ATMOSPHERIC INFRA-RED RADIATION

OVER CHRISTCHURCH, NEW ZEALAND.

A thesis

submitted in fulfilment

of the requirements for the degree

of

Doctor of Philosophy

in the

University of Canterbury

by

N.J. Tapper

University of Canterbury

1981

with 15 separate film strips in back pocket

ABSTRACT

The major concern of this study was to relate spatial and temporal variations of atmospheric infra-red radiation (IR↓) in Christchurch to peculiar attributes of the urban atmospheric environment, and to attempt to determine the relative role of IR↓ in contributing to the urban heat island.

This was approached in several ways including energy balance simulation of urban surface temperature to assess the likely effects of IR↓ variations on the heat island, urban-rural observations of radiation and other variables to establish variations in radiation transfer, and measurements of temperature, humidity and pollution in the vertical dimension to allow theoretical calculation of IR↓ and assessment of pollution effects on emissivity. Data collection was undertaken during 1978 and 1979 under clear-sky conditions to reduce the complicating effects of cloud cover.

The energy balance model, validated against field observations and making no direct allowance for IR↓ variation across the city, predicted Christchurch's nocturnal heat island with a reasonable degree of success indicating that the phenomenon was related more to surface effects of specific landuses rather than any atmospheric radiative effect. Urban-rural differences in incoming radiation showed an average clear-sky depletion of total solar radiation (SW↓) at the urban site of 3.5%, with individual daily depletions ranging above 10% and clearly related to atmospheric pollution. The urban SW↓ deficit appeared to be more than compensated for by an average clear-sky urban

excess IR↓ of 5.3% over the study period, and substantially more during winter and at certain times of day. While daytime excess IR↓ at the urban site was almost exactly balanced by a SW↓ deficit, the nocturnal continuation of urban IR↓ excess resulted in an excess radiant energy receipt at the urban site at that time. However, overall urban radiant energy excesses did not appear sufficient to account for the observed urban temperature excess.

Detailed investigations of the nature and composition of the urban atmosphere initiated to identify the source of observed urban IR↓ excess showed that the urban temperature excess present in the horizontal was also evident in the vertical, where warmer temperatures were consistently observed to approximately 300 m. The phenomenon was most marked at night and under a low windspeed regime. Atmospheric moisture regimes at the representative sites also showed distinctive urban and rural characteristics, with a nocturnal urban moisture excess extending approximately 350 m into the boundary-layer and a daytime urban moisture deficit existing to about 200 m. Significant urban-rural differences in air quality were also observed, with measurements emphasising the low level high concentration characteristics of Christchurch urban pollution, particularly during winter.

An emissivity approximation model, making no allowance for pollutant emissivity, showed that only a small proportion of observed urban-rural IR↓ difference in Christchurch could be accounted for by variations in temperature and water vapour across the city. Analysis of data for individual sites revealed a substantial component of atmospheric emissivity unaccounted for by profile characteristics, and this excess emissivity was observed higher at the urban site and during daytime. Detailed theoretical consideration of possible causes

of the excess emissivity at the urban site indicated the probable importance of particulate emission, and to a lesser degree emission by gaseous pollutants. Accordingly a mechanism to explain the urban-rural divergence in atmospheric infra-red radiation over Christchurch was proposed.

ACKNOWLEDGEMENTS

I would like to thank the many individuals and institutions that have made this study possible.

In particular I wish to express my sincere gratitude to Dr Ian Owens, my supervisor, whose assistance and advice at all stages of this study was invaluable and greatly appreciated. I will always look back on my time at Canterbury as being an enjoyable and stimulating one and this has in large part been due to Ian Owens. The advice and interest of Dr Andy Sturman of the Geography Department and Professor Peter Tyson, a visitor to the Geography Department at Canterbury, has also been most appreciated.

Second, I would like to thank those individuals and organisations assisting in the construction of the instrumented kytoon system. Particular thanks must go to Andy Sturman and Dr Bob Bennett of the Physics Department, University of Canterbury. The efforts of the Geography Department Technical staff in constructing the kytoon transporting trailer are also appreciated. The construction and operation of the kytoon system would not have been possible without the equipment and advice freely given by the New Zealand Meteorological Service and its staff.

Other institutions which must be thanked include the Department of Health and in particular its Air Pollution Section, which readily provided facilities, advice and data throughout the project. Facilities at Lincoln provided by the Soil Science Department, Lincoln

College and by Crop Research Division, Department of Scientific and Industrial Research are appreciated as is the storage space and equipment loaned by the Ghost Balloon Project (N.C.A.R.) at Christchurch International Airport. I am indebted to Ballins Industries (N.Z.) Ltd. and the University Grants Committee for providing financial support for this project.

Finally, a word of appreciation must go to my wife Liz, for her patience and encouragement throughout the study.

LIST OF CONTENTS

	Page
Abstract	ii
Acknowledgements	v
List of Figures	xiv
List of Plates	xx
List of Tables	xxi
List of Symbols	xxv
CHAPTER	
1 INTRODUCTION	1
RATIONALE	1
CHARACTERISTICS OF URBAN CLIMATES	3
Temperature Fields	3
Horizontal Structure	3
Vertical Structure	4
Moisture Fields	5
Wind Fields	6
THE ENERGY BALANCE OF URBAN AND RURAL AREAS	7
General	7
The Radiation Balance	9
Short-Wave Radiation	9
Infra-Red Radiation	11
The Heat Balance	15
MODELLING APPROACHES TO THE URBAN HEAT ISLAND	18
THESIS FRAMEWORK	21
Statement of the Problem	21
Aims and Approaches	22
Conceptual Framework and Thesis Format	23

Page

CHAPTER

2 A MODELLING APPROACH TO THE CHRISTCHURCH HEAT ISLAND 26

INTRODUCTION 26

THE MODEL 27

General Description 27

Sensitivity Analysis 33

APPLICATION AND VALIDATION OF THE MODEL 33

General 33

Physical Setting and Data Sources 36

Comparison of Observed and Simulated Temperatures 41

General Urban Effects 41
Spatial Temperature Patterns 42
Diurnal Temperature Variations 44

Energy Balance Fields Over Christchurch 47

Spatial Patterns of Simulated Energy Balance Components 47
Comparison of Observed and Simulated Energy Balance Components 52

Discussion 55

CONCLUSIONS 58

3 THE EXPERIMENTAL SITES AND INSTRUMENTATION 60

INTRODUCTION 60

GENERAL BACKGROUND 60

The Climate of Christchurch 60

Air Pollution in Christchurch 65

SITE REQUIREMENTS FOR THIS STUDY 69

General 69

Specific Consideration for Energy Balance Measurements 75

THE EXPERIMENTAL SITES 76

General Locational Characteristics 76

Suitability for Measurement of Energy Fluxes 79

CHAPTER		Page
3	View Factors	79
	Surfaces	83
	Height of Sensors Above Ground	84
	Air Quality	84
	Suitability for Kytoon Operations	84
	NEAR-SURFACE INSTRUMENTATION OF REPRESENTATIVE SITES	86
	General	86
	Radiant and Substrate Heat Flux Equipment	87
	Atmospheric Infra-Red Radiation	87
	Net All-Wave Radiation	88
	Short-Wave Radiation	88
	Substrate Heat Flux	90
	Data Recording Systems	92
	Sensor Calibration and Estimation of Error	93
	Meteorological and Air Pollution Equipment	93
	Screen Temperature and Humidity	93
	Windspeed and Direction	94
	Air Pollution	94
	Other Meteorological Data	95
	THE INSTRUMENTED KYTOON SYSTEM	96
	General	96
	Instrument Carrying System	96
	Kytoon Instrumentation	99
	Temperature and Humidity	99
	Windspeed and Direction	102
	Air Pollution	104
	THE DATA COLLECTION PROGRAMME	106
	Near-Surface Observations	106
	Kytoon Observations	107
4	URBAN-RURAL TEMPERATURE VARIATIONS IN THE CHRISTCHURCH AREA	110
	INTRODUCTION	110
	URBAN-RURAL VARIATIONS IN NEAR-SURFACE TEMPERATURES	112
	Previous Work	112
	General Results	113
	The Effect of City Size	115

CHAPTER		Page
4	Diurnal Variations and Urban-Rural Cooling Rates	117
	The Effect of Thermal Admittance	121
	URBAN-RURAL BOUNDARY-LAYER TEMPERATURE VARIATIONS	124
	Introduction	124
	General Results	125
	Nocturnal Profiles	125
	Daytime Profiles	128
	Elevated Inversions	130
	Urban Boundary-Layer Temperature Excess	132
	General	132
	Nocturnal Vertical Temperature Excess	134
	Daytime Vertical Temperature Excess	139
	CONCLUSIONS	143
5	URBAN-RURAL VARIATIONS IN THE CHRISTCHURCH MOISTURE FIELD	144
	INTRODUCTION	144
	URBAN-RURAL VARIATIONS IN NEAR-SURFACE MOISTURE CHARACTERISTICS	145
	General Results	145
	Diurnal Variations of Urban Moisture Excess	147
	URBAN-RURAL BOUNDARY-LAYER MOISTURE VARIATIONS	151
	Introduction	151
	General Results	152
	Nocturnal Profiles of Specific Humidity	152
	Daytime Profiles of Specific Humidity	152
	Diurnal Variation of Boundary-Layer Specific Humidities	155
	Urban Boundary-Layer Specific Humidity Excess	157
	General	157
	Nocturnal Urban Specific Humidity Excess	157
	Daytime Urban Specific Humidity Excess	159
	CONCLUSIONS	161

Page

CHAPTER

6 THE CHRISTCHURCH URBAN WIND FIELD AND ATMOSPHERIC POLLUTION 163

INTRODUCTION 163

VARIATIONS IN THE CHRISTCHURCH WINDFIELD 164

Introduction 164

Previous Studies of Spatial Variations Across Christchurch 164

Urban-Rural Differences Found in This Study 166

The Vertical Wind Profile Over Christchurch 172

ATMOSPHERIC POLLUTION OVER CHRISTCHURCH DURING THE STUDY PERIOD 180

Introduction 180

Near-Surface Variation of Atmospheric Pollution in Central Christchurch 180

The Vertical Profile of Atmospheric Pollution Over Christchurch 184

Introduction 184
Winter Smoke Particulate Profiles 186
Summer Nitrogen Oxides Profiles 195

CONCLUSIONS 201

7 CHARACTERISTICS OF CHRISTCHURCH'S URBAN RADIATION REGIME 204

INTRODUCTION 204

INCOMING SHORT-WAVE RADIATION CHARACTERISTICS 205

Urban-Rural Differences in Total SW↓ 205

Urban-Rural Differences in Atmospheric Transmissivity 208

General 208
Factors Involved in Urban-Rural Variations 215

INCOMING INFRA-RED RADIATION CHARACTERISTICS 219

Urban-Rural Differences in IR↓ 219

VARIATIONS IN INCOMING ALL-WAVE RADIATION AT THE REPRESENTATIVE SITES 232

CONCLUSIONS 235

Page

CHAPTER

8 PREDICTION OF ATMOSPHERIC IR↓ OVER CHRISTCHURCH :
I. THE USE OF SCREEN-LEVEL DATA 237

INTRODUCTION 237

A STATISTICAL APPROACH : REGRESSION ANALYSIS 237

Introduction 237

Relationships between Urban Excess IR↓ and Atmospheric Variables - Simple REgression Analysis 238

Atmospheric Pollution 238
Temperature 241
Vapour Pressure 244

The Relative Importance of Variables in Determination of Urban IR↓ Excess - Stepwise Multiple Regression 246

A SEMI-EMPIRICAL APPROACH : PREDICTIVE EQUATIONS FOR IR↓ 256

General 256

Empirical Formulae 257
A Derivable Formula - The Brutsaert Relation 258

Evaluation of IR↓ Predictive Equations 259

The Diurnal Variability of Predictive Errors 259
Performance Characteristics of Individual Equations 267

CONCLUSIONS 270

9 PREDICTION OF ATMOSPHERIC IR↓ OVER CHRISTCHURCH :
II. THE USE OF VERTICAL SOUNDINGS 272

INTRODUCTION 272

PREDICTION OF ATMOSPHERIC IR↓ FROM KYTOON AND RADIOSONDE PROFILES 273

General 273

The Prediction Method - Procedures and Assumptions 274

Prediction of Urban IR↓ Excess from Paired Profiles 280

Excess IR↓ at the Representative Sites 282

CHAPTER		Page
9	General	282
	Comparison with Previous Measurements	288
	Origin of the Excess Emissivity	289
	REFORMULATION OF THE BRUTSAERT RELATION	309
	CONCLUSIONS	314
10	CONCLUSIONS	316
	SUMMARY OF CONCLUSIONS	316
	SUGGESTIONS FOR FURTHER RESEARCH	320
	REFERENCES	324
APPENDIX		
I	PROGRAMME LISTING OF HEATIS	344
II	EQUIPMENT CALIBRATION PROCEDURES AND RESULTS	350
III	DETAILS OF THE INSTRUMENTED KYTOON SYSTEM	356
IV	STANDARDIZING OF PAIRED PROFILES	373
V	KYTOON PROFILES	378
VI	PROGRAMME LISTING OF 'FINALE'	379

LIST OF FIGURES

		Page
FIGURE 1.1	Diagrammatic Representation of Heat Balance of Urban and Rural Areas.	16
FIGURE 1.2	Conceptual Framework for Thesis.	24
FIGURE 2.1	Sensitivity Analysis for Mid-July Conditions Obtained over Christchurch Showing Daily Maximum and Minimum Temperatures with a Varying Model Input Parameter.	35
FIGURE 2.2	Simplified Landuse Map of Christchurch Showing the Points at which Temperatures were Measured on 10 July, 1979 and Location of Urban and Rural Representative Sites.	37
FIGURE 2.3	Average Winter Time Atmospheric Transmissivities for Incoming Solar Radiation over Christchurch.	39
FIGURE 2.4	Observed and Simulated (Model) Temperatures, ^{o}C, at 1400 h on 10 July, 1979.	43
FIGURE 2.5	Observed and Simulated (Model) Temperatures, ^{o}C, at 2230 h on 10 July, 1979.	45
FIGURE 2.6	Observed Windspeed and Direction Aloft and Vertical and Horizontal Temperature Gradients, ^{o}C, at 2230 h on 10 July, 1979.	46
FIGURE 2.7	Observed and Simulated (Model) Temperatures at Representative Sites on 10 July, 1979.	46
FIGURE 2.8	Average Winter Diurnal Variation of Energy Balance Components over Christchurch Rural and Urban (excluding C.B.D.) Sites under Clear Conditions.	48
FIGURE 2.9	Simulated Energy Balance Fields over Christchurch at 1200 h on Average Clear Winter Days.	50
FIGURE 2.10	Simulated Energy Balance Fields over Christchurch at 0400 h on Average Clear Winter Nights.	51
FIGURE 2.11	Diurnal Variation of Observed and Simulated Energy Fluxes for Urban and Rural Representative Sites, 10 July, 1979.	53

List of Figures (Continued)

		Page
FIGURE 3.1	Annual Average Concentrations of Pollutants in Central Christchurch, 1960-1980.	68
FIGURE 3.2	Location of Central City Experimental Site and Instrumentation.	77
FIGURE 3.3	Location of Lincoln Experimental Site and Instrumentation.	77
FIGURE 3.4	Central City Site View Factors.	80
FIGURE 3.5	Lincoln Site View Factors.	81
FIGURE 3.6	Block Diagram of the Data Acquisition System.	100
FIGURE 4.1	Distinction Between Urban Canopy-layer and Urban Boundary-layer.	111
FIGURE 4.2	Relationship Between Population and Intensity of the Urban Heat Island in North America, Europe and New Zealand.	116
FIGURE 4.3	Diurnal Screen Level Temperature Trends at the Urban and Rural Representative Sites in, a) Clear Summer Weather, and b) Clear Winter Weather.	118
FIGURE 4.4	Clear Weather Urban and Rural Cooling Rates for, a) The Average Summer Case, and b) The Average Winter Case.	120
FIGURE 4.5	Clear Weather Cooling Curves for the Urban and Rural Sites (Solid Lines), with Best Theoretical Approximations Shown (Dashed Lines).	123
FIGURE 4.6	Paired Urban and Rural Kytoon Profiles for 10 July, 1979, Showing, a) The 1440 h, and b) The 2230 h Situations.	133
FIGURE 4.7	Urban Nocturnal Vertical Temperature Excess, a) All Christchurch Data, b) Data for New York, (Bornstein, 1968) and Montreal (Oke and East, 1971), c) Christchurch Winter with Windspeeds $< 3\ ms^{-1}$, d) Christchurch Winter with Windspeeds $> 3\ ms^{-1}$, e) Christchurch Summer with Windspeeds $< 3\ ms^{-1}$. A Range of Plus and Minus One Standard Deviation is Shown.	135

List of Figures (Continued)

		Page
FIGURE 4.8	Urban Daytime Vertical Temperature Excess for Christchurch, a) All Data, b) With Easterly Wind Component, c) All Other Wind Components, d) Windspeeds < 3 ms^{-1}, e) Windspeeds > 3 ms^{-1}. A Range of Plus and Minus One Standard Deviation is Shown.	141
FIGURE 5.1	Clear Weather Diurnal Trends of Urban and Rural Absolute Humidity for, a) Christchurch Summer, b) Christchurch Winter, and c) Edmonton, Canada - Summer (Hage, 1975).	148
FIGURE 5.2	Time Progression of Boundary-layer Specific Humidities over Central Christchurch, 8 July, 1979.	156
FIGURE 5.3	Christchurch Nocturnal Urban Specific Humidity Excess for, a) All Nocturnal Data, b) Winter Nocturnal Data, and c) Summer Nocturnal Data. A Range of Plus and Minus One Standard Deviation is Shown.	158
FIGURE 5.4	Christchurch Daytime Urban Specific Humidity Excess for, a) All Daytime Data, b) Easterly Wind Component, c) All Other Wind Directions. A Range of Plus and Minus One Standard Deviation is Shown.	160
FIGURE 6.1	Diurnal Windspeed Variations at the Rural (L.S.) and Urban (C.C.S.) Representative Sites.	171
FIGURE 6.2	Mean Windspeeds Aloft (Open Circles) and Plotted Line of Best Fit (from Equation 6.1) for, a) Lincoln Site and b) Central City Site. c), d) and e) Show Data for the Central City Site under NE, E and SW Wind Directions Respectively.	176
FIGURE 6.3	a) Mean Daily Smoke Concentrations for the Two Study Years at the Central City Site. b) Mean Daily Concentrations of Nitrogen Oxides for the Two Study Years at the Central City Site.	181
FIGURE 6.4	Average Diurnal Variation of Smoke Particulate Concentration at the Central City Site During Winter Study Periods.	183
FIGURE 6.5	Average Diurnal Variation of Nitrogen Oxides at the Central City Site, a) During the Winter Study Periods, and b) During the Summer Study Periods.	185

List of Figures (Continued)

		Page
FIGURE 6.6	Composite of Nocturnal Profile Characteristics of Smoke Particulate, a) p.m. after Inversion Development and b) a.m. before Inversion Dissipation. Bars Show Plus and Minus One Standard Deviation and Extreme Values.	187
FIGURE 6.7	The Short Term Variability of Low Level Atmospheric Smoke Pollution, 12 July, 1978.	189
FIGURE 6.8	Typical Temperature and Pollution Profiles for a, a) Late Evening, and b) Early Morning Flight.	190
FIGURE 6.9	Composite of Daytime Profile Characteristics of Smoke Particulate, a) During Temperature Profile Transition, and b) Under Lapse Conditions. Bars Show Plus and Minus One Standard Deviation and Extreme Values.	192
FIGURE 6.10	A Typical Late Winter Lapse Profile and Smoke Concentrations, 3 September, 1978.	193
FIGURE 6.11	Composite of Nocturnal Profile Characteristics of Nitrogen Oxides (NOx and NO_2), Showing a) All Data, and b) Adjusted Data (Minus 5.4.79 and 14.4.79). Bars Show Plus and Minus One Standard Deviation and Extreme Values.	196
FIGURE 6.12	Elevated Inversions and Trapping of Pollutants Aloft, 26 April, 1979.	198
FIGURE 6.13	Composite of Nitrogen Oxides (NOx and NO_2) Profiles Under Daytime Lapse Conditions. Bars Show Plus and Minus One Standard Deviation and Extreme Values.	200
FIGURE 7.1	Relationship Between Urban Transmissivity Deficit and Log Urban Smoke Particulate.	218
FIGURE 7.2	Relationship Between the Winter Diurnal Variation of Clear Sky Apparent Atmospheric Emissivity and that of Other Atmospheric Variables for, a) The Rural, and b) The Urban Representative Sites.	228
FIGURE 7.3	Relationship Between the Diurnal Variation of Clear Sky Urban Excess $IR\downarrow$ and that of Other Atmospheric Variables Exhibiting Urban-Rural Differences, Showing a) the Summer/Autumn Case, and b) The Winter Case.	230

List of Figures (Continued)

		Page
FIGURE 8.1	Diurnal Variation of Clear-Sky Apparent Atmospheric Emissivity Estimation Error (Various Formulae).	260
FIGURE 8.2	Diurnal Variation of Clear-Sky Apparent Atmospheric Emissivity Estimation Error (Brutsaert Formula), Showing Variability of the Individual Point Deviations.	260
FIGURE 8.3	The Diurnal Variations of Clear-Sky Apparent Atmospheric Emissivity Estimation Error in Four Different Studies. The Zero Line (No Error) is Shown on the Right Hand Axis.	263
FIGURE 9.1	Example Profile from 'Finale' - Central City Site, 0605 h, 8 July, 1979.	279
FIGURE 9.2	Plot of Winter Time Fractional Excess Emissivity and Log_{10} Smoke Particulate Concentrations (Open Circles Show Daytime Relationship and Solid Circles the Nocturnal Relationship).	294
FIGURE 9.3	Dependence of the Mean Emissivity, $\bar{\varepsilon}$, of Aerosol in the Atmospheric Window and of the Effective Emissivity, $f\bar{\varepsilon}$, of the Atmosphere for Particles, on the Mass Absorption Coefficient, Ka, and on Aerosol Mass Concentration, M. Depth of Aerosol layer z is 150 m.	301
FIGURE 9.4	Prediction of Atmospheric Emissivity in Central Christchurch using, a) the Unadjusted, and b) The Pollution-adjusted Brutsaert Formula.	310
FIGURE 9.5	Prediction of the Diurnal Variability of Atmospheric Infra-red Radiation in Central Christchurch Using the Unadjusted and the Pollution-adjusted Brutsaert Formula.	313
FIGURE A.1	Aerostatic Lift Characteristics of a Helium Inflated Follmer 115 Kytoon.	357
FIGURE A.2	Circuit Diagram of Radiosonde Timing Mechanism.	359
FIGURE A.3	Plot of Radiosonde Temperature and Humidity Errors.	362
FIGURE A.4	Relationship Between Measured Windspeed and Kytoon Lift.	364

List of Figures (Continued)

		Page
FIGURE A.5	Equipment for Determination of Smoke Particulate at Altitude (O.E.C.D. Method).	364
FIGURE A.6	Flow Rates for NOx Pumps on Kytoon-System (Under Load).	371
FIGURE A.7	Measured and Predicted (Anfossi *et al.* Equation) Temperature Profiles Aloft, 7 July, 1979.	376

LIST OF PLATES

		Page
PLATE 3.1	Photochemical Smog Over Christchurch, 14 February, 1977.	70
PLATE 3.2	Adapted Net-radiometer for Measurement of IR↓.	89
PLATE 3.3	Net-radiometer for Determining Net All-wave Radiation. Note Levelling Device.	89
PLATE 3.4	Solarimeter and Shadow Ring Attachment.	91
PLATE 3.5	The Kytoon System Showing the Dirigible and Ground Station.	98
PLATE 3.6	Close-up of Radiosonde, Showing Temperature Sensor (on Outrigger) and Hygristor Filament.	101
PLATE 3.7	The Ground Station. Radio Receiver is on the Top Shelf and the Frequency Meter is Below it.	101
PLATE A.1	Kytoon Smoke Sampling Apparatus Showing Pump, Meter, Plastic Tubing and Filter Head.	365
PLATE A.2	Dismantled Filter Head Showing Filter Paper and Retaining Rings.	367
PLATE A.3	Kytoon Nitrogen Oxides Sampler Showing Portable Pump and Bubblers.	369

LIST OF TABLES

		Page
TABLE 2.1	Boundary Conditions for Clear Winter (July) Conditions and 10 July, 1979.	34
TABLE 2.2	Surface Boundary Conditions and Landuse Cagegories.	38
TABLE 3.1	Climatological Averages (1941-1970)	63
TABLE 3.2	Sunshine Percentage of Possible (1941-1970)	63
TABLE 3.3	Average Number of Days with Gusts Reaching 70 km h^{-1} or more (1941-1970).	63
TABLE 3.4	Categories of Synoptic Conditions and Relation to Air Pollution Levels for Christchurch Winter (1976).	64
TABLE 3.5	Fuel Consumption and Emissions - Three Winter Months (Mid-May to Mid-August).	67
TABLE 3.6	Variables Monitored in this Project.	72
TABLE 3.7	Air Pollution ($\mu g\ m^{-3}$) at Representative Sites, 18-28 August, 1978.	85
TABLE 3.8	Table of Boundary-layer Kytoon Temperature and Humidity Sensor Characteristics.	103
TABLE 3.9	The Data Record.	108
TABLE 4.1	Hourly Clear Weather Temperatures by Month (^{o}C).	114
TABLE 4.2	Nocturnal Temperature Profiles Showing, a) Nocturnal Profile Characteristics (Paired Profiles in Brackets), b) Percent Occurrence of Nocturnal Inversion Strengths, and c) Statistics of Nocturnal Inversion Characteristics.	126
TABLE 4.3	Daytime Temperature Profiles Showing, a) Daytime Profile Characteristics, b) Percent Occurrence of Lapse Strengths Under Unstable Conditions, and c) Daytime Lapse Strength Characteristics.	129

List of Tables (Continued)

		Page
TABLE 4.4	Percent Occurrence of Elevated Inversions.	131
TABLE 4.5	Statistics of 'Cross Over' Layer Parameters.	137
TABLE 4.6	Observed and Predicted Urban Mixing Heights Over Christchurch (m).	140
TABLE 5.1	Hourly Clear Weather Vapour Pressures by Month (mb)	146
TABLE 5.2	a) Distribution of Inversion and Lapse Conditions with Paired Nocturnal Humidity Profile Data, b) Summary Characteristics of Nocturnal Humidity Inversions, c) Distribution of Lapse and Inversion Conditions with Paired Daytime Humidity Profile Data, and, d) Summary Characteristics of Daytime Humidity Lapse Data.	153
TABLE 6.1	Average Hourly Wind Directions by Season for Lincoln and Central City Sites (% Occurrence)	167
TABLE 6.2	Mean Hourly Windspeed (ms^{-1}) by Wind Direction, Lincoln and Central City Sites.	170
TABLE 6.3	Typical Values of the Power Law Parameters.	174
TABLE 6.4	Central City Deviations (^{o}C) from Lincoln Wind Directions at Altitude.	179
TABLE 7.1	Daily Average SW↓ by Site (Wm^{-2})	206
TABLE 7.2	Previous Studies of Clear Weather Urban Total SW↓ Depletion.	207
TABLE 7.3	Average Daily Transmissivity by Site.	211
TABLE 7.4	Hourly Clear Sky Transmissivities by Season.	213
TABLE 7.5	Seasonal Hourly Transmissivities at Lincoln and Central City Sites.	214
TABLE 7.6	Summary of Regression Analysis - Urban Tr Deficit (%) and Pollution Characterisicts.	217
TABLE 7.7	Average Daily IR↓ by Site (Wm^{-2}).	220
TABLE 7.8	Average Daily Emissivity by Site.	222
TABLE 7.9	Seasonal Hourly IR↓ Values by Site (Wm^{-2})	224
TABLE 7.10	Seasonal Hourly Emissivity by Site.	226

List of Tables (Continued)

		Page
TABLE 7.11	Ratio of Urban-Rural Total Radiation.	233
TABLE 8.1	Summary of Regression Analysis (Log Pollution)	240
TABLE 8.2	Summary of Regression Analysis (Temperature)	243
TABLE 8.3	Summary of Regression Analysis (Vapour Pressure)	245
TABLE 8.4	Multiple Regression Analysis - All Data.	247
TABLE 8.5	Multiple Regression Analysis - Summer Data.	248
TABLE 8.6	Multiple Regression Analysis - Winter Data.	250
TABLE 8.7	Multiple Regression Analysis - Winter Days.	250
TABLE 8.8	Multiple Regression Analysis - Winter Nights.	251
TABLE 8.9	Multiple Regression Analysis - All Daily Data.	251
TABLE 8.10	Multiple Regression Analysis - Winter Daily Data.	253
TABLE 8.11	Multiple Regression Analysis - Individual Site Winter IR↓ Data.	254
TABLE 8.12	Summary of Studies from which Error Curves in Figure 8.3 were Obtained.	265
TABLE 8.13	Performance Statistics - Predictive Formulae.	268
TABLE 9.1	Measured Urban Excess IR↓ and Urban Excess IR↓ Calculated from Profiles.	281
TABLE 9.2	Summary of Profile Analysis - Central City Nocturnal Data.	284
TABLE 9.3	Summary of Profile Analysis - Central City Daytime Data.	285
TABLE 9.4	Summary of Profile Analysis - Lincoln Site Nocturnal Data.	286
TABLE 9.5	Summary of Profile Analysis - Lincoln Site Daytime Data.	287
TABLE 9.6	Summary of Regression Analysis - Winter C.C.S. Emissivity and Particulate Concentration (Log Smoke)	290

List of Tables (Continued)

		Page
TABLE 9.7	Summary of Regression Analysis - Summer C.C.S. Emissivity (Nocturnal Only) and Nitrogen Oxides Concentration (Log NOx)	292
TABLE 9.8	Fractional Excess Emissivity (γ) at Lincoln Site with Wind Direction.	296
TABLE 9.9	Size Distribution of Christchurch Winter Particulate Matter.	298
TABLE 9.10	Gaseous Absorbers in the Infra-red Showing Wave Length (μm) at the Centre of the Absorption Band.	307
TABLE 9.11	Improvement to Brutsaert Relation at Urban Site with Emissivity Adjustment for Pollution.	311
TABLE A.1	Summary of Radiation Instrument Calibrations, October, 1978.	351
TABLE A.2	Summary of Radiation Instrument Calibrations, November, 1979.	352
TABLE A.3	Summary of Flux Plate Calibrations.	355
TABLE A.4	Comparison of Ground Level Total Nitrogen Oxides ($NO + NO_2$) Measured with Kytoon Sampling Apparatus and Adjacent Monitor Laboratory Nitrogen Oxides Analyser.	372

LIST OF SYMBOLS

a	coefficient in regression : aerosol absorptivity
α	empirical coefficient
A	net advected energy : lot area : altitude of sun
AH	artificial urban heat production
b	coefficient in regression : constant term
B	Planck distribution
c_p	specific heat of air at constant pressure (1010 J kg^{-1} $^oC^{-1}$)
c_s	specific heat of substrate
C	pollutant concentration
d	depth of aerosol layer
e	vapour pressure
e_s	screen level vapour pressure
F	Fourier modulus
g	acceleration due to gravity
G	substrate heat flux
h	hour : hour angle of sun from noon : urban mixed height
$\overline{h}$	average height of roughness element
H	sensible heat flux
I	net infra-red radiation
IR↓	atmospheric infra-red radiation
IR↑	terrestrial infra-red radiation
j	node in heat conduction equation
k	Von Karman's constant
k_s	thermal conductivity of the substrate
K	bulk adiabatic transfer coefficient
Ka	mass absorption coefficient
Kh	coefficient of eddy diffusivity of heat
Km	coefficient of eddy diffusivity of momentum
Ke	coefficient of eddy diffusivity of vapour
L	latent heat of evaporation/condensation (2501 J g^{-1} at 0^oC)
LE	latent heat flux
m	optical air mass
M	mass concentration of aerosol

M_b	mass of kytoon
Ml	mass of unit length of tether line
M_L	potential kytoon payload
M_p	mass of payload
N	nitrogen oxides concentration (in regression equation)
p	atmospheric pressure
P	population : Richardson number correction factor
q	diffuse beam short-wave radiation
q_o	specific humidity at the surface
q_2	specific humidity at the reference level
Q	direct beam short-wave radiation
r	earth radius vector : correlation coefficient in regression analysis
R	evaporating fraction
Ri	Richardson number
Rn	net all-wave radiation
s	silhouette area of roughness elements
S	net solar radiation : smoke concentration (in regression equation) : standard deviation
S.E.E.	standard error of estimate
So	solar constant (1353 Wm^{-2})
SW↓	short-wave radiation toward the surface
SW↑	short-wave radiation from the surface
t	time : time step in heat conduction equation : transmissivity of aerosol layer
T	temperature
T_a	screen level air temperature
T_b	bulk atmospheric temperature
T_o	surface equilibrium temperature (model)
Tr	rural screen level temperature : atmospheric transmissivity
T_s	surface temperature
T_u	urban screen level temperature
T_z	temperature at depth z in substrate
T_2	reference level temperature
$\bar{u}$	mean windspeed
u_G	gradient windspeed at height z_G
$\bar{u}_z$	mean horizontal windspeed at height z
u_2	reference level windspeed
u_*	friction velocity
v	coefficient of variation in regression analysis

V	volume (of air)
V_b	volume of kytoon
W	total weight of pollutant
$\overline{X}$	arithmetic mean
z	depth in substrate or atmosphere
z_G	depth of frictional influence
z_i	depth of layer influenced by surface radiation
z_o	surface roughness
z_2	reference height
Z	solar zenith angle.
α	surface albedo: rural potential temperature gradient
γ	Richardson number correction factor : fractional excess emissivity
δ	solar declination, positive in Northerm Hemisphere
ε	emissivity
ε_a	emissivity of air, atmospheric apparent emissivity
ε_b	bulk atmospheric emissivity
ε_s	surface emissivity
$f\overline{\varepsilon}$	effective emissivity of atmosphere for pollution
λ	wave length of radiation
μ	population mean
θ	potential temperature
ρ	air density
ρ_s	substrate density
σ	Stefan-Boltzmann proportionality constant (5.67×10^{-8} Wm^{-2} K^{-4})
ϕ	latitude, positive in Northern Hemisphere
Δ	finite difference
$\Delta Tu-r$	urban-rural temperature differential.

CHAPTER 1

INTRODUCTION

RATIONALE

The distinctive three dimensional structure of urban heat islands[1] has long been recognized as one of the more dramatic influences mankind has had on his environment. For many years this phenomenon and its underlying mechanisms has received attention from climatologists and meteorologists and a considerable literature on the urban heat island has developed. Comprehensive selected bibliographies have been compiled by Brooks (1952) for the period 1833 to 1952, and more recently by Munn (1968), Chandler (1968) and Griffiths and Griffiths (1974). Kratzer (1956) provided an early review of the literature, while Tyson *et al.* (1973), Peterson (1969) and Oke (1974, 1979) give detailed reviews of the more recent literature.

It is surprising that despite accumulation of a vast amount of information about heat islands, we are still a long way from a complete understanding of causative mechanisms. Reasons to explain the relative warmth of urban areas have been many. Garnett and Bach (1965) supported Howard (1833) in his assertion that artificial heating is preeminent, while Kratzer (1956) attributed the heat island primarily to the

---

[1] Urban heat island in this text is taken to be synonymous with an urban temperature excess exhibited in three dimensions.

absorption and re-emission of infra-red radiation by urban atmospheric pollution. Oke and Fuggle (1972) and Rouse and McCutcheon (1972) attempted to quantify urban excess infra-red radiation, however the mechanisms leading to this excess and its relative contribution to the urban heat island were then, and have been since, in dispute. Other factors mentioned include the high heat capacities of pavement and building materials in urban areas (Duckworth and Sandberg, 1954; Chandler, 1967a; Oke and Maxwell, 1975), and a lack of evaporative cooling (Chandler, 1962a; Bornstein, 1968; Morgan *et al.*, 1977).

On a world scale urbanisation in New Zealand is of relatively modest proportions, although many related problems are emerging in the larger cities. It is not surprising that the little research done on urban climates in New Zealand has been concentrated in Christchurch, for it is a city providing a unique natural laboratory and an atmospheric environment comparable with a much larger city. Sham (1968) and Kingham (1969) have both described the urban temperature characteristics of Christchurch, while Ryan (1975) has discussed urban influences on local winds. Tuller (1977) made some general observations on Christchurch's overall urban climate. Durant (1979) described possible urban effects on Christchurch's rainfall patterns. Preliminary work on radiation transfers in Christchurch has been reported by Tapper (1976, 1977) and Tapper and Owens (1976).

Overall, there has been a large and disorderly body of literature on the urban heat island indicative of measurements being undertaken outside a conceptual framework of theory and giving little understanding of the complex inter-relationships between the physical processes that produce the heat island phenomenon. Most past research on urban climates has concentrated on statistical analysis of standard

climatic elements rather than a more fundamental examination of the physical attributes of urban areas and the way that these affect the basic processes of energy and mass transfer. The latter approach is essential to improve our knowledge of processes leading to heat island formation and would not only examine in detail the characteristics of the urban surface where most of the incoming energy is captured and redistributed, but also those of the urban boundary-layer. A precise knowledge of processes in the urban boundary-layer is crucial, and it is in this area that the present thesis is largely concerned. The boundary-layer is the layer in which energy is transferred between the atmosphere and the earth's surface in the form of radiation, water vapour, heat and momentum; it is also the layer in which all human and most biological activities take place.

This chapter will review the literature on urban heat islands and modelling approaches to the phenomenon and, after a consideration of objectives in light of the literature, will outline a conceptual framework for the thesis.

CHARACTERISTICS OF URBAN CLIMATES

Temperature Fields

Horizontal Structure

Probably the best documented of all urban-rural meteorological differences in time and space is the horizontal air temperature discontinuity. In the early nineteenth century Howard (1833) had reduced systematic observations from a large number of stations in and around London, clearly establishing that central London was warmer than

surrounding countryside. Urban heat islands have since been shown by Duckworth and Sandberg (1954) for San Francisco, Mitchell (1961) for Vienna, Chandler (1965) for London again, Oke (1968, 1973 for Montreal and other cities, Van Gogh (1979) for Pretoria and many others.

In general the nocturnal heat island intensity has been shown to be greater than daytime when differences observed are often difficult to distinguish from topographic effects. Heat island intensity has also been shown to be dependant on season and windspeed with windspeeds above 12 m sec^{-1} destroying the urban temperature excess, even in large cities (Oke and Hannell, 1968). Observations of heat island intensity have led to the suggestion that it is dependant on city size (Mitchell 1962), and Oke (1973) has shown a logarithmic relationship between the magnitude of the maximum urban-rural difference and the size of the urban area supplying the heat energy.

Vertical Structure

In comparison with the large body of literature relating to horizontal urban temperature patterns there is a relative paucity of information about the vertical structure of the atmosphere above cities. Those reporting on contrasting lapse rates over urban and rural areas include Duckworth and Sandberg (1954) for San Francisco, De Marrais (1961), McCormick and Baulch (1962), McCormick and Kurfis (1966) and Clarke (1969) for Cincinnati, Davidson (1967) and Bornstein (1968) for New York, Oke and East (1971) for Montreal, Angell *et al.* (1971) for Columbus, Tyson *et al.* (1972) for Johannesberg and Dirks (1974) for St. Louis.

Apart from some early tethered balloon observations by Duckworth and Sandberg (1954) in San Francisco most studies have obtained temperature from tower data (Munn and Stewart, 1967), or from airborne measurements. Generally results show less stable conditions in urban areas, with fewer surface based inversions. One peculiarity of the urban temperature profile indicated by many of these studies is the frequent occurrence of a weak, elevated inversion of relatively long duration (Bornstein, 1968; Clarke, 1969). However, there appears to be considerable variation in the exact nature of the urban temperature structure from place to place. The physical reasons advanced to explain urban warmth at the surface including artificial heating and surface characteristics cannot be directly related to the formation of a stable layer at some level above the city. One method proposed for the formation of elevated inversions is the advection of stable rural air over the warmer urban surface (Clarke, 1969; Leahey and Friend, 1971). Bornstein (1968) invoked the ideas of Sheppard (1958), suggesting radiative effects of polluted layers over a city as another possible cause. The modelling approach of Atwater (1971a, 1971b) lent further weight to this latter theory.

The development of mesoscale urban thermal plumes bending over surrounding rural areas under light wind conditions have been reported by several authors (Clarke, 1969; Bornstein, 1968; Tyson *et al.*, 1972).

Moisture Fields

As with temperature there is a divergence in atmospheric moisture between urban and rural areas. While there is general agreement that urban humidities are lower than surrounding rural areas

(Kratzer, 1956; Chandler, 1962b, 1965, 1967b; Kopec, 1973; Hage, 1975), the extent of dependence on variations in temperature is not always clear. Chandler (1965) cites an annual average urban vapour pressure deficit for London, but observed nocturnal vapour pressures were often found to be higher in the city than in outlying regions. Chandler attributed the former to lowered evaporation rates in the city and the latter to the moist daytime air being trapped between tall buildings and diffusing only slowly through the evening. One other explanation forwarded is the lack of cool surfaces for dew formation in the city as compared to rural areas, with moisture having to remain in the atmosphere.

Information on the vertical distribution of moisture in the atmosphere is limited and appears at first glance to be contradictory. Bornstein *et al.* (1972) produced evidence of a nocturnal moisture excess of 4% at heights of up to 700 metres over New York, while daytime specific humidity deficits have been identified over St. Louis, (Auer and Dirks, 1974).

Wind Fields

Observations have shown two distinct urban effects on wind characteristics which will cause deviations from regional wind flow patterns. Several investigations give evidence of reduced average windspeeds within cities (Landsberg, 1956; Frederick, 1964; Munn and Stewart, 1967; Graham, 1968), although Chandler (1965) suggested that urban-rural differences depended on such variables as seasonal and diurnal windspeed variations. Bornstein *et al.* (1972) produced evidence that at low windspeeds surface roughness and artificial heating combine to cause slightly higher windspeeds in the city. The work of Shklyarevich (1974) and Duchêne Marullaz (1976) is representative of

some of the more recent work on urban effects on the vertical wind profile.

Other investigators give evidence of changes in wind direction with airflow across urban areas. Early workers (Pooler, 1963; Georgii, 1970; Davidson, 1967; Angell *et al.*, 1968) showed local cyclonic convergence over cities at times of low windspeeds and generally ascribed it to the pressure effects of the urban heat island. Recently, frictionally induced turning of the wind in moderate and strong windflow conditions has been observed and detailed in several studies, including that of Angell *et al.* (1973). Oke (1974, 1979) contains an excellent review of studies of urban effects on local wind characteristics.

THE ENERGY BALANCE OF URBAN AND RURAL AREAS

General

That the observational characteristics of urban heat islands are generated by distinctive energy transfers over urban and rural surfaces is an unquestioned fact. It therefore becomes necessary to draw these various ideas and observations together by placing them within the context of energy balance theory.

Flows of energy to and away from the surface of the earth obey many laws of classical physics, the most important being the law of conservation of energy. It is this law that enables the energy balance for a city surface to be expressed as:-

$$(Q + q)\ (1 - \alpha) + IR\downarrow - IR\uparrow = Rn = LE + H + G + A - AH \qquad \ldots\ 1.1$$

where, Q and q - direct and diffuse beam short-wave radiation respectively, α - surface albedo, IR$\downarrow$ and IR$\uparrow$ - infra-red atmospheric emission and infra-red radiation emitted from the surface respectively, Rn - net all wave radiation, LE - latent heat transfer, H - sensible heat transfer, G - heat storage in the ground and in city surface materials, A - net advected energy and AH - urban artificial heat production. The left hand side of Equation 1.1 is generally termed the radiation balance and the right hand side the heat balance. If the radiation balance (given by the difference between incoming net short-wave and infra-red radiation) is positive, this represents a net gain of energy at the surface and *vice versa*. The heat balance terms are positive for a transfer of energy away from the surface, therefore are positive when they represent losses of heat for the surface and negative for gains. With removal of the artificial heat production term Equation 1.1 holds equally for any rural surface.

Most general factors physically affecting the energy balance components are discussed in standard texts such as Sellers (1972) and Oke (1978). Lowry (1970) more specifically outlines the ways that urbanisation may affect the components of the energy balance, through:-

(i) surface materials,

(ii) surface shapes,

(iii) heat sources,

(iv) moisture characteristics,

(v) air quality.

These can have definite individual effects on energy balance components and can also interact one with another to produce more complex effects. An examination of literature on the radiation and heat balance of urban and rural areas reflects the importance of these

characteristics in determining the magnitude and/or sign of the various energy balance components.

The Radiation Balance

Short-Wave Radiation

The driving force behind all energy and heat exchanges at the surface is the usable net radiant income Rn, of which SW↓ (Q + q) is the most important forcing function. Urban effects on SW↓ are very well documented. Short wave radiation receipt at the surface could be expressed as SW↓ = f (aerosols, atmospheric water vapour and trace gases, cloud amount, view factor, atmospheric path length and earth-sun distance). Few studies have attempted to unravel any of the complex inter-relationships involved, usually concentrating on the radiation response to one variable only.

One of the first documentations of the effect of a smokey atmosphere on the transmission of radiation was made by Hand (1943). With the passage of smoke from a forest fire he noted a decrease in short-wave radiation with little noticeable effect on the infra-red radiation. Concern for the environment stimulated research into climatic effects of atmospheric pollution in the early 1960's. Studies by Mateer (1961), Emslie (1964) and Bach (1973) indicated a weekly or annual cycle of solar radiation attenuation related to industrial pollution trends. Monteith (1966) showed an increased solar radiation in central London over the years 1957 - 1963 associated with a pollution abatement program.

Recent studies have concentrated more on contributing to an understanding of the total urban heat balance. Long term studies

include those by De Boer (1966), East (1968), Yamashita (1970), Probald (1972), Manes *et al.* (1975) and Camuffo (1979), while short term studies indicating urban-rural short-wave radiation differences include those by Bach and Patterson (1969), Rouse and McCutcheon (1972) and Sanderson *et al.* (1973). McCormick and Baulch (1962), Bach (1971) and Rouse and Bello (1979) reported variations in solar radiation attenuation with height over urban areas, with atmospheric transmissivity varying with meteorological and pollution conditions.

A recent advance in the examination of urban effects on solar radiation has been the application of the concept of climatonomy as proposed by Lettau and Lettau (1969) to urban areas (Yamashita, 1979). The development of a complete solar radiation budget had previously been limited by the difficulties posed in measuring directly the components of the solar radiation budget over the irregular and inhomogeneous surfaces of the city.

In summary, SW↓ radiation (0.3 - 4.0 μm wavelength) is found to be depleted by an annual average 10 - 15% in a polluted urban atmosphere compared to a clean rural site. Under heavy pollution conditions and when the solar path length is large (high solar zenith angles) attenuation can reach 30%. As well as gross depletion of total solar radiation, the spectral and directional character of the beam changes. Radiation nearer the ultra-violet is preferentially filtered out (Randerson, 1970; Peterson *et al.*, 1978; Bridgeman, 1980) and the proportion of diffuse to direct beam solar radiation is increased (Robinson, 1962; Montieth, 1962). Gross measurements of total solar radiation mask actual attenuation because a large proportion of lost direct beam solar radiation is regained at the surface as diffuse radiation (Sprigg and Reifsnyder, 1972).

Surface albedo (α) which is instrumental in determining outgoing short wave radiation ($SW\uparrow$), is directly influenced by the nature of the surface and thus may be expected to vary between city and country. Characteristic urban albedos reflect the influence of the colour and complex geometry of urban surfaces (Oke, 1974; Nunez and Oke, 1977). Many detailed studies of urban albedo (Kung *et al.*, 1964; Bach and Patterson, 1969; White *et al.*, 1978; Rouse and Bello, 1979) indicate a lowered albedo in urban areas in the order of 5 - 15%, but Oke (1974) urged caution in generalising lowered urban albedos in all cases. A numerical modelling approach (Craig and Lowry, 1972) indicates a decreased urban albedo due to multiple reflection. Rouse and Bello (1979) in one of the few studies of its type, examined the urban atmosphere over Hamilton, Ontario and found aerosol albedo to be similar to surface albedo.

Infra-Red Radiation

Urban-rural variations in atmospheric infra-red radiation ($IR\downarrow$) are poorly understood and documented and this results in a certain amount of confusion and controversy. Reasons for this are several, not the least of which is the current lack of intensive field studies in this area of urban climatology. Other problems include the small energy differences involved (less easily measured than $SW\downarrow$), the inability of most investigators to gather all information necessary for an understanding of $IR\downarrow$, and the current preoccupation with modelling rather than measuring infra-red radiative transfer.

It has generally been found that pollutants will decrease $SW\downarrow$ through absorption and scattering and it has been felt that this would in turn increase $IR\downarrow$. Robinson (1947) first identified an excess measured $IR\downarrow$ over that expected for a site near London. After careful

consideration of possible reasons for the phenomena, his most likely explanation related to the presence of atmospheric particulates. The often quoted paper of Sheppard (1958) is representative of standard ideas on effects of pollution in the atmosphere. The hypothesis in relation to urban radiation has been that an aerosol layer absorbs some incoming SW and outgoing IR radiation during the day, and outgoing IR radiation at night, then re-radiates this heat energy with a large proportion of it arriving at the surface as incoming IR radiation. This is the much publicised 'greenhouse' effect which has long been quoted as an important reason for the development of the urban heat island (Sham, 1968). Recently, doubt has been cast on the validity of this hypothesis. The main criticism is based upon the observation that any surplus energy from this source is unlikely to be sufficient for the development of an urban heat island (Oke and Fuggle, 1972; Probald, 1972), and that net IR losses are higher in the city due to increased IR↑ (Bornstein and Oke, 1979). In determining the contribution of IR↓ to the formation of the urban heat island we have the classical 'chicken and egg' situation of cause and effect. Each of air temperature and IR↓ is potentially capable of altering the other.

Bach and Patterson (1969) in a limited series of measurements in Cincinnati found an increase of IR↓ up to 8% in the central city as compared to a rural zone. However, differences were usually within instrumental error and therefore little confidence could be placed in them. Idso (1972a) noted a substantial increase in IR↓ during an Arizona dust storm. A later analysis of temperature records at Phoenix, Arizona, indicated a warming trend which was suggested to be associated with a build up of atmospheric pollution enhancing the 'greenhouse' effect (Idso, 1974).

Lettau and Lettau (1969) discussed the attenuation of solar radiation under various atmospheric conditions. They concluded that high turbidity in the atmosphere has the potential for atmospheric heating through aerosol absorption of solar radiation. Implicit in this atmospheric heating is an increase in IR↓ to the surface. Similarly, Atwater (1971b) showed in a modelling approach that concentrations of NO2 of 1 ppm could lead to strong atmospheric heating through absorption of solar radiation, and that a concentration of gases such as CO_2, SO_2, O_3, as well as aerosols, could lead to greater absorptivity of terrestrial IR↑. The findings of Atwater are similar to several other modelling approaches to IR radiative transfer (Reck, 1975; Ackerman *et al.*, 1976; Viskanka and Daniel, 1980).

Two of the most detailed field studies of urban-rural differences in IR↓ are those of Oke and Fuggle (1972) and Rouse *et al.* (1973). Both studies indicated a slight urban excess IR↓ on cloudless nights and the latter study described an excess IR↓ of up to 33% near midday. Since the variation of IR↓ at the surface is described by the Stefan-Boltzmann Law:-

$$IR\downarrow = \varepsilon_b \sigma T_b^4 \qquad \ldots 1.2$$

where ε_b - bulk atmospheric emissivity, σ - Stefan-Boltzmann proportionality constant = 5.67×10^{-8} $Wm^{-2} K^{-4}$, and T_b - bulk atmospheric temperature (^oK); variability of IR↓ across urban areas can only be explained by:

(i) an increase in urban atmospheric emissivity as a result of changes in atmospheric constituents, and/or

(ii) an increase in urban air temperature largely as a result of non-radiative warming of the atmosphere through the turbulent

sensible heat flux set up by artificial heat generation and stored city heat.

Oke and Fuggle (1972) tend to follow the second hypothesis. In the absence of vertical profiles of atmospheric temperature and water vapour, it appeared from a variety of empirical and theoretical considerations that the greater urban IR↓ emission was due to urban warmth rather than increased atmospheric emissivity. Hence, Oke and Fuggle decided that the observed increased IR↓ was probably an effect, rather than a cause of the urban heat island. The situation is complicated somewhat by the fact that some of the observed urban warmth may be due to radiative warming of pollution, however Oke and Fuggle discounted this, at least for the nocturnal situation.

Rouse *et al.* (1973) follow the first hypothesis. They took atmospheric radiative temperatures at 150 m and 2500 m above their industrial and control sites and found them to be similar. Therefore, application of the Stefan-Boltzmann relation (Equation 1.2) gave a computed sky emissivity which was significantly different for both sites.

Although only of limited sample size and rather simplistic in approach, these two studies remain the most comprehensive field data based accounts of urban-rural IR↓ differences. However, they cannot be compared directly as one relates only to the nocturnal situation and the other largely to the daytime situation. Neither attempts the integration or isolation of other likely controlling variables.

Brazel and Osborne (1976) also lend support to the observations of Rouse *et al.* (1973). Analysis of several months data for an urban site in Windsor, Ontario, suggested an increased urban IR↓ resulting from increased atmospheric emissivity due to the urban haze

layer. Dalrymple and Unsworth (1978) invoked aerosol emission as the most likely source of an observed IR↓ at rural sites in Britain and British Columbia.

In summary; whilst most studies agree that there is an excess IR↓ over polluted urban areas, most state the difference to be less than 5% and there is some controversy over the reasons for this excess. There have been no further studies to substantiate the larger differences reported by Rouse *et al.* (1973).

The Stefan-Boltzmann relation (Equation 1.2) holds equally for outgoing infra-red radiation (IR↑), where ε_s - surface emissivity, and T_s - surface temperature are appropriately substituted. Clearly both ε_s and T_s are surface properties that can be considerably altered in a city environment. Surface temperatures in particular are altered by the relatively high thermal admittances and storage capacities of urban building materials (Oke and Maxwell, 1975). Generally, observations of surface infra-red emission (Bach and Patterson, 1969; Landsberg and Maisel, 1972) indicate greater urban losses than for surrounding areas. Indirect measurements using remote sensing of urban surface temperatures (Outcalt, 1972b; Lewis *et al.*, 1976; White *et al.*, 1978) support these observations, although Bornstein and Oke (1979) suggest care in the interpretation of such approaches.

The Heat Balance

Figure 1.1 schematically represents the heat balance of urban and rural areas. It is assumed that artificial heat production is absent over rural areas and that the upwind rural surface is homogeneous allowing upwind advective influences to be ignored.

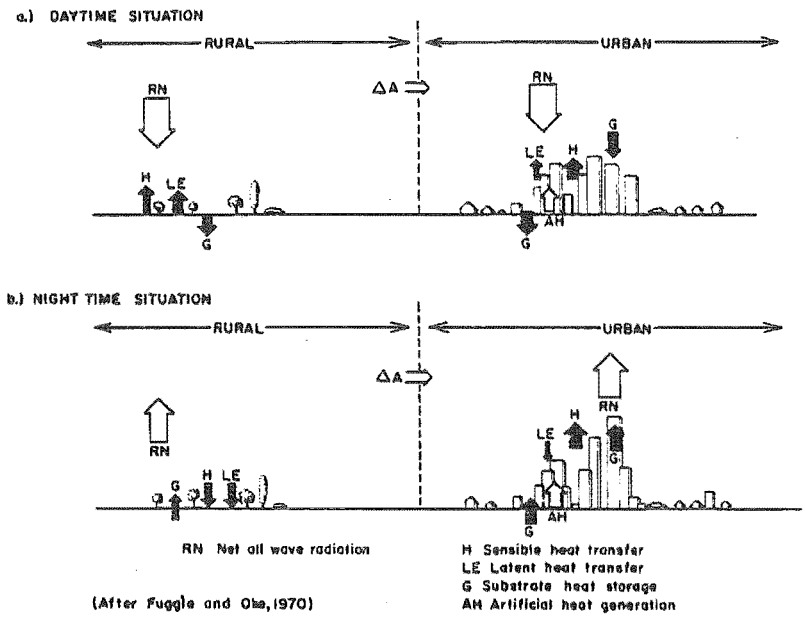

FIGURE 1.1 Diagrammatic Representation of Heat Balance of Urban and Rural Areas.

Until recently experimental quantification of heat balance components in urban areas had not been attempted, largely because of the problem of defining the 'representative' urban surface. Qualitative statements had been made suggesting that distinctions in urban and rural energy exchanges resulted from increased storage due to high heat capacities of building materials, reduced evaporative cooling and artificial heat production. It was hypothesised that by day (Figure 1.1a) a decreased evaporative cooling would be offset by enhanced sensible heat transfer and heat storage in urban materials. At night (Figure 1.1b) the flow of heat stored in building materials upwards into the atmosphere would dominate, partially balancing the nocturnal radiation loss and the reduced sensible heat transfer away from the surface.

Reviews of the role of artificial heating (AH) have been written and much of the data has been summarised (SMIC, 1971; Oke, 1974, 1979). Artificial heating varies seasonally and diurnally, having its greatest effect in winter and at night when domestic heating is at a maximum and receipt of solar radiation is absent.

Oke (1974, 1978, 1979) discussed the work of Oke *et al.* (1972), Yap (1973) and Yap and Oke (1974) which indicated that sensible heat flux away from the surface (H) and heat storage in the ground (G) was slightly higher by day in the city, with latent heat flux (LE) away from the surface reduced, although remaining an important energy sink. At night in the city the sensible heat term was often found to continue to be directed away from the surface while the heat stored during the day became an important energy loss.

The advection of energy (A) between urban and rural areas completely dominates other energy exchanges at windspeeds above 12 m sec^{-1} (Oke and Hannell, 1968) for large cities and at lower windspeeds for smaller urban centres. It is therefore only at low windspeeds that the energy balance processes operate to establish an urban temperature excess.

Because of the relative ease of defining a representative surface and the obvious agricultural and economic implications, the determination of the energy balance for rural areas has been well researched. One of the most detailed studies is for a rural grassed surface in Nebraska, (Lettau and Davidson, 1957). Energy balances of other rural land use types have been studied, including forests and crops where the works of Baumgartner (1956) and Wright and Lemon (1962) are representative. Energy balances for rural areas have also been undertaken for New Zealand (Fitzharris, 1974; Jamieson and Heine, 1976; and Jamieson, 1979).

By day (Figure 1.1a) the net radiant energy received by a vegetated surface is expended in the evaporation and transpiration of water, and turbulent transfer of heat to the atmosphere, and in the conduction of heat into the soil. Minor terms, usually able to be ignored include photosynthesis and the storage of heat energy within the biomass. At night (Figure 1.1b) the absolute losses through evaporation and turbulent transfer become less or are reversed, and the loss of energy by infra-red radiation is balanced by heat conduction from the soil.

MODELLING APPROACHES TO THE URBAN HEAT ISLAND

Given the apparent complexity of energy relationships responsible for the formation of heat islands, it is not surprising that there have been numerous attempts to simplify the phenomenon by reducing it to a model. There are four broad categories of heat island models that have been presented; statistical, mixing depth, energy balance and dynamic.

The most simplistic approach to urban heat island modelling has been statistical, where urban-rural temperature differentials are mathematically related to broad urban variables such as land use, meteorological parameters and city size. Sundborg (1951) related the strength of the urban heat island in Uppsala, Sweden, to variations in cloud, windspeed, water vapour pressure and temperature. Other statistical heat island models have been produced by Preston-Whyte (1970) and Clarke and Peterson (1973), while Oke (1973) related urban temperature excess to city size as inferred from population figures. A major problem with statistical models is that they do not in themselves answer questions concerning the causal mechanisms (Sundborg, 1951).

Mixing depth models derive from the theory that air flow over an urban area where there is an abrupt change in surface roughness, has induced in it an internal boundary layer that separates air influenced by the change in surface roughness from that unchanged (Tyson *et al.*, 1973). Summers (1965) introduced a thermodynamic model of the urban heat island on this basis showing urban temperature excess to be related to the difference between the dry adiabatic and the rural lapse rate and the depth of mixing. Leahy and Friend (1971)

modified and expanded on the original thermodynamic model.

The third area of urban heat island modelling is that of the energy balance model, first suggested by Myrup (1969, 1970) after the general models of Halstead *et al.* (1957) and Estoque (1963) where urban heat exchange is governed by the available net radiation and its subsequent partitioning into various other energy forms (Equation 1.1). His approach was to determine the heat balance in a one dimensional soil-air column for representative urban and rural characteristics. The energy balance is solved for a unique equilibrium temperature representative of that column alone. The original urban energy balance model has been enlarged and modified many times since, as in the work of Outcalt (1971, 1972a, 1972b), Miller *et al.* (1972) and Morgan *et al.* (1977). Major difficulties with this approach relate to problems in obtaining the extensive input data and in adequate validation. The major contribution of this model is in the detailed explanation and spatial resolution that is possible. Urban energy balance models are discussed in detail in Chapter 2.

Several models have been proposed to attempt to simulate the dynamic character of the urban heat island. Most of these involve the computer solution of a set of differential equations describing vorticity, continuity, thermodynamics and state. Representative is the work of Malkus and Stern (1953), Estoque (1961), Estoque and Bhumralker (1969) and Wagner and Yu (1972). While being more realistic than the steady-state models, the dynamic models still suffer from a lack of coupling between energy and momentum equations (Tyson *et al.*, 1973).

THESIS FRAMEWORK

Statement of the Problem

A poorly directed and fragmented body of literature on the urban heat island indicates the need for further work within the conceptual framework of energy balance theory. Because of the sheer magnitude of the task of a complete analysis of urban energy transfers, it is necessary to delimit this study to a detailed examination of atmospheric infra-red radiation (IR↓).

Urban IR↓ is probably that area of the urban energy balance requiring the most detailed and critical understanding. While increased urban IR↓ is often quoted as a major causative factor of urban heat islands, its precise relationship to the phenomenon must remain obscure until the mechanisms for urban IR↓ excess are clearly established.

Robinson (1977) remarked on the paucity of direct measurements of radiative transfer, particularly in relation to aerosol emission, and criticised the proliferation of mathematical models. He noted that the few measurements that have been made are notable for their limited sample size, contradictory conclusions and lack of the full information required, both at the surface and within the lower levels of the atmosphere. Dalrymple and Unsworth (1978, p. 996) suggest that the most likely explanations for excess IR↓ radiation over that expected will be revealed, "ultimately by experimental programmes combining measurements of longwave radiation at the ground with detailed studies of the composition and temperature of the lower atmosphere".

Aims and Approaches

Consideration of the problems outlined above suggest that a detailed and intensive study of variations in urban and rural $IR\downarrow$ under suitable conditions would be of use, especially if supplemented by detailed observations of the temperature and composition of the atmospheric boundary-layer.

Conceptually it would seem that consideration of the problem of $IR\downarrow$ over Christchurch within the framework of an energy balance model would be of value, both in identifying overall urban influences on local temperature patterns and in isolating shortcomings of standard prediction methods for various energy balance components, particularly that for $IR\downarrow$. Recently a direction to both qualitative and quantitative discussion has been given by the introduction of such models, but obstacles to their implementation arise from problems of few reliable measurements for input data and a notable absence of real world validation.

In more specific terms, the main objectives of this thesis are:-

i) to make a detailed survey of spatial and temporal variations of $IR\downarrow$ in Christchurch and to examine those attributes of the urban environment both at the surface and within the boundary-layer, potentially responsible for the variations.

ii) to determine the relative role of $IR\downarrow$ in contributing to the urban heat island.

Secondary objectives of this thesis include:-

i) the development of an energy balance model applicable to Christchurch to establish the relative effects of different energy

transfers on the urban heat island, and to establish a framework for the investigation of IR↓ for the remainder of the thesis.

ii) an examination of urban influences on the horizontal and vertical distribution of temperature, water vapour, windspeed and atmospheric pollution, and,

iii) the development of a computer method for the determination of IR↓ at the surface from atmospheric slab emissivities due to water vapour, carbon dioxide and ozone.

This study has several advantages over previous studies of urban influence on IR↓. Apart from the obvious advantage of considering all variables in the boundary-layer responsible for variations in IR↓, there are considerable advantages in using the city of Christchurch as a 'natural' laboratory for this study. The city is large enough to have a well defined urban effect and diverse enough to offer an almost complete range of land use types. In addition, local relief does not mask or distort urban influences, and it has a severe air pollution problem in winter.

Conceptual Framework and Thesis Format

The integration of procedures required to achieve the objectives outlined above is diagrammatically shown in Figure 1.2. The question of the interaction between IR↓ and the urban environment is initially approached by a review of the literature. This in turn suggests two avenues of investigation; the determination of the relative role of IR↓ in establishing an urban-rural temperature differential ($\Delta Tu-r$), and the evaluation of effects of the urban environment on IR↓. To test the role of relative energy transfers on $\Delta Tu-r$, an energy balance model for Christchurch is formulated and is validated

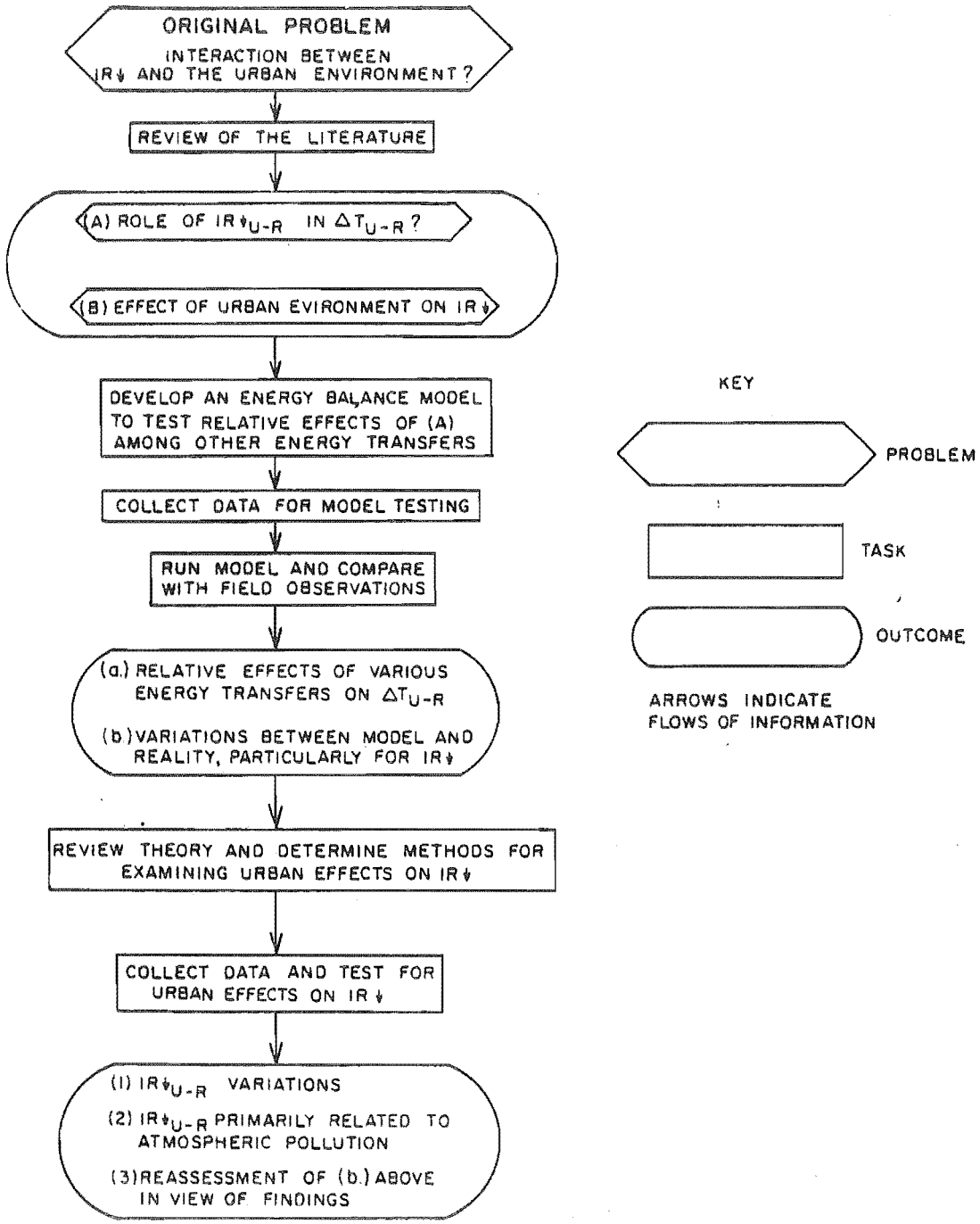

FIGURE 1.2 Conceptual Framework for Thesis.

against field observations. Shortcomings of the model suggest areas for more detailed examination of energy transfers, particularly in respect of IR↓. Further consideration of the theory of IR radiative transfer leads to the formulation of a field programme for a detailed examination of Christchurch's IR↓ regime incorporating observations in both the horizontal and the vertical. After collection of data and analysis, conclusions are drawn about reasons for the surface variation of IR↓, both in time and space, and a re-assessment of model prediction of IR↓ made accordingly.

The conceptual framework dictates the thesis format. Following this introductory chapter, Chapter 2 introduces the Christchurch energy balance model and attempts a validation. Chapter 3 outlines the materials and methods used in this study and the data collection program. Chapters 4, 5 and 6 examine the horizontal and vertical variation of parameters potentially responsible for variations in IR↓, while Chapters 7, 8 and 9 examine IR↓ variations and attempt an explanation in terms of atmospheric variables. Chapter 10 comprises a summary of conclusions and outlines areas for further research.

During preparation of this thesis some material has been published. A radiosonde system for use in the boundary-layer (Chapter 3) has been described in a paper appearing in New Zealand Journal of Science, while a paper on modelling the Christchurch urban heat island (Chapter 2) was presented in Journal of Applied Meteorology.

CHAPTER 2

A MODELLING APPROACH TO THE CHRISTCHURCH URBAN HEAT ISLAND

INTRODUCTION

The primary concern of this chapter is to present and validate an energy balance model for Christchurch under clear sky conditions and to establish a framework for more detailed studies of $IR\downarrow$ transfer over the city. Rather than a completely original model, the one described is a synthesis of aspects of previous models that appear most suited to the Christchurch environment. In contrast with most previous models the present one is extensively validated for actual conditions and includes carefully measured input data not possible in other studies.

Attempts at modelling urban heat islands have been reviewed by Tyson *et al.* (1973), Oke (1974, 1979) and Garstang *et al.* (1975). Those models relating to the spatial variation of energy balance over different types of urban surface have proved most successful in accounting for the surface form of the urban heat island. Energy balance models have been extended beyond the urban situation (Myrup, 1969; Terjung and Louie, 1973; Morgan *et al.*, 1977), to the simulation of needle ice occurrence (Outcalt, 1971), climatic change (Sellers, 1969), human thermal comfort (Morgan and Baskett, 1974) and the microclimatology of remote alpine areas (Marks and Dozier, 1979).

In New Zealand, Fitzharris (1974) has simulated the evaporation and water balance changes that may follow land use changes. Tapper (1976) used a simulation model developed by Outcalt (1971) to model the effects of air pollution and water vapour on atmospheric transmissivity over Christchurch, New Zealand. Hockey, Owens and Tapper (1980, 1981) have modelled the energy balance-thermal regime of the Hurunui River. Hitherto in New Zealand, no attempt has been made to model the urban heat island using the energy balance approach.

THE MODEL

General Description

Assuming a flat surface, uniform air mass and an even distribution of solar radiation over Christchurch and its immediately adjacent rural areas, the energy balance equation:-

$$Rn = H + LE + G - AH \quad \ldots 2.1$$

has been solved on a grid square basis to give the spatial characteristics of the Christchurch surface heat island (Equation 2.1 is a simplified and rearranged version of Equation 1.1). Advection of heat, moisture and momentum has been ignored.

The model is constituted by expressing infra-red outgoing radiation and sensible, latent and substrate heat fluxes as functions of surface temperature in Equation 2.1. Artificial heat generation has been taken as invariant with time and only broadly with space. The equation has only one solution which is determined iteratively using a secant algorithm (Acton, 1970), such that a subjectively

estimated initial temperature converges on the final equilibrium temperature of the surface. Care must be taken when reconciling surface equilibrium temperatures with observed temperatures as it is difficult to determine what actually constitutes the surface in an urban environment.

Net solar radiation is determined from:-

$$S = \frac{So}{r^2} (1 - \alpha) \cos Z \, Tr^m \qquad \ldots 2.2$$

where, So - solar constant (1353 Wm^{-2}), r - earth radius vector, Z - zenith angle (deg.), Tr - atmospheric transmissivity and, m - optical air mass. Values for transmissivity have been taken from Tapper's (1976) measurements for Christchurch. In their approach Dozier and Outcalt (1979) modelled diffuse radiation. Using a similar method, such modelling was done for Christchurch (Tapper, 1976), and was found to give an underestimation of actual conditions, so Tapper's empirical observations have been preferred.

Optical air mass is defined as:-

$$m = {}^{1}/\left[\cos Z + 0.15 (90 - Z + 3.855)^{-1.253}\right] \qquad \ldots 2.3$$

by Kasten (1966). No provision has been made for shading and view factor effects in urban canyons as has been suggested might be necessary by Terjung and Louie (1973) and Outcalt (1972b), who corrected for view factor and 'optical roughness'. Zenith angle is defined by:-

$$\cos Z = \sin\phi \sin\delta + \cos\phi \cos\delta \cos h \qquad \ldots 2.4$$

where, ϕ - latitude (deg.), δ - solar declination (deg.) and h - hour angle of the sun from noon.

Net infra-red radiation (I) has been determined by Brutsaert's (1975) method as used by Dozier and Outcalt (1979), and is given by:-

$$I = \varepsilon_a \sigma T_a^4 - \varepsilon_s \sigma T_o^4 \quad \ldots 2.5$$

and,

$$\varepsilon_a = 1.24 (e_s/T_a)^{1/7} \quad \ldots 2.6$$

where, ε_a - emissivity of air, T_a - air temperature (^oK), e_s - screen level vapour pressure (m b.), ε_s - emissivity of the surface and, T_o - surface equilibrium temperature (^oK). The Brutsaert approach has been used in preference to the more empirical Brunt (1932) method of determining infra-red radiation input favoured by Morgan *et al.* (1977). The Brunt method has proven unsatisfactory when tested on Christchurch data (Tapper, 1976). The diurnal variation of air temperature was simulated using maximum and minimum temperatures fitted to a sine wave with peaks at 1500 and 0300 h.

A Richardson number corrected bulk adiabatic transfer coefficient was used to determine sensible and latent heat fluxes in the manner advocated by Morgan *et al.* (1977). Turbulent transfer is estimated as the bulk adiabatic transfer (kg s^{-1} m^{-2}):-

$$K = k^2 \rho u_2 (1 - \gamma Ri)^P / (\ln z_2/z_o)^2 \quad \ldots 2.7$$

where, k - Von Karman's constant, ρ - air density (Kg m^{-3}), u_2 - reference level wind speed (m $s.^{-1}$), γ and P - Richardson number correction factors (described below), Ri - Richardson number, z_2 - reference height (m) and z_o - surface roughness (m). In Equation 2.7 it is assumed that the coefficient of eddy diffusivity of heat, momentum and vapour are equivalent (Kh = Km = Ke), that a logarithmic

profile describes the variation of windspeed with height and that neutral conditions obtain. In contrast with the Morgan *et al.* model, in this study the Richardson number correction factors have been clearly differentiated for stable and unstable conditions. Departures from neutral conditions are handled by the correction factor $(1 - \gamma Ri)^P$ where $\gamma = 16$ and $P = \frac{3}{4}$ for $Ri < 0$ and $\gamma = 5$ and $P = 2$ for $Ri > 0$ (Thom, 1975).

The Richardson number is estimated from:-

$$Ri = \frac{g(T_2 - T_o)\ (z_2 - z_o)}{u_2^2} \qquad \ldots 2.8$$

where, g - acceleration due to gravity (m $s.^{-2}$) and T_2 - reference level temperature (^oK).

In their model, Dozier and Outcalt (1979) determine the reference level z_2 by equating the bulk adiabatic diffusivity with the daily temperature disturbance penetration depth diffusivity following the method of Terzaghi (1952). In this study the level above which no urban-induced effect could be discerned was observed from tethered and pilot balloon observations.

Roughness lengths have been estimated using the method of Lettau (1969) in which:-

$$z_o = \frac{\bar{h}}{2} \frac{s}{A} \qquad \ldots 2.9$$

where, $\bar{h}$ - average height of roughness elements (m), s - silhouette area of roughness elements (m^2) and A - lot area (m^2).

Using the bulk adiabatic transfer, sensible heat flux is given by:-

$$H = Kc_p (T_2 - T_o) \quad \ldots 2.10$$

and the latent heat flux by:-

$$LE = KL (q_o - q_2) \quad \ldots 2.11$$

where, q_o - specific humidity at the surface (g g^{-1}) and q_2 - specific humidity at the reference level (g g^{-1}).

Actual surface humidity is estimated from the saturated specific humidity and relative humidity. The moisture of the air mass is taken as constant over the entire area and relative humidity is interpreted as the fraction of the total area occupied by freely evapotranspiring surfaces. Thus:-

$$q_o = R\left[3.74 + 2.64 (T_o/10)^2\right] 10^{-3} \quad \ldots 2.12$$

where, R - evaporating fraction (%).

Substrate heat flux is determined from:-

$$G = k_s (T_o - T_z)/z \quad \ldots 2.13$$

where, k_s - thermal conductivity of the substrate ($Wm^{-1}\ ^oC^{-1}$), T_z - substrate temperature (^oK) at depth in substrate z.

The temperature of the substrate is determined from the Fourier heat conduction equation in one dimension (Munn, 1966) in which:-

$$\frac{\partial T_z}{\partial t} = \frac{k_s}{\rho_s c_s} \frac{\partial^2 T_z}{\partial z^2} \quad \ldots 2.14$$

where, t - time (s), ρ_s - substrate density (kg m^{-3}) and c_s - specific heat of the substrate (J $Kg^{-1}\ ^oC^{-1}$).

The method used is that outlined by Dozier and Outcalt (1979), is fully implicit and is characterised by unconditional stability. The implicit scheme is given by:-

$$(1+2Fj^{t})(Tj^{t+1}) = Tj^{t}+Fj^{t}\ (Tj+1^{t+1}+Tj-1^{t+1}) \qquad \ldots\ 2.15$$

where the Fourier modulus (F) is given by $\frac{ks}{\rho_s c_s}\ \frac{\Delta t}{(\Delta z)^2}$, j indicates a node and t a time step. This leads to a tridiagonal system of simultaneous linear equations when applied to all nodes at one time with the top node given by the equilibrium surface temperature and the bottom node at 1 metre held constant.

$$\begin{bmatrix} 1+2F_1{}^t & -F_1{}^t & 0 & 0 & 0 \\ -F_2{}^t & 1+2F_2{}^t & -F_2{}^t & 0 & 0 \\ 0 & -F_3{}^t & 1+2F_3{}^t & -F_3{}^t & 0 \\ 0 & 0 & - & - & - \\ 0 & 0 & 0 & - & - \end{bmatrix} \begin{bmatrix} T_1{}^{t+1} \\ T_2{}^{t+1} \\ T_3{}^{t+1} \\ - \\ - \end{bmatrix} = \begin{bmatrix} T_1{}^t \\ T_2{}^t \\ T_3{}^t \\ - \\ - \end{bmatrix} \qquad \ldots\ 2.16$$

The model is cycled through two 24 h periods using a time step of 15 minutes.

The Christchurch model, unlike that of Morgan *et al.* (1977), allows for artificial heat production, albeit in a simplistic fashion with its magnitude being held diurnally constant and related to the evaporating fraction (R) as a surrogate for the amount of urbanisation.

A full and working listing of the Christchurch energy balance model appears in Appendix I.

Sensitivity Analysis

Using average winter input data for cloud-free 1979 July conditions, the model was run successively changing only one parameter at a time to enable its sensitivity to that parameter to be assessed. The non-varying input data are shown in Table 2.1 with the results of this analysis shown in Figure 2.1. The upper boundary conditions of temperature, windspeed (particularly below 5.0 m s^{-1}) and specific humidity are seen to be quite important in determining the maximum and minimum daily surface equilibrium temperature. Sensitive surface boundary parameters of note are evaporative fraction and surface roughness (particularly between a few centimeters and one meter). The surface boundary parameters of vapour pressure, albedo, soil heat capacity (not shown) and soil conductivity are relatively insensitive, particularly in the case of minimum temperatures.

APPLICATION AND VALIDATION OF THE MODEL

General

In this analysis the model is applied in three distinct ways. Initially the model is run for average clear sky July 1979 conditions and predicted temperatures compared with generally available data. Secondly, the model is applied for one day, July 10, 1979 for which detailed spatial patterns of measured temperature are available for the whole Christchurch urban-rural area. Finally, the model is applied to an urban and rural site for which detailed energy balance as well as diurnal temperature data are available for July, 10, 1979.

TABLE 2.1 Boundary conditions for clear winter (July) conditions and 10 July 1979.

UPPER BOUNDARY (300m)		WINTER CONDITIONS	10 JULY 1979
T_2 (^{o} C)		5.0	10.4
U_2 (m s^{-1})		3.0	5.0
q_2 (g g^{-1})		0.003	0.005
NEAR-SURFACE CONDITIONS			
e (mb)		5.5	7.8
INITIALISING TEMPERATURES			
maximum (^{o} C)		11.0	15.0
minimum (^{o} C)		1.0	3.0
SOLAR FACTORS			
latitude (degrees)		-43.3	-43.3
declination (degrees)		21.6	22.3
INITIAL SUBSTRATE TEMPERATURES (^{o} C)			
at depth (cm)	0	2.0	2.0
	20	3.5	3.5
	40	4.5	4.5
	60	5.5	5.5
	80	6.5	6.5
	100	7.0	7.0

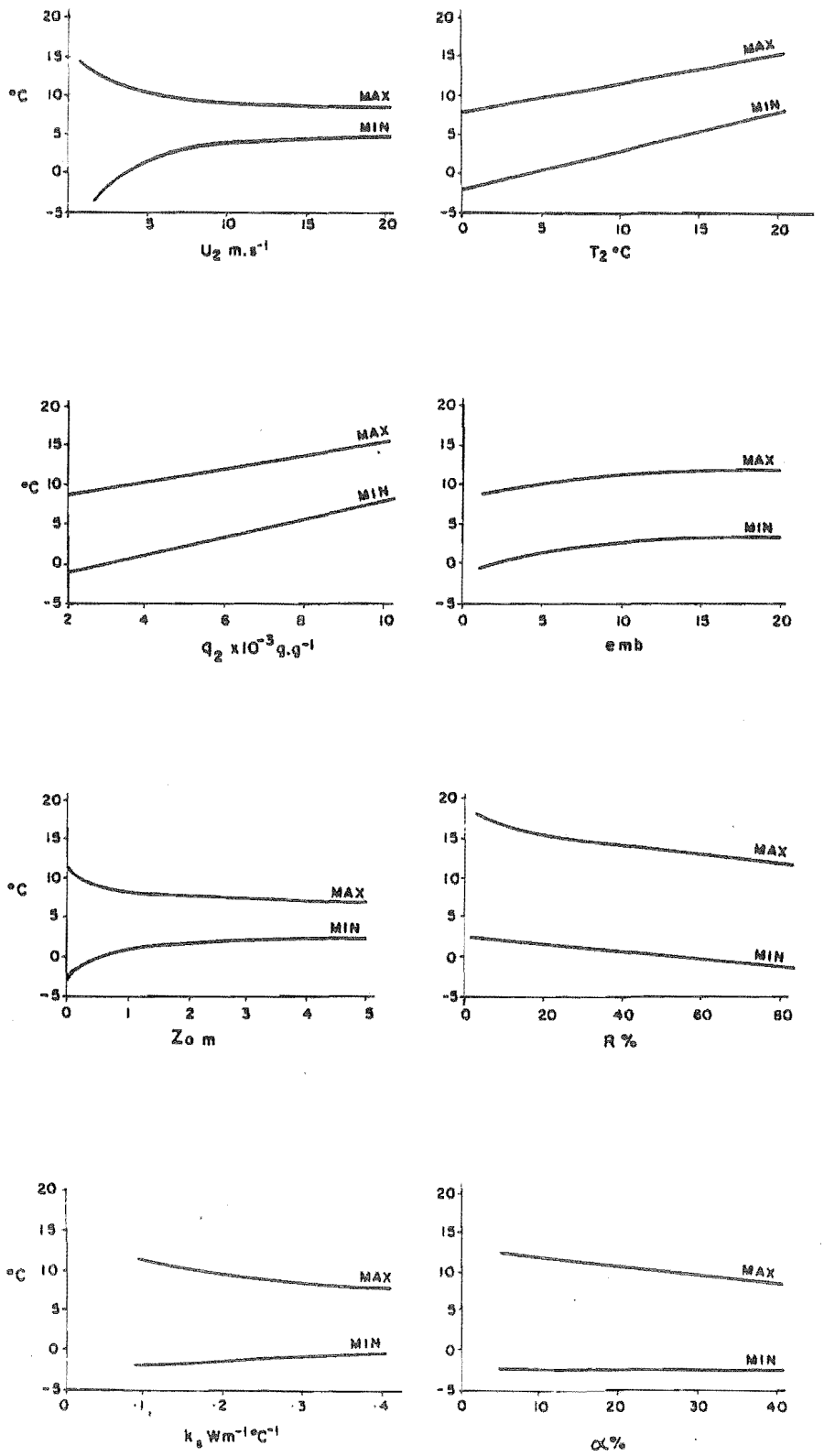

FIGURE 2.1 Sensitivity Analysis for Mid-July Conditions Obtained over Christchurch Showing Daily Maximum and Minimum Temperatures with a Varying Model Input Parameter.

Physical Setting and Data Sources

Situated on the eastern margin of the Canterbury Plains, the 140 km^2 city of Christchurch is an ideal site for the testing of an energy balance model owing to its flatness and relatively uncomplicated landuse (Figure 2.2).

Land use for each of 250 1 km^2 grid squares were determined by Hastie (1979) from aerial photographs and have been used here. Twelve categories were recognized and each assigned characteristic values of surface roughness, heat capacity ($\rho_s c_s$), albedo, thermal conductivity of the substrate and evaporating fraction (Table 2.2). For each grid square the percentage area occupied by a specific land use type was estimated. Input values for each category were then weighted by area of occurrence to determine a mean value for each parameter per square. Tapper's (1976) diagram of mean wintertime atmospheric transmissivities for Christchurch (Figure 2.3) was used for assigning to each grid square a specific transmissivity to account for attenuation of solar radiation by air pollution. Initial substrate soil temperatures were held constant for the whole 250 km^2 area (Table 2.1) and the value of thermal conductivity and heat capacity were assumed constant with depth.

The 'representative' rural and urban sites selected were, respectively, an open field of low cut (< 5 cm) grass situated in the area west of Halswell (Figure 2.2) and the flat, tarsealed roof of a single storied building located 1 km north of the C.B.D. These sites are described in detail in Chapter 3. Surface and atmospheric characteristics for these sites were estimated, or where appropriate, measured (albedo, surface roughness and evaporating fraction).

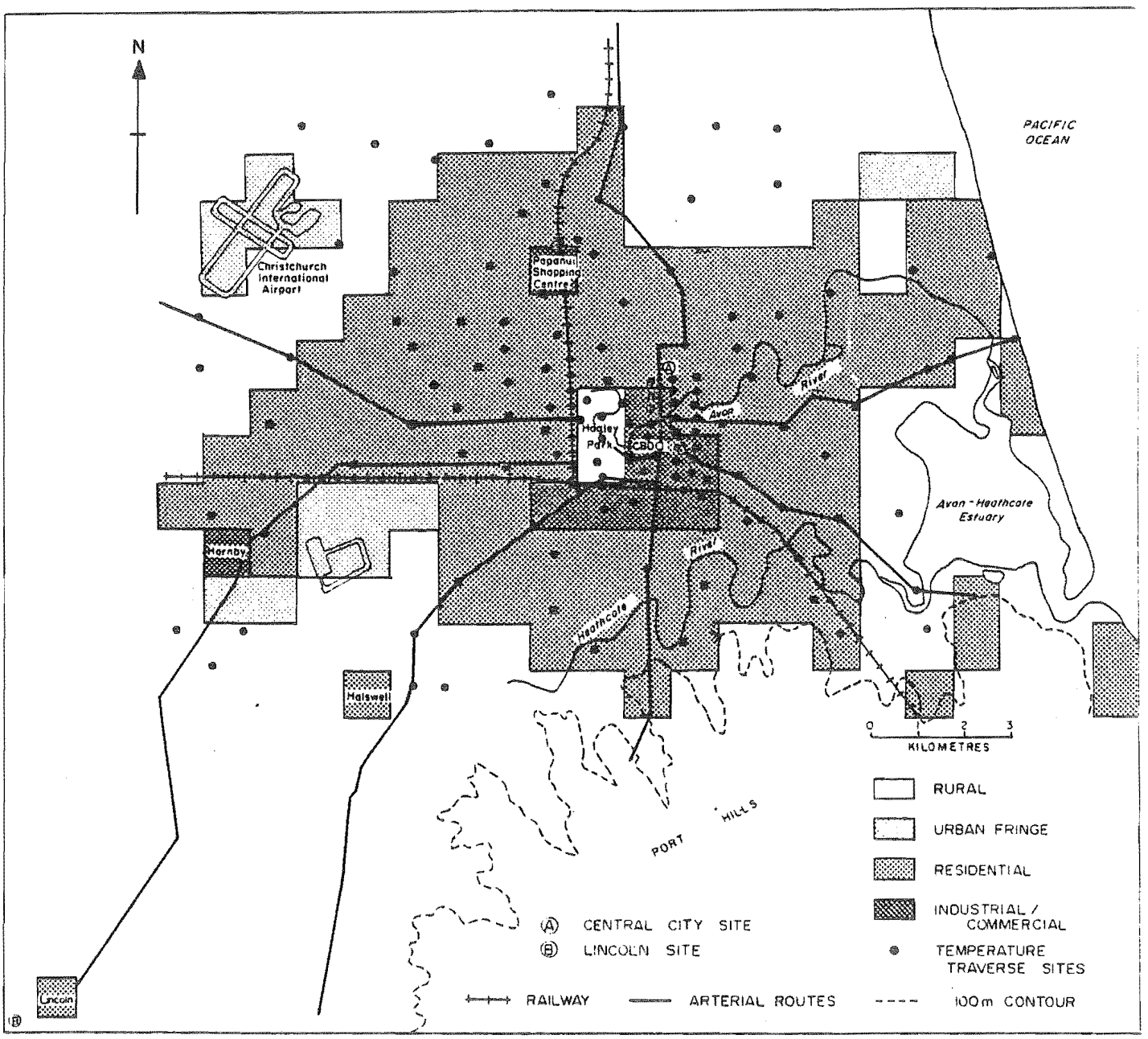

FIGURE 2.2 Simplified Landuse Map of Christchurch Showing the Points at which Temperatures were Measured on 10 July, 1979 and Location of Urban and Rural Representative Sites.

TABLE 2.2 Surface boundary conditions and land use categories

LAND USE	z_o (m)	$\rho_s C_s$ ($Jm^{-3}{}^oC^{-1} \times 10^6$)	α	k_s ($Wm^{-1}{}^oC^{-1}$)	R %
Residential	.41	1.80	.23	.096	60
Green areas					
trees	1.08	1.26	.10	.126	100
grass	.01	2.43	.20	.126	100
Central business district[1]	5.0	1.76	.30	.100	0
Industrial/shopping centres/schools[1]	3.0	1.88	.25	.096	0
Tar surfaces	.04	2.09	.11	.126	0
Bare ground[2]	.0058	2.18	.40	.126	100
Water	.0010	4.19	.08	.058	100

1. In these categories z_o refers only to buildings within the land use category and not to the category as a whole.

2. For much of winter, and certainly on 10 July 1979, bare ground was wet and assigned a wet fraction of 100.

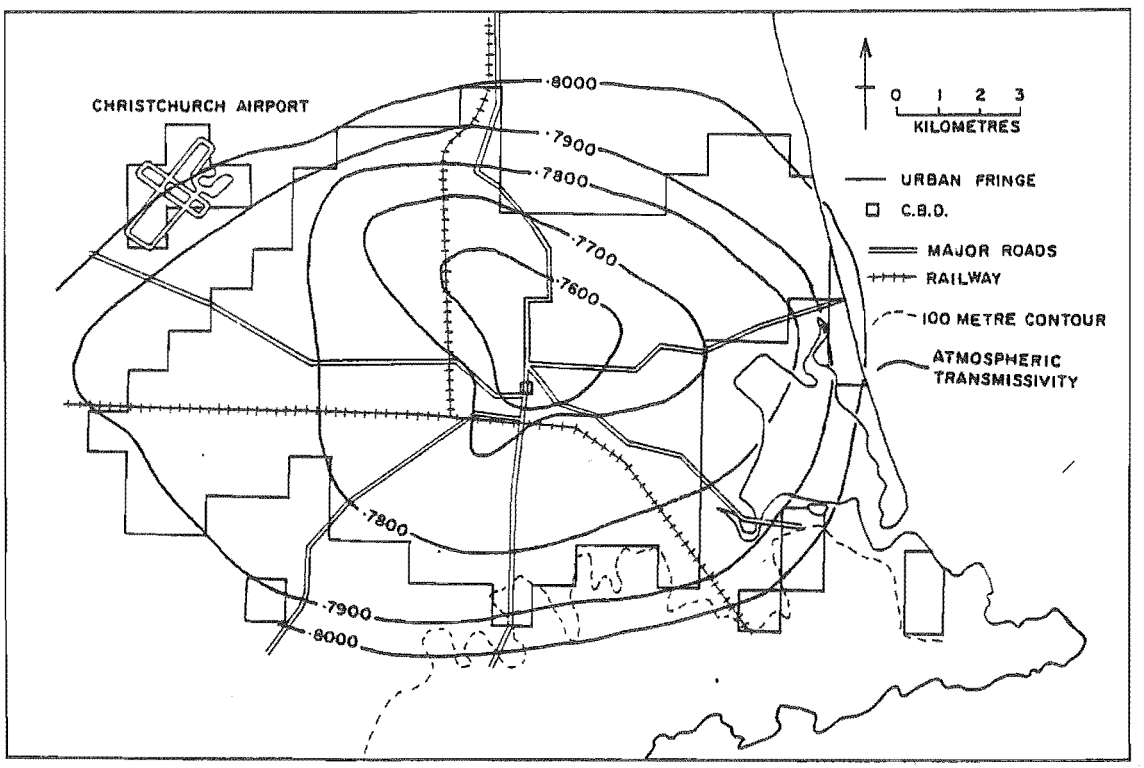

FIGURE 2.3 Average Winter Time Atmospheric Transmissivities for Incoming Solar Radiation over Christchurch.

Artificial heat generation has been estimated, using the method of Garnett and Bach (1965), from the daily consumption of fossil fuels and electricity for the city as a whole in the absence of data with a better temporal and spatial resolution. It would appear that 3.9 Wm^{-2} (approximately 3% of net shortwave radiation) are consumed in winter. Artificial heat production of this order is low by world standards (Garnett and Bach, 1965; Bach and Patterson, 1969; Kalma, 1974) and appears to be because of Christchurch's relatively low building and population densities in comparison with most other metropolitan centres. Artificial heat generation for the urban representative site has also been estimated according to heating, lighting and the metabolic rate of people using the building. The contribution of solar radiation through windows to the internal energy yield of the building has also been included. Loss of energy through the roof of the urban site has been estimated at a relatively constant 22.0 Wm^{-2}.

Urban boundary-layer lapse rates and wind profiles were measured using modified radiosonde equipment flown on a tethered balloon (Tapper and Sturman, 1980), and using pilot balloons. From the lapse rates and wind profiles upper boundary conditions were determined for the reference height above which no urban-induced effects could be discerned (Table 2.1). The reference level for July conditions in 1979 was 300 m.

In order to attempt a validation of the model, urban temperatures were collected in the early afternoon and evening of July 10, 1979 at 120 sites (Figure 2.2) on approximately one hour automobile traverses of the Christchurch area. All temperatures were taken with whirling psychrometers at screen level and standardised to 1400 and 2230 values. During the traverses urban and rural tethered

balloon data were collected and the release of pilot balloons permitted the vertical structure of the wind field to be determined.

At the 'representative' urban and rural sites, a hygrothermograph was installed one metre above the active surface to continuously monitor the diurnal temperature trends. At both sites energy balance instrumentation was operated continuously to monitor net radiation, incoming and outgoing infra-red radiation, direct and diffuse shortwave radiation and substrate heat flux. This instrumentation is described in detail in Chapter 3.

Comparison of Observed and Simulated Temperatures

General Urban Effects

Meteorological records for all 1979 July days give a mean minimum surface temperature of - 1.4° C for a near rural locality (Christchurch International Airport). The model prediction for clear conditions for the same site was - 2.9° C. The observed grass minimum for clear days was - 4.1° C. The observed screen maximum for clear days was 11.3° C; the model equilibrium surface temperature was 10.4° C (no midday grass temperatures are available for comparison).

Comparing the rural-residential and rural-C.B.D. temperature trends, the model predicts average urban heat islands for Christchurch of about 5.0° C and 8.0° C respectively. These values of the nocturnal heat island are of the same order as those observed by Kingham (1969) for August (6.7° C), Sham (1968) for clear winter nightime conditions (6.3° C) and Tapper (1976) for the average maximum winter heat island (5.4° C).

Spatial Temperature Patterns

Conditions for July 10, 1979, the day chosen for a specific test of the energy balance model, were typical of a clear Christchurch winter day. The evening of 9 July was characterised by light north westerly winds and cloud of $^{7}/_{8}$. Dewfall was heavy overnight. By 1045 h the sky had cleared and a sea breeze had developed on the coast and by 1120 h had extended inland to cover the whole city. The sea breeze prevailed until midnight, reaching a maximum depth of 350 m at 1700 h. Winds at Lincoln, near to the rural site, were variable during the day, except for a period of north-westerlies in the later afternoon.

Exact comparison of point-to-point temperatures is not possible since the observed temperature field is derived from a coarser network of stations than the 1 km spacing of the simulated temperatures. It must also be remembered that the model gives equilibrium surface temperature, whereas observed data are for approximately screen height. Nonetheless, comparison of the observed 1400 h temperature field with that predicted by the model is reasonable (Figure 2.4). Both fields are characterised by their flatness. In general the model underestimated the 1400 h temperatures over rural areas by about 3^{o} C and overestimated them in the city centre by about 1^{o} C. Near to the coast the cooling effect of the sea breeze is discernible in the observed temperature field, while the temperature field predicted by the model shows no advective effect. Temperatures over Hagley Park are slightly lower than elsewhere, evidencing the importance of the Park as a heat sink in the simulated temperature field. This cooler area is also discernible in the observed pattern. In the C.B.D. and industrial areas of the city the overestimated model

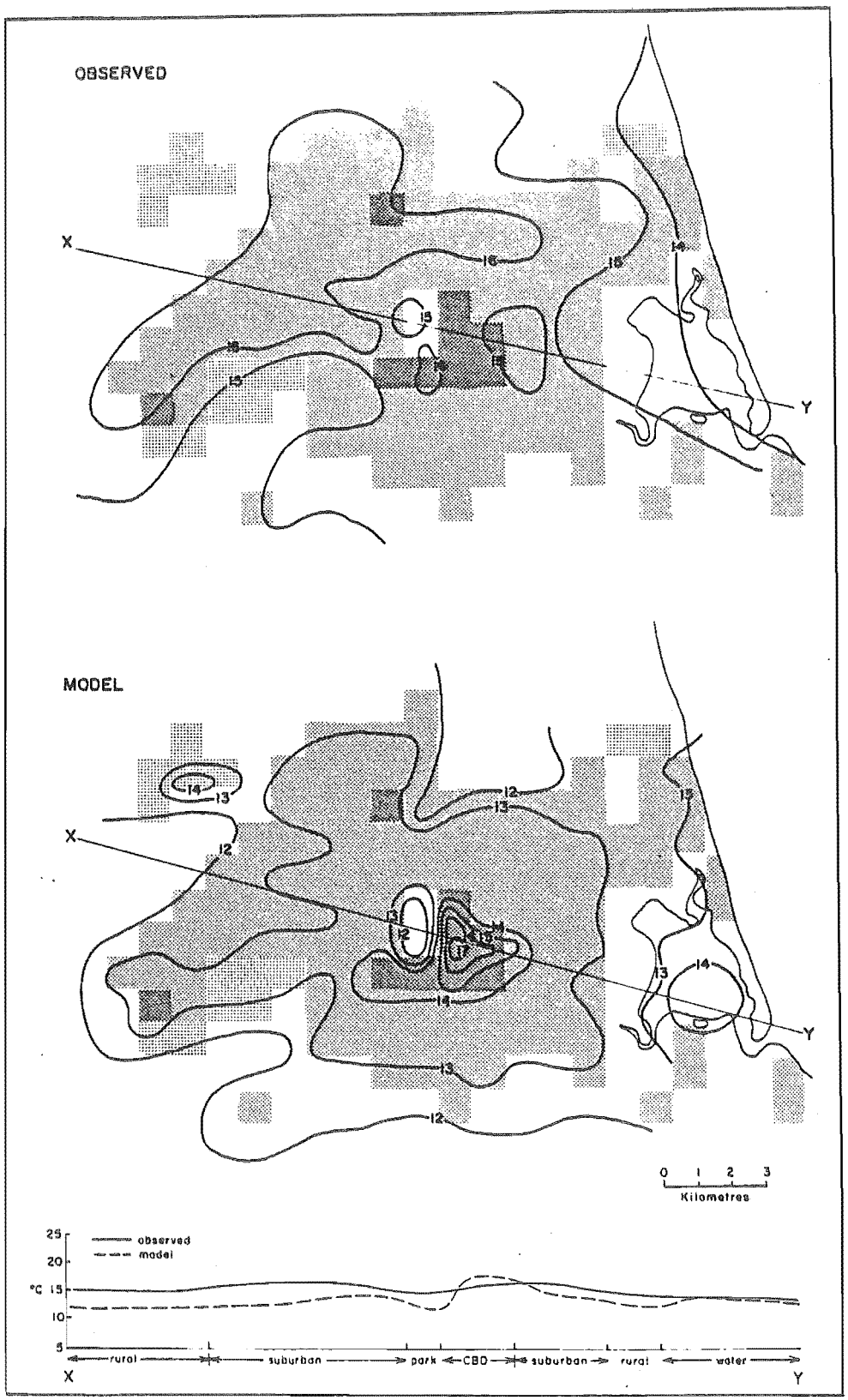

FIGURE 2.4 Observed and Simulated (Model) Temperatures, ^{o}C, at 1400 h on 10 July, 1979.

temperatures show the spurious occurrence of a heat island. This is largely due to the inability of the model to specify the appropriate wet fraction for dew-covered artificial surfaces (dew-moistened roads, where shaded, were observed to dry out only around midday). If, instead of specifying the wet fraction of the central areas as 12 to 25%, an arbitrary 10 to 15% had been added to account for dew-wetting of the surfaces, then the spurious C.B.D. heat island would not have been produced.

At night (2230 h) the agreement between observed and predicted temperatures is good, with the model being able to replicate all of the essential features of the surface temperature field over Christchurch (Figure 2.5). The Hagley Park heat sink and the central area enhancement of the heat island are apparent in the simulated temperature field, with the latter being overestimated by about 1^{o} C for the industrial area to the south of the C.B.D. and by about 4^{o} C within the one grid square constituting the core of the C.B.D. (an area where surface characteristics are especially hard to define). Along the periphery of the greater heat island, observed and simulated temperature gradients are virtually identical. Figure 2.6 shows that the surface heat island observed and modelled is continued into the boundary-layer. The Christchurch energy balance model, operating in two dimensions is unable to replicate the three dimensional heat island. Observations in the boundary-layer indicate urban warmth being advected by the sea breeze over rural areas to the south-west of the city.

Diurnal Temperature Variations

Observed and simulated daily temperature trends for July 10, 1979 have been plotted for the representative urban and rural site (Figure 2.7). Only times from 1000 h onward are shown, as it is only

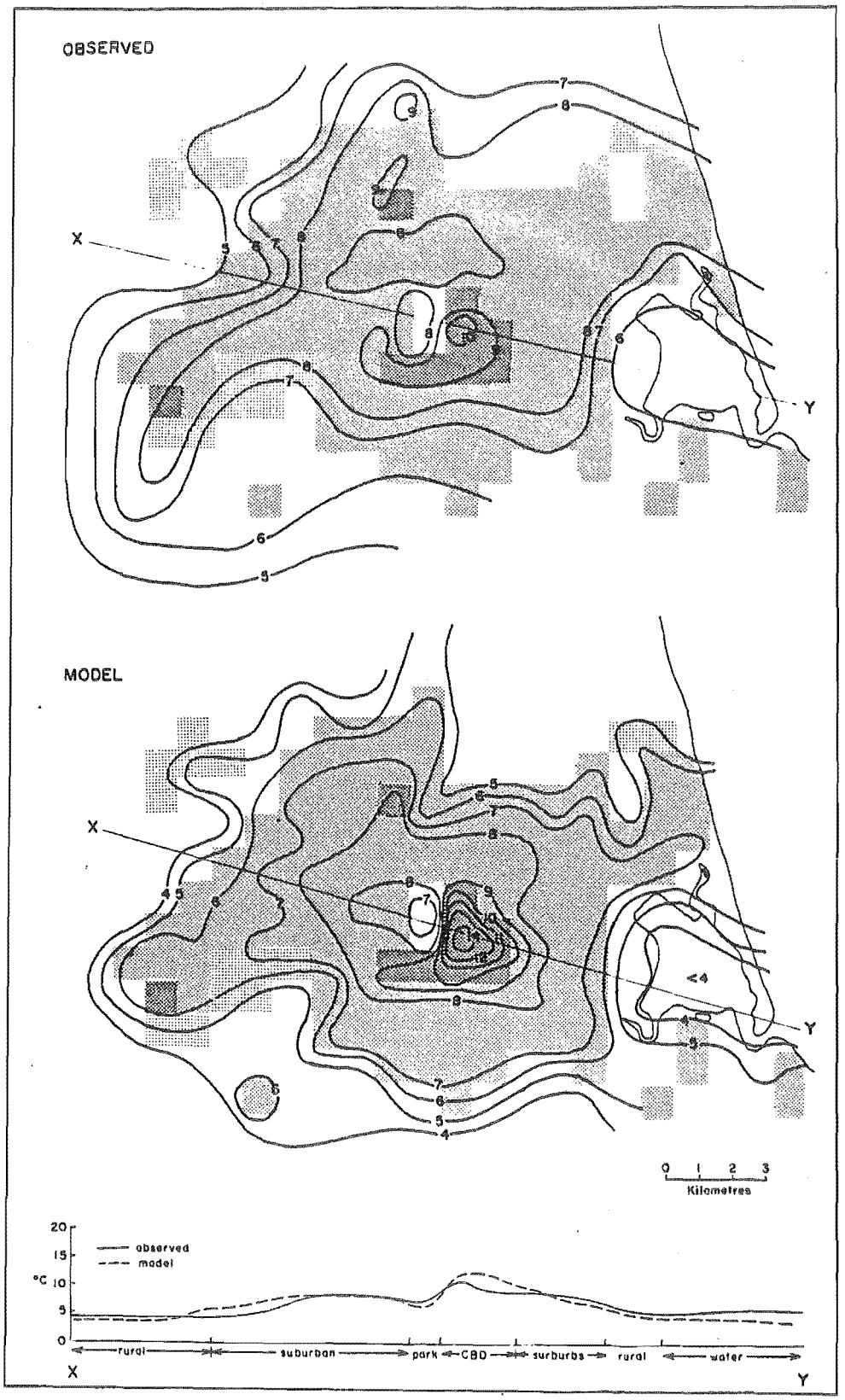

FIGURE 2.5 Observed and Simulated (Model) Temperatures, ^{o}C, at 2230 h on 10 July, 1979.

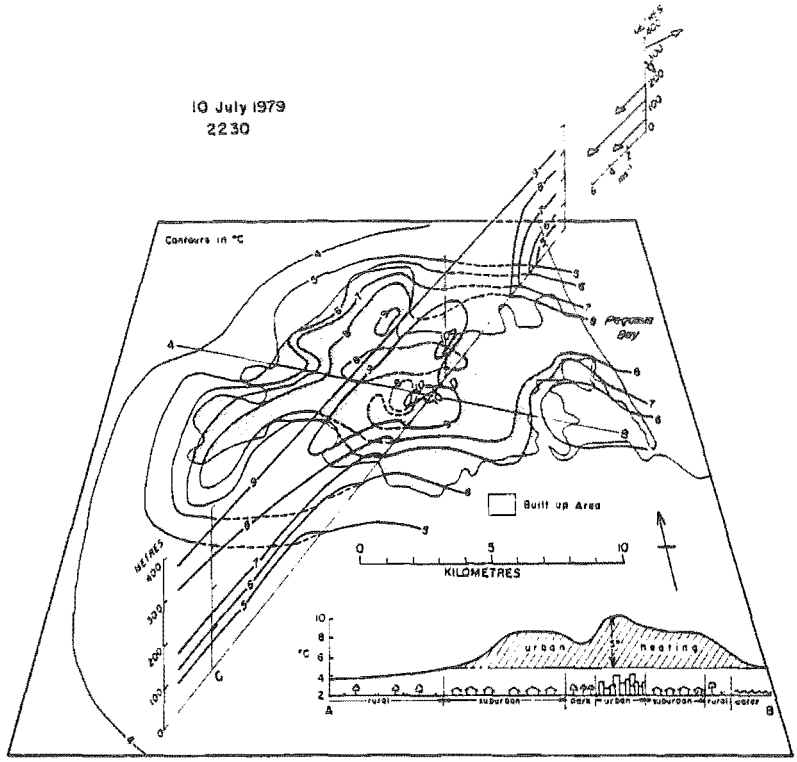

FIGURE 2.6 Observed Windspeed and Direction Aloft and Vertical and Horizontal Temperature Gradients, °C, at 2230 h on 10 July, 1979.

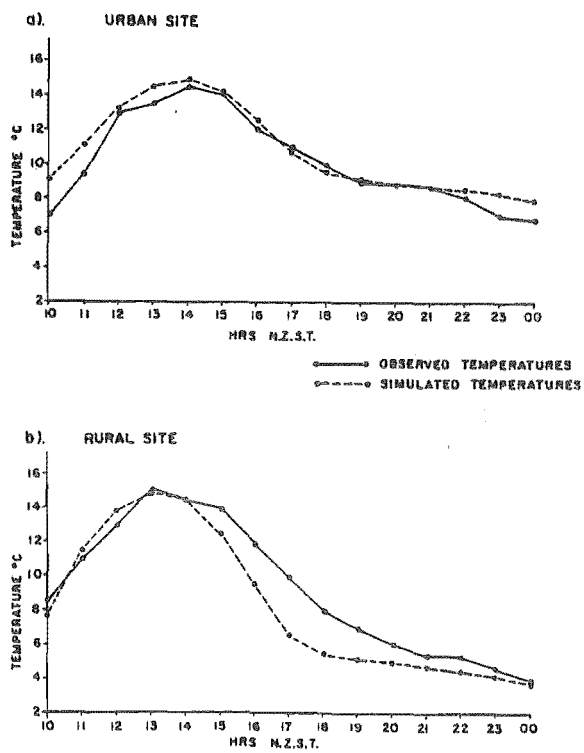

FIGURE 2.7 Observed and Simulated (Model) Temperatures at Representative Sites on 10 July, 1979.

from this time that the 'clear sky' criterion for the model can be applied. Urban observed and simulated temperatures are in close agreement, particularly from about 1200 h. A discrepancy of up to 2^{o} C earlier may be related to the previously discussed problem of dewfall evaporation from 'dry' urban surfaces. Temperature trends for the rural site are also in good agreement, except for the late afternoon-early evening period when observed temperatures are as much as 3.5^{o} C warmer than simulated temperatures. Reasons for this discrepancy are likely related to the advective effects of the warm north-westerly wind prevailing at the rural site at this time, which are not replicated by the model.

Given the reasonable ability of the model to simulate the spatial and temporal variation of the surface temperature field over Christchurch, an attempt has been made to estimate the likely partitioning of available net radiation and the spatial variation of energy fluxes over the city under typical clear winter conditions. A validation of the model's partitioning of energy at the urban and rural representative point sites is also made by comparison with detailed field observation.

Energy Balance Fields Over Christchurch

Spatial Patterns of Simulated Energy Balance Components

If the diurnal variation of the energy fluxes specified in Equation 2.1 are compared for a typical 1 km^2 rural and urban (not C.B.D.) grid square (Figure 2.8), then it is quite apparent that considerable differences exist in the partitioning of the net available radiant energy at midday. In the rural case the model suggests that in clear mid-winter conditions 40% of net radiation is used in

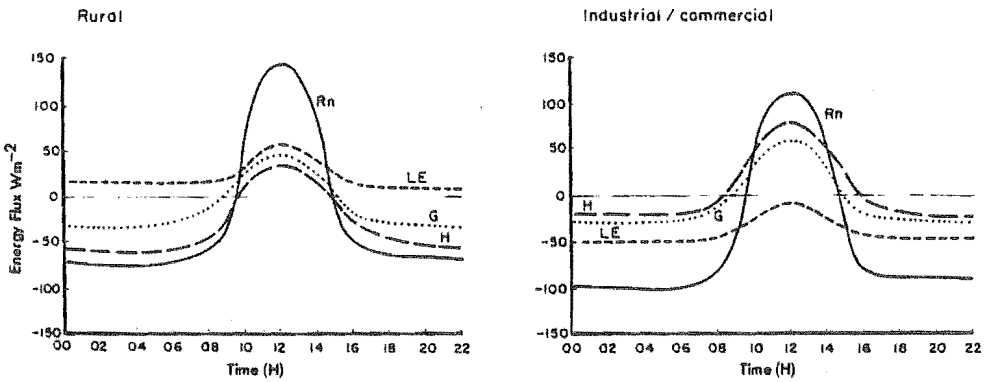

FIGURE 2.8 Average Winter Diurnal Variation of Energy Balance Components over Christchurch Rural and Urban (excluding C.B.D.) Sites under Clear Conditions.

evaporation, 26% in sensible heating and 33% in storage. By contrast in the industrial/commercial part of the city (with a low wet fraction) no energy is used in evaporation, 64% is converted to sensible heat and 46% goes into storage.

The spatial patterns of energy balance components at the times of maximum and minimum temperatures (Figures 2.9 and 2.10) clearly indicate an urban effect. Variations in energy fluxes occur over different land uses and in most cases the outer limit of the built-up area corresponds to discontinuities in the energy balance fields. Strongest gradients in the fields are always to be observed between the C.B.D. and the contiguous Hagley Park to the west. Shopping centres (e.g. at Papanui), dormitory residential areas (e.g. Halswell), discrete industrial areas (e.g. Hornby) and Christchurch International Airport usually feature as islands of enhanced or reduced energy fluxes depending on the time of day. The estuary of the Avon and Heathcote rivers is likewise an area exhibiting a distinctive set of energy fluxes. Areas receiving the lowest net radiation (C.B.D. and industrial/commercial zones) are generally warmest with sensible heating occurring at all times, not so much as a result of lower albedos, but mainly due to lack of evaporation.

The actual partitioning of net radiation varies with every grid square used in the simulation. As far as it is possible to generalise, at midday up to 36% of available net radiation goes into sensible heat over the urban area, excluding the C.B.D. where the figure is much higher. Up to 28% is used in evaporation and up to 48% goes into substrate heat storage. At 1200 h the sensible heat flux is everywhere positive with a maximum in central areas. The latent heat flux is likewise positive but decreasing towards the city centre where

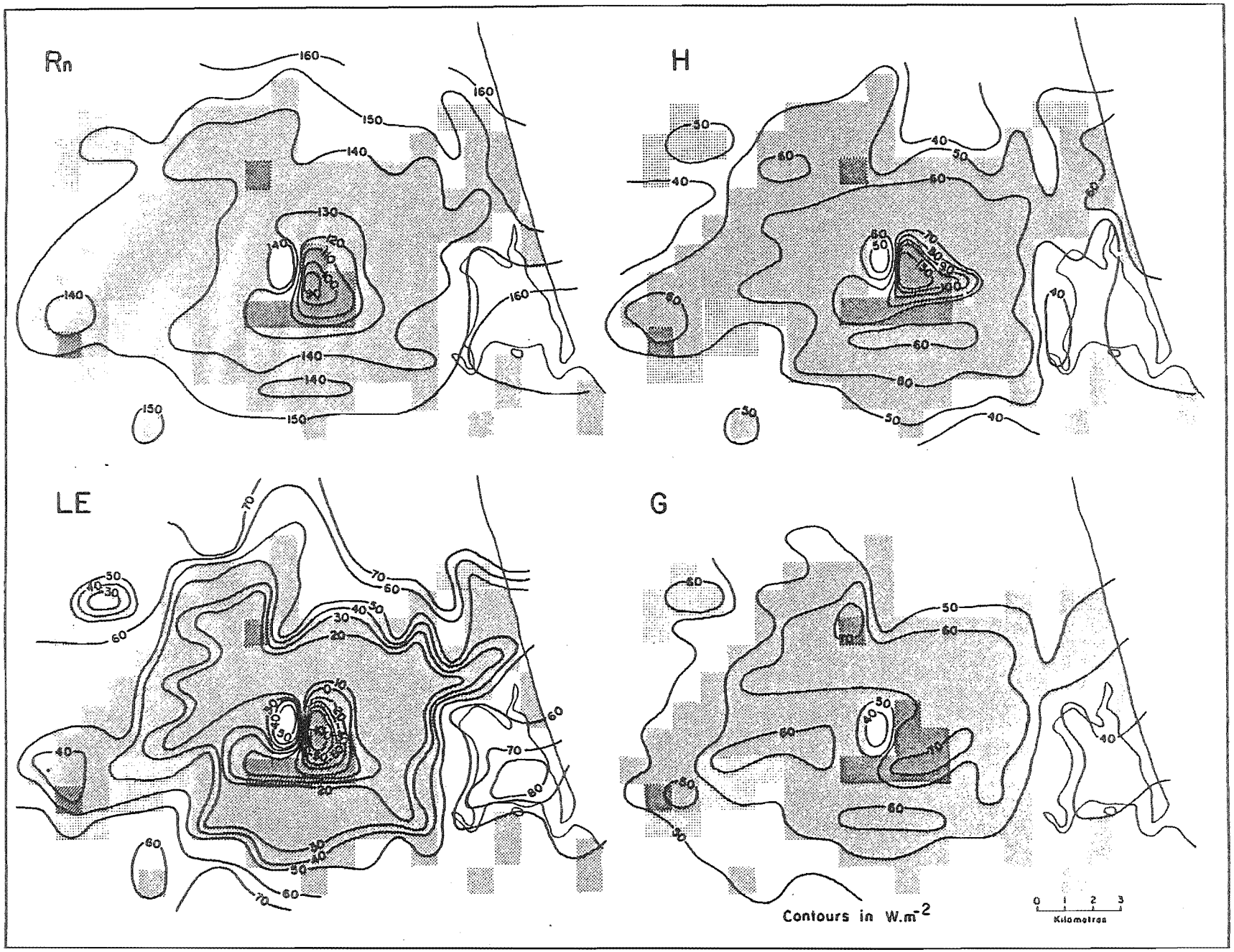

FIGURE 2.9 Simulated Energy Balance Fields over Christchurch at 1200 h on Average Clear Winter Days.

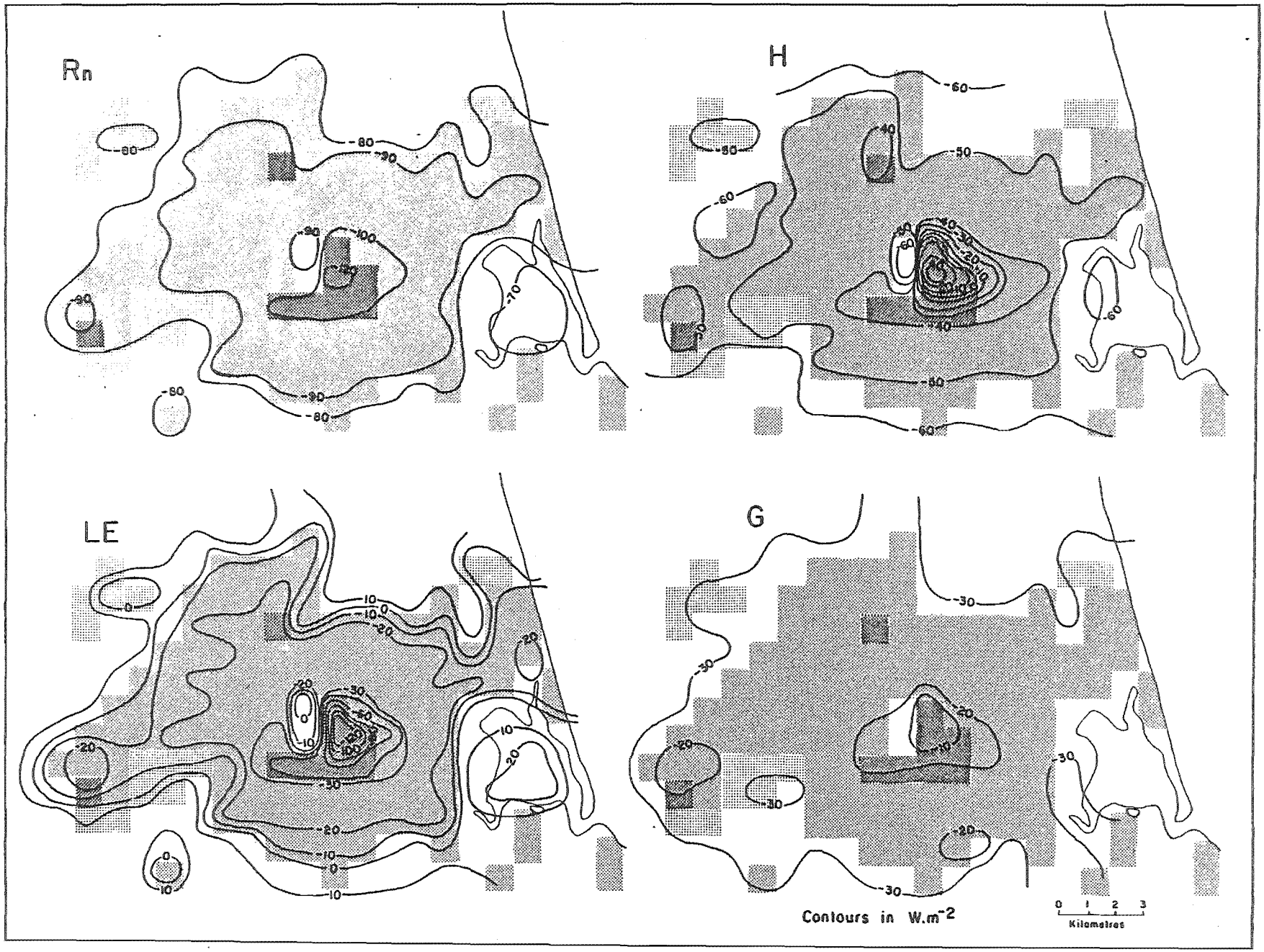

FIGURE 2.10 Simulated Energy Balance Fields over Christchurch at 0400 h on Average Clear Winter Nights.

a reversed flux implies heating by condensation. Only reflecting the urban influence in part, the midday heat storage field is quite complicated as heat is everywhere transferred from the surface into the substrate.

At 0400 h the maximum net radiation loss of energy occurs over the industrial/commercial and C.B.D. areas (Figure 2.10). Sensible heat flux is everywhere negative, except within the C.B.D., with the amount of cooling diminishing radially inwards. Within the C.B.D. the model suggests that equilibrium surface temperatures remain high enough to allow heat to be transported upwards. Elsewhere heat transport is towards the ground in the stable inversion conditions. Over the rural surroundings of Christchurch evaporation usually continues through the night. By 0400 h in the urban area dew fall is producing heat everywhere, with the latent heat flux increasing inwards towards the C.B.D. except over Hagley Park. The field of heat storage is negative, flat and rather featureless as everywhere heat is transferred from the substrate towards the surface.

Comparison of Observed and Simulated Energy Balance Components

Observed and simulated energy balance data for the representative urban and rural sites are presented in Figure 2.11a and 2.11b. As before, only data from late morning onwards are shown.

Both sites exhibit similar partitioning characteristics to those described in the previous section for typical urban and rural areas, although the selection of 'pure' surfaces has exaggerated the distinctions. Of special note is the convergence of simulated with observed components in some cases and divergence in other cases. At the urban site net solar radiation and substrate heat flux show only

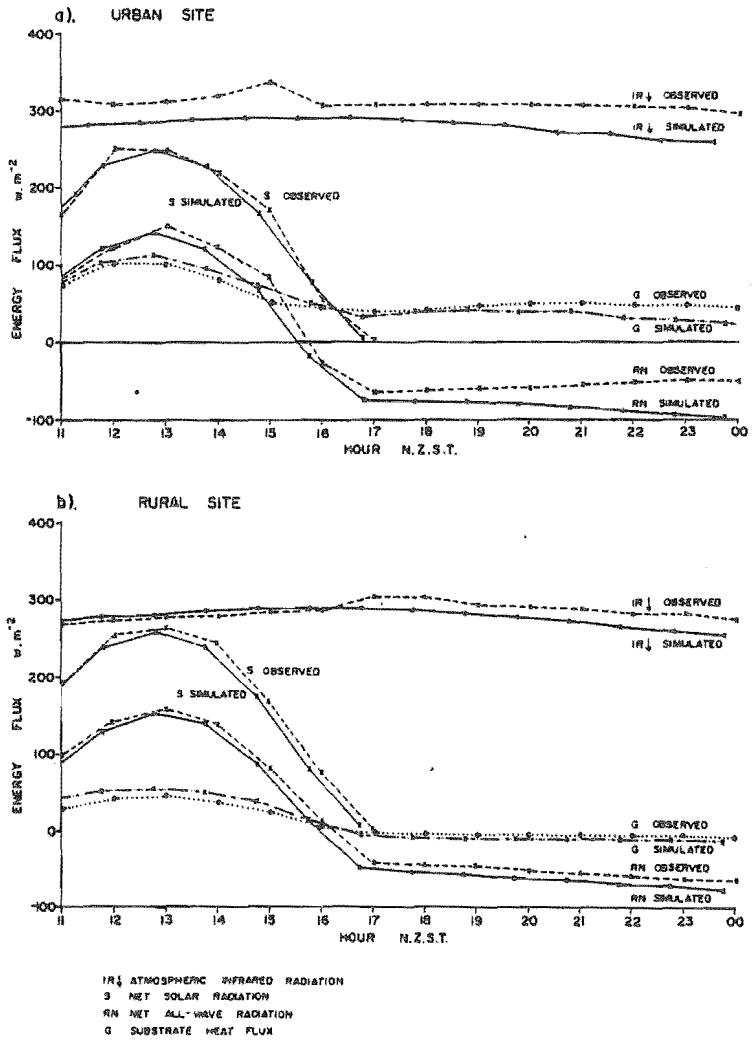

FIGURE 2.11 Diurnal Variation of Observed and Simulated Energy Fluxes for Urban and Rural Representative Sites, 10 July, 1979.

slight divergences, a maximum of 15 Wm^{-2} and 17 Wm^{-2} for net solar radiation and substrate heat flux respectively. Substrate heat flux shows a slight systematic divergence, with the simulated flux higher than observed during the day and lower at night. Simulated atmospheric infra-red radiation (IR↓) consistently underestimates the observed data. The observed IR↓ excess peaks at about 50 Wm^{-2} at 1500 h and increases again to above 40 Wm^{-2} later in the evening. Understandably, this pattern is reflected in a comparison of observed and simulated net all-wave radiation, where from around midday there is an observational excess flux. After sunset the trend of excess observed net all-wave radiation is similar to the IR↓ pattern, indicating that the divergence is not artifact. The increase in all radiant fluxes at 1500 h is possibly due to cloud effects above the urban site.

The rural site data (Figure 2.11b) again shows the systematic divergence of observed and simulated substrate heat flux exhibited in the urban case. This divergence is always small, in the order of 10 Wm^{-2} maximum. Simulated net solar radiation consistently under estimates observed fluxes from 1200 h by approximately 15 Wm^{-2}, indicating that the arbitrarily selected rural model transmissivity for this day (0.80) was too low. Observed IR↓ at the rural site is similar or slightly below that modelled during the day but becomes progressively higher than the simulated flux during the evening, reaching a maximum excess of 18 Wm^{-2} by 2300 h. Trends of simulated and observed net all-wave radiation reflect those of both net solar radiation and IR↓ with the daytime excess observed net solar radiation and the nightime excess observed IR↓ combining to keep observed net all-wave radiation consistently higher than that simulated.

Discussion

In modifying and extending the work of Myrup (1969), Outcalt (1972), Morgan *et al.* (1977) and Dozier and Outcalt (1979) and in developing a model for application to the flat-terrain city of Christchurch, a number of points emerge.

In contrast with Dozier and Outcalt a more empirical approach to the problem of solar radiation generation instead of a modelling approach has been found satisfactory. Additionally, the use of a bulk adiabatic transfer to obtain sensible heat fluxes in the manner of Morgan *et al.* (1977) has been found superior to the use of Businger-Dyer functions as preferred by Dozier and Outcalt. The height of the reference level (z_2) in this study has also been determined empirically in preference to the theoretical approach of Dozier and Outcalt.

The magnitudes of the Christchurch energy balance terms appear similar to those reported for Sacramento by Morgan *et al.*, except that, whereas in the Sacramento study LE appears to have been set at zero at night in C.B.D. and industrial areas, this has not been done in the Christchurch study. The apparently high nocturnal Christchurch C.B.D. LE values of the order of - 50 to - 100 Wm^{-2} seem to be of the same magnitude as those reported for central urban Vancouver (Oke, 1978). By day the negative direction of the LE flux over the Christchurch C.B.D. appears inadmissable. Whereas there is no doubt that evaporation of dewfall from the previous night is retarded on many clear winter days, there is little doubt that moistened surfaces do dry out by midday. If the degree of moistening could be assessed objectively and included in the model, more realistic C.B.D. temperatures would be predicted. Urban surface roughness is similarly difficult to

determine in the C.B.D., even with the method given in Equation 2.9. It is likely that poor estimates of this parameter may have induced errors in predicted C.B.D. temperatures.

Local scale advective effects have been ignored in this model leading to some minor discrepancies between observed and simulated temperature fields. Over Christchurch when synoptic-scale circulations are weak, two wintertime local winds are likely to affect the urban heat island. The first is the regularly occurring north-easterly sea breeze, the other a cold air drainage seawards across the Canterbury Plains from the Alps. The forcing exerted by these mesoscale circulations could usefully be incorporated into future models.

Artificial heat generation has been handled in a crude manner. Lack of data in the spatial application of the model precludes a grid by grid evaluation of this term. However, knowledge of the temporal variation of energy consumption (Pullen, 1970) should make it possible to incorporate the morning and evening peaks into the model, instead of holding artificial heat generation to be invariant with time. The reasonable similarity in observed and simulated substrate heat flux at the urban representative site suggests that, at least for this site, heat release from within this building is relatively constant from 1100 h through 0000 h.

Perhaps the most significant point arising from this application of the model is that it predicts Christchurch's heat island with a reasonable degree of success while making no direct allowance for $IR\downarrow$ variation across the city. The modelling exercise, although simplistic in approach, indicates that the Christchurch heat island

is related to surface effects associated with specific land uses, including the effect of thermal admittance, evaporative fraction and surface roughness, rather than any atmospheric radiative effect. In the model warmer temperatures over the city generate slightly higher IR↓, but this results largely from the influence of other factors and does not appear a direct cause of the urban heat island. There is a degree of feedback between IR↓ and ΔTu-r in the model however, which is difficult to assess.

A further point worth noting is the behaviour of the observed and simulated IR↓ fluxes at the representative urban, and to a lesser extent, rural sites (Figure 2.11a and 2.11b). The consistent underestimate of IR↓ fluxes by the model in the urban situation suggests processes operating that are not sufficiently accounted for by the usually reliable Brutsaert equation (Equation 2.6). Similar processes also appear to be operating at the rural site from late afternoon to cause an increasing divergence of observed from simulated IR↓ fluxes. The average underestimate of the model (IR↓ observed - IR↓ simulated/ IR↓ simulated) is 9.0% at the urban site with a maximum underestimate of 15% at 1500 h. Rural site data shows an average model underestimate of 3.9% with individual hourly values varying from an overestimate of 2.2% at 1400 h to an underestimate of 9.2% at 2300 h. In addition, a comparison of observed urban and rural IR↓ indicates an average excess urban IR↓ of 6% with differences ranging as high as 20% at 1500 h. These differences are of a similar magnitude to those obtained for a different urban and rural site in Christchurch in 1976 (Tapper, 1976).

A consideration of Equation 2.6 indicates two possible properties of the urban atmosphere which could account for the deviation of urban IR↓ observed from that simulated and which could also account

for the observed urban-rural IR↓ differences. Either the urban atmosphere has a higher emissivity than the rural atmosphere at altitude and as predicted by the Brutsaert equation, or the vertical temperature structure of the city is such that warm temperatures aloft are producing higher IR↓ at the surface than would be expected from near surface temperatures. Möller (1951) has shown that variations in vertical temperature gradient are capable of producing marked differences in IR↓ from clear skies. Higher emissivities in the urban atmosphere could be possibly due to a factor included in the Brutsaert equation, water vapour, or could be due to other constituents such as particulates, not included in the Brutsaert equation. The increasing divergence of observed from simulated IR↓ during the evening at the rural site in Figure 2.11 may be similarly considered.

Several quite plausible and reasoned explanations could be advanced to explain all of these phenomena, but a detailed answer requires a careful consideration of the composition and temperature of the atmosphere across the city in relation to surface IR↓ fluxes as suggested by Robinson (1977) and Dalrymple and Unsworth (1978). This is the approach followed in the present study

CONCLUSIONS

(i) A simple energy balance model has been presented for Christchurch which appears to give acceptable predictions of the Christchurch surface nocturnal heat island in winter. All essential features of the surface heat island have been replicated, including the urban fringe discontinuity, heat sinks and suburban heat sources and

the major central area heat source. Temperature predictions for the C.B.D. and during daytime simulation were less exact.

(ii) The major advantage of the model lies in its ability to delimit in detail the spatial variation of energy fields over Christchurch. These vary with land use in a manner that is qualitatively reasonable and provide a sound basis for the understanding of the physical processes which support and maintain the Christchurch heat island.

(iii) Energy balance simulation of the variation of surface temperature over Christchurch indicates that surface characteristics such as roughness, thermal properties and evaporative fraction are the primary influence on heat island occurrence.

(iv) Detailed consideration of observed and simulated energy fluxes for a rural and urban site indicate that there is room for improvement in the prediction of $IR\downarrow$, particularly for urban areas. Comparison of observed $IR\downarrow$ at the urban and rural sites and a consideration of theory suggests that differences between urban and rural sites and between observed and predicted $IR\downarrow$ might best be reconciled by detailed investigations of atmospheric temperature and composition in the boundary-layer.

CHAPTER 3

THE EXPERIMENTAL SITES AND INSTRUMENTATION

INTRODUCTION

The major concern of this chapter is to describe the experimental sites and the methods used in this study of urban effects on atmospheric infra-red radiation. After discussing the general climatic and air pollution characteristics of Christchurch, the experimental sites are discussed, equipment for monitoring energy transfers, meteorological parameters and air pollution is described and the data collection programme outlined.

GENERAL BACKGROUND

The Climate of Christchurch

Christchurch's latitude places it between the subtropical anticyclones and disturbed mid-latitude westerlies. Mean winds at undisturbed levels are therefore westerly, but because of the large-scale topographic effects of the Southern Alps winds below 1000 m usually have a north east or south west component. The synoptic scale weather of the area is dominated by a regular progression of eastward moving anticyclones, with a recurrence interval of one week to ten days

(de Lisle, 1969). Anticyclones have a trough between them usually containing one or more cold fronts, therefore conditions of stagnant weather seldom persist for long.

Other effects associated with the Southern Alps include the retarding of the passage of cold fronts and the creation of low pressure areas in their lee (Sevelle, 1968), and the presence of low humidity föhn winds, particularly during spring and autumn (Lamb, 1970). Christchurch's comparatively low rainfall regime can be attributed to the rainshadow effect of the Alps acting on the dominant westerly flow.

With westerly flow at undisturbed levels and high mountains upwind, skies are frequently clear. This promotes strong night cooling of lower level air layers with frequent nocturnal inversions, especially in winter anticyclonic conditions. In such conditions drainage of cold air (katabatic wind flow) is readily established, both off the plains and foothills to the northwest, and off the Port Hills to the south, with 'ponding' of the cold air occurring in the Christchurch area (Ryan, 1975).

A further important local feature of the climate is an onshore sea breeze, often augmented by a gradient northeast wind which is particularly well developed in the Christchurch area due to the funnelling effect of Banks Peninsula (Sturman and Tyson, 1981). This breeze continuing into the evening is often responsible for bringing onshore low-level stratocumulus cloud originating from cooling and turbulence of moist low level air along the north-east coast of Banks Peninsula. This phenomenon, present on perhaps 30% of clear nights (pers. comm., H. Kingham, New Zealand Meteorological Service, 1980). often results in part of the city being covered in cloud while areas

to the north and west remain cloud free.

Characteristic features of Christchurch's climate are endorsed by comparison with other New Zealand cities, although it should be remembered that New Zealand as a whole is characterised by high sunshine hours and high windiness, even when compared to other mid-latitude areas (Garnier, 1958). Table 3.1 shows that Christchurch has a lower rainfall, fewer raindays and a greater temperature range than the other cities. As shown in Tables 3.2 and 3.3 Christchurch has a relatively high frequency of clear days in winter and is less windy. In addition calms occur 20% of the time and, being more frequent in winter, are an important factor in determining the high pollution potential of Christchurch.

Owens and Tapper (1977) analysing daily synoptic and air pollution data for Christchurch for a four month period in the winter of 1976 were able to relate pollutant levels to different synoptic conditions with a very high level of statistical significance. Part of the analysis is summarised in Table 3.4. Two categories of synoptic conditions were associated with high levels of atmospheric pollution in Christchurch. They were anticyclonic conditions (category A), and conditions where a gradient wind from the northwest aloft is associated with variable winds at the surface (category D), both conditions promoting the development of inversions and the suppression of surface winds. In the period under study these conditions occurred on 39% of days, conditions associated with moderate pollution on 21% of days and conditions associated with low pollution (all including strong gradient winds at the surface) occurred 40% of the time.

TABLE 3.1 Climatological Averages (1941-1970)

STATION	RAIN DAYS	RAINFALL (mm)	MEAN TEMP (°C)	MEAN DAILY MAX. (°C) Jan.	MEAN DAILY MAX. (°C) July	MEAN DAILY MIN. (°C) Jan.	MEAN DAILY MIN. (°C) July	MEAN ANN. MAX.	MEAN ANN. MIN.
Auckland	140	1268	15.3	23	14	16	8	27	3
Wellington	124	1271	12.4	20	11	13	5	26	1
Christchurch	85	658	11.4	21	10	12	1	32	-4
Dunedin	119	772	10.9	19	10	11	3	30	-2

TABLE 3.2 Sunshine Percentage of Possible (1941-1970)

STATION	SUMMER %	WINTER %
Auckland	51	44
Wellington	52	42
Christchurch	46	45
Dunedin	41	43

TABLE 3.3 Average Number of Days with Gusts Reaching 70 km hr^{-1} or more (1941-1970)

STATION	NOV.-APRIL	MAY-OCT.	YEAR
Auckland	20	28	48
Wellington	90	98	188
Christchurch	31	23	54
Dunedin	28	32	60

Source: New Zealand Yearbook 1980.

TABLE 3.4 Categories of Synoptic Conditions and Relation to Air Pollution Levels for Christchurch (Winter 1976).

CLASS	DESCRIPTION		POLLUTION CATEGORY [1]
A	Anticyclone		S
B	Depression		M
C	Northerly flow		L
D	Northwest flow undeveloped at Christchurch		S
E	Northwest flow		M
F	Moist east to northeast flow		L
G	Westerly flow	Following passage of a cold front	M
H	Southwesterly flow		L
I	Southerly flow		L

1. Average daily total pollution concentration -

$\overline{\Sigma}$ sulphur dioxide + smoke + nitrogen oxides

S > 150 μg m^{-3}, M 100 - 150 μg m^{-3}, L < 100 μg m^{-3}

After Owens and Tapper 1977.

The above discussion indicates that Christchurch is well situated for the frequent occurrence of conditions conducive to high pollution potential in winter. However, even in winter the city is generally well ventilated so that daytime pollution levels after about midday, when the nocturnal surface inversion has been destroyed by surface heating, are almost always low. Only in situations where the inversion is forced to persist (category D) do pollution levels remain high during the day. Fortunately these conditions appear to be present on 10% or less of days (Owens and Tapper, 1977). The tendency towards nocturnal inversions in Christchurch means that sources of nocturnal air pollution (mainly domestic open fires) have a more dominant influence than their emission would suggest.

Air Pollution in Christchurch

The peculiar problems of air pollution in Christchurch have long been recognized. Tapper (1976) reviewed some of the early work on air pollution in Christchurch and traced the evolution of a monitoring programme up to the current detailed observations undertaken by the Department of Health. In recent years pollution levels and relative quantities of various types of emission have shown marked variation in response to changing energy sources due to factors both within and outside New Zealand.

Particulates, including smoke, dust and grit and gaseous pollutants such as sulphur, nitrogen and carbon oxides are the principal pollutants in the Christchurch atmosphere. The burning of fossil fuels produces carbon dioxide and to a certain extent nitrogen oxides and carbon monoxide. Smoke is produced from incomplete combustion, while dust and grit originate primarily from industrial boiler plants and

are emitted in flue gases. According to Pullen (1970) the sources of smoke in Christchurch in order of quantity produced are as follows:

a) the domestic open fire,

b) industrial combustion,

c) incinerators for the disposal of wood waste,

d) heavy trucks, buses and motor vehicles.

Table 3.5 indicates fuel consumption and smoke emission from various sources within the city over the three winter months for the 16 years to 1976. A decreasing coal usage for domestic purposes is evident to 1975 with a slight increase in 1976. Although data is not presently available, evidence is that the annual usage of domestic coal has continued to increase to the present (pers. comm., D.R. Pullen, Air Pollution Control, Department of Health, 1981). An increase in consumption of motor spirits and diesel oil up to 1973, followed by a levelling off of demand has also occurred. These trends are reflected in the amount of smoke emitted from various sources with only industrial emissions remaining relatively constant.

Along with emissions of smoke, smoke pollution levels in the central city in winter months from 1960 - 1976 show a definite decrease (Fig. 3.1), which is paralleled by a decrease of sulphur oxides (both by-products of coal combustion). This general trend of decreasing particulate and sulphur oxide pollution can be explained by:

a) changing domestic heating methods,

b) the use of coal of lower sulphur content (Kennedy *et al.*, 1974.

Subsequent to 1976 there has been a substantial increase in both smoke and nitrogen oxides. The reason for the increase in smoke has been

TABLE 3.5 Fuel Consumption and Emissions Three Winter Months (mid May - mid August)

	1960	1961	1962	1963	1964	1965	1966	1967	1968	1969	1970	1971	1972	1973	1974	1975	1976
Fuel (thousands tons)																	
Domestic Coal Usage	36.9		44.9	14.0	38.2	38.7	34.5	28.3	23.4	24.7	19.2	27.2	19.5	29.0			
Industrial Coal Usage	19.8		22.1	21.8	22.4	21.5	20.6	23.5	21.4	29.4	23.2	21.5	18.7	22.3			
Motor Spirits and Diesel Oil	17.8		21.3	23.2	24.4	26.4	28.2	30.4	31.2	31.3	32.4	33.3	33.5	33.6			
Smoke Emissions (tons)																	
Domestic	1292		1572	1575	1337	1354	1207	990	819	864	672	850	682	1014			
Industrial	198		221	218	224	215	206	235	214	294	232	215	185	223			
Motor Vehicles	57		68	75	78	100	110	123	122	104	96	109	94	99			
Domestic % of total	80		83	83	79	79	79	73	71	69	67	72	71	75			
Motor Vehicles % of total	3.5		4	4	5	6	7	9	11	8	10	9	10	7			
Industrial % of total	16.5		13	13	16	15	14	18	18	23	23	19	19	18			

Source: Health Department Data

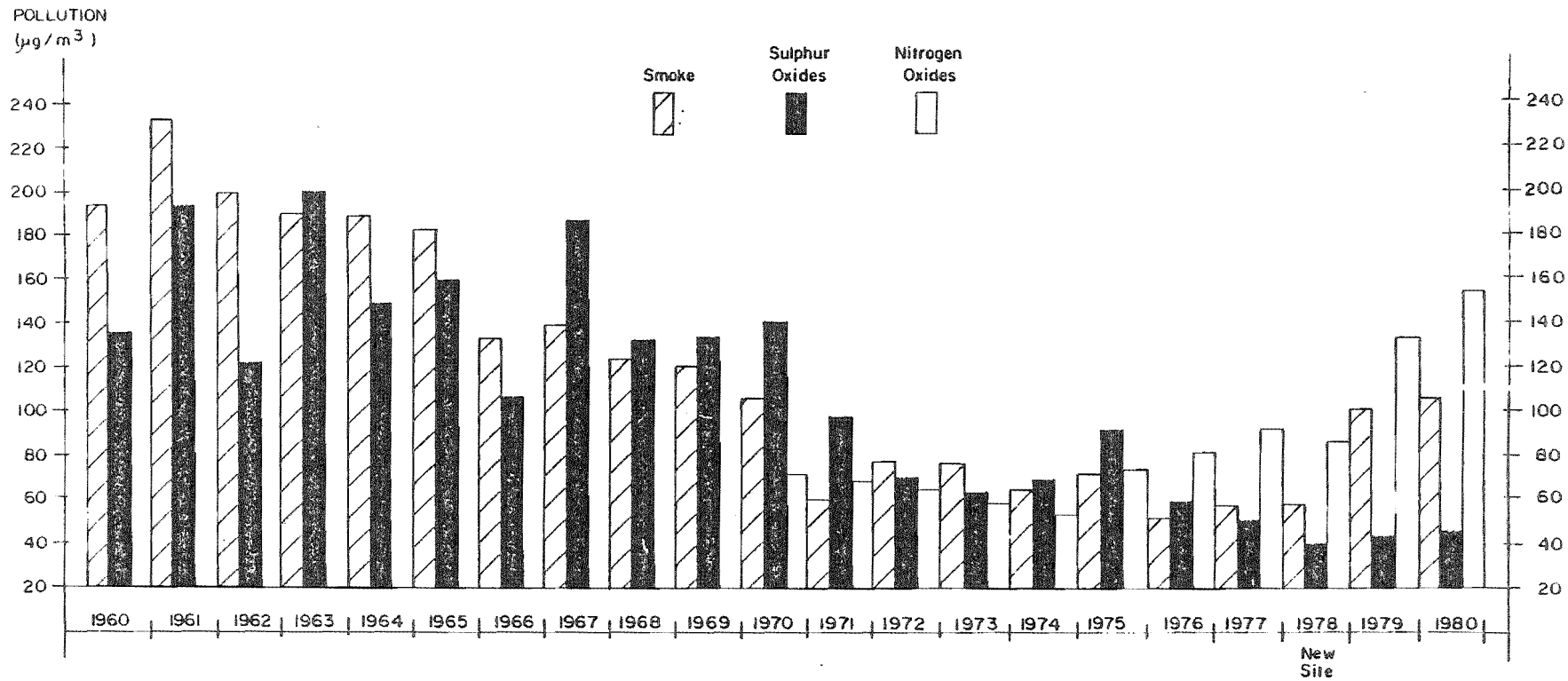

FIGURE 3.1 Annual Average Concentrations of Pollutants in Central Christchurch, 1960-1980.

the reversion to coal as a form of domestic heating, although the low sulphur content of that coal has helped keep sulphur oxide pollution low. With average winter smoke concentrations currently $\sim$ 100 $\mu g.\ m^{-3}$ in central areas, Christchurch's pollution levels are high even by world standards (Paterson and Pullen, 1979). In 1979, readings at the Department of Health's Bealey Avenue monitoring site exceeded 120 $\mu g.m^{-3}$ on 22 days, 15 days in excess of WHO recommendations.

Although the Christchurch air pollution problem is largely a winter one, the relatively constant emission rates of some pollutants, such as nitrogen oxides and hydrocarbons from motor vehicles provide the potential for high summertime pollution under suitable meteorological conditions. Tapper (1976) discussed possibilities for a photochemical type smog in Christchurch on the basis of known climatic data and trends in motor vehicle emission. Since that time several such photochemical smog episodes have been monitored, although they have been minor in comparison with problems elsewhere. Plate 3.1 shows a photochemical smog over Christchurch on 14th February, 1977.

SITE REQUIREMENTS FOR THIS STUDY

General

Because of the expense and sophistication of instruments for measurement of energy transfers over different surfaces, the number of sites is usually restricted. In urban effects studies this is often reduced to one urban and one rural site, and while this has been criticised (Lowry, 1977), it remains a valuable approach and is the approach used here. However, considerable care must be taken in site

PLATE 3.1 Photochemical Smog Over Christchurch, 14 February, 1977.

selection so that they are as representative as possible and do not reflect other influences such as topography and presence of water bodies. Also of importance in site selection are the variables to be measured. Variables measured in this study are included in Table 3.6. Note that net all-wave radiation and substrate heat flux were required for the modelling exercise only.

The following criteria were employed in the selection of areas in the Christchurch region suitable for establishment of representative urban and rural sites.

a) Distance from lateral boundaries - the urban site had to be representative of the city environment, thus a location which may be influenced by advection from rural areas was unsuitable. Similar considerations were applied in the selection of a rural site.

b) Long westerly fetch - clear weather periods of high pollution potential in Christchurch are usually associated with a light westerly katabatic wind (Ryan, 1975). As it is under these conditions that urban-rural radiative differences can be assumed to be greatest, an urban site with sufficient westerly fetch to allow wind, temperature, humidity and air pollution in the boundary-layer to adjust to surface influences was required. The rural site should be well upwind of the city under such conditions.

c) Surface discontinuities - the relative simplicity of topography in the Christchurch area provides few problems for placement of urban and rural experimental sites. Discontinuities at the periphery of the city include the ocean to the east and prominent hills to the south. Within the city the only major discontinuity is contiguous Hagley Park.

TABLE 3.6 Variables Monitored in this Project

URBAN SITE

CONTINUOUS MEASUREMENTS

A) Energy balance variables at surface

1. Atmospheric infra-red radiation
2. Total incoming solar radiation
3. Diffuse solar radiation

B) Meteorological and air pollution variables at surface

1. Screen level temperature
2. Screen level vapour pressures
3. Wind speed
4. Wind direction
5. Smoke, sulphur dioxide and nitrogen oxide pollution.

NON-CONTINUOUS MEASUREMENTS

A) Energy balance variables at surface (modelling exercise only)

1. Net all-wave radiation
2. Substrate heat flux

B) Vertical Profiling of Meteorological and air pollution variables

1. Temperature
2. Humidity
3. Smoke and nitrogen oxide pollution
4. Wind speed
5. Wind direction.

TABLE 3.6 (continued)

RURAL SITE

CONTINUOUS MEASUREMENTS

A) Energy balance variables at surface

1. Atmospheric infra-red radiation
2. Total incoming solar radiation
3. Diffuse solar radiation

B) Meteorological variables at surface

1. Screen level temperature
2. Screen level vapour pressure
3. Wind speed
4. Wind direction.

NON-CONTINUOUS MEASUREMENTS AT SURFACE (Modelling exercise only)

A) Energy balance variables

1. Net all-wave radiation
2. Substrate heat flux.

B) Air pollution variables

1. Smoke, sulphur dioxide and nitrogen oxide pollution.

C) Vertical profiling of meteorological and air pollution variables

1. Temperature
2. Humidity
3. Windspeed
4. Wind direction

TABLE 3.6 (continued)

In addition backup information was obtained from the New Zealand Meteorological Service (N.Z.M.S.) station at Christchurch International Airport, including:-

1. Upper air temperature
2. Upper air humidity
3. Atmospheric air pressure
4. Cloud amount
5. Wind speed
6. Wind direction.

d) Continuity of landuse - for the urban site a uniform type, function, density and height of building in the area was sought, while open pastureland was sought for the rural site. Sites were also chosen where no significant changes would occur over the study period.

e) Proximity to an established air pollution monitoring station - the incorporation of existing facilities operated by the Department of Health would avoid duplication of equipment for monitoring ground level air pollution.

f) Proximity to an open area - at the urban site a major requirement was an adjacent open area suitable for the launching of an instrumented kytoon.

g) Power supply and shelter - the relatively sophisticated nature of the recording equipment for the project required a reliable and continuous power supply and adequate shelter to ensure data quality over the long periods of measurement.

h) Site elevation - in selection of sites it is essential to ensure that observations are made at similar heights above ground level, particularly in the case of atmospheric infra-red radiation.

Specific Considerations for Energy Balance Measurements

In addition to the general site restrictions, certain further restraints were imposed on sites intended for energy balance measurements.

a) For all upward facing radiation sensors the view factor, or proportion of unobstructed sky out of the total hemisphere in view, should be as high as possible and should vary little between comparative sites.

b) The area viewed by the lower surface of the radiation sensor must be representative of an integrated urban or rural area.

c) Substrate heat flux, while obviously unable to be measured in an integrated urban or rural surface medium, should be measured in a medium that is representative of a large proportion of the surface of that urban or rural area.

THE EXPERIMENTAL SITES

General Locational Characteristics

An urban observational site consistent with respect to all of the above criteria was established on the roof and in the car park of the Department of Health, School for Dental Nurses, while the rural site was established on the roof of a building at Lincoln College and in adjacent pastureland. The general location of sites is given in Figure 2.2 with greater detail appearing in Figures 3.2 and 3.3.

The urban site (alternatively referred to as the Central City Site or C.C.S.) is situated 800 m due north of Cathedral Square, the heart of Christchurch's central business district (Fig. 3.2). A few buildings in the city centre exceed 60 m but most are two or three storied (8 - 12 m) or less. To the south-west Hagley Park extends to within 800 m of the site. Christchurch Women's Hospital, 30 m tall and 200 m away is the nearest large building. The majority of buildings in the area of the urban site are small office buildings, light industrial plants or rented accommodation, usually one or two storied. To the north land use becomes progressively more residential. In common with the rest of the city, the area around the urban site is well vegetated

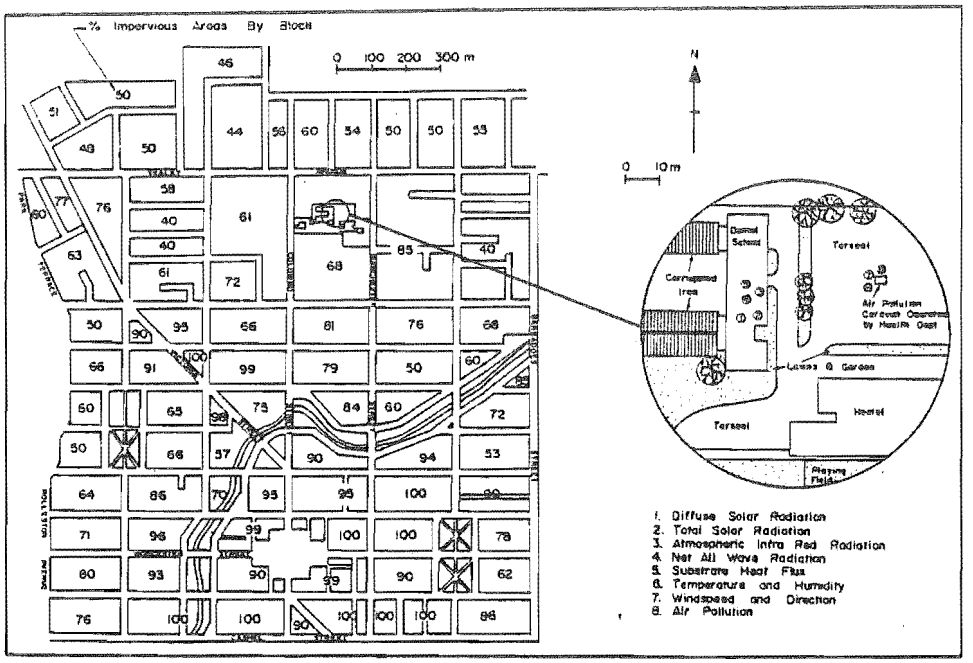

FIGURE 3.2 Location of Central City Experimental Site and Instrumentation.

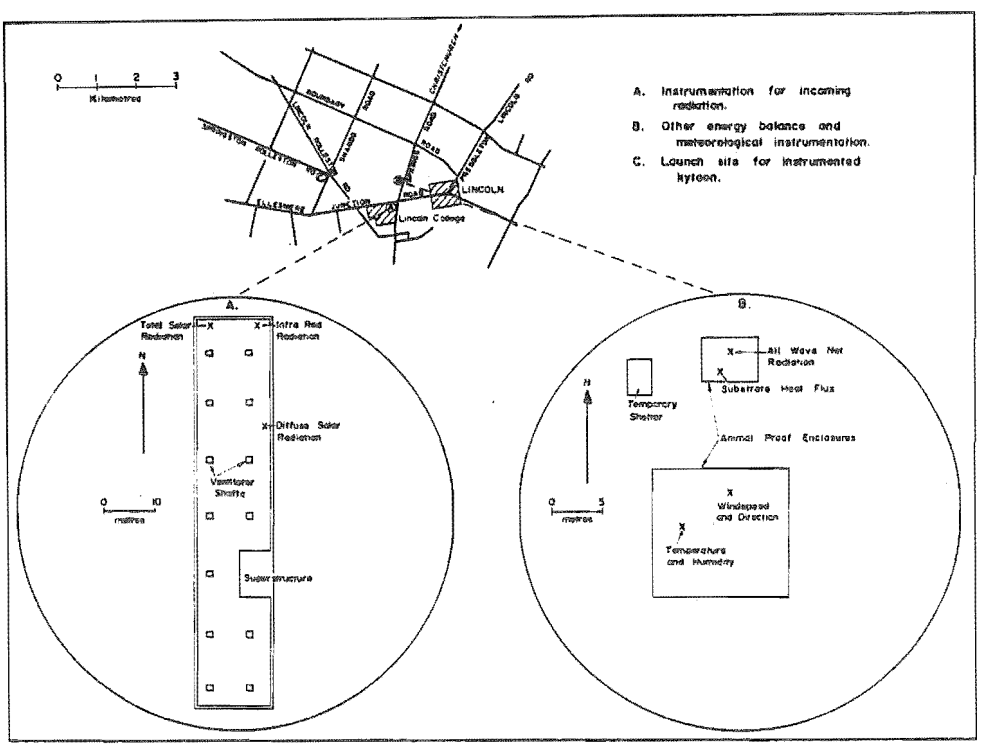

FIGURE 3.3 Location of Lincoln Experimental Site and Instrumentation.

for an urban area, with many mature trees generally corresponding in height with adjacent buildings. Using air photographs a survey of the percentage of horizontal surface area of each block covered by impervious materials indicates that values range from 100% within the C.D.B. to approximately 50% in the dense residential areas to the north of the representative site. The urban site is near the centre of a block (68% impervious) bound by Colombo and Manchester Streets and Bealey Avenue (Fig. 3.2), some of the busiest streets in the city.

All energy balance instrumentation was located on the flat, tarsealed roof of the School for Dental Nurses, 7 m above ground level, while meteorological and air pollution data were collected 30 m away in a car park. The position of equipment is shown in Figure 3.2. Immediately adjacent the urban site is the St Marys College playing field, a suitable site for launching of the instrumented kytoon.

Previous investigation (Tapper, 1976) had shown that sites located on the periphery of Christchurch could easily be influenced by the urban pollution dome. Detailed analysis of 15 years of radiation data at Christchurch International Airport, 10 km northwest of the city centre, indicated a steady decrease in solar radiation significant at the 1% level and probably related to urban encroachment. It was therefore considered that a rural site located at Lincoln (alternatively referred to as the Lincoln Site or L.S.), 30 km west southwest of the city centre, would be reasonably representative of a rural area, while still being close enough geographically to assume a uniform air mass and distribution of solar radiation under conditions operative in this study.

Lincoln College proper (Fig. 3.3) occupies a 0.8 km^2 site set amongst open farmland comprising both crop and pastureland. The College comprises an assortment of buildings ranging to 30 m in height. Open farmland in the vicinity is interrupted only by occasional tree wind breaks, scattered farm buildings and the small rural service centre of Lincoln (population 1590).

Instrumentation for the measurement of incoming radiation was located on the flat roof of a building at the north east margin of the College at a height of 18 m above ground level. Remaining energy balance equipment was established over pastureland at a meteorological site operated by Crop Research Division, Department of Scientific and Industrial Research and located slightly north of Lincoln College (Fig. 3.3). A temporary shelter was erected at that site to house recording equipment. To comply with Civil Aviation Authority requirements, the instrumented kytoon was operated from an open paddock 2.8 km west of the College (Fig. 3.3).

Suitability for Measurement of Energy Fluxes

View Factors

An important consideration in the measurement of incoming radiation characteristics is the representativeness of sites used, one to another. Complete similarity is an impossibility, hence possible limitations should be accepted and accounted for. In the case of outgoing radiation, the surface should be representative of an integrated urban or rural area.

Figures 3.4 and 3.5 illustrate upper and lower hemispheric view factors for all radiation sensors installed. As view factor

A.

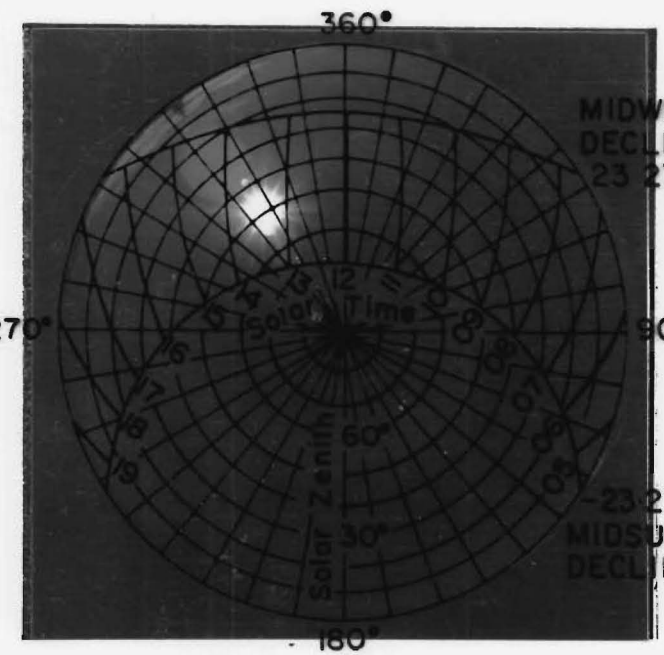

UPPER HEMISPHERIC VIEW FACTORS

SKY	·9510
TREES	·0380
BUILDINGS	·0110

B.

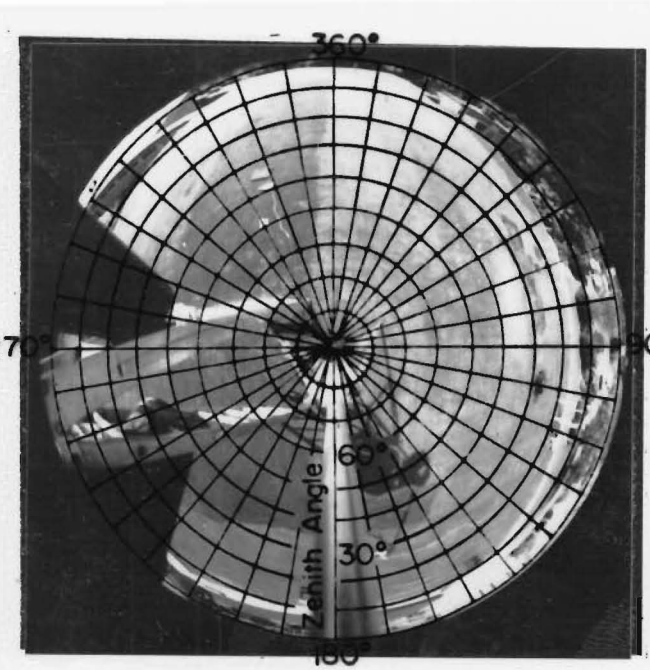

LOWER HEMISPHERIC VIEW FACTORS

TARSEAL ROOF	·8800
OTHER SEAL	·0450
VEGETATION	·0700
INSTRUMENTS	·0050

FIG. 3·4 CENTRAL CITY SITE VIEW FACTORS

A.

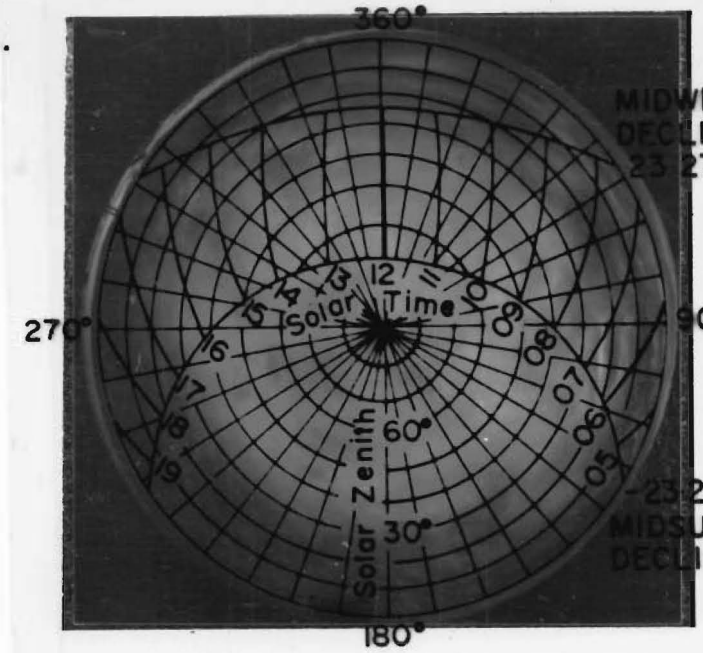

LINCOLN ROOF
UPPER HEMISPHERIC VIEW FACTORS

SKY	·9810
BUILDINGS	·0100
VEGETATED HILLS	·0090

B.

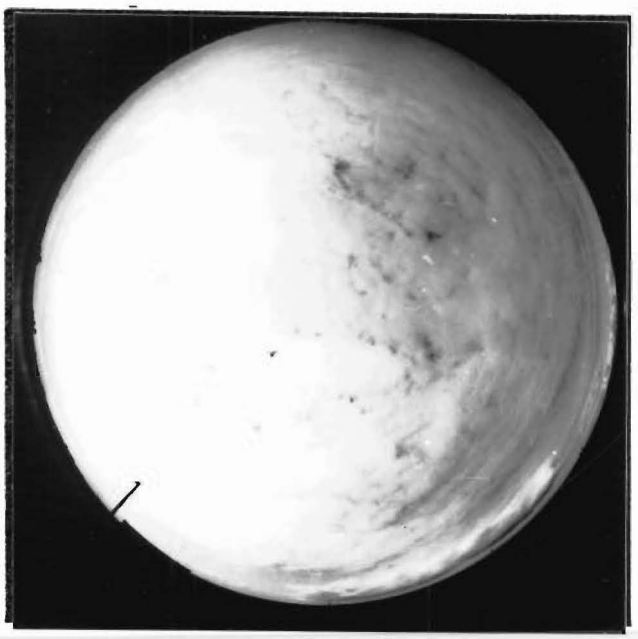

LINCOLN FIELD
UPPER HEMISPHERIC VIEW FACTORS

SKY	·9890
BUILDINGS	·0030
VEGETATED HILLS	·0080

C.

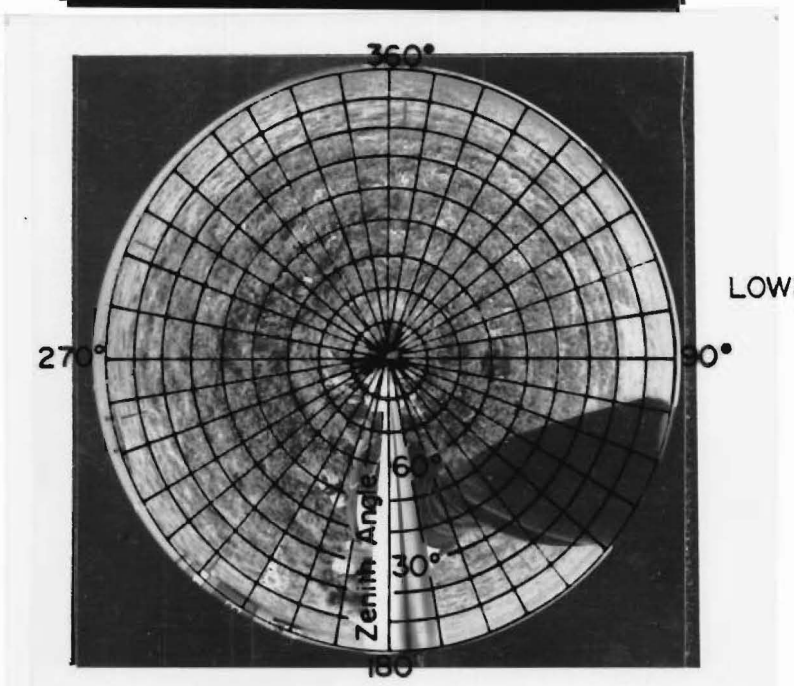

LINCOLN FIELD
LOWER HEMISPHERIC VIEW FACTORS

PASTURE	·9680
TREES	·0180
BUILDINGS	·0100
INSTRUMENTS	·0040

FIG. 3·5 LINCOLN SITE VIEW FACTORS

differences resulting from sensor positioning are extremely small, only one upper hemispheric diagram is presented for each site. All photographs have been taken using an 8 mm f/2.8 Fisheye-Nikkor Auto lens providing a full 180^{o} hemispheric view with minimal distortion. Optical distortion has been allowed for in the drawing of polar grids and calculation of view factors. Polarity has been reversed photographically in Figures 3.4(A) and 3.5 (A and B) to give standardisation with normal compass bearings. Areal proportions occupied by various elements within the hemispheric fields of view have been obtained using a digitiser interfaced with a Wang 2200T minicomputer.

The most critical view factor comparisons in this study are for the upper hemispheric view factors at the Central City Site (Fig. 3.4A) and the Lincoln roof site (Fig. 3.5A) as these are the view factors for the infra-red and solar radiation sensors. Upper hemispheric view factors have two important effects on incoming radiation. For solar radiation, obstructions can directly interfere with the solar beam or reflect radiation onto the sensor, while obstruction of sky for infra-red radiation has the effect of a warmer object blocking out the colder radiating sky. Sky view factors are high at both the urban and rural sites, 0.9510 and 0.9810 respectively. Simple calculations using very large sky - obstruction temperature differences and assuming infra-red radiation intensity equal from all angles, indicate differences in infra-red radiation due to view factor variations to be less than 1.5%. Under most circumstances and given that the greater proportion of incident infra-red radiation is from directly above the sensor, the difference in radiation due to view factor would be much less. As important as the proportion of sky covered is the part of sky obscured, particularly with regard to direct beam solar radiation. Figures 3.4

(A) and 3.5 (A) show solar paths for mid-summer and mid-winter. In both cases most obstructions are toward the south and the maximum intrusion into field of view is 15^{o} for the urban site and 10^{o} for the rural site. At neither site do obstructions block the solar beam at times of low sun angles. In terms of incoming radiation the two sites are considered representative enough for direct comparisons to be made without recourse to view factor corrections.

Lower hemispheric view factors for radiometers established at a height of 2 metres above the surface at the Central City and Lincoln Sites are shown in Figures 3.4 (B) and 3.5 (C). At the Central City Site the proportion of the field of view occupied by impervious urban surfaces is 0.9250 with the roof of the School for Dental Nurses comprising 0.8800 of the area. This proportion is similar to many inner city areas of Christchurch, although somewhat overrepresentative of impervious surfaces in the block in which the Central City Site is located (Fig. 3.2). At the Lincoln field site view factors are considered representative of rural areas, with non-rural surfaces occupying only 1.4% of the lower hemispheric field of view.

Surfaces

The roof of the School for Dental Nurses is entirely covered with a 3 cm layer of tarseal with a fine chip base constituent. This surface is similar in most respects to other urban surfaces including sidewalks, carparks and some road surfaces. Measured albedo and emissivity of the material is 0.095 and 0.95 respectively, similar to values reported for other similar urban surfaces (Oke, 1978, page 247). Substrate heat flux was measured through a layer of similar tarseal chip set onto the roof.

At the Lincoln Site rye grass pasture within the enclosures was kept at ∿ 5 cm length during experimental periods. Albedo over the grass averaged 0.24 and emissivity 0.92, similar to values compiled from several sources (Oke, 1978, page 15).

Height of Sensors Above Ground

The variation of IR↓ with height in the lower atmosphere is a well known phenomenon reported in many standard texts, for example Sellers (1972, page 46). An emissivity approximation model utilising atmospheric soundings (Chapter 9) showed that IR↓ radiation differences resulting from the different height of placement of sensors at the two major sites were small, usually less than 1% in conditions operative.

Air Quality

Since air quality is known to be important in transfers of both IR↓ and SW↓, a short period of air pollution observations was undertaken at the Lincoln Site (Lincoln College) in August, 1978 to ascertain if air quality was synonymous with a true rural site. Table 3.7 indicates that for all major pollutants, levels at the Lincoln Site are low, usually at the threshold of detection. Although pollutant levels are slightly higher than true rural background levels, for most purposes Lincoln can be deemed a rural site in terms of air quality.

Suitability for Kytoon Operation

The 150 by 80 m playing field adjacent to the urban site provides adequate facilities for the operation of the instrumented kytoon system. There are no significant aerial obstructions for operation in winds from any direction. Other advantages include

TABLE 3.7 Air Pollution ($\mu g\ m^{-3}$) at Representative Sites, 18 - 28 August, 1978

	SO_2		SMOKE		NOX		AMMONIA	
	C.C.S.	L.S.	C.C.S.	L.S.	C.C.S.	L.S.	C.C.S.	L.S.
18 - 20 August	39	4	71	5	90	10	7	1
20 - 23 August	27	3	8	0	50	4	4	0
23 - 25 August	23	3	9	0	62	7	4	0
25 - 28 August	21	2	20	3	35	2	3	0

proximity to radiation and air pollution measuring equipment (50 m away) and a telephone for communication with Air Traffic Control as well as on-site access for support vehicles. Only under exceptional circumstances was it not possible to obtain permission from the authorities for flights from this site.

The rural kytoon site was relocated 2.8 km from Lincoln College to be away from the flight path to R.N.Z.A.F. Base Wigram and, apart from the relative distance from surface based sensors, was quite suitable in terms of other criteria. Elevation, topography and land use are identical to the Lincoln Site. Detailed observations of screen level temperature at times of kytoon flights, showed differences at the two sites in the order of 1^{o} or less, indicating that boundary-layer temperatures would vary little above each site.

NEAR SURFACE INSTRUMENTATION OF REPRESENTATIVE SITES

General

The long term measurement of energy fluxes and related parameters requires two things in relation to instrumentation; durability under all conditions, and accuracy. Generally, these requirements are well satisfied with the instrumentation used in this study. As this study is designed specifically to investigate the variation of $IR\downarrow$ in response to other atmospheric variables, it is convenient to consider energy balance instrumentation separate from the meteorological and air pollution instrumentation, and surface based equipment separate from kytoon borne equipment.

Radiant and Substrate Heat Flux Equipment

Atmospheric Infra-Red Radiation

Sensors employed for measurement of IR↓ at both sites were Swissteco Model S-1 versions of the C.S.I.R.O. Funk net radiometer (Swissteco Pty. Ltd., Australia), adapted for measurement of IR↓. The instrument and its characteristics have been described in detail by Funk (1959, 1962a, b, c, d) and MacDowall (1954). Upper and lower surfaces of the sensor are enclosed within a pair of thin (0.05 mm) moulded polythene hemispheres having absorption bands centred at 3, 5, 7 and 14 μm (Funk, 1959), but narrow enough to have little effect on absolute accuracy. To minimise systematic differences between sensors in this study, selected hemispheres extruded from the same polythene sheet were ordered from the manufacturer. The fitted polythene hemispheres were regularly cleaned and were replaced two-weekly during observation periods to maintain sensor efficiency. Hemispheres were kept rigid with air flow from a small 230 Volt A.C. pump via a silica gel drying chamber. After passing through the instrument air was vented at exterior ports which directed airflow over the polythene surfaces.

Measurement of IR↓ was effected by attaching a black body cavity to the underside of the radiometer. The cavity, coated on the inside with optically black paint and on the outside with reflective white paint, contained a silicone diode temperature sensor which measured the radiating temperature of the inner surface. Experimental evidence suggested that the effective emissivity of the cavity was sufficiently close to unity for a value of 1.0 to be used.

After calculating IR↑ from the cavity using the Stefan Boltzmann relation (Equation 1.2), IR↓ was given by the following equations:-

night-time $IR\downarrow = Rn + IR\uparrow$ 3.1

daytime $IR\downarrow = Rn + IR\uparrow - SW\downarrow$ 3.2

Solar radiation input to the equation was derived from an adjacent solarimeter and the manufacturer's calibration coefficients were applied to convert from readings in millivolts to the energy units used in this study (Wm^{-2}).

Plate 3.2 shows the adapted net-radiometer mounted on its metal frame, levelled and oriented with respect to solar north.

Net All-Wave Radiation

Net radiometers indentical to those used for $IR\downarrow$, but without black-body adaptors, were used at each site to determine net all-wave radiation (Rn) for the modelling exercise. The polythene hemispheres were inflated and treated in the same way as for the $IR\downarrow$ instrumentation. Sensors were mounted on a levelling device at a height of two metres above the surface (Plate 3.3). The radiometer mast was securely guy-wired to the ground.

Short-Wave Radiation

Total incoming short-wave radiation (Q + q) and the diffuse component (q) were obtained using Kipp and Zonen CM5 dome solarimeters (Kipp and Zonen, Delft, Holland) at each site. These solarimeters are suitable for long term outdoor operation as the sensing thermopile is enclosed in a moisture proof, optically correct, double walled glass dome (transparent from 0.3 to 2.8 μm). Specifications of these solarimeters are accuracy ± 2%, linearity of response ± 1%, good adherence to the Lambert cosine response law and independence from ambient temperature effects.

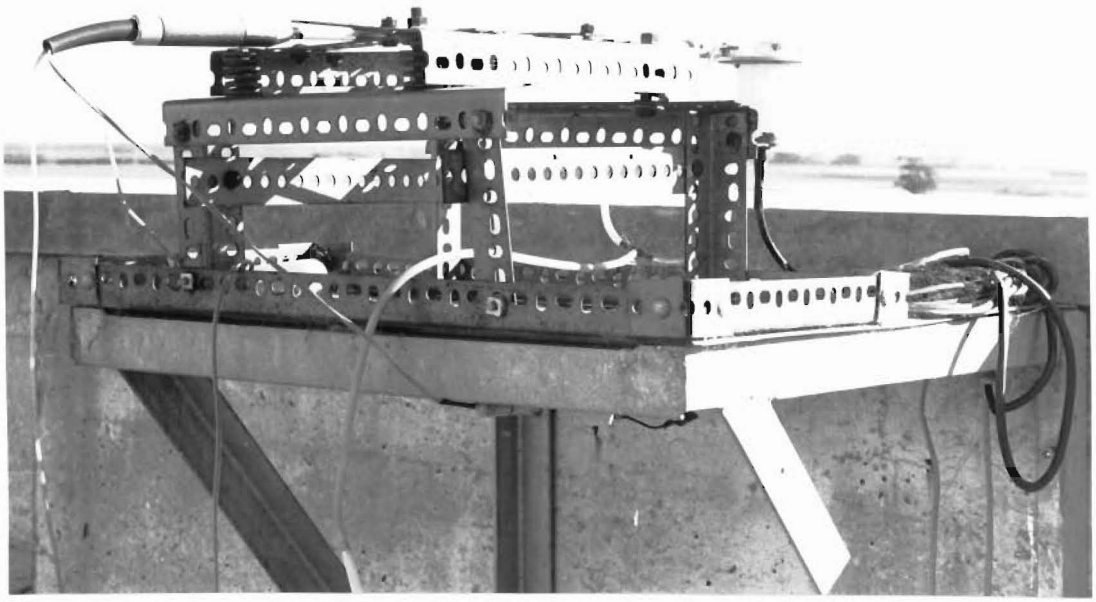

PLATE 3.2 Adapted Net-radiometer for Measurement of IR↓.

PLATE 3.3 Net-radiometer for Determining Net All-wave Radiation. Note Levelling Device.

At each site the solarimeters for measurement of total short-wave radiation were levelled and oriented in relation to solar north. One solarimeter at each site was employed using a shadow ring designed and manufactured within the Geography Department, University of Canterbury. The purpose of this device was to shield the sensor of the solarimeter from direct beam radiation, thereby measuring only diffuse sky radiation. Plate 3.4 shows the shadow ring with the solarimeter mounted within it. Specifications of the shadow ring are, a width of 66 mm and an overall radius of 190 mm.

Two shadow ring adjustments are necessary for a particular site. Latitude is set by altering the angle the ring makes with the horizontal plate of the solarimeter, while solar declination is adjusted by moving the ring along its slide according to the time of year. In this study it was found necessary to make adjustments once every three days (or more frequently near the equinoxes) to ensure a shadow centred over the solarimeter dome. One further adjustment must be made to the raw data to account for the loss of diffuse sky radiation due to the presence of the shadow ring. The correction method used in this study follows that of Drummond (1955) and is described in detail by Tapper (1976).

Substrate Heat Flux

Heat storage at both sites for the modelling exercise was measured by heat flux plates of non-commercial manufacture. The method of construction and characteristics of these flux plates are discussed in Tanner (1963) and Moran (1971). As with all flux plates the temperature differential through the plate is measured by means of a thermopile which produces an electromotive force (e.m.f.) proportional to this temperature difference.

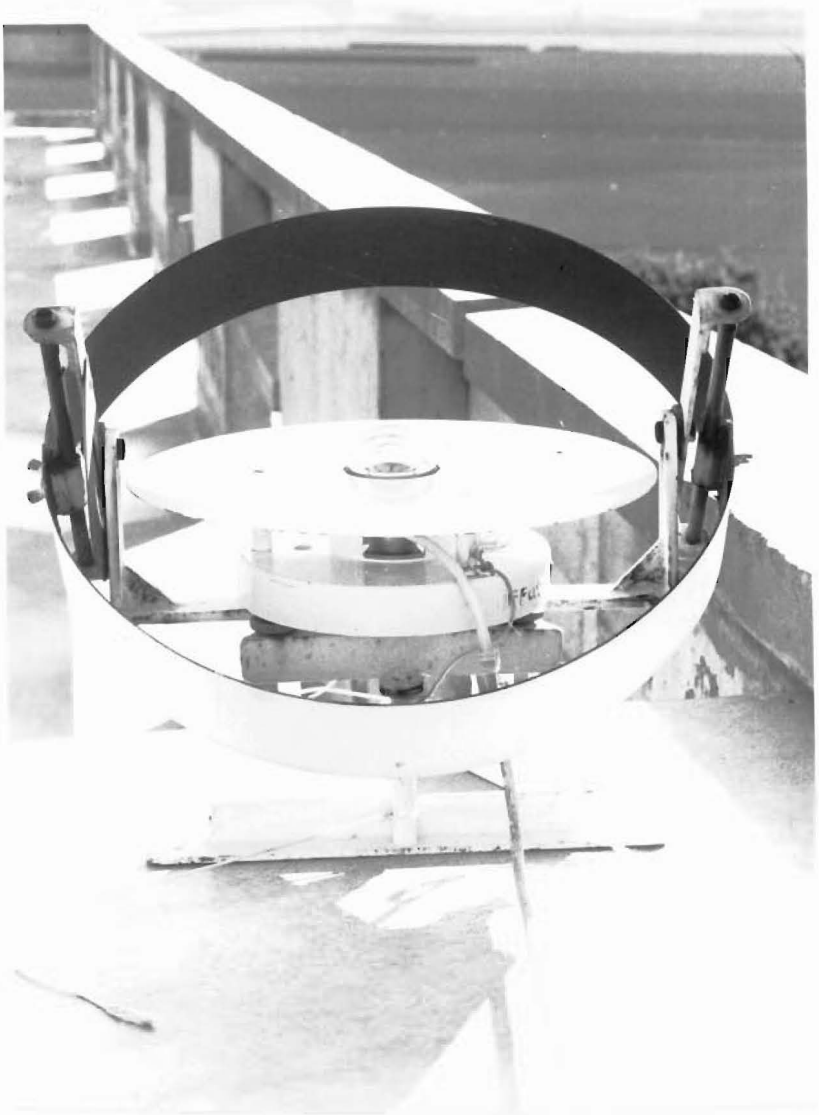

PLATE 3.4 Solarimeter and Shadow Ring Attachment.

Problems involved in the usage of flux plates are outlined by Tanner (1963), but can largely be overcome by the correct placement of the plates at a sufficient depth within the soil structure (Tanner, 1963). In the present application the urban site flux plate was embedded in tarseal chip at a depth of 2 cm, while at Lincoln the plate was buried at the same depth in soil under pasture. The depth selected was a compromise between a depth of 5 cm or more recommended by Tanner (1963) in order to ensure minimal disruption of natural moisture and heat transfer and maximum soil contact, and a position closer to the surface where the actual surface flux would be more closely approximated. As the measurement of substrate heat flux was of secondary consideration in this study, at neither site were corrections made for flux divergence in the overlying surface layers, therefore values of substrate heat flux at both sites are conservative.

Data Recording Systems

Signals from all of these transducers were recorded automatically and continuously during data collection periods. At the urban site all energy flux parameters and black body cavity temperature were recorded on an Integrating Millivoltmeter System 601 (Technical Enterprises Ltd., Christchurch, N.Z.). Printouts for all channels were obtained hourly and the count rate of the machine could be varied according to the required accuracy, or the individual output from each sensor. Before each period of observation the integrator was calibrated by the manufacturer.

At the rural site infra-red radiation (including black body cavity temperature) was recorded on a two channel Toa Electronic Polyrecorder Model EPR.3T and total and diffuse short-wave radiation on a National Pen Recorder UP6539 and Honeywell Multichannel Versaprint

chart recorder respectively. During intermittent periods of observation at the field site, net-radiation was recorded on a Lloyd CR553 and substrate heat flux on a Heathkit single channel recorder model IR 18M. All chart records were integrated on an hourly basis using an electronic digitiser to give mean hourly data values.

Because of external electronic noise it was found necessary to adequately shield and earth all instrument cables, particularly at the rural site where long cables were employed.

Sensor Calibration and Estimation of Error

In order to obtain as much accuracy as possible in this study two detailed calibration periods were used; the first in October 1978, part way through the study, and the other in November 1979 at the completion of the study. Two calibrations were undertaken to minimise problems resulting from any progressive changes in instrument sensitivity over a long data collection period. Details of calibration procedures and results are included in Appendix II. Results show relative errors to be 5% or better for all paired energy balance data utilised in this study.

Meteorological and Air Pollution Instrumentation

Screen Temperature and Humidity

Temperature and humidity at both sites was recorded at standard screen level on Kohari thermohygrographs (humidity 0-100%, temperature -15°C to 40°C) which recorded a pen and ink trace on paper charts. Before and after periods of operation the two instruments were carefully calibrated to give maximum errors of 0.25°C and 3% in temperature and humidity respectively. The data was converted into

vapour pressure or specific humidity for use in this study.

Wind Speed and Direction

Wind data at the urban site was provided by a Climatronics WM - I Wind System (Climatronics Corpn., U.S.A.). Manufacture specifications include ranges of 0 - 100 knots (± 1%) and 0 - 360° (± 2.5%). The three cup anemometer and vane were installed on top of a 10 m mast in the grounds of the School for Dental Nurses (Fig. 3.2). A Lambrecht Mechanical Anemograph (three cup anemometer) installed at a height of 7 m at the Lincoln field site provided wind run and direction at that site.

Air Pollution

Department of Health air pollution data were available at the Central City Site for the whole study period, but only smoke pollution data in winter and nitrogen oxides data in summer were utilised in this study. Data was available on a continuous basis (2 hourly averages for smoke) for much of the study period.

For several reasons, smoke pollution is a particularly useful pollutant on which to concentrate. These are:-

a) Smoke is Christchurch's worst pollutant in terms of atmospheric loading, particularly during the winter months.

b) The presence of smoke particulate in the atmosphere has well known influences on both solar and infra-red radiative transfer (Hand, 1943; Sheppard, 1958; Atwater, 1971b; Volz, 1972; Pueschel and Kuhn, 1975; Viskanta and Daniel, 1980).

c) It is easily measured and is a reasonable indicator of the presence of, and variations in, other urban air pollutants such as

SO_2 which are potentially important in radiative transfer; this given that meteorological conditions favourable for smoke pollution are the same as those for other pollutants.

Nitrogen oxides were utilised during summer periods when smoke levels were at or below the level of detection. Nitrogen oxides, while not themselves directly important in infra-red radiative transfer were monitored because:-

a) They are also an indicator of the presence of, and variations in other urban air pollutants.

b) Nitrogen dioxide (NO_2) formation is one of the indicators of photochemical activity in the atmosphere and Ozone (O_3) is known to absorb very strongly in the infra-red. NO_2 has also been shown by Atwater (1971b) to lead to strong atmospheric heating due to absorption of solar radiation, even when present in small quantities (1 p.p.m.).

Smoke levels were recorded using a Research Appliance Company A.I.S.I. model F2 sampler utilising a timing mechanism and continuous paper tape to monitor average smoke concentrations over required time intervals. With knowledge of airflows and smoke stain density (obtained with a D.S.L. smoke stain Reflectometer) it is possible to determine average smoke concentrations in micrograms per cubic metre ($\mu g\ m^{-3}$) using the recommended W.H.O. procedure (W.H.O., 1976). Continuous records of nitrogen oxides pollution ($\mu g\ m^{-3}$) were obtained with a M.L. Nitrogen Oxides Analyser Model 8440 (Monitor Laboratories Inc., U.S.A.).

Other Meteorological Data

In addition to data collected at the two main sites, occasional use was made of New Zealand Meteorological Service data recorded at

Christchurch International Airport. Where necessary upper air temperature and humidity data was obtained from daily or twice daily radiosonde soundings. Atmospheric air pressure and cloud amount were also available from this source, as were surface wind speed and direction data when data from the representative sites was missing.

THE INSTRUMENTED KYTOON SYSTEM

General

The design requirements of a kytoon system for this study were that it:-

a) provide reliable and accurate boundary-layer data,

b) be mobile for movement between sites,

c) be able to be operated by one person, and

d) be of a low capital cost.

Tethered balloon systems meeting some of the above requirements and for similar applications have been described by Klein, 1969; Painter, 1970; Perroud *et al.*, 1973; Morris *et al.*, 1975; and several systems are available commercially. But as none of the systems completely met all requirements, a small tethered kytoon system was developed specifically for the present project.

The Instrument Carrying System

The complete system comprises a small polyethylene kytoon, airborne sensors for meteorological and air pollution measurements, a tether line and winch, and a ground station. A specially constructed

trailer with a canvas canopy enables the kytoon to be transported and stored in its inflated state.

The dirigible-shaped kytoon (Plate 3.5) is a Follmer Model 115 (V.J. Follmer, Minnesota, U.S.A.), with a nominal volume of 3.25 m^3 in launch condition. A section in the tail extends during ascent to maintain internal stability and provide near-constant lift. Inflated with pure grade helium gas, lift at sea level in calm conditions is 1.9 kg. Aerostatic lift characteristics of the kytoon are included in Appendix III.

Kytoon altitude was calculated from clinometer measurements of the angle from the vertical and distance to the kytoon obtained from the length of graduated tether line corrected for catenary sag. With the 1000 m tether line marked at 10 m increments by coloured embroidery cotton, altitude could be estimated to an accuracy better than 5 per cent. A standard surf life saving reel mounted on the drawbar of the transporter was used as a winch, enabling the kytoon to be raised or lowered at a rate of 100 m min^{-1}.

For ambient wind speeds of greater than, or less than 8.0 ms^{-1} respectively, a heavy grade tether line (4.5 gm m^{-1}) of 160 kg breaking strain, or lighter grade line (2.0 gm m^{-1}) of 80 kg breaking strain was used. The length of tether line a kytoon can support in relation to the payload in aerostatic conditions is given in Appendix III. Seldom was sufficient lift generated to take all instrumentation aloft during one flight. Accordingly, meteorological and air pollution data were obtained on individual flights, usually separated in time by less than ten minutes.

PLATE 3.5 The Kytoon System Showing the Dirigible and Ground Station.

To keep operational costs acceptable, a regular leak testing procedure was instituted to reduce helium consumption. Facilities and equipment, including a halogen leak detector, belonging to the Ghost Flight Station (National Centre for Atmospheric Research) in Christchurch were utilised for this purpose.

Kytoon Instrumentation

Temperature and Humidity

General

A block diagram of the temperature and humidity data acquisition system is shown in Figure 3.6. The basis of the measurement system is a Plessey 72.2 Mhz radiosonde unit comprising a frequency modulated transmitter, a switching mechanism and relay, and temperature and humidity elements. The mobile ground station (housed inside the towing vehicle) comprises an intermediate frequency amplifier from a SCR 522 receiver requiring 250 V A.C. and 12 V D.C. The signal is passed through an audio filter to a frequency meter, where the modulating frequency is recorded. Plates 3.6 and 3.7 show the radiosonde and ground station respectively.

The original radiosonde, where an aneroid baroswitch causes the temperature and humidity measurements to be transmitted alternately as pressure decreases during ascent, has been modified for use in the boundary-layer. The modification involving a timing device is described in Appendix III. Power for the modified radiosonde was provided by the standard 18 V water activated battery (Viz Type 1271-058) which lasts approximately four hours of continuous operation.

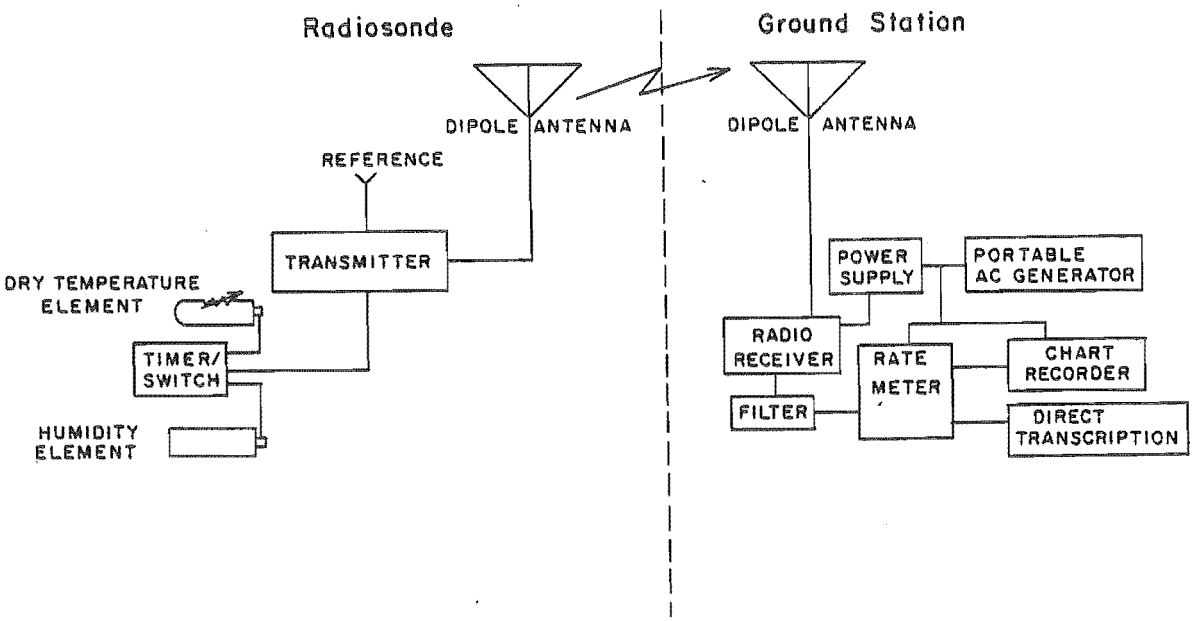

FIGURE 3.6 Block Diagram of the Data Acquisition System.

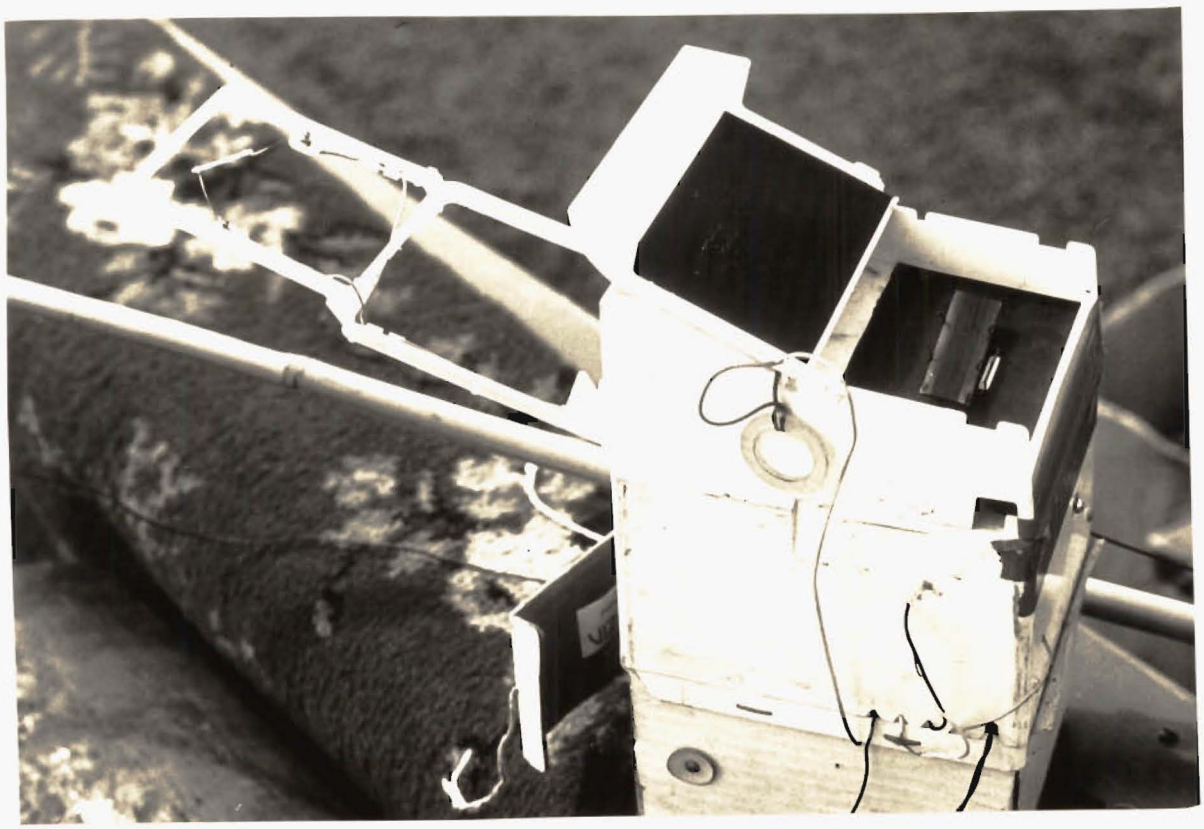

PLATE 3.6 Close-up of Radiosonde, Showing Temperature Sensor (on Outrigger) and Hygristor Filament.

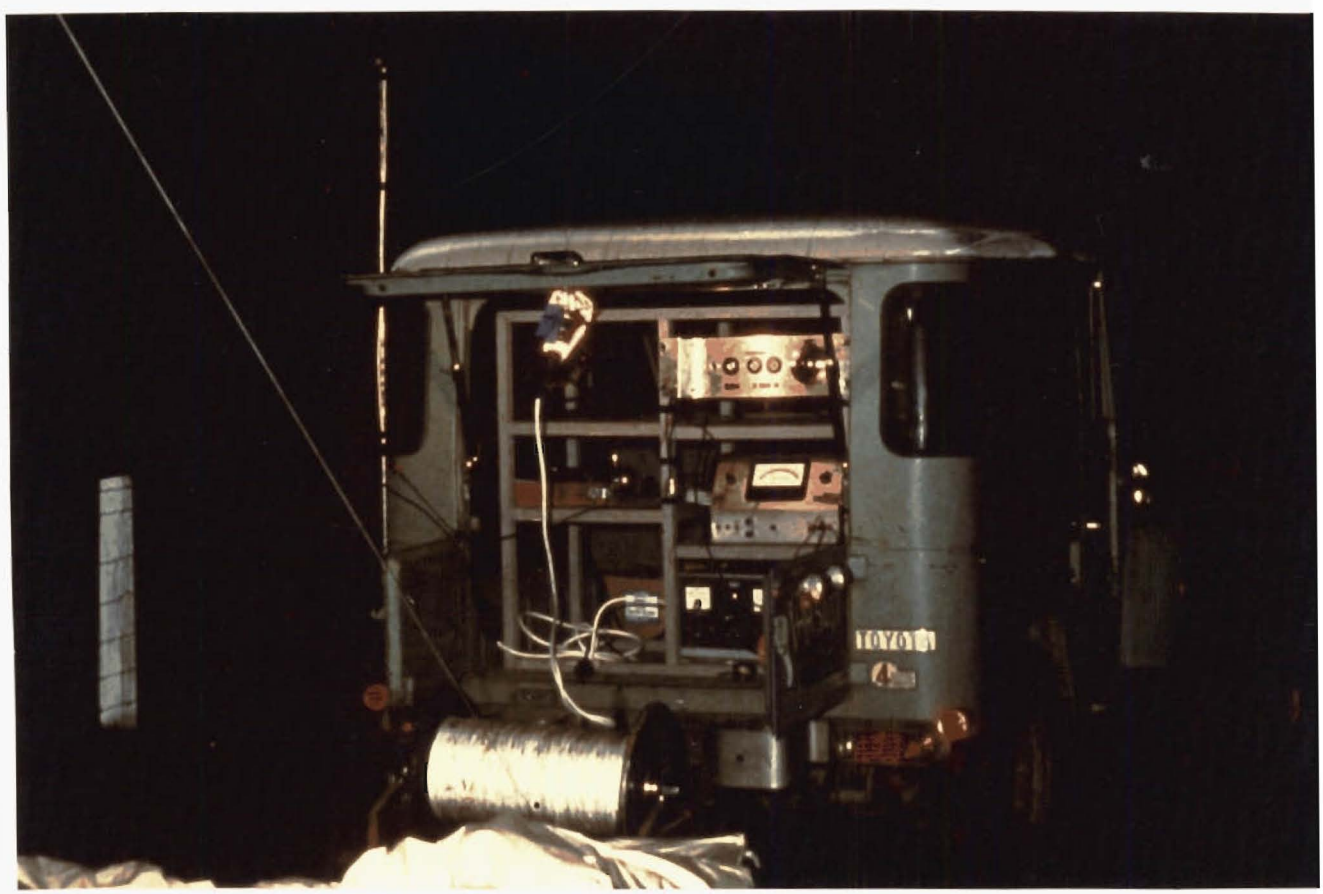

PLATE 3.7 The Ground Station. Radio Receiver is on the Top Shelf and the Frequency Meter is Below it.

The unit, weighing 850 gm complete with battery, was attached to the tether harness immediately beneath the kytoon, with the dipole antenna held torsionally rigid to prevent rotation. The given mass of payload and tether line meant that there were no problems reaching this study's maximum operational height of 500 m. Although capable of operating to 500 m, altitude restrictions below that nominated level were sometimes imposed by the Civil Aviation Authority, these restrictions being more frequent at the urban site.

Radiosonde Operation and Accuracy

The mode of operation of the equipment and its accuracy are discussed in detail in Appendix III. The radiosonde was operated according to standard New Zealand Meteorological Service procedures in a pre-determined pattern of measurements in the boundary-layer. It is considered that radiosonde temperature and humidity data are accurate to 0.5°C and 5% R.H. respectively, this accuracy and resolution similar to that offered by commercial units for which information is available. Temperature and humidity sensor characteristics are summarised in Table 3.8.

Windspeed and Direction

With payload a major consideration for kytoon performance, it became necessary to determine wind data aloft independent of further kytoon borne instrumentation. Experience with flights in the initial part of this project suggested that kytoon lift generated by wind aloft could be used indirectly to determine windspeed. Accordingly, a series of controlled experiments were made relating windspeed to kytoon aerodynamic lift. These experiments and the results are reported in Appendix III. The resultant plot of measured windspeed and kytoon lift has been used to estimate windspeed aloft to an accuracy of approximately $\pm$ 1.0 ms^{-1}, an accuracy consistent with the secondary importance of wind

TABLE 3.8 Table of Boundary Layer Kytoon Temperature and Humidity Sensor Characteristics

VARIABLE SENSED	SENSOR	ELECTRICAL ELEMENT	TOTAL RANGE	PRECISION	RESOLUTION
Temperature	White Ceramic Thermistor	Resistance	-60 to +40°C	± 0.5°C	0.1°C
Humidity	Carbon Coated Plastic Filament (Hygristor)	Resistance	0 to 100% RH	± 5% RH	1% RH

characteristics in this project.

Wind directions aloft have been simply estimated from a visual determination of kytoon orientation (assuming the kytoon is an effective vane) in relation to a compass bearing taken at ground level. The highly reflective nature of the kytoon surface ensures visibility at all levels in most conditions. When the kytoon was not visible, it was possible to obtain a broad estimate of wind direction by using the orientation of the kytoon radiosonde dipole antenna in conjunction with the ground station dipole antenna; radio signal strength being greatest when antennae were in phase. It is considered that wind direction could generally be ascertained to within $\pm 15^{o}$ with practice.

Observations of windspeed and direction were made at 100 m intervals during all radiosonde flights, except for some early flights when wind direction observations only were made.

Air Pollution

In comparison with data on the variation of air pollution concentration at ground level, relatively few measurements have been made of vertical profiles of air pollution concentration. The main reasons for this are the considerable instrumentation problems involved. Various solutions to the problem have been sought through the instrumentation of tall buildings (Giovanardi *et al.*, 1959; Nkemdirim and Lunn, 1975), of aircraft (Gartnell and Carpenter, 1955; Davidson, 1967; Olsson *et al.*, 1974) and of captive balloons (Hewson and Gill, 1943; Munger, 1951; Stewart *et al.*, 1958; Braun and Wilson, 1961; Perroud, *et al.* 1973). Problems with using buildings include a limited vertical extent and unknown convectional and air current effects, while sampling from aircraft is imprecise and expensive. Balloon sampling provides a

relatively inexpensive means of obtaining pollution concentrations in free air at relatively precise points, although the weight of instrumentation is a problem with small balloons and large balloons are difficult to use in built up areas.

Pollution sampling balloons described in the above studies are all considerably larger than the Follmer 115 kytoon used in this study, so emphasis has been placed on designing extremely light sampling equipment. A further consideration for the sampling trains employed was that they be consistent with methods currently used by the Air Pollution Section, Department of Health. In keeping with the surface based sampling described previously, kytoon pollution sampling was of smoke and nitrogen oxides respectively in the winter and summer half-years. It appears from the literature that neither of these pollutants have been sampled from balloon systems before.

Methods employed on the kytoon system for smoke and nitrogen oxides determination and operational procedures are described in detail in Appendix III. Both systems rely on a standard type of pollution sampling train involving the following elements:-

a) an air mover or pump,
b) a flow measuring device or meter,
c) a sample collector, and,
d) some form of contaminant detector.

Concentration of pollutant is then obtained from:-

$$C = W/V \qquad \ldots\ldots 3.3$$

where, C - pollutant concentration ($\mu g\ m^{-3}$), W - total weight of pollutant (μg), and, V - total volume of air moved (m^3).

THE DATA COLLECTION PROGRAMME

Near-Surface Observations

The observational programme ran semi-continuously from February, 1978 to September, 1979. Continuous data collection (except for occasional loss of record through equipment malfunction) occurred over two summer/autumn periods and two winter/early spring periods, including 2 February - 4 April, 1978; 13 July - 6 October, 1978; 7 February - 27 April, 1979 and 22 June - 13 September, 1979. The first of these four periods of observation was of limited use owing to the fact that the instrumented kytoon was not yet operational.

While clear sky conditions were sought in order to isolate atmospheric variables responsible for radiation variations, equipment was operated continuously during these periods for two major reasons.

a) The time involved in re-establishing operations at the two sites after a close down was prohibitive, particularly given that clear stable conditions in Canterbury often establish rapidly after the passage of a cold front and that such conditions seldom last for longer than two days. In addition, the presence of local stratocumulus over Christchurch in otherwise clear conditions is difficult to predict, often appearing and disappearing rapidly, or extending only partly across the city from the coast.

b) Equipment is usually more reliable in continuous rather than short period operation. Particular problems in re-establishing operation include recorder stability and moisture in equipment. By maintaining a programme such as this it was possible to include in the total record observations where only a few hours data were available.

Another advantage was that, at the expense of slightly more maintenance time, it was possible to free manpower during clear weather periods for other essential duties including kytoon operation.

Selection of clear weather periods was made by reference to the N.Z.M.S. hourly record of cloud amount in octas recorded at Christchurch International Airport. Generally speaking, only periods with no observed cloud were included in the record, although intervals with no more than one eighth cloud in an otherwide completely clear record were admitted. Additionally, only days with more than ten continuous hours fitting the above criteria were included. In this way it was possible to extract 720 hours from the total record. A breakdown of the total available record is given in Table 3.9 . Since paired data was always used, and equipment failure occasionally occurred, the actual data base was less than this total. In the case of IR↓, only approximately 600 hours was available.

Kytoon Observations

Whenever cloud free intervals occurred within the overall data collection periods, observations with the instrumented kytoon system were initiated. Kytoon observations were generally paired, with flights being made from the respective Central City and Lincoln Sites as close in time as possible. Profiles were corrected later for time progressions (approximately an hour elapsed) in the manner described in Appendix IV. When clear weather persisted, paired flights continued at regular intervals until interrupted. At the Central City Site, the sequence of operation was usually an air pollution sampling flight followed immediately by a radiosonde flight. At Lincoln, radiosonde flights only were undertaken, this because none of the initial air

TABLE 3.9 The Data Record

OBSERVATIONAL PERIOD	TOTAL HRS	CLEAR HRS	% TOTAL	COMPLETE DAYS	PART DAYS
2 Feb - 4 Apr 1978	1,440	72	5.0	3	0
13 Jul - 6 Oct 1978	2,040	237	11.6	8	5
7 Feb - 27 Apr 1979	1,896	251	13.2	8	4
22 Jun - 13 Sep 1979	1,992	160	8.0	5	6
	7,368	720	9.8	24	15

sampling flights showed any detectable pollution. Surface based sampling (Table 3.7) also suggested pollution aloft would be below the level of detection.

During kytoon operations 82 radiosonde/wind data flights were made, slightly over half at the Central City Site. Thirty-five air pollution sampling flights were made. Of all flights, approximately two thirds were made during night-time hours.

CHAPTER 4

URBAN-RURAL TEMPERATURE VARIATIONS IN THE CHRISTCHURCH AREA

INTRODUCTION

At any given time the downward flux density of infra-red radiation under clear skies is itself composed of the partial flux densities due to the presence in the atmosphere of H_2O, CO_2, O_3, aerosol and other trace gas emitters, each radiating proportionally to temperature. This section of the thesis examines certain of these variables as background to a detailed analysis of IR↓ across Christchurch. This chapter is concerned with urban-rural variations in temperature through time and in the vertical dimension in response to seasonal and diurnal changes.

Following Oke (1976), the terms 'urban canopy' and 'urban boundary-layer' are used to distinguish between the layers below, and above, roof level respectively. Oke suggests that the urban canopy is dominated by processes operating at the microscale largely related to site materials and building geometry, while the urban boundary-layer is a mesoscale phenomenon resulting from the presence of an urban area at its lower boundary and the consequent interchange of heat and matter. This modified layer is conceived to develop as an advective internal boundary-layer and may remain intact over downwind rural areas as an 'urban plume' overlying the rural boundary layer (Figure 4.1).

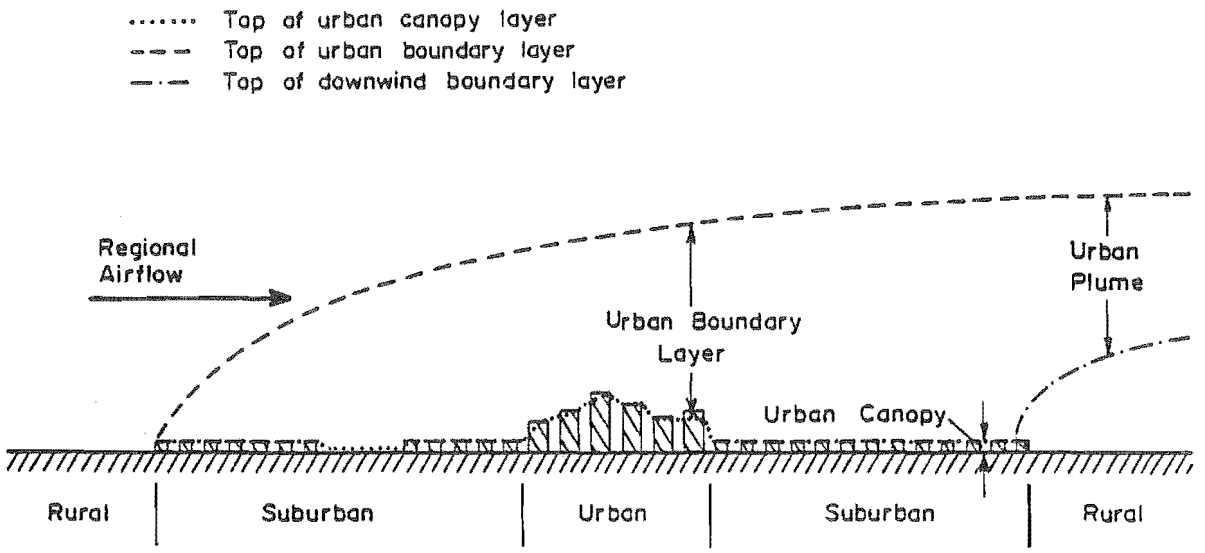

After T. R. Oke 1976.

FIGURE 4.1 Distinction Between Urban Canopy-layer and Urban Boundary-layer.

Although IR↓ at the surface depends mainly on variations within the boundary-layer, the urban canopy is also considered here because it has important influences on the boundary-layer and because many previous studies of urban temperature have considered only the urban canopy. In this chapter all data collected at screen level in the city refer to the urban canopy, while kytoon observations are almost entirely in the boundary-layer. There is no synonymous rural canopy, and all data, including that collected at screen level, are considered to have been collected in the rural boundary-layer. Spatial patterns of temperature across the Christchurch urban-rural area have already been discussed in Chapter 2. The present discussion relates to the relative behaviour of temperature at the discrete urban and rural representative sites and in the boundary-layer immediately above these sites.

URBAN-RURAL VARIATIONS IN NEAR SURFACE TEMPERATURES

Previous Work

The urban heat island effect is the most obvious atmospheric modification attributed to urbanization. The Christchurch urban heat island has been studied previously by Sham (1968), Kingham (1969), Tapper (1976) and Tuller (1977). All of these investigators have found considerable urban-rural differences. Sham found a maximum heat island intensity of up to 6.3° C, with the intensity being governed by meteorological factors such as windspeed and cloudiness. Kingham, in a limited number of motor vehicle transects, found urban temperature excesses ranging between 2.2° C and 5.6° C. Tapper, using data from

two continuously recording stations, found an average hourly all weather heat island in Christchurch of 0.6° C over a six month summer to winter period, although it was suspected that the 'rural' station was subject to urban influences. Tapper also found a clear weather average maximum heat island intensity of 5.4° C. Tuller found a maximum heat island intensity of 5.4° C averaged over two wintertime motor vehical traverses.

General Results

Table 4.1 tabulates the mean hourly temperature by month for all clear weather data from the two years of observations. This indicates the effect of a heat island which gives differences in hourly average temperature for each month statistically significant at the 0.01 level using the t-test:-

$$\mu \text{ urban} = \mu \text{ rural},$$

where the observations are paired variates and μ is the population mean.

Weighted term means (allowing for monthly differences in observation numbers) for the whole study are 10.3° C at the urban site and 7.7° C at the rural site, a difference of 2.6° C over the term. While a large urban-rural difference, it appears in keeping with an all-weather average 1.0° C urban excess temperature quoted by Geiger (1973) for a number of northern hemisphere cities. It is also more than the 0.6° C all-weather average previously reported for an urban and semi-rural station in Christchurch (Tapper, 1976). Perhaps surprisingly, there is no observed trend for an increasing heat island intensity toward the winter months in Table 4.1, although some of the largest observed mean hourly differences occur during the month

TABLE 4.1 Hourly Clear Weather Temperatures by Month (^{o} C)

	FEB		MAR		APR		JUL		AUG		SEPT	
HR TO	L	CC	L	CC	L	CC	L	CC	L	CC	L	CC
01	13.8	18.0	12.2	15.2	5.2	10.5	1.6	3.3	1.0	3.6	4.0	6.2
02	13.0	17.2	11.7	14.8	4.2	9.7	1.2	2.4	0.2	3.1	3.5	5.7
03	12.8	16.3	10.7	14.8	3.1	9.3	0.7	2.3	0.1	2.6	3.2	5.5
04	12.7	16.3	10.2	14.5	2.4	8.3	0.4	1.7	-0.2	2.2	3.0	5.2
05	11.5	15.3	10.2	14.3	1.9	7.4	0.3	1.5	-0.4	2.0	2.5	5.1
06	11.3	15.2	10.5	14.0	1.3	6.8	0.0	1.1	-0.7	1.4	2.0	5.0
07	11.5	14.8	9.8	14.5	0.8	6.4	-0.2	0.5	-1.0	1.0	1.8	4.7
08	11.7	14.5	10.2	14.0	1.1	6.3	-0.2	0.1	-1.1	0.7	2.5	4.7
09	14.0	15.8	12.0	14.8	4.1	7.4	-0.2	-0.1	0.0	1.2	4.8	5.5
10	17.5	18.5	13.7	17.5	7.7	10.2	1.5	1.0	3.0	4.3	8.5	8.0
11	19.8	21.0	15.0	19.0	10.9	13.1	4.2	3.6	5.6	7.6	10.5	10.7
12	21.3	22.5	17.2	20.5	12.6	14.6	6.2	6.7	7.9	9.4	11.8	12.2
13	22.0	23.0	18.5	22.0	13.5	15.7	7.3	8.2	9.2	10.7	12.2	12.7
14	22.3	23.3	19.0	22.0	14.0	16.0	8.1	9.0	9.9	11.4	12.8	12.8
15	22.3	23.3	19.5	22.0	13.8	16.0	8.2	9.4	10.0	11.7	12.8	12.8
16	21.8	23.3	20.5	20.8	13.5	15.7	8.2	9.4	9.6	11.7	12.5	12.5
17	21.2	23.2	19.7	20.0	12.5	15.1	7.1	8.8	8.5	10.7	11.5	12.0
18	20.6	22.7	19.5	20.2	9.5	14.1	5.2	7.6	6.9	9.7	10.0	11.3
19	19.8	22.2	18.8	20.0	9.2	13.2	3.9	6.5	5.0	8.7	8.2	10.5
20	19.0	21.5	16.7	20.3	7.7	12.2	3.1	5.7	4.2	7.9	7.0	9.5
21	18.0	20.0	15.2	19.0	6.9	12.5	2.7	5.1	3.7	7.5	5.5	8.5
22	17.3	19.7	14.5	18.3	6.4	11.3	2.1	5.0	3.5	7.0	4.5	7.5
23	16.3	19.3	13.7	17.0	5.9	10.8	1.9	4.3	3.0	6.5	4.0	7.0
00	16.1	19.0	12.5	16.2	5.7	10.5	1.7	3.4	2.9	6.1	3.0	6.5
$\bar{X}$	17.0	19.4	14.7	18.5	7.2	11.4	3.2	4.4	3.8	6.2	6.8	8.4
$\bar{X}_{CC} - \bar{X}_{L}$	2.4		3.8		4.2		1.2		2.4		1.6	

Weighted term means $\bar{X}_{CC}$ $\bar{X}_{L}$

10.3 7.7

Term difference 2.6^{o}C

of April.

The Effect of City Size

The mean maximum urban-rural difference (ΔTu-r (max)) is one of the more frequently used comparative indices of the urban heat island effect. Oke (1973, 1976) addressed the question of the effect of city size on ΔTu-r, showing ΔTu-r (max) to be highly correlated with the logarithm of population (P) where windspeed ($\bar{u}$) approaches zero. Figure 4.2 shows two different slopes and equations obtained by Oke for North American and European cities. The mean maximum winter heat island intensity of 5.1° C observed in the current data (37 clear nights with $\bar{u} \sim 0$) and the value of 5.4° C obtained in a previous study (Tapper, 1976) have been plotted along with data for other New Zealand cities (McBoyle, 1970), to give a relationship for New Zealand.

In statistical models such as these, population appears to be a surrogate for the physical structure of the centre of cities, including such features as the sky view factor, amount of green area, type of surface material and amount of artificial heat released. As such, the relative position of slopes for the European and New Zealand data suggests basic differences in city structure from North American cities. Oke (1976a) attributes differing heat island intensities between North America and European cities of similar population to factors such as greater surface evaporation from more vegetation, lower thermal admittances of urban surfaces and less artificial heat generation in European cities. Although the New Zealand data base is limited, it seems that the heat island intensity for a given population is lower still than the European case, for similar reasons.

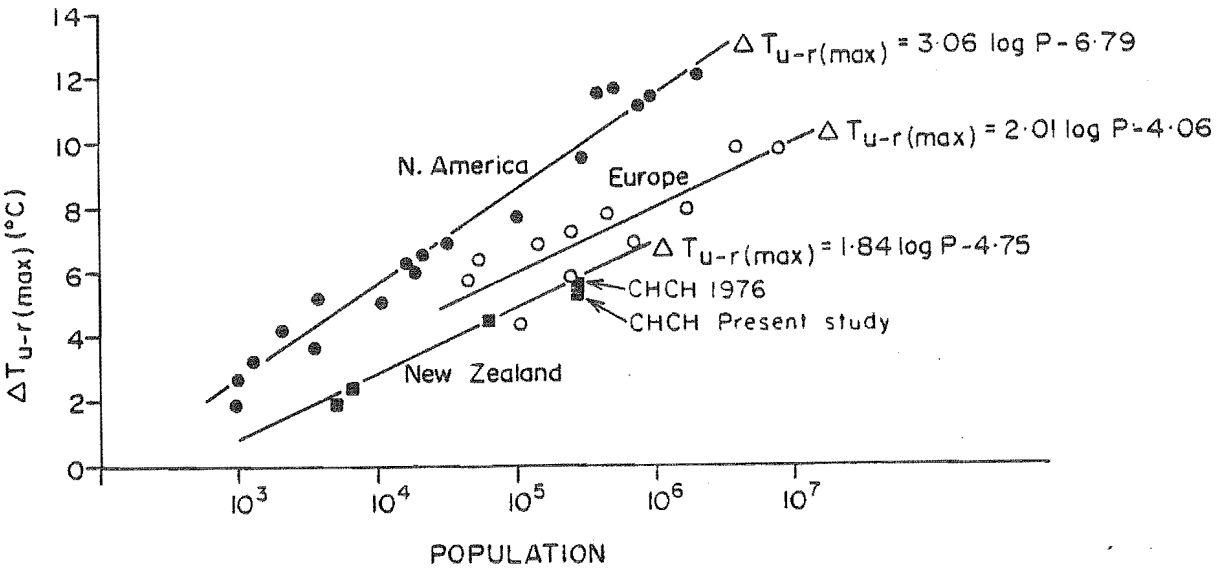

FIGURE 4.2 Relationship Between Population and Intensity of the Urban Heat Island in North America, Europe and New Zealand.

Diurnal Variations and Urban-Rural Cooling Rates

While a detailed consideration of heat island morphology at an instant in time (as in Chapter 2) or absolute magnitudes (above) tend to highlight special landuse or scale effects, they are not especially helpful in a search for governing mechanisms. A close examination of the temporal nature of heat island behaviour, particularly of urban-rural cooling rates, enables the development and decay of the heat island to be viewed in terms of fundamental differences in energy exchange rates.

Data from Table 4.1 has been reduced to summer and winter diurnal temperature curves for the Lincoln and Central City Site (Figure 4.3a and b). The equinoxial month of April has been excluded from the summary data. Diurnal patterns are similar for both summer and winter plots. In the summer case, ΔT_{u-r} is at a minimum in the early afternoon and reaches a maximum some 3 - 5 h after sunset. These findings are similar to those of Mitchell (1962) who suggested that the trend was due to differing thermal capacities of nearby surfaces at each site; rural surfaces heating and cooling more rapidly than urban surfaces. This is unfortunately an overly simplistic view of the situation as the following discussion will indicate.

The winter diurnal temperature pattern is different from that of summer in one important respect. While ΔT_{u-r} (max) is once again 3 - 5 h after sunset, the minimum ΔT_{u-r} has shifted forward to mid-morning and has become small indeed. This distinct summer-winter pattern infers some influence over and above differing heating rates of surfaces. Without detailed further analysis here, it appears that this may be an urban canopy layer effect, where a relatively low winter

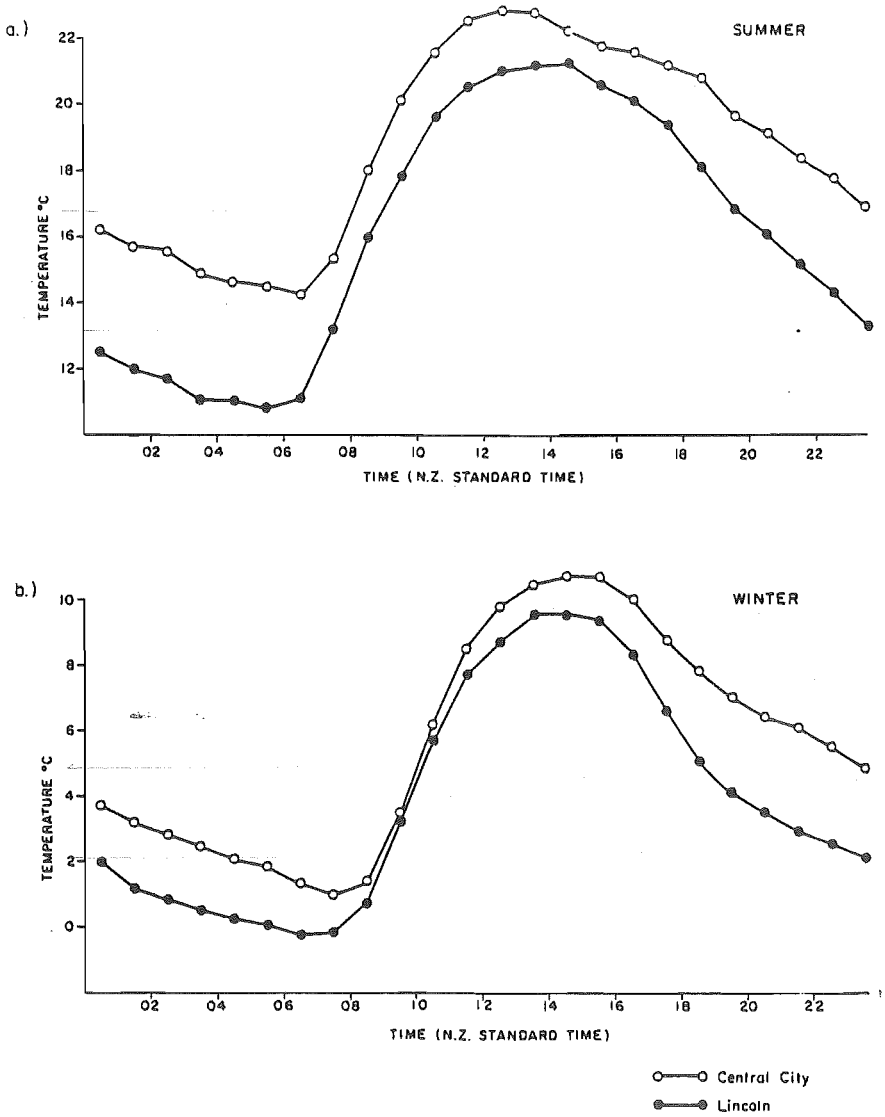

FIGURE 4.3 Diurnal Screen Level Temperature Trends at the Urban and Rural Representative Sites in, a) Clear Summer Weather, and b) Clear Winter Weather.

sun ($Z > 70^{o}$ for most of the morning) does not reach below roof level to ground level horizontal urban surfaces until relatively late in the morning compared with an unobstructed rural area. This would have obvious effects on heating rates within urban canyons.

The investigation of nocturnal cooling rates to a $\Delta Tu\text{-}r$ (max) is important in determination of the energy dissipation capabilities of various surface types. Clear weather urban and rural cooling rates for the average summer and winter case are shown in Figures 4.4a and b. In the summer case (Figure 4.4a) the urban cooling rate is a relatively constant 0.5^{o} C h^{-1} from 4h before sunset to 8 h after sunset. The rural cooling rate diverges strongly to show its greatest value at sunset, followed by a decline where it approaches the urban cooling rate approximately 5 h after sunset. Correspondingly, $\Delta Tu\text{-}r$ reaches its maximum at that time.

In the winter case, both sites pass from a net heating to a cooling rate 1 to 2 h before sunset and both experience an increasing rate of cooling to 1 h after sunset, although the increase of rural cooling is more extreme. 4 h from sunset the cooling rate for both sites has declined to 0.5^{o} C h^{-1} and the $\Delta Tu\text{-}r$ (max) occurs at that time. Reasons for the urban cooling rate increasing markedly in winter near sunset and not in summer are unclear, but may relate to a larger surface - sky temperature differential than occurs in summer. This is supported in part by the fact that rural cooling rates are also greater around sunset in winter than summer.

Oke and Maxwell (1975) have attempted an explanation of similar patterns for Montreal and Vancouver. They suggest that on calm, clear nights, the principal heat loss from the rural surface will

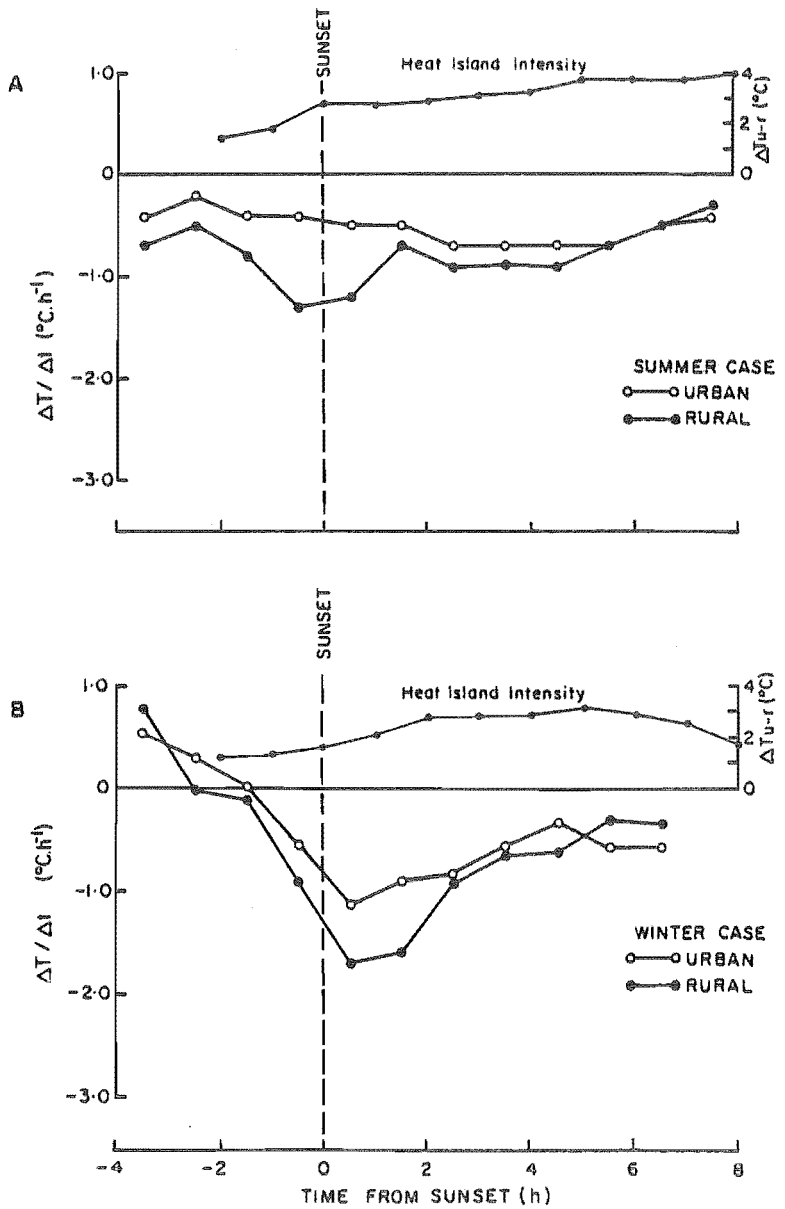

FIGURE 4.4 Clear Weather Urban and Rural Cooling Rates for, a) The Average Summer Case, and b) The Average Winter Case.

be net infra-red radiation to an open and radiatively cold night sky. As the rural surface does not store large amounts of energy by day due to the thermal nature of the surface and the fact that most available energy is used in evaporation from moist rural surfaces, (Chapter 2, Figure 2.9), the energy store is rapidly expended in the early evening when the surface - sky temperature differential is greatest and solar input is absent. In addition, any slight regional airflow present adds to surface cooling. Urban cooling rates by comparison depend less upon the nature of the sky and any regional airflow. This is especially so within the urban canopy, where the radiative environment is often dominated by surrounding man-made structures and subsequently lower sky view factors. Additionally, the urban fabric is better able to store heat for subsequent release into the atmosphere and the heated air below roof-level often remains stagnant.

The Effect of Thermal Admittance

As described above, the urban heat island is at least partially due to the special thermal properties of building materials. Urban surfaces such as concrete, brick and tarseal are characterised by large volumetric heat capacities (c) [$c = \rho c$, where ρ is the density and c the specific heat of a material], and high thermal conductivity k_s. During the day therefore, urban surfaces allow more penetration and storage of heat, while at night the upward directed heat flux helps to maintain higher surface temperatures and retard urban cooling.

Oke and Maxwell (1975) describe a method for approximating the thermal admittances of urban and rural surfaces based on Brunt's (1941) surface cooling equation. At night and in the absence of advection, the surface energy balance can be written:-

$$I = H + LE + G \quad \ldots 4.1$$

where IR* is the net infra-red radiation flux density. In very light winds and in the absence of surface condensation and artificial heating, the surface loss of infra-red radiation (I) is balanced by an upward flux of stored heat (G). Under such assumptions, Brunt (1941) has theoretically determined surface cooling from the equation:-

$$\Delta T_{t-s} = \frac{-2}{\pi^{\frac{1}{2}}} \cdot \frac{I}{(k_s c_s)^{\frac{1}{2}}} t^{\frac{1}{2}} \quad \ldots 4.2$$

where ΔT_{t-s} is the decrease in temperature in the time (t) from sunset, and the product $(k_s c_s)^{\frac{1}{2}}$ is the material's thermal admittance. From a knowledge of ΔT_{t-s} and I with t and assuming constancy of k_s and c_s, it is therefore possible to determine thermal admittance from equation 4.2. In the present application such a thermal admittance might be representative of an integration of a multitude of urban or rural surfaces.

Figure 4.5 shows the mean winter cooling curve for the urban and rural sites from sunset and the best-fit Brunt cooling curves for each data set. For input to Equation 4.2 a mean measured value for I of -50 Wm^{-2} was determined for both sites. The best fit with observed rural data was achieved with a thermal admittance of 1500 $Wm^{-2} S^{\frac{1}{2}} {}^{o}K^{-1}$, a value identical to that given by Lettau (1951) for a sandy clay with 15 per cent moisture.

The urban situation is quite different. An obviously higher thermal admittance is required and the best approximation possible was a value of 2000 $Wm^{-2} S^{\frac{1}{2}} {}^{o}K^{-1}$, part way between the rural value and a value of 2380 $Wm^{-2} S^{\frac{1}{2}} {}^{o}K^{-1}$ determined by Ingersoll, *et al.* (1948) for a concrete slab. The fit however, is not particularly good, with

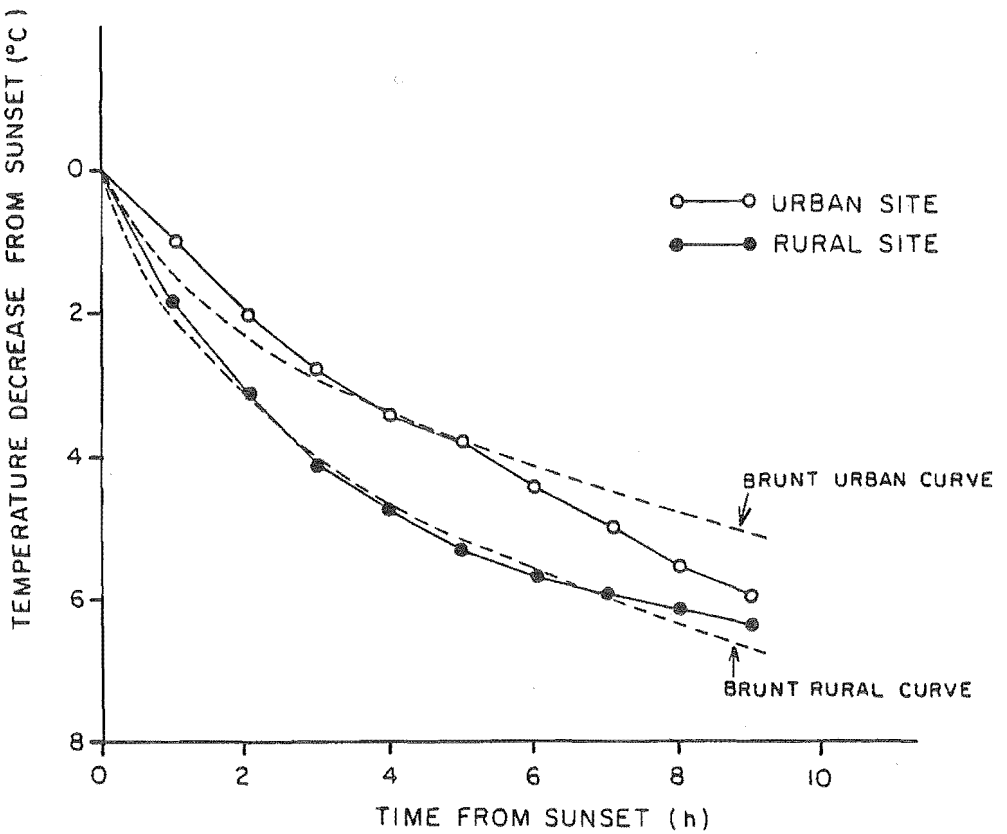

FIGURE 4.5 Clear Weather Cooling Curves for the Urban and Rural Sites (Solid Lines), with Best Theoretical Approximations Shown (Dashed Lines).

actual urban cooling being substantially less than predicted in the initial 4 h and greater than predicted subsequently. Unlike the square root of time decay for the rural observed data, the urban decrease is more nearly linear.

Similar differences in the urban and rural temperature decrease were noted by Oke and Maxwell (1975), who suggested processes separate from those governing normal Brunt-type cooling were operating in the urban area. They suggested that these processes operated to flatten the measured cooling curve and could conceivably include the release of artificial heat or the transfer of sensible heat away from the urban surface. These possibilities appear equally valid for Christchurch, where reasonably high levels of artificial heat input occur near the city centre and there is evidence of sensible heating (Chapter 2, Figure 2.10). As Oke and Maxwell remark, the action of processes such as these would undermine the validity of assumptions underlying the derivation of Equation 4.2.

URBAN-RURAL BOUNDARY LAYER TEMPERATURE VARIATIONS

Introduction

Because of the substantial data base (82 individual kytoon flights), most of the subsequent analysis is of summarised data, without recourse to individual profile characteristics. Plotted individual flight data is included in Appendix V. All flights were undertaken during clear weather, 48 at night, 26 during the middle of the day and the remainder under conditions of profile transition (most during the morning inversion decay).

One convenient method of classifying temperature profiles is according to a lapse rate (^{o} C 100 m^{-1}) to give a broad indication of stability. For this analysis three types of static stability have been recognized:-

unstable : lapse rate greater than the dry adiabatic lapse rate (0.98^{o} C 100 m^{-1}).

stable : lapse rate between the dry adiabat and isothermal.

inversion : lapse rate showing an increase of temperature with height.

In all cases the degree of stability was assessed according to the lapse rate between the surface and 100 m, or the surface and the top of any surface based inversion present. The subsequent analysis excludes all transitional profiles.

General Results

Nocturnal Profiles

Table 4.2a outlines the distribution of nocturnal profiles within the three classifications, for all flights at the individual sites, and for those where a paired flight at the other site was available (offering easier urban-rural comparison). Of immediate note is the dominant occurrence of inversion conditions at both sites. None of the rural nocturnal profiles exhibited other than inversion characteristics, while only three nocturnal urban profiles out of 27 showed stable or unstable characteristics. This especially high frequency of nocturnal inversions within the Christchurch urban area is somewhat unexpected in view of observations elsewhere. Duckworth and Sandberg (1954) found radiation inversions in 30 out of 32 rural temperature soundings and in only seven out of 32 urban soundings undertaken in varying weather conditions in and near San Francisco. De Marrais (1961) found that whereas

TABLE 4.2a Nocturnal Profile Characteristics (Paired Profiles in Brackets)

	INVERSION	STABLE	UNSTABLE
Central City Site	24 (15)	2 (1)	1 (0)
Lincoln Site	21 (16)	0 (0)	0 (0)

TABLE 4.2b Percent Occurrence of Nocturnal Inversion Strengths (^{o}C 100 m^{-1} to top of inversion - Paired Profiles in Brackets)

	0-2	2.1-4.0	4.1-6.0	6.1-8.0	8.1-10.0	10.1-12.0	12.1-14.0	>14.1
Central City Site	0(0)	26(40)	21(13)	25(20)	12(7)	4(0)	8(13)	4(7)
Lincoln Site	5(0)	14(6)	24(25)	19(19)	6(6)	9(12)	9(13)	14(19)

TABLE 4.2c Statistics of Nocturnal Inversion Characteristics (Paired Profiles Only)

CHARACTERISTIC		CENTRAL CITY SITE	LINCOLN SITE
Depth of Inversion (m)			
All data	$\bar{X}$	59	79
	σ	28	54
	Range	15 - 110	25 - 200
	N	16	16
Winter	$\bar{X}$	52	92
	σ	26	44
	Range	15 - 95	35 - 200
	N	11	11
Summer	$\bar{X}$	74	63
	σ	28	69
	Range	35 - 110	25 - 200
	N	5	5
Inversion Temperature Increase (^{o}C)			
	$\bar{X}$	4.1	5.2
	σ	2.1	1.8
	Range	0.5 - 8.5	2.8 - 8.6
Inversion Strengths (^{o}C 100 m^{-1})			
	$\bar{X}$	6.7	9.3
	σ	3.8	4.6
	Range	2.1 - 15.1	1.2 - 18.0

nocturnal inversions were frequent in most weather conditions over rural land uses, they were comparatively rare in the Louisville urban area. Similar observations were made by Munn and Stewart (1967) for sites in Southern Ontario, Vdovin (1973) for Leningrad, and Machalek (1974) for Vienna. It would appear that the characteristics of the Christchurch urban area (low building density and high evaporative fraction) discussed previously are at least partially responsible for the high proportion of nocturnal inversions. In addition, all flights in the present study were undertaken in conditions conducive to the development of radiational inversions.

Strength characteristics of nocturnal inversion profiles have been examined in greater detail in Table 4.2b. This table indicates greater urban effects, with urban inversion strengths considerably less than rural. For example, 40% of paired urban profiles exhibit inversion strengths of less than 4.1° C 100 m^{-1} compared with 6% of rural profiles. Conversely, only 7% of urban profiles showed inversion strengths greater than 14.1° C 100 m^{-1} as against 19% at the rural site. General urban and rural inversion characteristics have been summarised in Table 4.2c. The Central City Site exhibits overall lower inversions particularly during wintertime (52 m as against 92 m at Lincoln), smaller temperature increases to the top of the inversion and a smaller mean inversion intensity (6.7° C 100 m^{-1} compared with 9.3° C 100 m^{-1} at Lincoln). These features all appear to be related to atmospheric heat input in urban areas.

Daytime Profiles

The distribution of daytime temperature profiles within the stability classification scheme is given in Table 4.3a. Unstable conditions associated with lapse profiles are the dominant stability

TABLE 4.3a Daytime Profile Characteristics
(Paired Profiles in Brackets)

	INVERSION	STABLE	UNSTABLE
Central City Site	1 (0)	0 (1)	15 (8)
Lincoln Site	0 (0)	1 (1)	9 (8)

TABLE 4.3b Percent Occurrence of Lapse Strengths under Unstable Conditions (Temperature decrease to 100 m in ^{o}C 100 m^{-1} Paired Profiles in Brackets)

	1.1-3.0	3.1-5.0	5.1-7.0	7.1-9.0	9.1-11.0
Central City Site	27(37)	33(37)	20(26)	13 (0)	7 (0)
Lincoln Site	40(37)	20(20)	30 (20)	10 (10)	0 (0)

TABLE 4.3c Daytime Lapse Strength Characteristics
(^{o}C 100 m^{-1} - Paired Profiles only)

	CENTRAL CITY SITE	LINCOLN SITE
$\bar{X}$	3.75	4.25
σ	1.6	4.4
Range	1.2-7.0	2.0-8.6

classification for both urban and rural sites. A consideration of daytime lapse rate strengths (Tables 4.3b and c) reveals small urban-rural differences with rural lapse rates tending to be slightly stronger (mean urban lapse rate of 3.75^{o} C 100 m^{-1} compared with 4.25^{o} C 100 m^{-1}). These results are consistent with the daytime observations of De Marrais (1961).

Elevated Inversions

Analysis of profile data thus far has concentrated largely on the lowest 100 m of the boundary-layer. Many profiles however indicate the presence of one or more elevated inversions at some distance above the surface, and these inversions appear to occur largely irrespective of time of day. Table 4.4 gives the percent occurrence of elevated inversions on a diurnal basis for both experimental sites, indicating that the phenomenon is more frequent over the Christchurch urban area and in summer. Bornstein (1968) and Clarke (1969) found similar patterns for New York and Cincinnati respectively, which Clarke attempted to explain in terms of a model proposed by Summers (1965). In this model, input of heat into the urban atmosphere, combined with enhanced turbulent mixing over rough urban surfaces, forms an adiabatic mixing layer which progressively deepens with distance from the upwind rural-urban boundary. Above the urban boundary-layer a new inversion forms, becoming the elevated inversion. This explanation does not appear entirely satisfactory in the Christchurch situation, as there is seldom the formation of a surface based adiabatically mixed layer over the city in the manner described. In addition, the relatively high frequency of elevated inversions over the rural site, particularly during summer, suggests that the reasons for occurrence are not entirely urban related, but rather may be due to mesoscale influences such as

TABLE 4.4 Percent Occurrence of Elevated Inversions (to 500 metres)

	NOCTURNAL PROFILES	DAYTIME PROFILES	COMBINED
All Profiles			
Central City Site (N = 51)	37	50	42
Lincoln Site (N = 32)	23	22	22
Summer Profiles Only			
Central City Site (N = 14)	100	85	93
Lincoln Site (N = 8)	60	66	63

the complications introduced by the proximity of the land-sea boundary. A fuller understanding of mechanisms responsible for the development of these elevated inversions awaits a depth of study not possible in this thesis.

Urban Boundary-Layer Temperature Excess

General

The magnitude of near surface urban temperature excess has been discussed previously in this chapter. An extension of the investigation of urban excess temperatures into the vertical is essential, not only for a fuller understanding of the urban heat island, but also because variations in vertical temperature gradients are capable of producing marked differences in $IR\downarrow$ received at the surface from clear skies as Moller (1951) has shown.

Figures 4.6a and b are typical paired urban and rural profiles, in this case from the afternoon and evening of 10 July, 1979, the day of the heat island modelling exercise. In the daytime situation (1440 h) the temperature profiles are similar, exhibiting a typically weak winter lapse to 100 m with relatively isothermal conditions to 400 m. By comparison, the nocturnal profiles (2230 h) show a consistent urban excess warmth to approximately 350 m where the profiles merge. At both sites surface based temperature inversions are present. Because similar consideration of all paired profiles is laborious and potentially not very rewarding with regard to explaining urban-rural temperature variations, composite profiles were constructed by interpolating temperature differences at 25 m intervals in the manner of Bornstein (1968) and Oke and East (1971). These composites can then be stratified according to various possible influencing factors. This method-

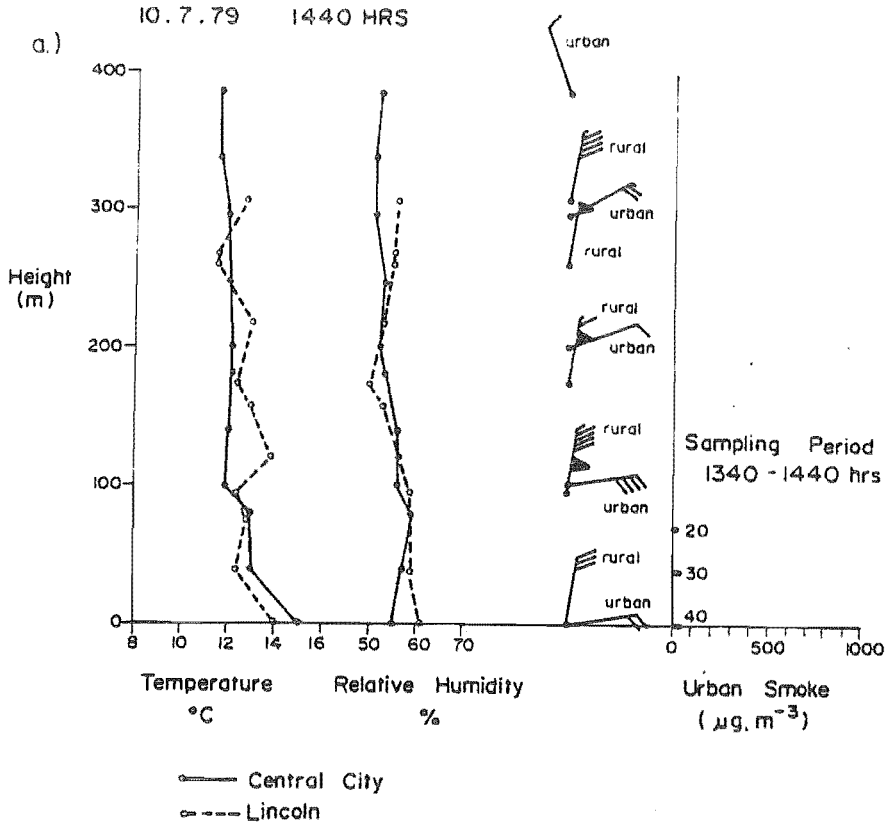

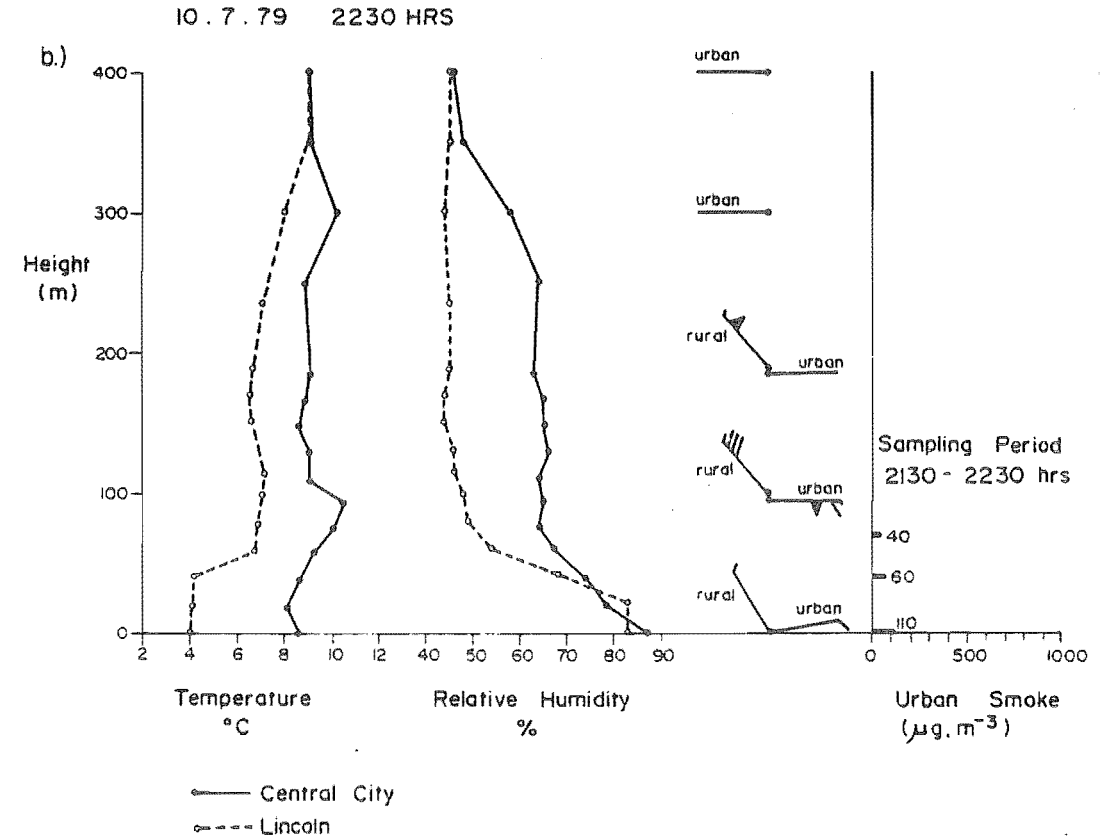

FIGURE 4.6 Paired Urban and Rural Kytoon Profiles for 10 July, 1979. Showing a) The 1440 h and

ology can only be properly accomplished if occurrences where advective warming occurs at one site but not the other, are excluded from the analysis. To this end four paired flights where north-westerly winds were warming the rural boundary-layer have been separated from the rest of the data base and will be discussed separately. The following analysis relates mainly to the 23 remaining paired profiles.

Nocturnal Vertical Temperature Excess

Figure 4.7a is a composite of all nocturnal data, showing the mean urban excess temperature and standard deviation at 25 m increments to 500 m. Above 400 m, lack of data precludes calculation of standard deviations and accordingly inferences cannot be made above that level. This generalised picture for all data shows a maximum urban heat island of almost 2.5° C near the surface, decreasing only slowly to 100 m (2.2° C), apart from a marked discontinuity at 25 m. Above 100 m the profile shows an almost linear decrease in urban excess temperature to zero at 290 m. Above 290 m an urban temperature deficit exists to 350 m, although the deficit (always $\leq$ 0.25° C) is within the accuracy of the recording system. Similar extensions of urban warmth into the atmosphere have been noted by many other investigators, including Duckworth and Sandberg (1954) for San Francisco, De Marrais (1961) for Louisville, Clarke (1967) for Cincinnati, Bornstein (1968) for New York, Oke and East (1971) for Montreal, and more recently Vdovin (1973) and Shklyarevich (1974) for Leningrad, and Dirks (1974) for St Louis.

Figure 4.7b gives mean urban excess temperatures near sunrise for New York (Bornstein, 1968) and Montreal (Oke and East, 1971). Unlike the present study neither of these studies was restricted to clear weather data only. The similarity between the Christchurch urban

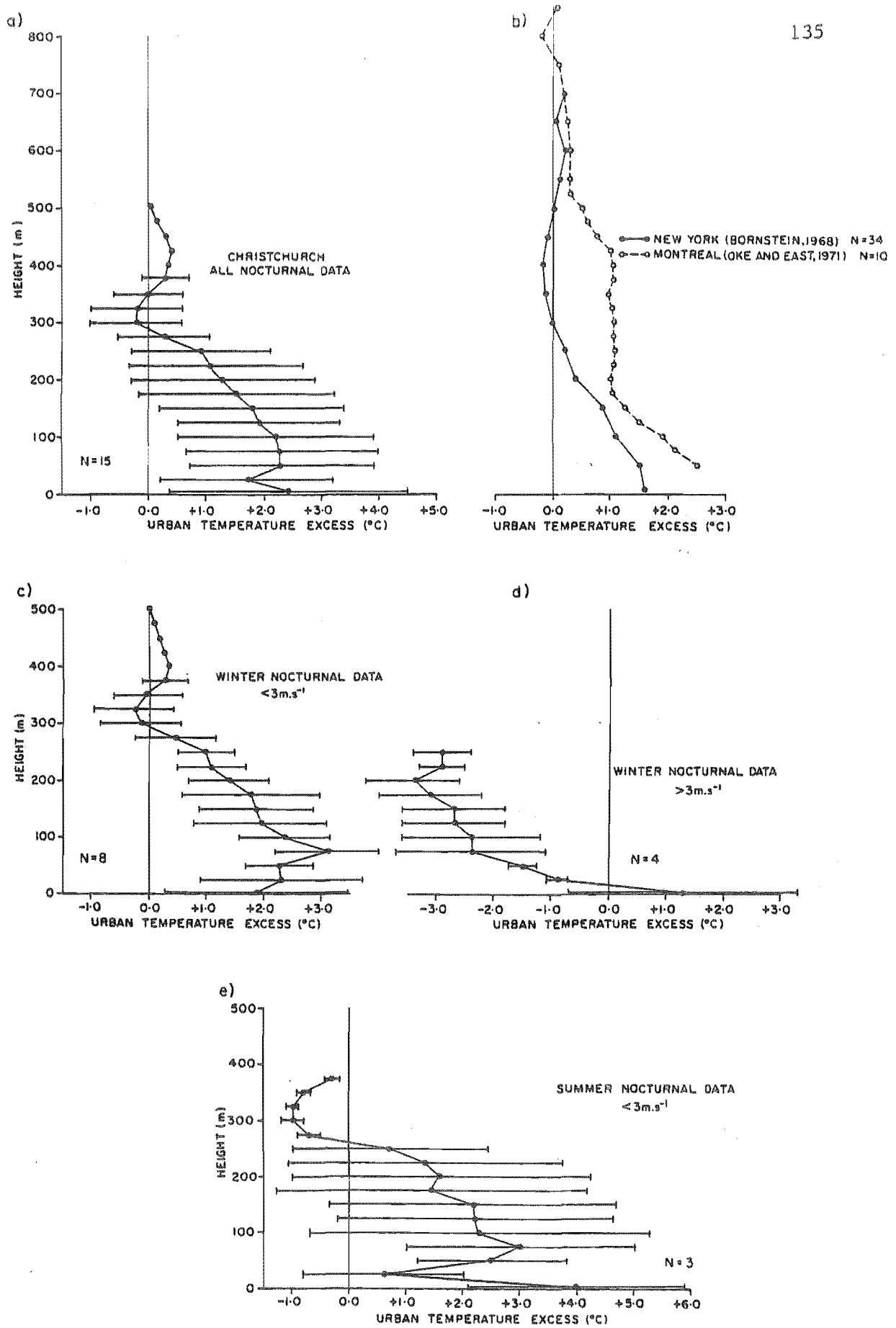

FIGURE 4.7 Urban Nocturnal Vertical Temperature Excess, a) All Christchurch Data, b) Data for New York, (Bornstein, 1968) and Montreal (Oke and East, 1971), c) Christchurch Winter with Windspeeds < 3 ms^{-1}, d) Christchurch Winter with Windspeeds > 3 ms^{-1}, e) Christchurch Summer with Windspeeds < 3 ms^{-1}. A Range of Plus and Minus One

excess temperature profile and that of New York is remarkable, all the more so because of city size differences. Both profiles indicate an elevated cooler layer over the city based near 300 m, although the cool layer in New York appears to have a greater vertical extent. The urban excess temperature reported for Montreal is much deeper, extending to 700 m. Evidence also exists for an elevated cooler layer in Montreal, but at a considerably higher altitude than any previously reported.

The first investigators to observe an elevated layer of urban cooling were Duckworth and Sandberg (1954) who dubbed it the 'cross over'effect, where urban temperatures become cooler than rural. Several possible theories explaining this 'cross over' effect have been advanced, including enhanced vertical mixing through greater urban turbulence and subsequent entrainment of cooler air from aloft, an urban convection cell with compensating subsidence over peripheral rural areas, and radiational cooling from polluted urban layers. Bornstein (1968) favoured the hypothesis of radiational cooling and that explanation has been further supported by the theoretical work of Atwater (1971a) who showed that infra-red radiative cooling in a pollution layer (aerosols in particular) can produce the cooling necessary for elevated inversions over urban areas.

Various statistics relating to the 'cross over' effect over Christchurch are included in Table 4.5. The phenomenon was observed to occur during 10 out of 11 paired nocturnal temperature profiles and the average vertical extent of the layer was 60 metres. The maximum rural excess temperature observed within a 'cross over' layer was 1.3^{o} C.

TABLE 4.5 Statistics of 'Cross Over' Layer Parameters

	$\bar{X}$	Range	σ
Base of Layer (m)	290	100 - 500	92
Depth of Layer (m)	60	30 - 200	-
Level of Maximum Rural Excess (m)	325	120 - 520	-
Maximum Rural Excess (^{o}C)	0.25	0.1 - 1.3	-

Nocturnal winter urban excess temperatures under low windspeeds (Figure 4.7c) show a similar pattern to that described above, except that the standard deviations are smaller, and the maximum heat island of 3.2° C is evident at a height of 75 m. Reasons for this elevated maximum urban excess are unclear, but may relate to the influence of heat sources above the ground level. The only winter nocturnal data relating to surface windspeeds greater than 3 m s^{-1} is for situations where warm föhn north-westerlies were present at Lincoln and undeveloped in the city due to the persistence of sea breezes. Figure 4.7d, produced for comparative purposes only, shows the urban excess temperature profile under such conditions, where, except in the lowest layers, any urban warmth is completely submerged by advective warming at the rural site.

Figure 4.7e gives the urban nocturnal temperature excess during summer with windspeeds < 3 m s^{-1} (no summer nocturnal observations were made in windspeeds above 3 m s^{-1}). This profile is similar to the winter case, except for a marked discontinuity at 25 m where the urban excess temperature is less than 1° C. As with the winter case there is a marked warmer layer over the city between 50 and 100 m, with the urban excess being as great as 3° C at 75 m. The transition to the elevated cool layer over the city appears to be more marked than the winter case (urban excess temperatures decrease from + 1.0° C to - 1.0° C within 50 m) and the 'cross over' layer appears deeper, but the data base is much smaller and standard deviations greater. Above 350 m the profile tends toward zero urban-rural difference.

Summers (1965) suggested that the depth of the urban mixed height (h) can be related to size of the urban heat island by the simple equation:-

$$Tu = Tr + \alpha h \quad \ldots 4.3$$

where Tu and Tr are the urban and rural surface temperatures respectively and α is the rural potential temperature gradient (^{o} C m^{-1}). Leahey (1969) and Oke and East (1971) both found good agreement between predicted and observed values of h for New York and Montreal data. Using the standard equation for potential temperature:-

$$\Theta = T \left(\frac{1000}{p}\right)^{0.288} \quad \ldots 4.4$$

where p is measured surface pressure (mb) and T is temperature (^{o} C), urban mixing depths for all nocturnal profiles were calculated and compared with observed mixing depths. A summary of this analysis appears in Table 4.6, with the model predicting wintertime urban mixing heights quite well ($\overline{X}$ error 37 m), but predicting summertime urban mixing heights less successfully ($\overline{X}$ error 125 m). This indicates that at least in the case of winter data, the rural lapse rate and heat island intensity have a strong bearing on the height of urban warming. Ludwig (1970) similarly demonstrated a strong relation between the rural lapse rate and urban heat island intensity.

Daytime Vertical Temperature Excess

Generally speaking, daytime temperature profiles where mesoscale influences become important exhibit greater variability than nocturnal profiles where circulations are generally weak.

Figure 4.8a is a plot of urban temperature excesses for all daytime profiles. As the excess is always within instrumental error (0.5^{o} C) and the observations exhibit marked variability it is not possible to determine obvious urban warming with any confidence. When the daytime data is stratified according to the boundary-layer wind

TABLE 4.6 Observed and Predicted Urban Mixing Heights Over Christchurch (m)

	$\bar{X}$ (CALCULATED)	$\bar{X}$ (OBSERVED)	$\bar{X}$ (ERROR)
Winter	232	269	37
Summer	133	208	125

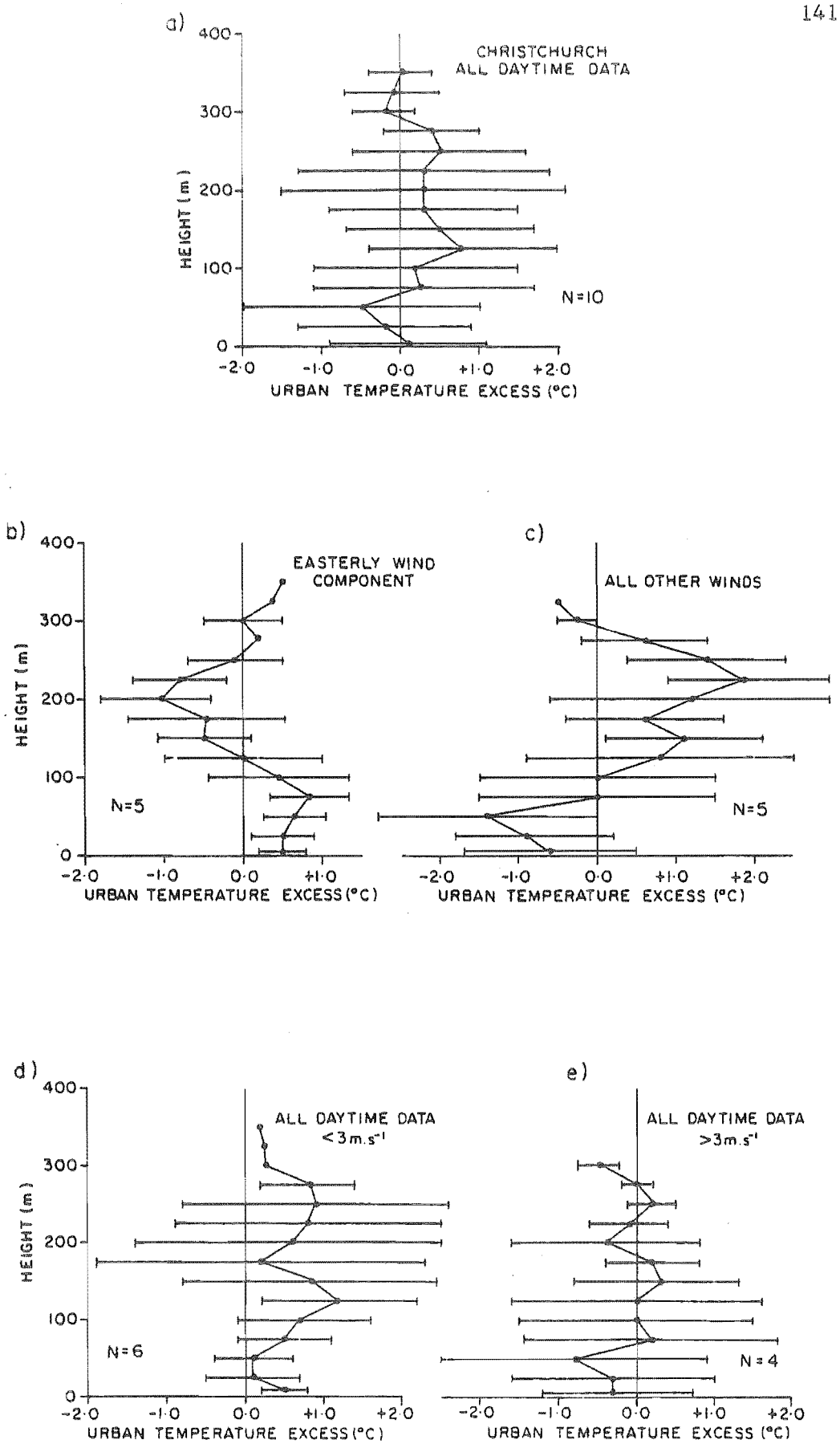

FIGURE 4.8 Urban Daytime Vertical Temperature Excess for Christchurch, a) All Data, b) With Easterly Wind Component, c) All Other Wind Components, d) Windspeeds < 3 ms^{-1}, e) Windspeeds > 3 ms^{-1}. A Range of Plus and Minus One Standard Deviation

component at the Lincoln site an interesting pattern emerges. With an easterly component (Figure 4.8b) there is a small but significant warm layer (0.5 - 0.7^{o} C) to 100 m over the city above which a cooler layer (rural temperatures up to 1^{o} C warmer) dominates the profile to 260 m. This appears to evidence the occurrence of an urban heat plume, centred at about 200 m, being advected over Lincoln and its subsequent replacement with cooler non-urban air (in this case maritime) over the central city. With a composite of all other wind components (Figure 4.8c) there is far greater variability in the mean urban temperature excess, but a mirror image to the easterly data appears to apply, with considerable urban warmth above 200 m. In general terms, windspeeds are lower in non-easterly clear sky conditions (mean windspeeds at 200 m 3.5 m s^{-1} as against 6.6 m s^{-1} for easterly data) and this appears to have aided urban warming in those layers where urban warmed air aloft has not been displaced. Reasons for the apparent cool layer under 75 m are unclear, but standard deviations about the means are large (up to 125 m). An example of advected urban warmth over the Lincoln site has been shown previously in Figure 2.6.

Windspeed influences on daytime urban excess temperatures are indicated in Figures 4.8d and e. With windspeeds < 3 m s^{-1} there is evidence of urban warmth, especially above 100 m, although above 150 m there is considerable variability about the means. Evidence of urban warmth becomes indefinite with windspeeds above 3 m s^{-1}.

CONCLUSIONS

The most important points arising from this study of Christchurch urban heat island characteristics may be summarised as follows:-

(i) A clear weather mean surface hourly temperature difference of 2.6° C between the Central City and Lincoln sites existed during the study period, the monthly urban excess temperature being significant by t-test.

(ii) The magnitude of Christchurch's maximum urban heat island appears lower for a similar population size than North American and European cities indicating the more 'rural' character of Christchurch's physical structure.

(iii) Heating and cooling curves for the Lincoln and Central City sites indicate basic differences in site characteristics, particularly relating to types of materials and view factors.

(iv) Radiational inversions were found to predominate on clear nights at both the urban and rural sites, although rural inversion strengths were greater. Lapse rates under daytime conditions were found to be slightly stronger at the rural site.

(v) Nocturnal vertical urban temperature excesses were consistently observed to approximately 290 m, with the maximum excess generally between 50 and 100 m and related to the urban heat input. Above 290 m a shallow 'cross over' layer was observed with urban temperatures cooler than rural.

(vi) Daytime observations indicate only slight urban excess temperatures in the boundary-layer, the excess present especially under low windspeeds. Advection of an elevated urban heat plume over the rural site was evidenced under winds with an easterly component.

CHAPTER 5

URBAN-RURAL VARIATIONS IN THE CHRISTCHURCH MOISTURE FIELD

INTRODUCTION

In comparison with temperature, study of the spatial, temporal and vertical variation of moisture fields over cities is a neglected aspect of urban climatology. This lack of interest in urban moisture fields has been reflected in New Zealand, where, apart from some limited observations of urban-rural differences by McBoyle (1970), Tapper (1976) and Tuller (1977) no relevant work has been undertaken. McBoyle found the relative humidity in Cambridge and Te Awamutu to be about 10 per cent below that of surrounding rural areas, and the value in downtown Hamilton to be up to 15 per cent lower. Tapper found a 0.2 mb rural excess vapour pressure averaged over a five month term in Christchurch; but more importantly found a diurnal reversal with daytime rural and nocturnal urban vapour pressures being higher than the respective urban and rural vapour pressures. Also in Christchurch, Tuller found urban nocturnal vapour pressures to be about 0.5 mb above outlying rural areas.

URBAN-RURAL VARIATIONS IN NEAR-SURFACE MOISTURE CHARACTERISTICS

General Results

Table 5.1 gives mean hourly clear weather vapour pressures by month for the study period. This indicates a divergence between vapour pressures measured at the Lincoln and Central City Sites, with an average daily urban excess vapour pressure ranging from 3.2 mb in February to -0.1 mb in July. The difference is significant at the 0.01 level by t-test for all months except July. The weighted term difference amounts to an average Central City site excess vapour pressure of 1.0 mb.

These findings are not entirely consistent with previous investigations of long term urban-rural vapour pressure difference. Kratzer (1956) reported average urban deficits of 0.2 to 0.5 mb for various European cities, this being confirmed by Chandler (1965) for the annual vapour pressure deficit over London. The present results are also somewhat at variance with those long term observations obtained previously for Christchurch (Tapper, 1976), suggesting that the results may be partly due to particular characteristics of the Central City site. Set adjacent to extensive areas of lawn, garden and mature trees (Chapter 3), there is evidence that humidities may be artificially high for an urban area and that extensive irrigation, especially during summer months, may be an important influence. A decreasing urban excess vapour pressure toward winter lends support to this hypothesis. Possible irrigation effects on diurnal variations of absolute humidity are discussed below. Table 5.1 also reveals a trend toward lower vapour pressures at both sites in the wintertime, evidencing the decreased ability of a cooler atmosphere to hold moisture.

TABLE 5.1 Hourly Clear Weather Vapour Pressures by Month (mb)

	FEB		MAR		APR		JUL		AUG		SEPT	
HR TO	L	CC	L	CC	L	CC	L	CC	L	CC	L	CC
01	15.8	17.9	13.3	14.8	8.8	10.4	6.7	6.6	6.0	6.7	7.8	8.7
02	13.7	17.3	13.0	14.6	6.8	10.2	6.5	6.4	5.7	6.4	7.5	8.4
03	12.3	16.4	12.0	14.5	7.5	10.0	6.3	6.3	5.7	6.3	7.4	8.4
04	12.5	16.3	11.7	14.3	7.2	9.5	6.1	6.1	5.5	5.9	7.3	8.2
05	12.4	15.9	11.7	13.9	6.9	9.1	6.0	6.1	5.6	6.0	7.0	8.2
06	11.7	15.9	11.7	13.9	6.7	8.8	5.9	5.7	5.5	5.8	6.8	8.0
07	11.0	15.3	11.6	14.0	6.4	8.5	5.8	5.5	5.5	5.7	6.7	7.8
08	10.4	13.7	11.9	13.6	6.5	8.5	5.7	5.3	5.5	5.6	7.0	7.8
09	10.9	12.7	12.8	13.4	7.8	8.3	5.7	5.3	5.7	5.7	7.8	8.0
10	10.8	12.1	14.0	13.2	8.5	8.4	6.1	5.5	6.2	5.6	9.5	8.0
11	10.6	12.9	15.0	13.0	9.2	9.0	6.7	5.6	6.7	6.4	9.4	8.2
12	10.3	13.0	14.6	13.5	9.3	9.4	7.1	6.2	6.8	6.8	8.7	8.4
13	10.0	13.7	15.7	14.0	9.1	9.6	7.2	6.6	6.7	6.9	8.4	8.2
14	10.3	14.1	13.7	14.1	9.0	9.9	7.2	6.9	6.5	6.6	8.2	8.4
15	10.5	14.5	14.5	13.5	9.4	10.1	7.3	6.9	6.5	6.8	8.5	8.6
16	10.7	14.7	12.9	15.5	9.5	9.9	7.3	7.2	6.6	7.2	9.6	8.9
17	10.7	14.8	12.5	15.5	9.7	10.2	7.7	7.7	7.7	8.2	9.7	9.3
18	11.0	14.7	12.2	15.3	10.1	10.4	7.6	7.8	8.1	9.4	10.1	10.0
19	11.4	14.9	11.3	15.8	10.2	10.5	7.4	7.6	7.9	9.2	9.8	9.9
20	12.0	15.5	10.5	14.7	9.9	10.6	7.1	7.5	7.9	9.0	9.4	10.2
21	12.7	15.8	10.3	13.9	9.6	10.8	7.1	7.3	7.8	8.7	8.6	9.8
22	13.2	15.8	10.5	13.6	9.4	11.0	6.9	7.7	7.6	8.4	8.6	9.3
23	13.1	15.7	10.5	14.6	9.2	10.8	6.9	7.3	7.3	8.3	7.7	9.2
00	13.0	15.5	10.0	14.6	9.0	11.0	6.8	7.0	7.4	8.3	7.2	9.0
$\bar{X}$	11.7	14.9	12.4	14.2	8.6	9.7	6.7	6.6	6.4	7.0	8.2	8.7
$\bar{X}_{CC} - \bar{X}_{L}$	3.2		1.8		1.1		-0.1		0.6		0.5	

Weighted term means $\bar{X}_{CC}$ $\bar{X}_{L}$

9.5 8.5

Term difference 1.0

Although not tabulated here, urban relative humidities are consistently lower than at the rural site. This contrast with vapour pressures is related to the consistently warmer urban temperatures and the observation is in general agreement with those of other workers including Kratzer (1956), Chandler (1967), Kopec (1973) and Hage (1975).

Diurnal Variations of Urban Moisture Excess

The diurnal variation of the urban moisture excess (or deficit) is of greater significance for the determination of mechanisms responsible for urban-rural differences in moisture than absolute values or annual trends as described above. A diurnal trend in urban-rural vapour pressure difference for each month can be discerned from Table 5.1. For comparative purposes this data has been converted into absolute humidities (g m^{-3}) and grouped into summer and winter data (the month of April excluded). The results, along with a summer pattern for Edmonton, Canada (Hage, 1975) are shown in Figure 5.1. The Christchurch summer pattern shows air in the urban canopy layer remaining more moist at all times than at the rural Lincoln site. The urban excess moisture is at a minimum early to mid-morning and is at a maximum slightly before sunset. While urban absolute humidities decrease rapidly after sunrise to 0900 h and subsequently increase slowly to a mid-evening maximum, the rural absolute humidity exhibits a 'double wave' with peaks several hours after sunrise and sunset.

The winter pattern is similar for rural absolute humidities, but quite different for urban absolute humidities and for the behaviour of urban-rural differences. Unlike the summer pattern, the winter urban data exhibits similar 'double wave' characteristics to the rural data, with peaks after sunrise (somewhat later in the urban case) and

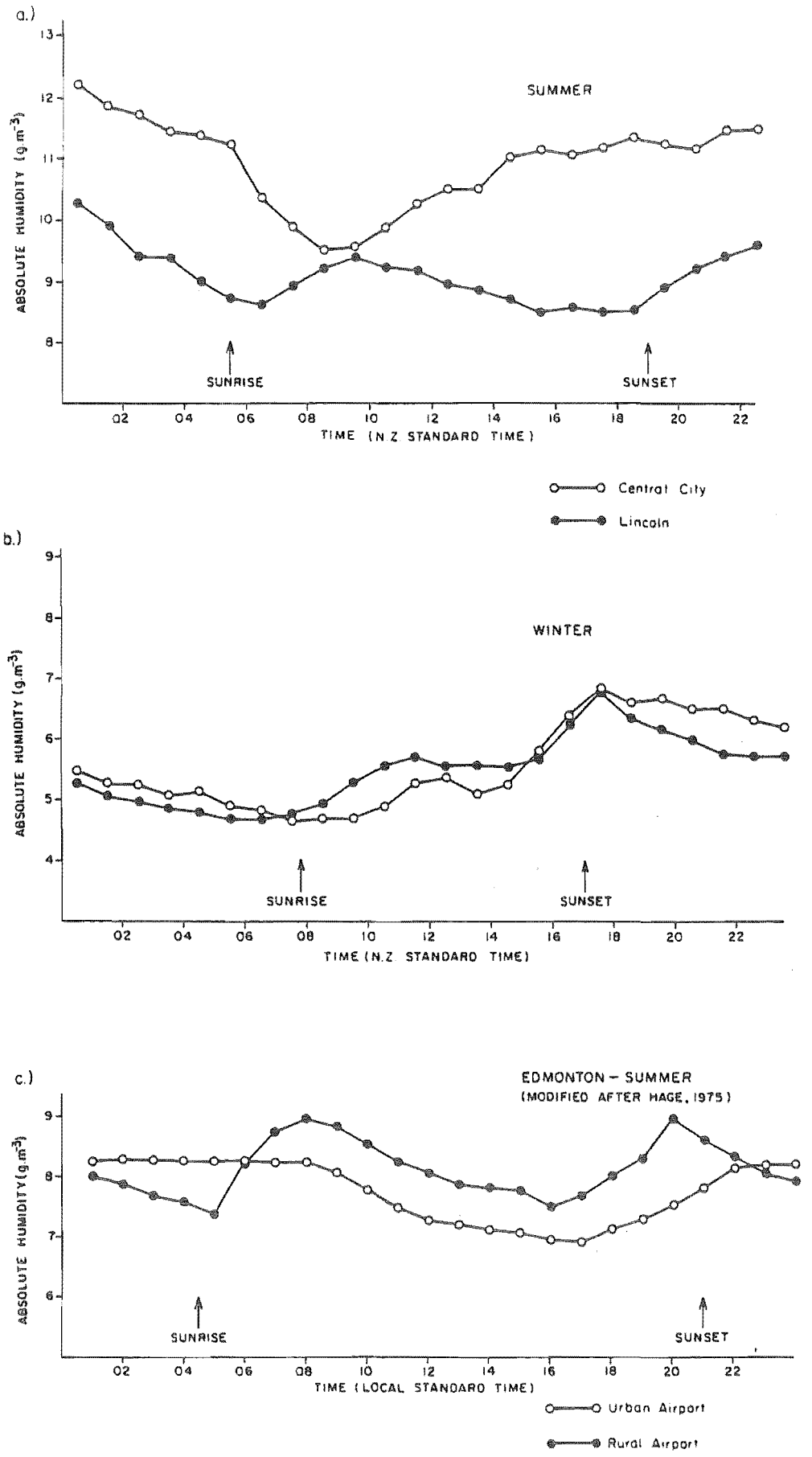

FIGURE 5.1 Clear Weather Diurnal Trends of Urban and Rural Absolute Humidity for, a) Christchurch Summer, b) Christchurch Winter, and c) Edmonton, Canada - Summer (Hage, 1975).

at sunset. There is also a noticeable diurnal reversal of absolute humidities, with urban canopy layer humidities being lower by day and higher at night.

Geiger (1973) suggested that the 'double wave' phenomenon described above is characteristic of rural locations in dry climates. Hage (1975) examined in detail similar patterns for the Edmonton summer situation (Figure 5.1c). For the rural case, Hage ascribes the peak after sunrise to the rate of moisture input by evapotranspiration into a stable lower atmosphere exceeding the upward transport to higher levels, with convection not yet well developed. During the rest of the day absolute humidities decrease as upward diffusion in an unstable atmosphere becomes increasingly efficient. Near sunset, absolute humidities peak through vapour convergence as evapotranspiration continues to add moisture to an increasingly stable atmosphere. Absolute humidities begin to fall steadily during the night as dewfall continues to deplete the lower boundary-layer moisture store. In the urban case for Edmonton, the pattern was quite different. A reduced urban evapotranspiration and enhanced mixing combine to keep urban daytime humidities below their rural equivalents. Hage ascribed the gradual increase in urban humidities into the evening to continued evapotranspiration and anthropogenic moisture input to the urban atmosphere and possibly to downward mixing of moisture from above the urban boundary layer due to urban induced turbulence.

In terms of the rural data for Christchurch, it appears possible to apply in some measure Hage's interpretation of physical mechanisms responsible for rural absolute humidity variations. Processes operating in the urban situation, particularly in summer, appear to be somewhat different. Winter urban absolute humidities

(although lower during the day and higher at night) exhibit the same general trend as the rural data, suggesting that the high proportion of green area in the proximity of the Central City site (Chapter 3) invests in the city some characteristics of a more rural climate. Both sites exhibit a mid-morning peak in absolute humidities, followed by a decline into the afternoon (coincident with the erosion of the wintertime nocturnal temperature inversion in the late morning). Subsequently, absolute humidities once again increase with the development of more stable conditions in the late afternoon.

Superimposed on the above trend are some obvious urban influences. Daytime urban humidities are lower than rural because of increased mechanical and thermal mixing (urban areas 1 - 2^{o} C warmer) and subsequent moisture diffusion, while urban evapotranspiration is reduced (40 - 90% impervious area compared with zero at the rural site). Conversely nocturnal absolute humidities remain higher within the city. Apart from the mechanisms invoked by Hage (continued urban evapotranspiration, input of anthropogenic moisture from combustion and the downward mixing of moister air by turbulence), other possible reasons for higher urban nocturnal humidities include decreased dewfall because of higher surface temperatures, and the trapping of moist daytime air within urban canyons, with a consequently lowered diffusion rate (Chandler, 1967). Within the scope of this discussion, it is not possible to determine the relative importance of each of these factors.

The summer pattern of urban absolute humidities shown in Figure 5.1a is sufficiently different to suggest an entirely separate source of urban canopy layer moisture. In addition, the magnitude of the urban excess (2.5 g m^{-3}) over much of the day suggests an urban moisture source unavailable at the rural site. From available

evidence, it appears that evaporation from irrigated surfaces is the source of increasing absolute humidities during late morning and early afternoon. At the Central City site continuous irrigation of lawns and gardens occurs from 0800 h to 1700 h on all clear summer days. Following removal of the moisture source, humidities gradually decline through the evening for reasons described previously. No irrigation occurred in the region of the Lincoln site, so the characteristic 'double wave' feature of nocturnal rural environments is preserved at that location.

URBAN-RURAL BOUNDARY-LAYER MOISTURE VARIATIONS

Introduction

The subsequent analysis of boundary-layer moisture characteristics is derived from the same data base used for describing boundary-layer temperature characteristics. Relative humidity, height and temperature data from all paired profiles collected has been converted to specific humidities (g kg^{-1}) to allow valid comparison, site to site and with varying altitude.

As with temperature data, a convenient method of broadly classifying humidity profiles is according to lapse rate characteristics (g kg^{-1} 100 m^{-1}). Two categories only have been used:

moisture inversion : where the humidity lapse rate shows an increase of humidity with height.

moisture lapse : where the humidity lapse rate shows a decrease of humidity with height.

In all cases the lapse rate has been determined between the surface and 100 m, or in the case of a humidity inversion, to the top of the inversion.

General Results

Nocturnal Profiles of Specific Humidity

Table 5.2a shows the distribution of nocturnal profiles between humidity lapse and inversion classifications. At both sites inversion conditions predominate at a ratio of 2 : 1 on clear nights, indicating that at the time of profiling on most nights (approximately 2300 h) dewfall is depleting the moisture store in the lower boundary-layer. Considering nocturnal humidity inversions alone (Table 5.2b), certain urban-rural differences in profile characteristics are revealed. Rural humidity inversions are generally lower and more intense than for the urban site, the stronger gradient indicating less turbulence induced mixing and greater dewfall depletion in the lower rural boundary-layer. At the city site the overall increase in specific humidity to the top of the humidity inversion indicates a larger supply of moisture aloft within the urban area.

Daytime Profiles of Specific Humidity

Daytime specific humidity profiles typically exhibit lapse characteristics at both sites (Table 5.2c). These humidity lapse situations are associated with the daytime occurrence of high surface evapotranspiration moisture inputs associated with efficient upward moisture diffusion in an unstable atmosphere. Consideration of urban-rural differences in daytime lapse characteristics (Table 5.2d) indicates the effect of an enhanced daytime rural moisture supply with the mean rural humidity lapse (1.52 g kg^{-1} 100 m^{-1}) almost double that

TABLE 5.2a Distribution of Inversion and Lapse Conditions with Paired Nocturnal Humidity Profile Data

	NO. OF OBSERVATIONS	HUMIDITY INVERSIONS	HUMIDITY LAPSE
Central City Site	16	11	5
Lincoln Site	16	11	5

TABLE 5.2b Summary Characteristics of Nocturnal Humidity Inversions

CHARACTERISTIC	CENTRAL CITY SITE	LINCOLN SITE
Inversion Height (m)		
$\bar{X}$	78	35
σ	38	18
Range	25 - 100	25 - 75
N	11	11
Humidity Increase to Top of Inversion ($g\ kg^{-1}$)		
$\bar{X}$	1.48	0.94
σ	0.92	0.72
Range	0.45 - 3.4	0.17 - 2.38
N	11	11
Humidity Inversion Strength ($g\ kg^{-1}\ 100\ m^{-1}$)		
$\bar{X}$	2.0	3.0
σ	0.93	2.7
Range	0.9 - 3.9	0.68 - 9.52
N	11	11

TABLE 5.2c Distribution of Lapse and Inversion Conditions with Paired Daytime Humidity Profile Data

	NO. OF OBSERVATIONS	HUMIDITY INVERSIONS	HUMIDITY LAPSE
Central City Site	9	0	9
Lincoln Site	9	1	8

TABLE 5.2d Summary Characteristics of Daytime Humidity Lapse Data

CHARACTERISTIC	CENTRAL CITY SITE	LINCOLN SITE
Humidity Lapse Rate Strength ($g\ kg^{-1}\ 100\ m^{-1}$)		
$\bar{X}$	0.85	1.52
σ	0.49	0.85
Range	0.26 - 1.81	0.50 - 3.14

of the urban site.

Diurnal Variations of Boundary-Layer Specific Humidities

The transition from nocturnal humidity inversion to daytime lapse can best be illustrated with an example drawn from the data base. Figure 5.2 is a typical time progression of boundary-layer specific humidities for the Central City site on 8 July, 1979. This reveals a complex interaction between micro-, meso- and macroscale influences on boundary-layer humidities.

Surface effects are largely confined to below 100 m where a light sea breeze persists most of the day. A surface based humidity inversion with its top at 50 - 75 m is present throughout the night and becomes strongest just before sunrise at 0800 h as near-surface humidities continue to drop through dew-fall. 0800 h coincides with the time of the maximum surface based temperature inversion. After sunrise, the input of surface moisture into a still stable atmosphere rapidly erodes the surface humidity inversion to a slight lapse by 1100 h. At that time a slight humidity inversion exists above 150 m, but appears associated with the synoptic wind at that time. Maximum humidity lapse rates are reached by 1500 h when surface humidities exceed 4.0 g kg^{-1} (< 3.0 g kg^{-1} at 100 m). By 2000 h a surface based humidity inversion has once again become established.

Synoptic effects on the boundary-layer specific humidity appear largely above 100 m and at no stage dominate surface effects, although perhaps compressing the surface-based specific humidity inversion until 0900 h. Extremely dry air of a N-NW origin gradually descends through the morning with specific humidities as low as 1.0 g kg^{-1} at 130 m by 0800 h. Between 0900 and 1100 h an abrupt change

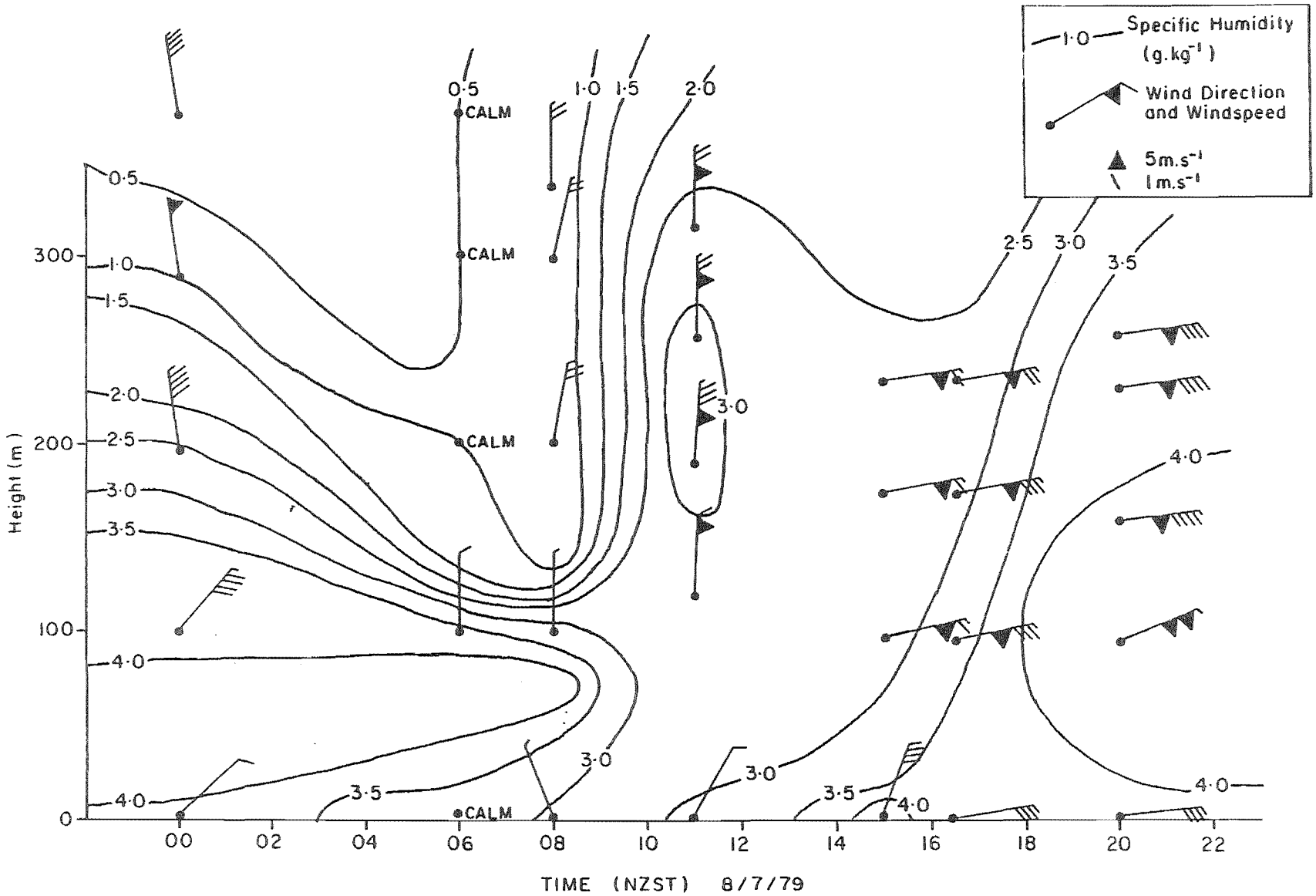

FIGURE 5.2 Time Progression of Boundary-layer Specific Humidities over Central Christchurch, 8 July, 1979.

in the character of the air mass above 100 m occurs, with the air becoming much more moist. Although the wind direction has not altered significantly at 1100 h it has freshened throughout the layer, perhaps associated with the onset of the sea breeze. By early afternoon the northerly has been replaced throughout the layer by a strong easterly sea breeze and a more normal specific humidity lapse through the profile. The sea breeze continues into the evening with the final kytoon flight of the day occurring at 2000 h.

Urban Boundary-Layer Specific Humidity Excess

General

As with temperature, the magnitude of any urban excess humidity is potentially of great importance in the determination of urban-rural differences in IR↓. Water vapour has long been recognized as the single most important gaseous constituent of the atmosphere in determination of IR↓, this evidenced by the multitude of prediction equations for IR↓ that include atmospheric water vapour as well as temperature as input (Ångström, 1916; Brunt, 1932; McDonald (Sellers, 1972); Brutsaert, 1975).

Composites of all humidity profile data have been constructed in the manner of the boundary-layer temperature data, to give a mean excess specific humidity and standard deviation at 25 m increments to 100 m, and 50 m increments thereafter. The composites once again have been stratified according to potential influencing factors.

Nocturnal Urban Specific Humidity Excess

Figure 5.3a is a composite of all nocturnal data. This shows an increase in the urban excess specific humidity from 0.7 g kg^{-1}

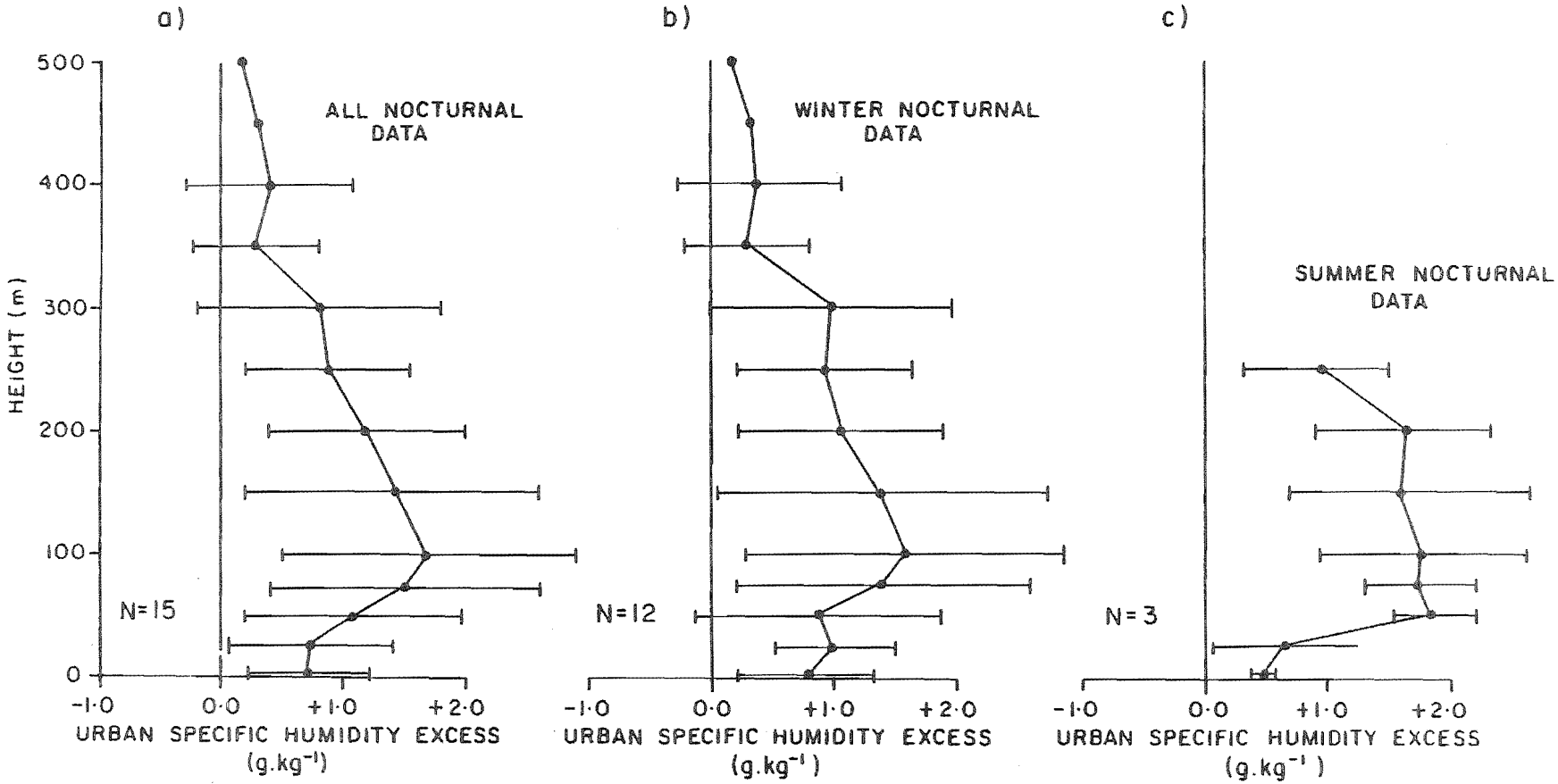

FIGURE 5.3 Christchurch Nocturnal Urban Specific Humidity Excess for, a) All Nocturnal Data, b) Winter Nocturnal Data, and c) Summer Nocturnal Data. A Range of Plus and Minus One Standard Deviation is Shown.

near the surface to a maximum excess of 1.7 g kg^{-1} at 100 m. Above this level the mean urban excess humidity declines steadily to approach zero at 350 m. At no point on the profile is there evidence of a consistent nocturnal urban moisture deficit and this is in complete agreement with the surface based observations described previously.

The extension of the nocturnal urban moisture excess deep into the boundary-layer lends especially strong support to one of the several explanations advanced previously for the near-surface humidity excess; that of enhanced vertical mixing over the city. None of the other mechanisms; continued evapotranspiration, decreased dewfall, moisture trapping and anthropogenic moisture input; with the possible exception of the latter, appear to have influence to the heights of urban excess moisture observed. The height of mean maximum moisture excess (100 m) also suggests that the major causative factor is not surface based. Bornstein, Lorenz and Johnson (1972) also reported a nocturnal moisture excess of about 4% to 500 - 700 m over New York and ascribed the anomaly to enhanced vertical mixing over central areas of that city.

The winter nocturnal situation (Figure 5.3b) is very similar to that described, while summer nocturnal data (Figure 5.3c) exhibits an especially strong increase in the urban specific humidity excess between the surface and 50 m, where the mean maximum urban excess humidity is recorded.

Daytime Urban Specific Humidity Excess

As with winter surface based data, the daytime profile of specific humidity excess for all data (Figure 5.4a) shows an urban deficit near to the surface. The mean maximum urban deficit of 1.0

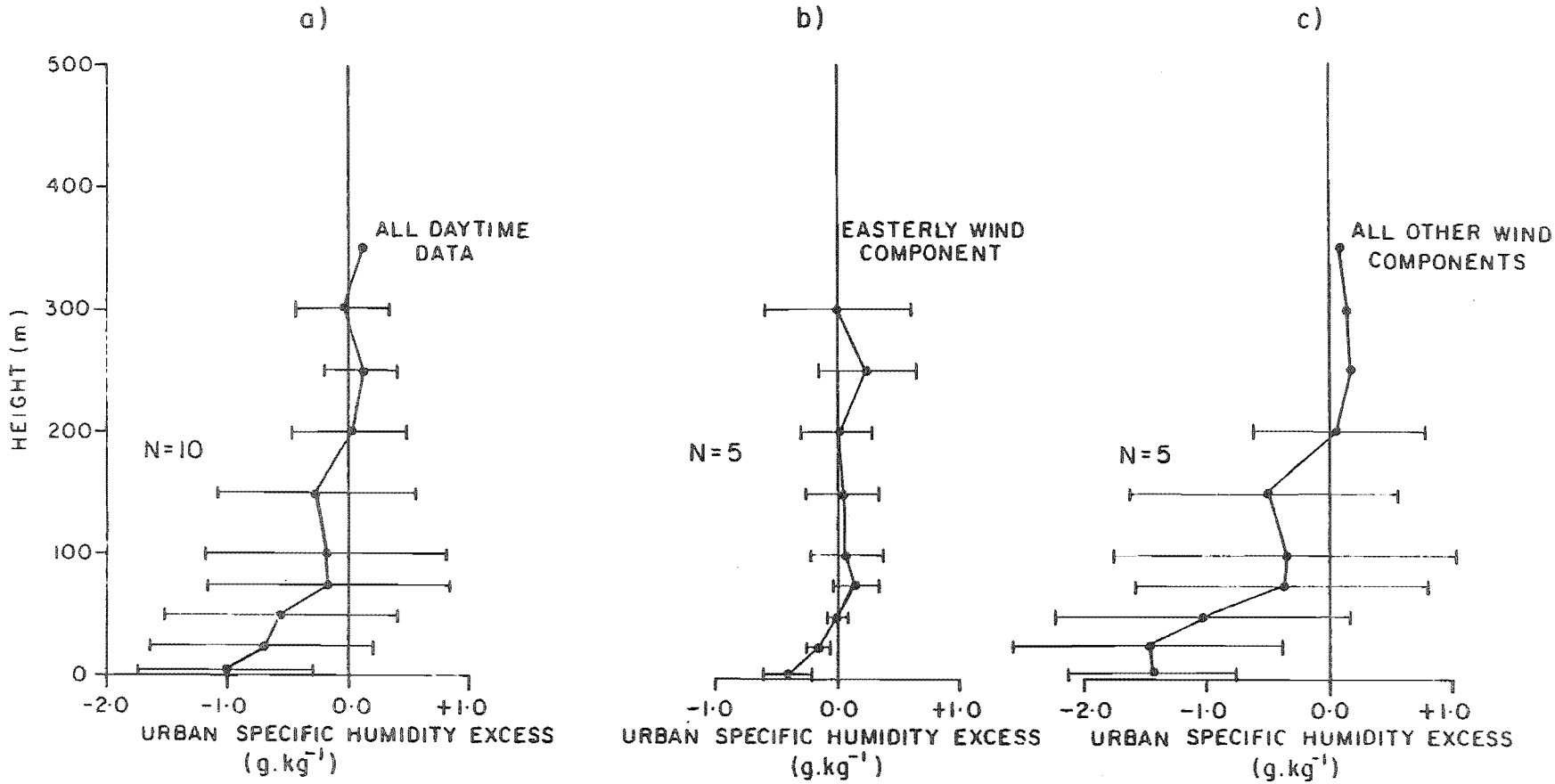

FIGURE 5.4 Christchurch Daytime Urban Specific Humidity Excess for, a) All Daytime Data, b) Easterly Wind Component, c) All Other Wind Directions. A Range of Plus and Minus One Standard Deviation is Shown.

g kg^{-1} near the surface decreases rapidly to 0.15 g kg^{-1} at 75 m and to zero at 200 m. Although thermal and mechanical turbulence may be partially responsible, the surface-based maximum deficit suggests that the surface mechanism of reduced urban daytime evapotranspiration is responsible for the urban daytime anomaly. These observations are consistent with other investigations of urban-rural boundary-layer humidities which have been almost entirely confined to the METROMEX project over St Louis (Auer and Dirks, 1974; Dirks, 1974; Spangler and Dirks, 1974). They identified an anomaly in the urban mixing layer with humidity deficits of 1.0 g kg^{-1} over and downwind of the city, although the urban deficits were found to exist to much higher levels than was apparent for the Christchurch data.

Stratifying according to the component of wind direction at Lincoln yields Figures 5.4b and c. With an easterly component, the urban humidity deficit disappears by 50 m, swamped by the relatively strong moist sea breezes. Above 200 m there is evidence of a slight urban excess, possibly related to the advection of the drier urban plume over the rural site in the manner described in the previous chapter. With all other daytime wind components the urban deficit is greater and exists to 200 m.

CONCLUSIONS

The major conclusions arising from this consideration of the Christchurch urban moisture field can be summarised as follows:-

(i) A clear weather urban mean hourly near surface vapour pressure excess of 1.0 mb over the Lincoln site was observed during

the study period, the excess being greater during summer months and related strongly to site characteristics.

(ii) Although near surface urban absolute humidity was observed consistently higher in summer, the diurnal variation of near surface absolute humidity in winter showed an urban nocturnal excess and a daytime deficit.

(iii) Humidity inversions were found to predominate on clear nights at both the urban and rural sites, the major reason being related to dewfall from the lower boundary-layer. Humidity inversions were observed to be lower and more intense at the rural site, due to increased dewfall and reduced mixing.

(iv) Daytime humidity lapse profiles were characteristic at both sites, although the higher rural lapse indicated the effect of enhanced daytime moisture supply at that site.

(v) A nocturnal vertical specific humidity excess was observed to about 350 m over the city, with a maximum average excess of 1.7 g kg^{-1} at 100 m. The excess appeared to be related to enhanced vertical mixing over the city in conjunction with continued evapotranspiration, decreased dewfall and anthropogenic moisture input near to the surface.

(vi) Daytime observations indicated a mean urban moisture deficit (maximum deficit 1.0 g kg^{-1} at the surface) existing to 200 m. Evidence suggested that the deficit was due to reduced evapotranspiration from city surfaces in comparison with rural areas.

CHAPTER 6

THE CHRISTCHURCH URBAN WIND FIELD AND ATMOSPHERIC POLLUTION

INTRODUCTION

Meteorological factors (atmospheric temperature and water vapour) capable of influencing clear-sky infra-red radiative transfers across the Christchurch urban area in a direct manner have been considered in the two preceding chapters. The radiative ability of the atmosphere is also strongly dependent on the variability of gaseous and particulate matter in the atmosphere.

All phases of the pollution process are weather dependant. The origin and quantity of emission is affected by meteorological factors, as is the dispersion of emissions. The most important factor lies in the ability of the atmosphere to disperse pollutants, this varying by a factor of 100,000 between extreme cases (Scorer, 1958). The degree of turbulence and hence pollution dispersal from a point of emission source depends on the nature of the surface, windspeed, vertical wind profile and, most importantly the vertical temperature profile. These last three factors are themselves affected by turbulence, therefore there is a degree of interdependence.

In this chapter, wind characteristics capable of indirectly affecting $IR\downarrow$ through their influence on pollution are discussed initially, followed by an analysis of atmospheric pollution over central Christchurch during the study period.

VARIATIONS IN THE CHRISTCHURCH WINDFIELD

Introduction

In the boundary-layer steady state winds are governed by a unique balance of forces; the horizontal pressure gradient force, the virtual force associated with coriolis acceleration and the frictional stress imposed by the surface. On traversing an urban area, windflow encounters changes in surface and atmospheric characteristics necessitating a redistribution of forces compared with upwind (and downwind) rural areas. Of particular importance in urban areas is the greater frictional drag exerted on the airflow by rougher surfaces, and the alteration of windflow characteristics (mainly directional) by the existence of a three-dimensional deformation of the overall pressure field imposed by the presence of an urban heat island. The former effect is much more readily recognised in field observations than the latter (Oke, 1979).

Previous Studies of Spatial Variations Across Christchurch

The effect of Christchurch's urban area on the overall windflow regime has received only scant attention in the past. A report by the Christchurch Air Pollution Advisory Committee (1966) indicated that from data gathered over four previous winters by the New Zealand

Meteorological Service, windspeeds near the centre of Christchurch were nearly exactly half those at Christchurch International Airport on the urban fringe. This was perceived as a particular problem in view of Christchurch's severe air pollution.

Ryan (1975) undertook a detailed investigation of low-level airflow patterns over Christchurch on 'calm' nights of high pollution potential in winter, using smoke tracer and a dense network of observers to ascertain the movement of any airflows determined by topography and/or urbanisation. It was found that flow patterns on almost all occasions belonged to one of three types; a northeast, southwest or northwest flow. The northwest flow is a downslope katabatic wind resulting from subsiding air off the Canterbury Plains, and often evolves later in the night from the other two flow patterns. Usually this wind is of a surface origin and unless the other winds are particularly weak, the northwest flow does not usually penetrate far into the urban area. This was ascribed by Ryan to vertical mixing, associated with greater surface roughness and the urban heat island operating to destroy the shallow layer of light northwest flow. There was also evidence of katabatic flow off the Port Hills to the south of the city, although the influence of this flow appeared to be local and mimimal. Ryan also suggested that because flow patterns appeared to be strongly influenced by topography in Christchurch, little evidence of a heat island induced circulation could be deduced. It appears that apart from the katabatic flows, the surface wind flow patterns over Christchurch on relatively calm nights are determined by the large scale weather situation, operating in conjunction with Christchurch's position relative to Banks Peninsula.

Tuller (1977) undertook some limited observations of windflow characteristics on clear, cold nights in Christchurch. In contrast with Ryan some evidence of a cyclonic circulation around the heat island in calm conditions was noted, although in view of the limited number of observation sites and times involved, it is possible that the detected flow was in fact an interaction between the downslope katabatic wind to the north and west of the city and a sea breeze to the south and east.

Sturman and Tyson (1981) in an investigation of the North Canterbury coastal sea breeze noted the effect of the interaction of Banks Peninsula with local winds in the Christchurch area. It was noted that the developing sea breeze over Christchurch failed to adjust to Coriolis force in the manner described elsewhere and predicted by theory. With an increasing velocity during the day the easterly sea breeze over Christchurch should back northeast, but the east-west orientation of the northern flanks of Banks Peninsula appeared to prevent this from occurring.

Urban-Rural Differences Found in This Study

Table 6.1 tabulates the frequency of occurrence of hourly wind directions at each of the observational sites for the two year study period. The table is for all weather data and has been stratified into a late summer (February, March, April) and late winter (July, August, September) situation. Both seasonal and site differences are evident from the data.

At both sites in both seasons the predominate wind direction is a sea breeze, a northeasterly at Lincoln site and an easterly at the

TABLE 6.1 Average Hourly Wind Directions by Season for Lincoln and Central City Sites (% Occurrence)

		N.	N.E.	E.	S.E.	S.	S.W.	W.	N.W.	CALM
SUMMER (February, March, April)	L.S.	10.1	40.8	6.4	2.5	13.9	8.8	2.9	6.4	8.2
	C.C.S.	0.6	16.8	37.5	0.7	7.3	15.5	4.1	0.9	16.6
WINTER (July, August, September)	L.S.	12.2	35.0	5.8	2.3	10.7	11.1	5.3	8.0	9.6
	C.C.S.	0.6	13.6	29.7	0.5	5.2	20.7	6.6	0.9	22.1

Central City Site, As there is no misalignment of sensor, the difference must stand as real, and appears related to the topographic influence of Banks Peninsula previously described by Sturman and Tyson (1981). Located south of the city and east-southeast of Lincoln (Figure 2.2) the presence of this large ($\sim$ 1000 m) mass in an otherwise flat landscape appears to deflect the easterly sea breeze airflow along the North Canterbury coast southward through 40^{o} - 60^{o} as it passes over Lincoln. A similar phenomenon occurs with winds of a southerly component, where southerly winds at Lincoln appear deflected eastward by Banks Peninsula and arrive over the Central City site as a southwesterly. This south or south westerly is the second most frequent wind direction occurring.

One further important difference between the sites is the exposure to winds from the northwest. The percent occurrence of northwest airflow is considerably greater at Lincoln (Table 6.1), this being entirely due to its position further inland and greater exposure to both synoptic and katabatic northwest winds off the Canterbury Plains. At the Central City Site the land breezes (particularly the low-level katabatic flow) have to overcome the onshore sea breeze and the frictional effects of the city surface. A final important site difference is evident in the occurrence of calms; calm conditions at the Central City Site being twice as frequent as those at rural Lincoln. This is also largely due to the frictional effects of the urban fabric on wind flow.

Certain seasonal trends are indicated in Table 6.1. At both sites there is a slight decrease in the sea breeze (northeast or east) component between summer and winter, and there is also evidence of a slight increase in winds from a southwesterly direction due to

the more strongly developed meridional flow at that time of year. At the Lincoln Site particularly, westerly and northwesterly winds increase into the winter season due to a strengthening of the katabatic gravity wind off the Plains in cooler weather. A winter trend toward a greater frequency of calm periods is also evident from Table 6.1, particularly at the Central City Site. This is of particular importance in relation to atmospheric pollution.

Table 6.2 groups the above data into mean windspeeds for each wind direction category. For both sites in both seasons, mean hourly windspeeds are greatest for the sea breeze (northeast at Lincoln and east at the Central City). North-west winds are also very strong in summer, particularly at the more exposed Lincoln Site, but exhibit a marked seasonal decrease to be one of the lightest wind speed categories in winter. This is further evidence of the impact of winter nocturnal katabatic winds. For all wind directions except easterly (the Central City sea breeze), windspeeds are 50 - 60% stronger at the rural site, evidencing the strong frictional effect exerted on the wind profile by the city surface.

The diurnal variation of windspeed at both instrumented sites is shown in Figure 6.1. This provides further evidence of the deceleration of airflow imposed by urban surface characteristics. Both sites exhibit a characteristic diurnal cycle of windspeed, with higher daytime windspeeds related to daytime instability and enhanced vertical mixing of the wind profile. Although mean windspeeds decrease by one third from summer to winter, the urban-rural windspeed ratio remains a near constant 0.55 - 0.56, similar to that previously reported for Christchurch (Air Pollution Advisory Committee, 1966). These urban windspeed reductions appear slightly higher than those of other

TABLE 6.2 Mean Hourly Windspeed ($m\,s^{-1}$) by Wind Direction Lincoln and Central City Sites

		N.	N.E.	E.	S.E.	S.	S.W.	W.	N.W.
SUMMER									
	L.S.	3.2	4.2	2.3	2.1	3.8	2.9	2.3	3.8
	C.C.S.	2.0	2.5	3.0	1.3	2.2	1.7	1.4	2.3
WINTER									
	L.S.	1.8	2.9	2.0	1.5	2.4	2.5	1.8	1.6
	C.C.S.	1.1	1.7	1.9	0.9	1.4	1.5	1.0	1.0

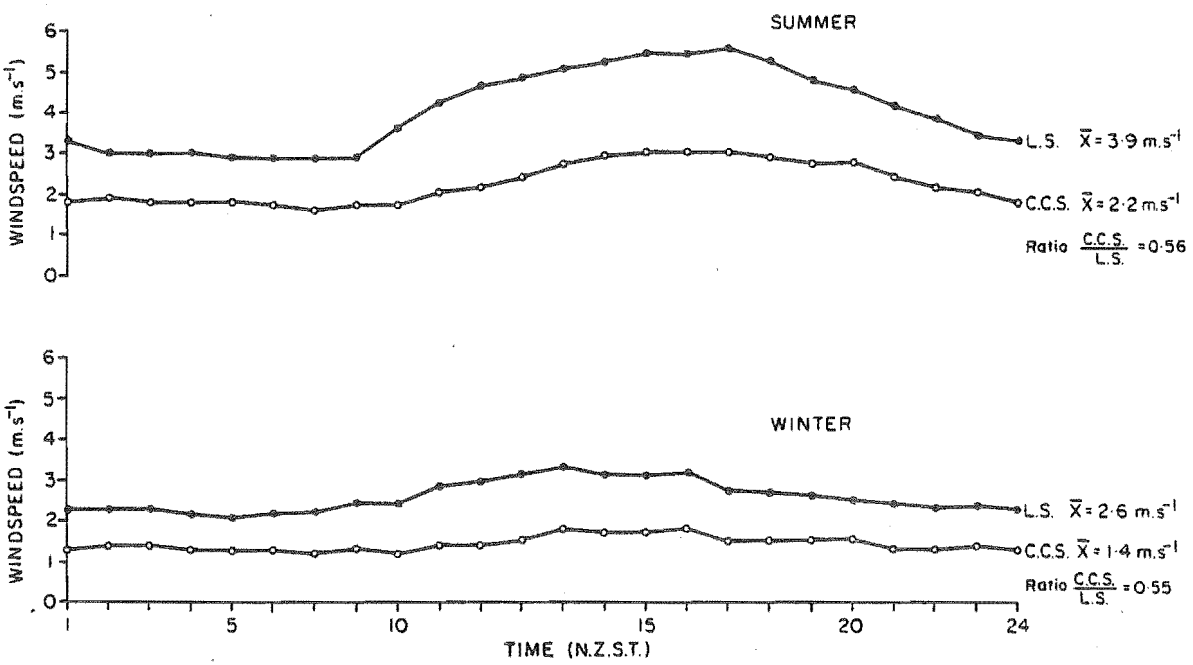

FIGURE 6.1 Diurnal Windspeed Variations at the Rural (L.S.) and Urban (C.C.S.) Representative Sites.

investigators using standard exposures of anemometers (Landsberg, 1956, 1958; Frederick, 1964; Chandler, 1965; and Munn and Stewart, 1967), but are not as great as those reported by Clark (1972) for street level winds. Recent and much more detailed investigations over New York (Bornstein, Lorenzen and Johnson, 1972; Loose and Bornstein, 1976) show that while the above is true for strong winds, for windspeeds below 15 km h^{-1} at night there is a slight increase in velocity within the city and that frontal movement is enhanced or retarded over the urban area dependent on position relative to, and strength of, the heat island induced pressure field. The Christchurch data shows no evidence of enhanced urban windspeed at times of low velocity airflow; indeed the frequency of calms in the Central City indicates that the reverse is true, but it should be borne in mind that the anemometers employed in this study are not sensitive to windspeeds below 1 m s^{-1}.

Given the high frequency of low windspeeds and calms in the central Christchurch area and the nature of city vertical temperature profiles under clear, calm, winter nocturnal conditions (mean inversion depth of 52 m and strength of 6.7° C 100 m^{-1}), conditions of high pollution potential are a regular occurrence. The concentration profile of pollution above a city however, depends on the wind velocity gradient as well as the stability of the atmosphere and the height at which pollution is emitted. This is considered below.

The Vertical Wind Profile Over Christchurch

Throughout the kytoon observational program wind direction measurements at approximate 100 m increments were made as a matter of routine, but it was only in the last series of flights (July/August, 1979) that reliable measurements of windspeed aloft were undertaken.

Reasons for obtaining such data were two-fold; to determine sources and ventilation rates for pollutants, and to determine the effects of relative landuse types on wind velocity gradients with a view to estimating values of surface roughness. Altogether 42 flights were undertaken where wind direction and windspeed data were both available.

The increase in surface roughness in urban areas is an obvious urban effect, but it has been difficult to obtain reliable quantitative estimates of the surface roughness length, z_o, from urban wind profile measurements (Oke, 1974). A proper specification of z_o from urban wind profiles is dependent upon neutrality, and urban areas are often characterised by weak instability rendering the determination of z_o by standard methods difficult (Shklyarevich, 1974).

Problems associated with standard logarithmic wind profile analysis over urban areas have lead some investigators (Newberry and Eaton, 1974; Penwarden and Wise, 1975; and Counihan, 1975) to relate the wind speed near the surface under strong wind conditions and/or neutral stability to the gradient wind, generally defined as the level where surface frictional influences disappear and the synoptic pressure field determines the wind speed. This relation is expressed as a simple power law:-

$$\bar{u}_z = u_G \left(\frac{z}{z_G}\right)^a \qquad \ldots 6.1$$

where, $\bar{u}_z$ - mean horizontal wind speed at the height z, U_G - gradient wind speed at the height z_G (i.e. depth of frictional influence), a - empirical co-efficient which depends on surface roughness and stability. Typical values for z_G and a for selected terrain types are shown in Table 6.3. Counihan (1975) has extended the relationship one stage further to provide a relation between a and z_o under

TABLE 6.3 Typical Values of the Power Law Parameters (z_G and α) for Three Categories of Surface Roughness (z_o) Based upon Measurements with Strong Winds and/or Neutral Stability (after Oke 1979)

TERRAIN	z_o[1] (m)	z[2] (m)	α[1]
Open countryside	0.01 - 0.2	275	0.13 - 0.16
Woodland, suburbs, small towns.	1.0 - 1.5	400	0.20 - 0.23
Dense urban, city centre	2.0 - 4.0	500	0.25 - 0.40

[1] Counihan (1975)

[2] Penwarden and Wise (1975)

adiabatic conditions:-

$$a = 0.096 \log_{10} z_o + 0.016 (\log_{10} z_o)^2 + 0.24 \quad \ldots 6.2$$

This relationship has been criticized for not using available theory (Oke, 1979), but for practical use in the urban atmosphere it appears to give quite reasonable results. Typical values of z_o derived by Counihan for different terrain are also given in Table 6.3.

To meet the criteria for Equation 6.1 of moderate to strong windspeeds (surface wind > 1.5 m s^{-1}) and/or neutral stability, the original wind profile data base was reduced to 20 individual profiles (eight from the Lincoln Site and twelve from the Central City Site). Figure 6.2a is a composite of the Lincoln profile data showing mean windspeeds at 2, 100, 175 and 275 m (open circles). Also plotted is the line of best fit from Equation 6.1 using the value of 275 m for z_G suggested by Penwarden and Wise (1975) for open countryside. The derived a coefficient for the best relationship is 0.18 which yields a surface roughness of 0.20 m using Equation 6.2. The values of $a = 0.18$ and $z_o = 0.2$ m are consistent with values for open countryside suggested by Counihan (Table 6.3).

Central City data has been similarly treated but with the composite profile extended to 400 m. While the suggested z_G for dense urban terrain is 500 m, the suburban nature of the land use around the Central City Site and operational constraints suggested that 400 m (typical of suburban areas) would have to be adequate. Figure 6.2 b is a plot of composite mean urban windspeeds aloft (open circles), where the line of best fit yields $a = 0.22$ and $z_o = 0.60$ m, somewhat lower than would be expected from Table 6.3. Stratifying the data according to wind direction produces interesting results. Figure

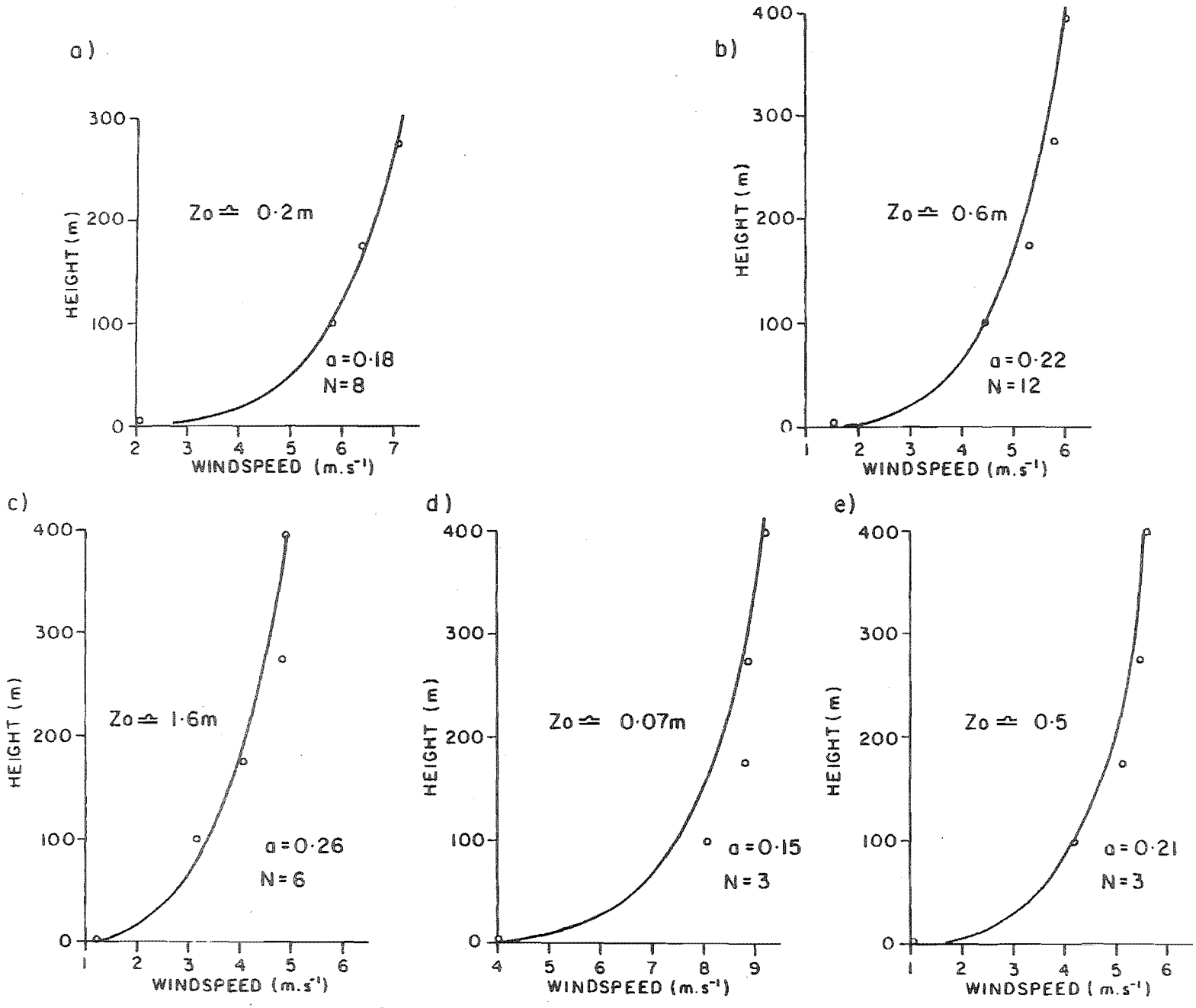

FIGURE 6.2 Mean Windspeeds Aloft (Open Circles) and Plotted Line of Best Fit (from Equation 6.1) for, a) Lincoln Site and b) Central City Site. c), d) and e) Show Data for the Central City Site

6.2c (six cases) for a northeasterly wind fetch yields a more typical urban/suburban z_o value of 1.6 m, while the easterly case (Figure 6.2d) indicates an extremely small z_o of 0.07 m, although the fit of the curve is particularly poor. For the southwesterly case (Figure 6.2e), the indicated surface roughness is 0.5 m. Despite the low number of profiles available for analysis (particularly for the easterly and southwesterly fetches), a large variability in urban z_o is apparent with differing wind fetches. Similar variability has been recognized by other investigators. Dûchene-Marullaz (1976) showed that z_o values at a suburban site in Nantes ranged between 0.4 and 2.3 m depending on direction of fetch.

For the Christchurch case the variability of z_o in the central city appears clearly related to wind fetch across nearby landscape features. Thirty metres to the north and north-east of the kytoon launch site is a large (25 m high) wooden building flanked by many large (20 m) deciduous trees. These features appear to have increased the z_o value with a fetch from that direction. Easterly winds have no such obstructions, are funnelled between two large buildings 150 m away, and run the length of a playing field before reaching the kytoon launch site. Similarly, winds from a southwesterly direction (although from the direction of the city centre), have no large nearby obstructions and are in fact funnelled by nearby buildings toward the launching site, with a resultant low z_o value.

The above analysis has only considered profiles undertaken with conditions approaching stability. With increasing stability even higher values of wind velocity gradient than those described become apparent. It is clear that the effect of wind velocity gradient is to increase dilution of pollution with a windflow increasing with

height, but it is also clear that it is difficult to separate effects of atmospheric stability on the vertical pollution profile from those of the wind velocity gradient. It should always be remembered that it is a combined effect on atmospheric pollution that is being observed.

The only feature of wind direction data aloft discussed here is the systematic deviation of airflow between the two representative sites. This phenomenon has been discussed previously for the surface based data. Table 6.4 shows the systematic altitudinal wind direction deviations between the Lincoln and Central City sites for paired ascents. Only those wind direction categories with at least five paired ascents available for analysis have been included in Table 6.4. For all direction categories there is a positive (clockwise) deviation at the Central City Site, although the deviation becomes less with increasing altitude. Except in the northwesterly case, standard deviations of mean departures also become less at altitude. The deflecting influence of Banks Peninsula once again appears to be the cause, although in the case of northwesterly flow at Lincoln, the deviations may also relate to the position of the Lincoln and Central City Sites in relation to the boundary between the northwesterly and easterly sea breeze. Especially large mean deviations (+ 100^{o} to + 105^{o}) near the surface under such conditions lend support to this hypothesis.

TABLE 6.4 Central City Deviations (°) from Lincoln Wind Directions at Altitude (all Paired Data)

WIND AT LINCOLN	ALTITUDE (m)	$\bar{X}$ DEPARTURE	σ	RANGE
Northerly (338°-022°)	0	+ 66°	27°	+30° to +120°
N = 10	100	+ 52°	26°	+20° to +110°
	200	+ 53°	21°	+30° to + 95°
	300	+ 43°	18°	+30° to + 80°
	400	+ 10°	22°	-30° to + 30°
Northwesterly (292°-338°)	0	+100°	21°	+80° to +130°
N = 5	100	+105°	32°	+60° to +140°
	200	+ 80°	40°	+30° to +130°
	300	+ 20°	-	-
	400	+ 30°	-	-
Southerly (157°-202°)	0	+ 80°	49°	+40° to +150°
N = 5	100	+ 42°	22°	+20° to + 70°
	200	+ 22°	5°	+20° to + 30°
	300	+ 20°	-	-

ATMOSPHERIC POLLUTION OVER CHRISTCHURCH DURING THE STUDY PERIOD

Introduction

In this discussion only two of the many atmospheric pollutants are considered. They are smoke particulate and nitrogen oxides pollution during the winter and summer study periods respectively. The physical reasons for isolating these pollutants for investigation have been mentioned previously (Chapter 3). Because pollution levels are generally at, or below the threshold of detection at the Lincoln site (as described in Chapter 3), this discussion of surface and vertical variability of pollution is restricted to the Central City site.

Near-Surface Variation of Atmospheric Pollution in Central Christchurch

The mean daily smoke concentrations by month for the two study years are shown in Figure 6.3a, along with an indication of the periods of intense study within those two years. Mean daily concentrations vary from 3 $\mu g\ m^{-3}$ (maximum daily value 8 $\mu g\ m^{-3}$) in December to 80 $\mu g\ m^{-3}$ (maximum daily value 385 $\mu g\ m^{-3}$) in June. These concentrations are similar to those of the previous few years in Christchurch, but are high even by world standards. The W.H.O. standard of no more than seven days per year exceeding an average daily mean of 120 $\mu g\ m^{-3}$ was exceeded on two occasions in 1978 and fifteen occasions in 1979. The seasonal trend in smoke pollution can be attributed to two factors; seasonal differences of climatic and fuel usage factors. The importance of domestic smoke emission has been mentioned previously and it can be appreciated that during the summer season, emission from that source is cut significantly. However, seasonal changes in climatic parameters relating to dispersion discussed previously are an important consideration.

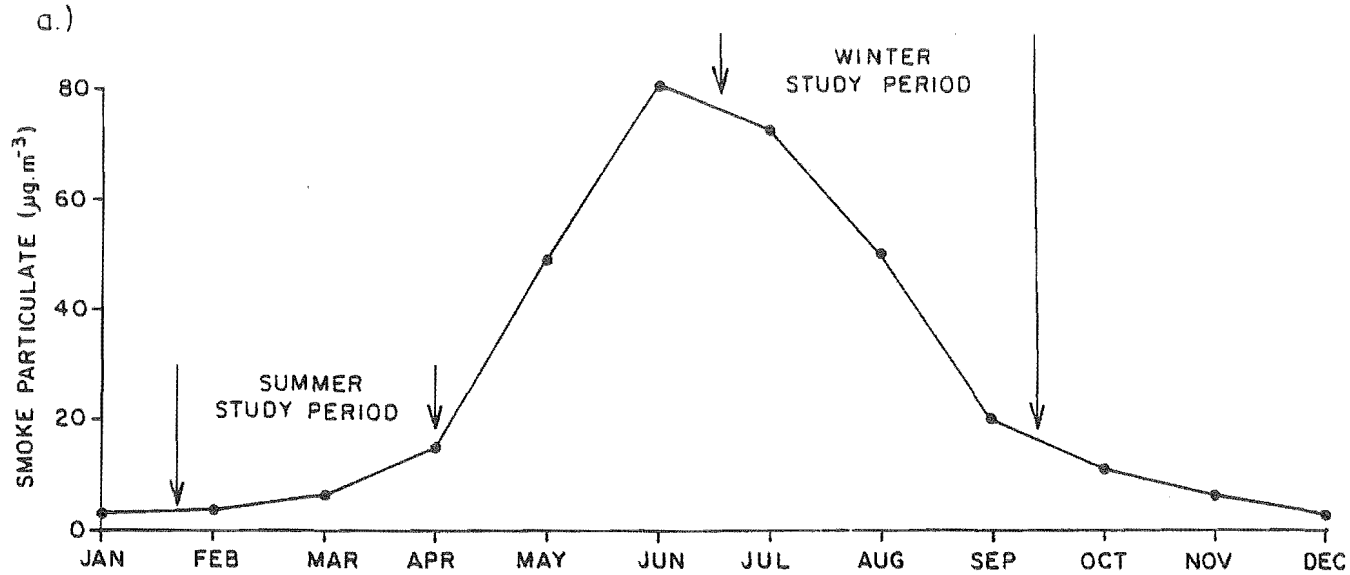

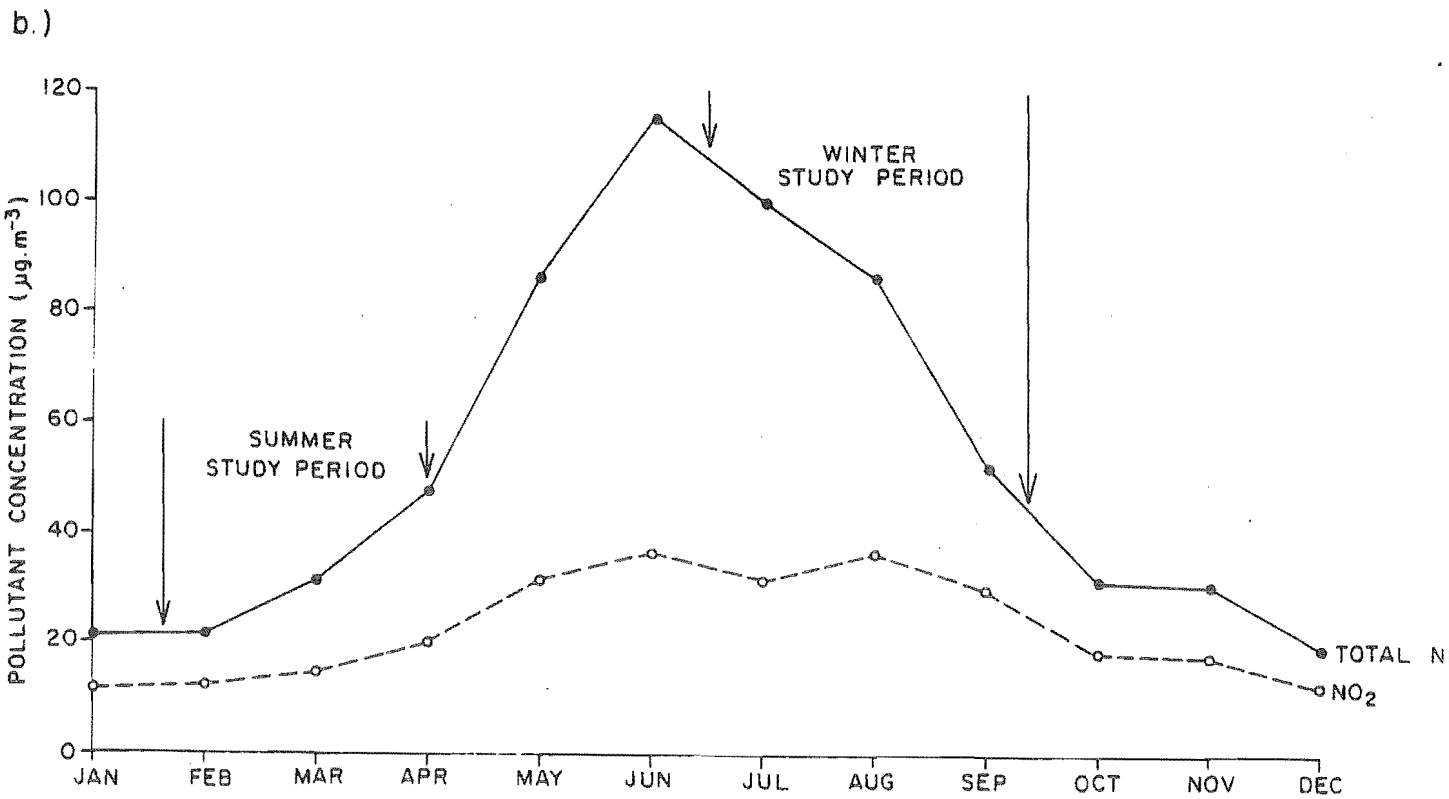

FIGURE 6.3 a) Mean Daily Smoke Concentrations for the Two Study Years at the Central City Site. b) Mean Daily Concentrations of Nitrogen Oxides for the

ation. The seasonal trend in mean daily nitrogen oxides (NOx) pollution for 1978 and 1979 (Figure 6.3b) is similar to that for smoke, but as the emission rate of NOx is relatively constant annually (largely a motor vehicle pollutant), the trend for NOx is related almost entirely to seasonal atmospheric dispersion capabilities. Mean daily concentrations of NOx range from 20 $\mu g\ m^{-3}$ in December (NO_2 - 12 $\mu g\ m^{-3}$) to 116 $\mu g\ m^{-3}$ in June (NO_2 - 37 $\mu g\ m^{-3}$). The NO_2 proportion of NOx is greater during summer months than in winter, due to more efficient photochemical oxidation of NO during summer months. Although NO_2 is produced in some chemical and nitration industries, it is primarily a secondary contaminent and is considered to be one of the more important indicators of photochemical activity (Levaggi *et al.*, 1973).

Superimposed on seasonal trends are those of smaller amplitude, including synoptic trends in response to the passage of weather systems, and at an even smaller scale, daily trends in response to diurnal stability and wind characteristics. Figure 6.4 shows the average daily variation in smoke concentration for the winter study periods at the Central City Site. The most important features of this graph are the two smoke peaks, a small one of 61 $\mu g\ m^{-3}$ at 0900 h and a much larger peak of 158 $\mu g\ m^{-3}$ at 2100 h. The Report of the Air Pollution Advisory Commiteee (1966) relates reasons for these peaks largely to emission factors, but meteorological factors are also a consideration. In winter, with the frequent occurrence of clear calm conditions, an overnight temperature inversion develops, further suppressing windflow and inhibiting dispersion. From 0700 h pollution builds up quickly in the stable atmosphere as domestic fires are lit, traffic begins to move, and industrial activity begins. By late morning the overnight inversion breaks up and windspeeds increase in response to solar heat

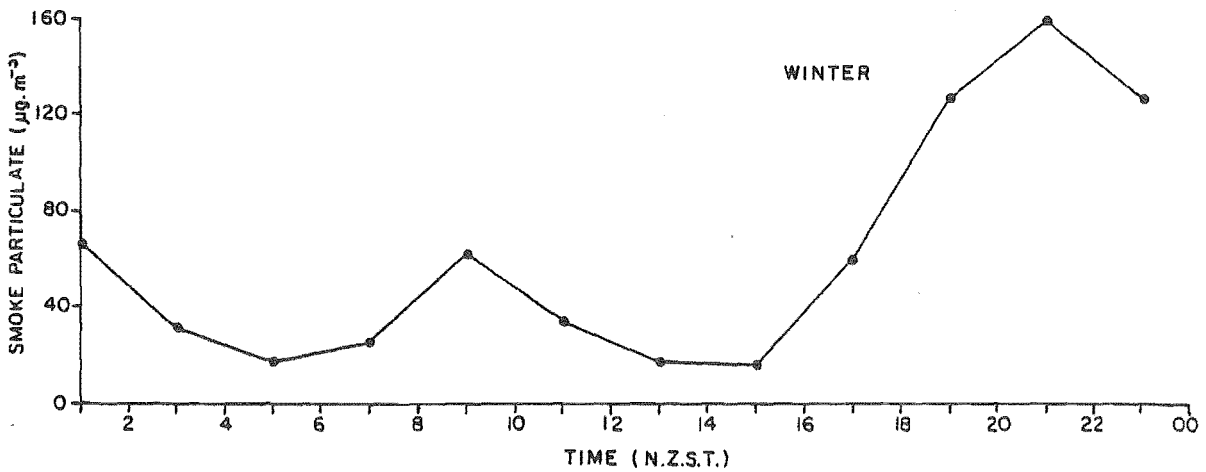

FIGURE 6.4 Average Diurnal Variation of Smoke Particulate Concentration at the Central City Site During Winter Study Periods.

input and pollution levels drop through the middle of the day. In late afternoon the inversion redevelops and pollution climbs in response to the lighting of domestic fires.

The diurnal pattern of wintertime NOx pollution during the two winter study periods is similar (Figure 6.5a), with a primary peak of 220 μg m^{-3} occurring at 0900 h and two secondary peaks occurring at 2000 h and 0000 h. These peaks are related to the meteorological factors discussed above and periods of high traffic movement. The proportion of NO_2 to NOx in winter is a relatively low 0.36. Summertime trends of daily NOx (Figure 6.5b) are similar, but of much lower amplitude than winter due to meteorological conditions being more conducive to dispersion. A primary peak level of NOx at 50 μg m^{-3} is evident at 0900 h with a sustained build up to a secondary peak of 44 μg m^{-3} at 2300 h. Of considerable interest is the much higher summer proportion of NO_2 to NOx (0.69) averaged throughout the day, evidencing the importance of photochemical oxidation in the summer, particularly during the middle of the day.

The Vertical Profile of Atmospheric Pollution Over Christchurch

Introduction

Of 54 profiling operations undertaken at the Central City Site, 48 involved an associated pollution profile. The winter pollution profiling data base (all of smoke particulate) comprises 35 individual profiles, 20 nocturnal and 15 daytime. Profiling of summertime nitrogen oxides comprises 13 profiles, seven nocturnal and six daytime.

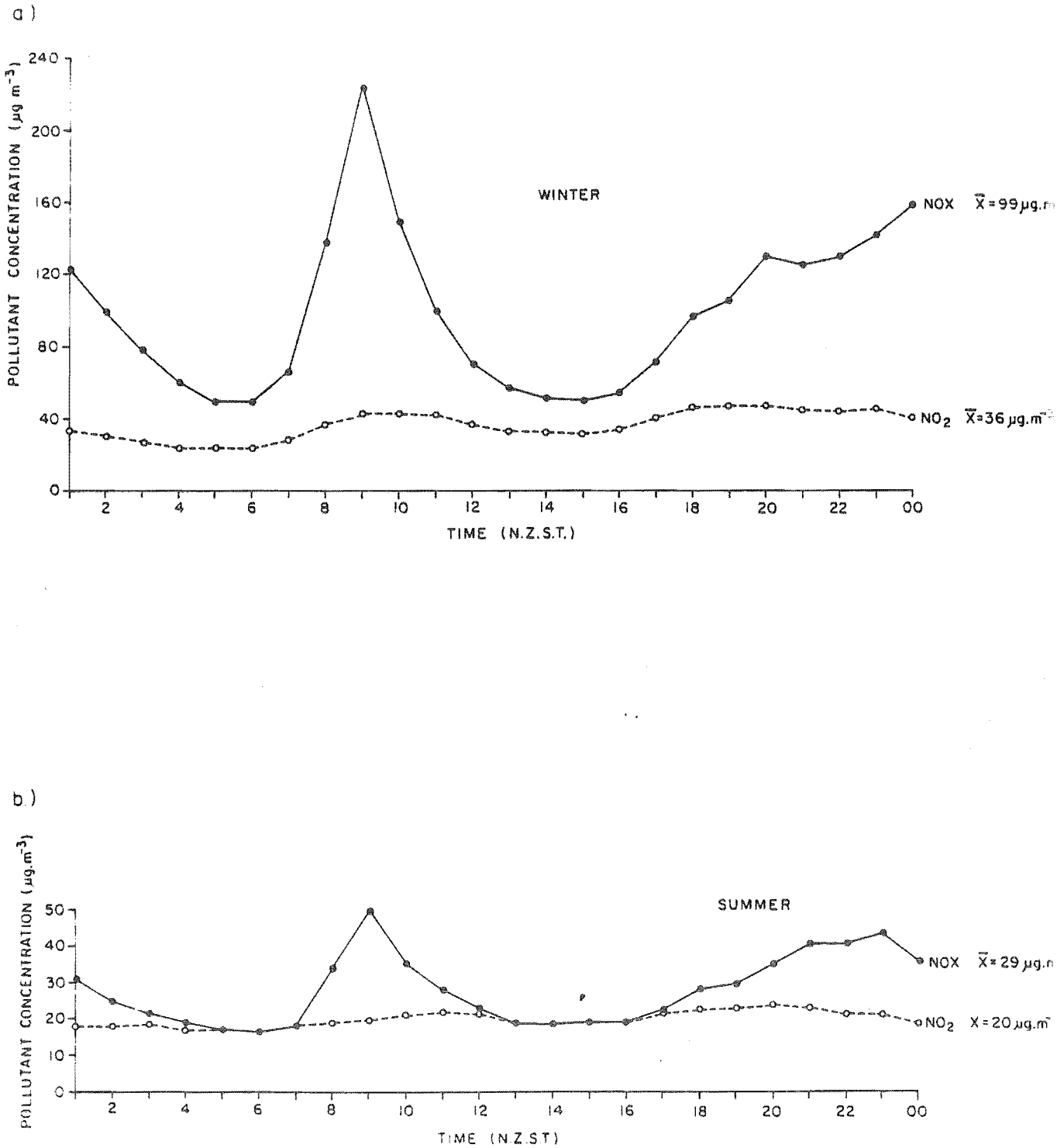

FIGURE 6.5 Average Diurnal Variation of Nitrogen Oxides at the Central City Site, a) During the Winter Study Periods, and b) During the Summer Study Periods.

The bulk of analysis undertaken here is in terms of composite profiles of stratified data. Although the inherent variability of atmospheric pollution compared with such parameters as temperature and water vapour content creates certain problems, this probably remains the best method of summarising results. To tie pollution profiles to causative mechanisms, some data from individual days are also used.

Winter Smoke Particulate Profiles

Nocturnal Profiles

Nocturnal smoke particulate profiles (all under inversion conditions) have been stratified into late evening (2100 - 2300 h) and early morning (0500 - 0800 h) flights; this is because although stability situations are similar, pollution concentrations during the latter period are generally much lower (refer Figure 6.4) and are related to a different set of emissions and/or are residuals of the peak from the previous evening. Figure 6.6a shows the mean smoke particulate concentrations at mean heights (the ground level height being the only fixed height) for all evening pollution profiles. For each point on the composite pollution profile, the standard deviation and maximum and minimum concentration and height for all observations is given. Of particular note is the extremely rapid reduction in pollution concentration with altitude between the 2 m level (415 $\mu g\ m^{-3}$) and the 37 m level (73 $\mu g\ m^{-3}$). At the 66 m level, the top of the profile, the pollution concentration is further reduced to a mean value of 36 $\mu g\ m^{-3}$. Also evident is a decreasing variability of pollution with height, the standard deviation dropping from 226 $\mu g\ m^{-3}$ near the surface to 35 $\mu g\ m^{-3}$ at the 66 m level.

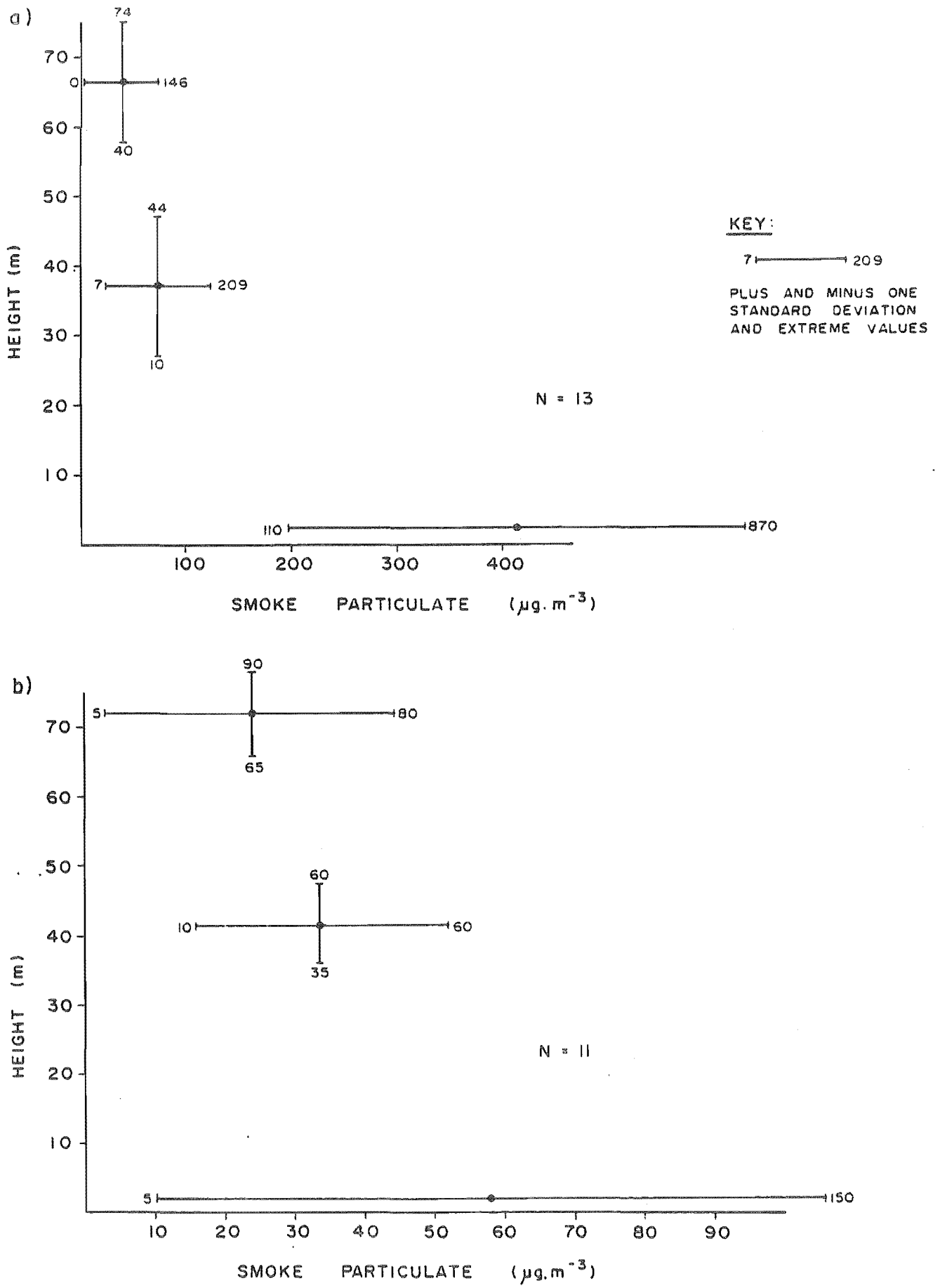

FIGURE 6.6 Composite of Nocturnal Profile Characteristics of Smoke Particulate, a) p.m. after Inversion Development and b) a.m. before Inversion Dissipation. Bars Show Plus and Minus One Standard Deviation and Extreme Values.

Both the high concentrations and variability of near-surface pollution can be related to the strength ($\bar{x}$ 6.7° C 100 m^{-1}) and height ($\bar{x}$ 52 m) of the wintertime nocturnal inversion over Christchurch. These characteristics, associated with the low height of emission of domestic fires (∿ 5 metres), ensure that most pollution is contained in the lowest 10 - 20 m. The variability of near-surface smoke pollution, even within a short time frame, is illustrated with data from 12 July, 1978 (Figure 6.7). During a 2 h period on that evening, near-surface smoke concentrations ranged from 310 µg m^{-3} to 1025 µg m^{-3} and back to 530 µg m^{-3}, while above 60 m concentrations varied only slightly. Unfortunately temperature profile data were not available for these flights which took place early in the study period.

A composite of all early morning pollution profiles illustrates a slightly different pattern of smoke pollution (Figure 6.6b). At all levels, and particularly near ground level, smoke concentrations are lower. Whereas in late evening flights the smoke levels at ∿ 40 m were 0.17 those at 2 m, in the early morning flights the proportion is nearer 0.60. As the stability situation is similar to flights earlier in the night, the lower concentrations and reduced height differences appear entirely related to reduced near surface smoke emission at this time, and may in fact be residuals of the high concentrations of the previous evening.

Typical late evening and early morning temperature and pollution profiles are given in Figure 6.8. Despite similarities in inversion height and strength there are considerable differences in pollutant concentration and distribution. In the case of the evening flight of 22 July, 1978, high near-surface smoke concentrations of 490 µg m^{-3} drop rapidly with altitude to 96 µg m^{-3} slightly below the top

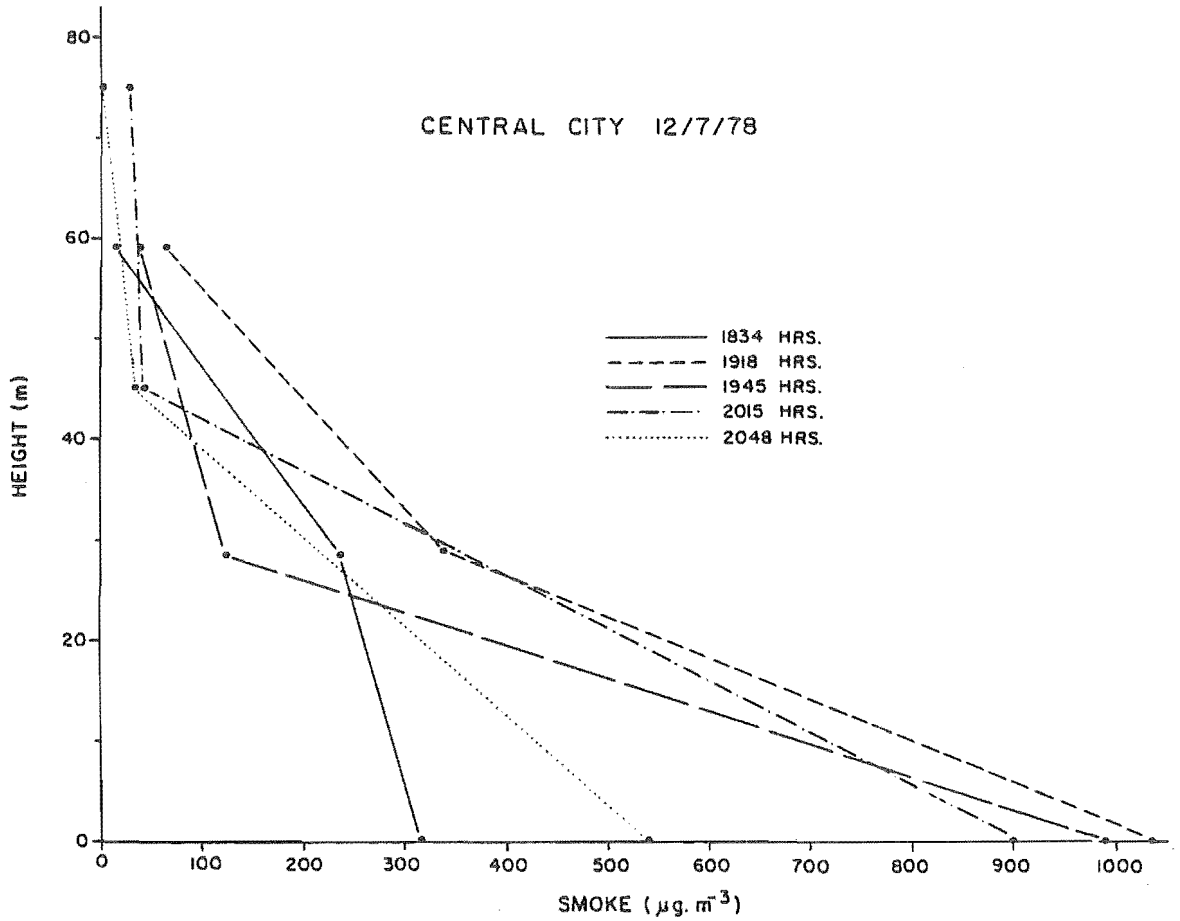

FIGURE 6.7 The Short Term Variability of Low Level Atmospheric Smoke Pollution, 12 July, 1978.

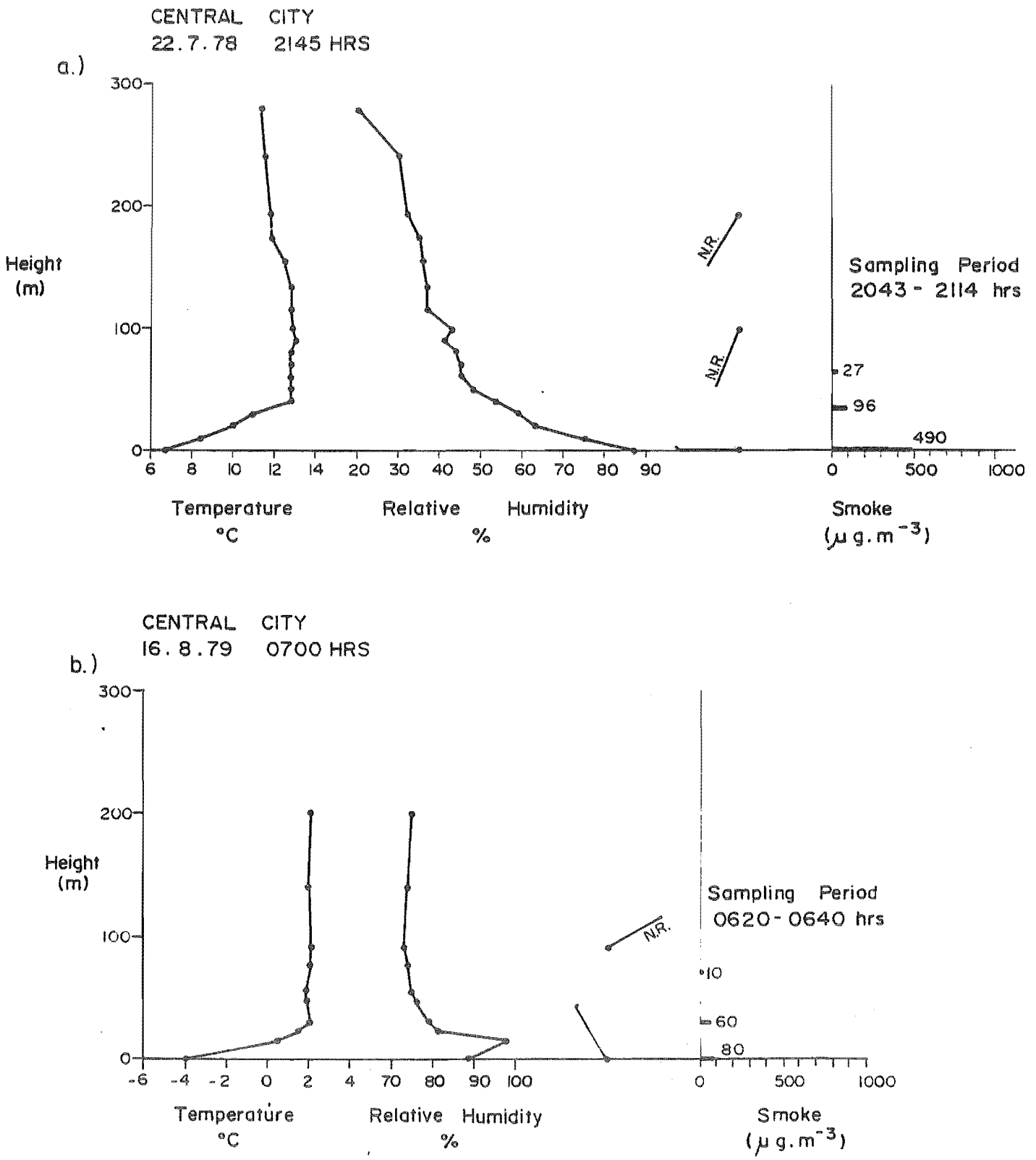

FIGURE 6.8 Typical Temperature and Pollution Profiles for a, a) Late Evening, and b) Early Morning Flight.

of the inversion at 40 m. Above the inversion concentrations drop rapidly to 27 μg m^{-3} at 64 m. By comparison, the early morning flight of 16 August, 1979 shows only moderate, but well mixed, concentrations of smoke (60 - 80 μg m^{-3}) below an inversion at 32 m. Above the inversion there is a marked reduction in pollution to 10 μg m^{-3} at 60 m.

Daytime Profiles

Daytime winter smoke pollution profiles have been subdivided into those made during the break up of the nocturnal surface inversion, where pollution levels are still relatively high, and those under daytime lapse conditions when concentrations are low.

With small sample numbers (N = 3) little can be inferred from the composite pollution profile under transitional conditions (Figure 6.9a). Concentrations of pollution with altitude are similar to those of the early morning composite pollution profile under inversion conditions. Under pure lapse conditions the daytime smoke pollution profile (Figure 6.9b) once again shows decreasing smoke concentrations with altitude, although mean concentrations at all levels are below 10 μg m^{-3}. At the ∿ 67 m level pollution concentrations of 2 μg m^{-3} are at the threshold of detection. In common with the other composites, there is considerable variability around the mean concentrations, particularly near to the ground.

A typical late winter pollution situation under lapse conditions is shown in Figure 6.10. With a reasonably strong temperature lapse of 4.0° C 100 m^{-1} near to the surface, upward diffusion of pollution is quite efficient. Accordingly smoke concentrations decrease from 20 μg m^{-3} at the surface to zero at 65 m.

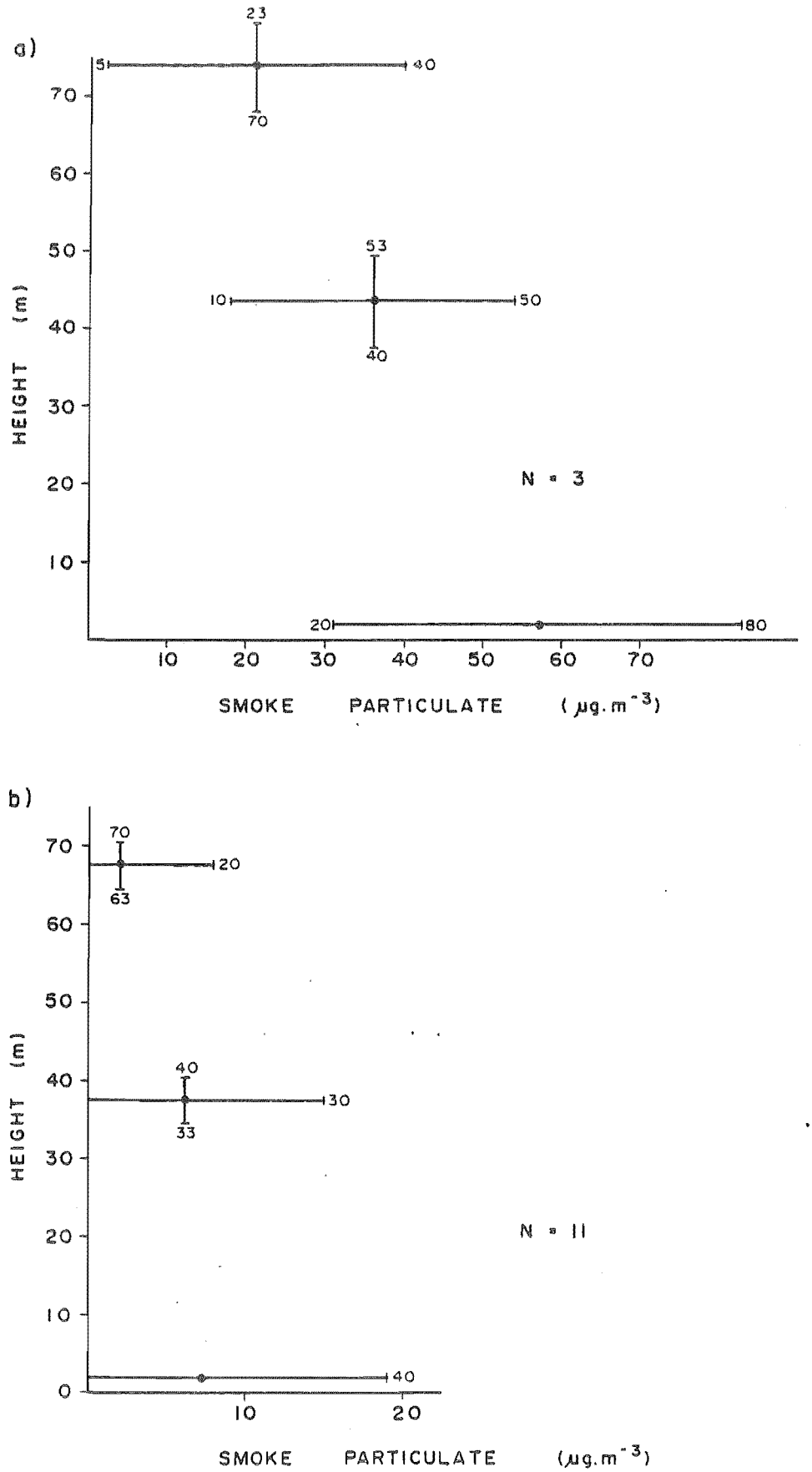

FIGURE 6.9 Composite of Daytime Profile Characteristics of Smoke Particulate, a) During Temperature Profile Transition, and b) Under Lapse Conditions. Bars Show Plus and Minus One Standard Deviation and Extreme Values.

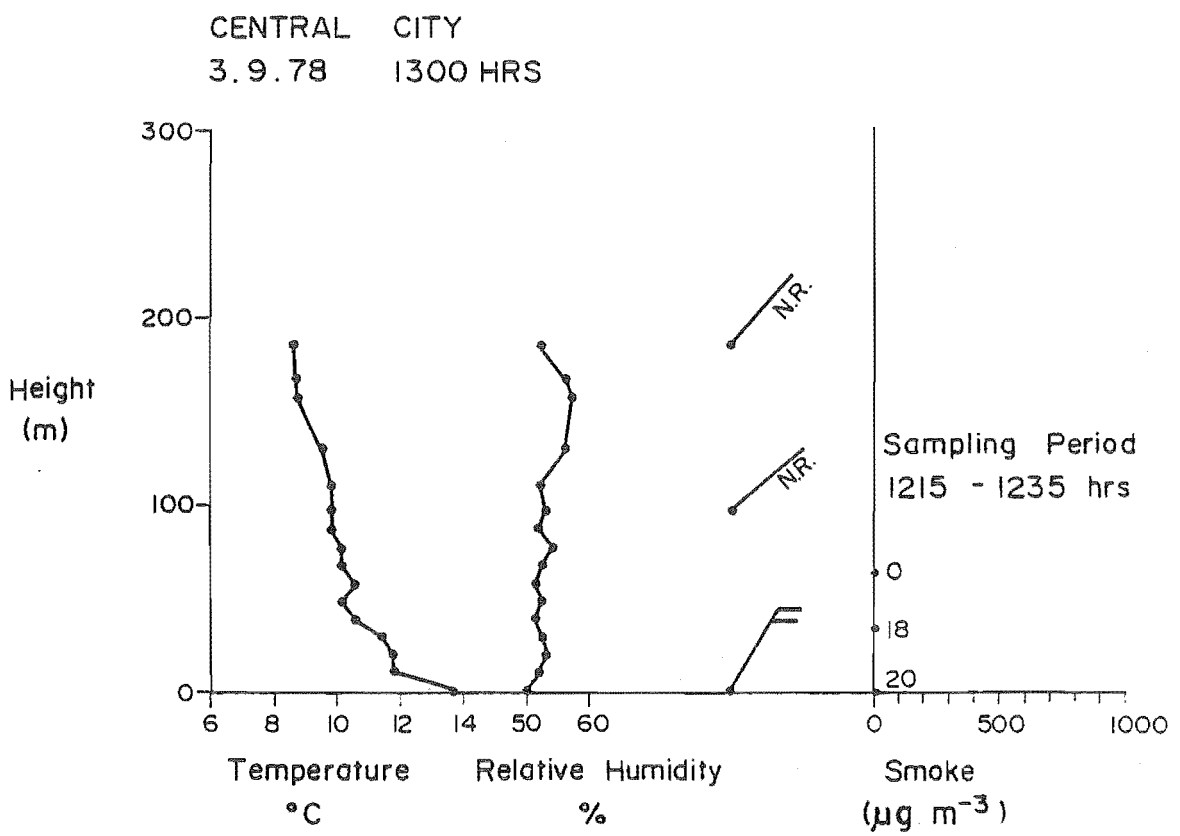

FIGURE 6.10 A Typical Late Winter Lapse Profile and Smoke Concentrations, 3 September, 1978.

Discussion

Notwithstanding the limited numbers of sampling points on each profile and the relatively small numbers of profiles involved, two significant points emerge from this brief summary of wintertime vertical pollution profiles.

Firstly, irrespective of whether a lapse or inversion temperature profile is present, pollution concentrations show a decrease with altitude. This is because under stable conditions the upward movement of air pollution is hindered, and as in the Christchurch case the pollution input is at very low levels, this is where the higher concentrations remain. Also, as wind speeds increase with height, so does the ability of the atmosphere to disperse and dilute pollutants. Under daytime lapse conditions upward diffusion in an unstable atmosphere ensures that pollution decreases away from its source near the surface. Higher winds aloft again ensure that the rate of dispersal in the upper boundary-layer is greater than at the surface.

Secondly, actual concentrations of pollution in the boundary-layer are dependent on the rate of emission as well as atmospheric stability. The two extremes can be seen between late evening profiles when both emissions and stability levels are high, and daytime profiles when emissions are low and there is pronounced instability. The importance of emission factors alone on the pollution concentration profile is evident from a comparison of morning and evening concentration profiles under inversion conditions.

Comparison of the vertical profile of pollution over Christchurch with other studies is difficult since previous studies of atmospheric pollution in free air over cities have been few and largely

limited to isolated case studies which cannot be related easily to the composite pollution profiles used here.

High concentrations of near-surface atmospheric pollution during conditions of surface based inversions have also been noted previously by Braun and Wilson (1961) for balloon sampling of SO_2 over London, Davidson (1967) for helicopter sampling of SO_2 over New York, and Ahlquist and Charlson (1968) for aerosol light scattering coefficients measured by aircraft over Seattle. Bach *et al.* (1970) constructed composite profiles of mean turbidity from helicopter flight under conditions of high air pollution potential over Cincinnati. They found a rapid decrease in mean turbidity away from the surface.

The results of Nkemdirim *et al.* (1975) for surface based inversion conditions in Calgary are somewhat at variance. Using data gathered from a tall building they found a pollution (coefficient of haze) inversion with an elevated pollution plume, but there was evidence that it was a phenomenon peculiar to Calgary and related to advective effects and emission from a source at some height above the surface. Observations of a pollution lapse under daytime conditions of instability by the Calgary investigators are in accordance with observations elsewhere.

Summer Nitrogen Oxide Profiles

Nocturnal Profiles

Figure 6.11a is a composite of seven pollution profiling flights undertaken on summer/autumn evenings under clear-sky inversion conditions. Both the concentration of total nitrogen oxides (NOx) and nitrogen dioxide (NO_2) at the 2 m, $\sim$ 76 m and $\sim$ 142 m levels are shown. Figure 6.11a is somewhat atypical as it includes two profiles

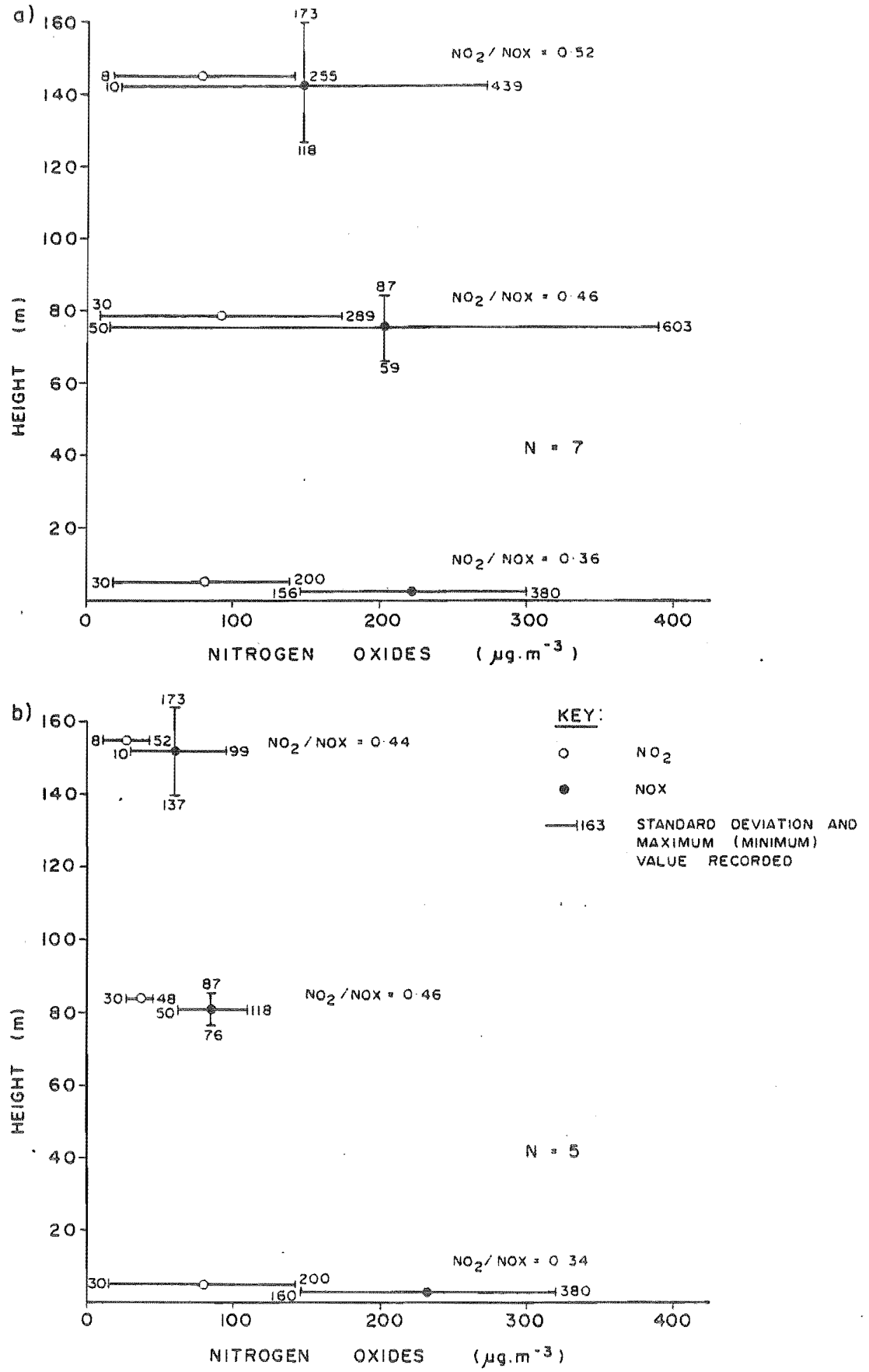

FIGURE 6.11 Composite of Nocturnal Profile Characteristics of Nitrogen Oxides (NOx and NO_2), Showing a) All Data, and b) Adjusted Data (Minus 5.4.79 and 14.4.79). Bars Show Plus and Minus One Standard

from rather unusual days where the top of the inversion lay above the operational limit of the kytoon, and where pollution concentrations were much higher than normal at the two upper sampling stations. Removal of these two profiles (5 April, 1979 and 14 April, 1979) from the composite yielded Figure 6.11b which is considered to be more representative of the summertime nocturnal nitrogen oxides profile under inversion conditions.

Figure 6.11b exhibits a marked decrease in NOx between the surface (232 $\mu g\ m^{-3}$) and $\sim$ 80 m (85 $\mu g\ m^{-3}$). The $\sim$ 80 m level lies above the mean height of the top of the nocturnal summer temperature inversion (74 m). Above $\sim$ 80 m the concentration decreases still further to 60 $\mu g\ m^{-3}$ at $\sim$ 152 m. As with wintertime smoke pollution, variability of pollution concentration diminishes away from the surface. The pattern of NO_2 concentration with altitude is slightly different. The decrease of NO_2 concentration away from the surface is less than that of NOx, therefore the proportion of NO_2 to NOx increases with altitude, from 0.34 near the surface to $\sim$ 0.45 at the two higher levels. Above the top of the surface based inversion nitrogen oxides concentrations remain relatively high in comparison with the winter situation above the surface based inversion. This appears to be related to the greater summertime frequency of elevated inversions (Chapter 4), which trap pollution which would otherwise disperse above the surface inversion.

An example from 26 April 1979 (Figure 6.12) illustrates how elevated inversions are capable of forming elevated pollution plumes over the Christchurch urban area. Although the surface based inversion is not yet properly developed by 2315 h, quite high levels of nitrogen oxides (380 $\mu g\ m^{-3}$) are concentrated below 28 m, the height of the top of the lowest inversion. Above this level pollution concentrations

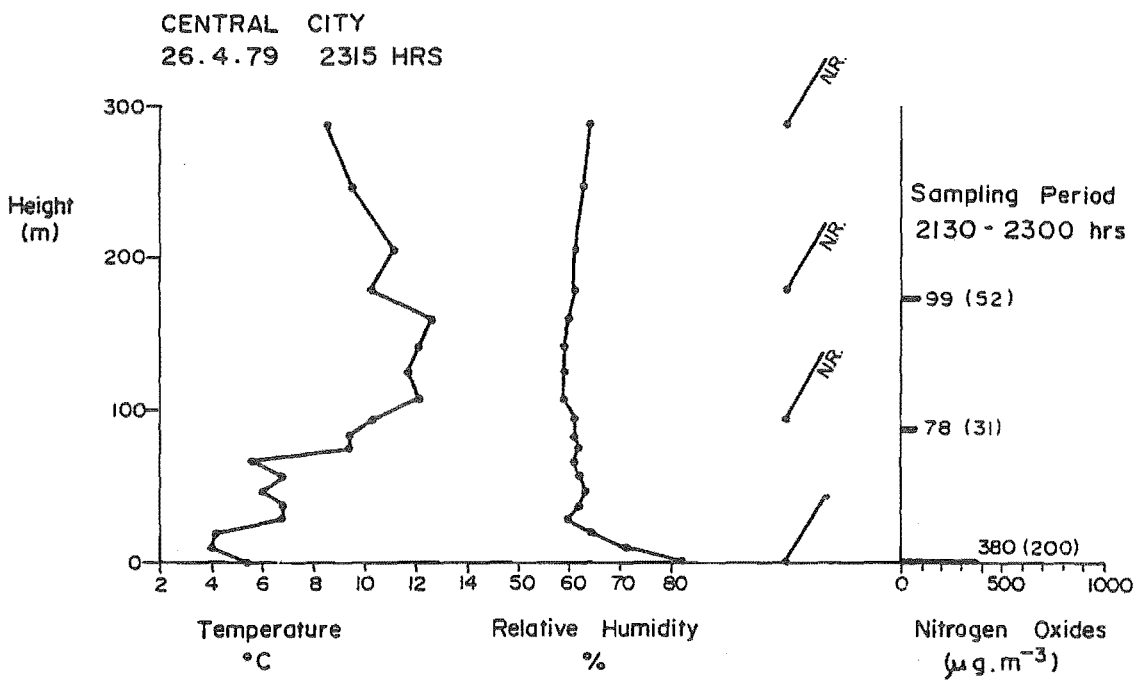

FIGURE 6.12 Elevated Inversions and Trapping of Pollutants Aloft, 26 April, 1979.

are relatively low (78 μg m^{-3} at 87 m). Trapped below an elevated inversion centred at 180 m however, there is a layer of rather more polluted air with a concentration of 99 μg m^{-3} at 173 m.

Daytime Profiles

Under daytime lapse conditions (Figure 6.13) concentrations of nitrogen oxides are low, generally near or below the limits of chemical detection. What concentrations were detected show a decrease away from the surface, and none of the six profiles detected any NOx at the upper (∿ 140 m) level. As with nocturnal NOx profiles, the proportion of NO_2 to NOx increases away from the surface, from 0.33 at 2 m to 0.50 at ∿ 70 m.

Discussion

Although a different pollutant and time of year was involved, the nocturnal and daytime profiles of pollution under summer and winter clear-sky conditions show similar characteristics. As with wintertime smoke pollution, summertime nitrogen oxides pollution showed decreasing concentrations and variability away from the surface day and night, and for similar reasons. The major reason for similarities in clear-sky profiles, despite basic differences in their physical nature, is that both pollutants have their source near ground level. Additionally, clear-sky temperature profiles in winter and summer are similar in character (although not in degree).

Trapping of pollutants under elevated inversions over urban areas, occasionally observed in the Christchurch summer data, has been reported previously by Davidson (1967) for New York as well as Perroud *et al.* (1973) and Olsson *et al.* (1974) for Grenoble and Stockholm respectively. Davidson's observations of pollution trapping

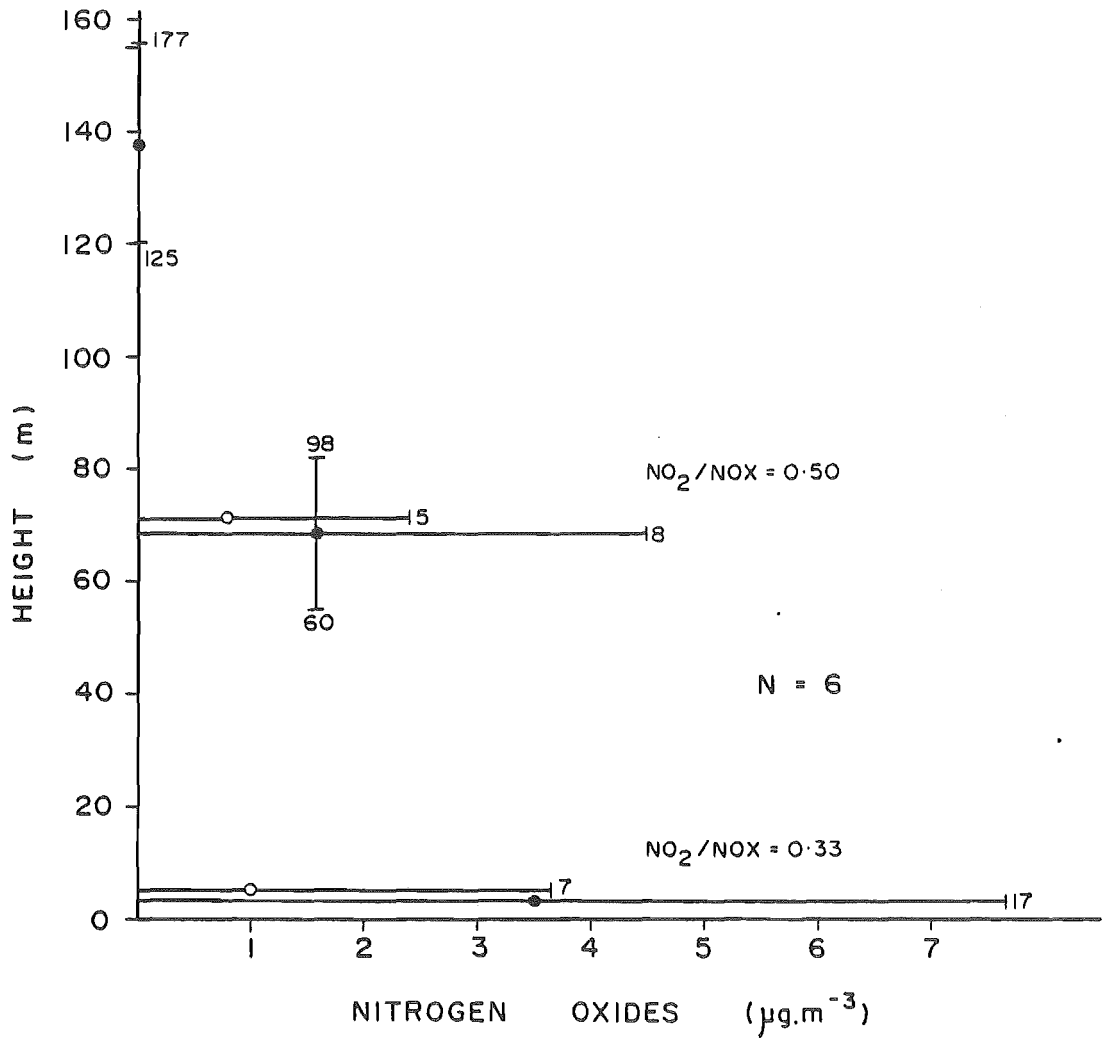

FIGURE 6.13 Composite of Nitrogen Oxides (NOx and NO_2) Profiles Under Daytime Lapse Conditions. Bars Show Plus and Minus One Standard Deviation and Extreme Values.

beneath elevated urban inversions were in fact more frequent than observations of trapping beneath surface based inversions which appear to be largely a rural phenomenon in New York.

Of potential significance for the Christchurch summer pollution profile data is the changing proportion of NO_2 to NOx away from the surface. In the absence of major chemical industry in the central Christchurch area, it must be assumed that much of the measured NO_2 is derived from NO in conjunction with photochemical oxidation processes, and that high proportions of NO_2 exhibited at night are residuals of daytime photochemical processes.

The increasing proportion of NO_2 to NOx with time and down wind of a source under favourable conditions has been reported previously (W.H.O. 1976), but does not appear to have been reported previously in the vertical dimension.

CONCLUSIONS

Significant points arising from this consideration of the Christchurch urban wind field and atmospheric pollution can be summarised as follows:-

(i) The large landform feature of Banks Peninsula exerts considerable influence on the regional windflow, particularly at lower levels of the boundary-layer. The predominant easterlies and southerlies near to the surface are deflected 40 - 60° as they pass over the area.

(ii) For most directions, winds at the rural site are 50 -

60% stronger than at the Central City Site and calms are significantly less frequent. This is related to the nature of the surfaces, and analysis of vertical wind profiles suggest that rural z_o values are near 0.20 m, while those within the city range as high as 1.60 m, depending on wind direction.

(iii) Both smoke and nitrogen oxides surface pollution exhibit yearly and daily concentration trends in line with stability and emission factors, pollution levels being highest in winter and during the evening. Lower annual variability of nitrogen oxides pollution reflects the fact that this emission is largely unrelated to climatic conditions.

(iv) Irrespective of stability conditions, wintertime smoke concentrations and variability show a decrease with altitude, although under inversion conditions near surface concentrations and variability are higher and the reduction of pollution between the surface and upper levels is considerably greater.

(v) Despite physical and seasonal differences, the vertical distribution of summertime nitrogen oxides follows a similar pattern to wintertime smoke. The NO_2 proportion of NOx is observed to increase away from the surface source in much the same way as that occurring with horizontal distance from an emission source.

(vi) The fact that the vertical profile of pollution under all conditions gives a maximum concentration near to the surface is of immense significance when considering what radiative effects the pollution might have. With highest pollution concentrations near to the surface, maximum radiative effects will be near to the surface, as it is the atmosphere immediately adjacent which contributes most to $IR\downarrow$. Also, because near surface pollution concentration can be measured much more readily than vertical profiles, predictions of pollutant radiative

effects in Christchurch should be relatively straightforward.

CHAPTER 7

CHARACTERISTICS OF CHRISTCHURCH'S URBAN RADIATION REGIME

INTRODUCTION

The primary concern of this chapter is to examine clear-weather variations in urban and rural IR↓ through the study period. Any consideration of IR↓, particularly during daytime hours, should not be separated from an examination of urban effects on solar radiation over Christchurch, as this is the ultimate source of the energy manifest in IR↓.

This chapter, the first of three dealing specifically with IR↓ is primarily descriptive. The two subsequent chapters seek to establish causative mechanisms for IR↓ variations by adopting a predictive approach, firstly through a statistical and semi-empirical approach utilising surface-based meteorological input data, and secondly, using a more sophisticated method of calculating IR↓ from profiles of atmospheric temperature, water vapour, carbon dioxide and ozone.

INCOMING SHORT WAVE RADIATION CHARACTERISTICS

Urban-Rural Differences in Total SW↓

Table 7.1 shows daily average total SW↓ (direct and diffuse solar radiation) for 28 days or parts of days chosen from throughout the study period for a complete lack of cloud cover. The average urban solar radiation deficit for the 28 clear days was 3.5% with individual daily differences ranging from -1.6% to 10.3%, for one winter day.

An average clear weather solar depletion of 3.5% over Christchurch appears lower than that previously reported for other generally much larger cities (Table 7.2), although the maximum daily depletion of 10.3% appears comparable with other cities. This clear weather depletion is also much lower than the previously reported average SW↓ urban deficit for Christchurch (Tapper, 1976). Precise reasons for the discrepancy are unclear, but are probably related to the small sample size and limited seasonal extent of the earlier study. Several problems are inherent with comparisons with clear weather depletions in other cities. Some of the studies reported in Table 7.2 refer only to heavily polluted times of the year, whereas the Christchurch data have a greater seasonal spread. In addition, Yamashita (1973) showed that solar radiation reduction could be related to pollution levels by the cosine of the altitude of the sun. The fact that solar radiation attenuation is affected by both pollution concentration and the path length of the solar beam through the urban layer suggests that direct comparison between cities of different latitudes, or observations made at different times of year may be difficult and misleading. Also, relatively low solar depletions found in recent studies may be related to different pollution sources and/or the effect of pollution controls

TABLE 7.1 Daily Average SW↓ By Site (Wm^{-2})

DATE	RURAL	URBAN	URBAN DEFICIT %	SIGNIFICANCE BY t-TEST
Feb 11/78	589	556	5.9	
Feb 22/78	557	539	3.3	
Feb 12/79	562	562	0.0	
Feb 24/79	531	506	4.9	
Feb 27/79*	627	600	4.6	0.01
March 1/78*	630	611	3.2	
March 18/79*	406	397	2.1	
Summer $\bar{X}$	557	539	3.3	
April 3/79*	466	474	-1.6	
April 14/79*	406	387	4.8	
April 15/79*	269	255	5.7	
April 16/79	351	339	3.5	0.01
April 22/79	332	316	5.1	
April 26/79	331	314	5.2	
Autumn $\bar{X}$	359	347	3.4	
July 15/78	248	245	0.9	
July 17/78*	227	230	-1.3	
Aug 5/78	301	291	3.5	
Aug 12/78	325	313	3.8	
Aug 19/78*	399	372	7.2	
Aug 20/78	334	324	2.9	
Sept 2/78	381	383	-0.6	
Sept 3/78*	398	393	1.0	0.01
July 7/79	226	208	8.8	
July 8/79	225	208	8.1	
July 21/79	265	247	7.2	
July 22/79	275	252	9.3	
Aug 3/79	271	260	4.2	
Aug 10/79	328	297	10.3	
Aug 16/79*	387	393	-1.6	
Winter $\bar{X}$	306	294	4.1	
Term $\bar{X}$	380	367	3.5	

* Incomplete solar day but including at least six consecutive clear hours.

TABLE 7.2 Previous Studies of Clear Weather Urban Total SW↓ Depletion

AUTHOR(S)	LOCATION	AVERAGE DEPLETION %	MAXIMUM DEPLETION %
Bach (1969)	Cincinnati	6	
Yamashita (1970)	Tokyo	10	
Yamashita (1973)	Toronto	5 - 15	
Rouse and McCutcheon (1972)	Hamilton (Ontario)	12	17
Sanderson (1973)	Windsor (Ontario)	9	25
Peterson and Flowers (1974)	St Louis	3	
Manes *et al.* (1975)	Bet-Dagan (Tel Aviv)	7	
Tapper (1976)	Christchurch	14	30

(Oke, 1979).

Although not obviously reflected in the seasonal means, the trends in daily differences shown in Table 7.1 appear to be clearly seasonal in character. The lowest daily differences occur in late summer and autumn, while the highest differences (as well as greatest variability) occur during the more heavily polluted winter term. The major reasons for this seasonal trend relate to an increased solar path length through an increasingly polluted urban atmosphere. For all seasons total SW↓ differences tested on an hourly basis are significant by t-test.

Urban-Rural Differences in Atmospheric Transmissivity

General

Direct beam short-wave radiation is that part of total SW↓ which reaches the surface without any form of scattering in the atmosphere by particulate and gaseous matter. Direct beam solar radiation (Q) is therefore an important measure of atmospheric opacity. A major disadvantage of using standard measures of solar radiation for comparative purposes is that they are not constant throughout the day and year and cannot be directly compared. It is therefore desirable to express direct beam SW↓ as an atmospheric transmissivity coefficient (Tr) which is given by:-

$$Tr = \left(\frac{Q}{S_o / r^2 \ (\sin A)} \right)^{1/m} \qquad \ldots 7.1$$

where, S_o - the mean solar radiation constant (1360 Wm^{-2}), r - the radius vector (which corrects S_o for the earth-sun distance), A - the altitude of the sun given by latitude, solar declination and time of day, Q -

measured direct beam SW↓, m - optical air mass (relative amount of atmosphere that radiation has to pass through), depends on air pressure and solar altitude. This equation yields a coefficient varying between 0 and 1, which expresses the proportion of direct beam radiation that would penetrate the atmosphere with the sun at its zenith. Hence the measure is independent of time of the year or day and latitude, and is an ideal measure for the examination of urban effects on the transmission of solar radiation.

Several previous studies have indicated atmospheric transmissivities that can be expected for different atmospheric conditions. In Japan, Nishizawa and Yamashita (1967) suggested that clear-sky atmospheric transmissivities for heavily polluted areas were generally < 0.65, less polluted areas < 0.75 and clear rural areas > 0.80. Sanderson *et al.* (1973) quoted urban transmissivities for a site in Windsor, Ontario, at 0.782 averaged over nine clear winter days, while at a nearby rural site the average Tr was 0.853. In a later study Sanderson (1974) quotes Tr values from 56 cloudless days for an urban site in Windsor. In this sample no days had a Tr > 0.80, 45% of days had values between 0.70 and 0.80, 38% between 0.60 and 0.70, and 17% of clear days had a Tr < 0.60. The average urban Tr recorded was 0.65, considerably lower than the urban Tr quoted in the earlier study. Differences between the two studies may be related to changes in site characteristics, computational procedure, or may be due to differences in atmospheric constituents (atmospheric water vapour and pollution) between the winter study (Sanderson *et al.*, 1973) and the other study, which drew on data from throughout the year.

It is unfortunate that none of the papers defines the transmissivity coefficient, and it is not clear whether they include a

correction for optical air mass (m), as in this study, or merely consist of a ratio of measured direct beam radiation corrected for solar altitude to that predicted for the top of the atmosphere. For example, at a solar altitude of 30^{o} and pressure of 1020 mb, the optical air mass (m) is 2.4. If the ratio of radiation at the top of the atmosphere with that measured under these conditions was 0.65, this would give a Tr value of 0.8344 in this study. For this reason comparison with these studies is on rather uncertain grounds.

In an earlier study in Christchurch, Tapper (1976) and Tapper and Owens (1976) found a mean rural Tr of 0.8253 and urban Tr of 0.7844, averaged over 20 clear days drawn from throughout the year, but concentrating on the winter half year. That study employed an urban site in the heavily polluted inner suburbs of Christchurch, and a rural site at Christchurch International Airport beyond the north-west margin of the city. A subsequent study concentrating on summer days and utilising the identical urban and rural sites to those of the present study (Tapper, 1977) found a mean rural Tr of 0.8194 and urban Tr of 0.7833, a difference of 3.9%.

Table 7.3 gives average daily transmissivities for the same 28 days represented in Table 7.1. As with total SW↓, urban-rural differences tend to become greater toward the winter half year. Individual daily differences range from an urban excess Tr of 0.9% (February 12, 1979), to a maximum urban deficit Tr of 4.7% (July 7, 1979). The overall urban Tr deficit throughout the term is 2.6%, with a mean rural Tr of 0.8524 and urban Tr of 0.8308.

While both urban and rural transmissivities reported here are higher, and urban-rural % differences lower than in the Tapper (1976)

TABLE 7.3 Average Daily Transmissivity by Site

DATE	RURAL	URBAN	URBAN Tr DEFICIT (%)
Feb 11/78	.8472	.8199	3.3
Feb 22/78	.8190	.8119	0.9
Feb 12/79	.8239	.8314	-0.9
Feb 24/79	.8563	.8292	3.3
Feb 27/79*	.8169	.8105	0.8
March 1/78*	.8224	.8148	0.9
March 18/79*	.8275	.8050	2.8
Summer $\bar{X}$	.8304	.8175	1.6
April 3/79*	.8716	.8739	-0.3
April 14/79*	.8665	.8351	3.8
April 15/79*	.8549	.8114	5.3
April 16/79	.8749	.8526	2.6
April 22/79	.8380	.8181	2.4
April 26/79	.8612	.8300	3.7
Autumn $\bar{X}$	.8612	.8368	2.9
July 15/78	.8350	.8235	1.4
July 17/78*	.8490	.8436	-0.3
Aug 5/78	.8666	.8534	1.5
Aug 12/78	.8589	.8286	3.7
Aug 19/78*	.8629	.8212	3.8
Aug 20/78	.8617	.8418	2.3
Sept 2/78	.8424	.8387	0.4
Sept 3/78*	.8182	.7884	3.8
July 7/79	.8784	.8390	4.7
July 8/79	.8103	.7764	4.4
July 21/79	.8871	.8533	4.0
July 22/79	.9106	.8710	4.5
Aug 3/79	.8687	.8503	2.2
Aug 10/79	.8924	.8412	6.1
Aug 16/79*	.8524	.8505	0.2
Winter $\bar{X}$	.8591	.8347	2.9
Term $\bar{X}$	.8524	.8308	2.6

* Incomplete solar day, but includes at least six consecutive hours.

study, the results are comparable with the 1977 study in Christchurch utilising the same representative sites. Rural transmissivities observed in this study are very similar to those observed by Sanderson (1973), although Christchurch's urban transmissivity indicates considerably lower urban radiation attenuation than over Windsor, Ontario.

Average hourly transmissivities for all clear weather data for both urban and rural sites have been tabulated and classified according to percentage occurrence in each transmissivity grouping by season (Table 7.4). All clear weather transmissivity data have been included in these tables; 291 hours from the rural site and 283 hours from the urban site. Transmissivity values are greater at the rural site in comparison with the urban site in all seasons, with the trend becoming more pronounced toward the winter season as would be expected with increasing pollution and greater solar path through the atmosphere. Throughout the term only 1% of rural transmissivities lie below 0.75, while 8% of urban transmissivities are below 0.75. At the other end of the scale 52% of rural transmissivities are above 0.85 compared to only 27% of urban values. Examination of rural transmissivities (assumed unaffected by atmospheric pollution) indicates an increased atmospheric transmissivity toward winter (19% of summer observations > 0.85, 65% of winter observations > 0.85). This is probably related to a decreased atmospheric water vapour content toward winter.

Table 7.5 compares the seasonal mean hourly transmissivity values for each site. In all seasons there is a trend toward increased urban transmissivity deficits during early to mid-morning and again in the late afternoon. This appears to be the result of an interaction between solar path length and pollution levels throughout the day in a similar manner to seasonal trends. The times of maximum solar

TABLE 7.4 Hourly Clear Sky Transmissivities by Season (Percentage Occurrence)

	Tr	RURAL	URBAN
a) Summer	> 0.85	19	9
	0.81 - 0.85	59	46
	0.76 - 0.81	21	40
	0.71 - 0.75	1	1
	< 0.71	-	4
		N = 80	N = 78
b) Autumn	> 0.85	63	36
	0.81 - 0.85	32	38
	0.76 - 0.81	5	11
	0.71 - 0.75	-	10
	< 0.71	-	5
		N = 62	N = 52
c) Winter	> 0.85	65	33
	0.81 - 0.85	29	50
	0.76 - 0.81	4	10
	0.71 - 0.75	2	4
	< 0.71	-	3
		N = 149	N = 153
d) Term	> 0.85	52	27
	0.81 - 0.85	38	47
	0.76 - 0.81	9	18
	0.71 - 0.75	1	4
	< 0.71	-	4
		N = 291	N = 283

TABLE 7.5 Seasonal hourly transmissivities at Lincoln and Central City Sites

TIME N.Z.S.T.	SUMMER (FEB, MARCH)				AUTUMN (APRIL)				WINTER (JULY, AUG, SEPT)			
	RURAL	URBAN	URBAN Tr DEFICIT (%)	NO_x ($\mu g\, m^{-3}$)	RURAL	URBAN	URBAN Tr DEFICIT (%)	NO_x ($\mu g\, m^{-3}$)	RURAL	URBAN	URBAN Tr DEFICIT (%)	SMOKE ($\mu g\, m^{-3}$)
5- 6	.8200	.8180	0.2	15	-	-	-	-	-	-	-	-
6- 7	.8295	.8118	2.2	18	-	-	-	-	-	-	-	-
7- 8	.8167	.8063	1.3	34	.8500	.8350	1.8	40	.8769	.8546	2.6	25
8- 9	.8182	.7742	5.6	50	.8459	.8117	4.2	91	.8828	.8170	8.0	50
9-10	.8196	.7975	2.8	35	.8535	.8395	1.7	66	.8510	.8090	5.2	61
10-11	.8216	.8135	1.0	28	.8496	.8247	3.0	50	.8499	.8348	1.8	47
11-12	.8256	.8050	2.5	23	.8525	.8519	0.1	41	.8435	.8327	1.3	34
12-13	.8295	.8166	1.6	19	.8560	.8595	-0.4	27	.8483	.8441	0.5	25
13-14	.8315	.8205	1.3	19	.8570	.8466	1.2	28	.8542	.8456	1.0	17
14-15	.8326	.8178	1.8	19	.8643	.8553	1.0	28	.8588	.8496	1.1	16
15-16	.8466	.8222	2.9	19	.8730	.8507	2.6	30	.8620	.8465	1.8	16
16-17	.8372	.7926	5.6	28	.8862	.7944	11.5	48	.8712	.8325	4.6	37
17-18	.8488	.8249	2.9	28	.8662	.8400	3.1	40	.9016	.8464	6.5	59
18-19	.8424	.8500	-0.9	19	-	-	-	-	-	-	-	-

attenuation in all seasons correspond closely with periods of maximum pollution build up. Depletion of the urban solar beam is enhanced because the times of maximum pollution are coincident with relatively long solar paths, this increasing the depth of polluted atmosphere the solar beam has to pass through. The daily trend in urban transmissivity deficit is shown well in the winter case (Table 7.5). Between 0700 - 0800 h the urban-rural difference is small, along with relatively low pollution amounts. Between 0800 - 0900 h attenuation of solar beam is greatest (8.0%) due to an increasing level of pollution and relatively low solar altitude. An hour later attenuation is dropping once again because of a higher solar elevation, despite highest daytime pollution levels. With daytime instability and relatively high solar altitudes, attenuation during the middle of the day is at a low level, but increasing pollution and lower solar altitudes after 1600 h combine to increase the depletion of the urban solar beam.

Factors Involved in Urban-Rural Variations in Transmissivity

All recent studies of solar radiation attenuation in urban areas isolate atmospheric pollution as the dominant agent of reduction (Oke, 1979). Tapper (1976), in stepwise multiple regression analysis on Christchurch data also found that smoke pollution was the dominant influence on wintertime urban-rural transmissivity differences, and that meteorological variables controlling pollution levels (windspeed and atmospheric stability) were also indirectly related to atmospheric transmissivity through their effects on pollution. Wind direction was also found to be important according to whether the windflow was pushing polluted urban air over the nearby rural site, or whether the air mass over the rural site was rural in character.

Simple linear regression analysis of pollution plotted against hourly urban Tr deficit (%) has been performed on the current data stratified according to summer and winter observations (Table 7.6). Because of the log-normal distribution of pollution concentrations, analysis has been performed on $\log_{10}$ pollution values only. Clear seasonal trends are indicated in Table 7.6, with correlations being better for the winter data (urban Tr deficit with smoke pollution), than for the summer data (urban Tr deficit with NOx pollution). As would be expected, the relationship between reduction in urban transmissivity and increased smoke pollution is a positive one. Figure 7.1 illustrates the relationship between winter time urban Tr deficit and $\log_{10}$ urban smoke pollution (S). The equation of the line is given by:

$$\text{URBAN Tr DEFICIT} = 4.3 \log S - 1.88 \quad \ldots 7.2$$

This is almost identical to the rate of attenuation increase with increasing smoke pollution found previously by Tapper (1976).

Monteith (1966) stated that for London, a 10 $\mu g\ m^{-3}$ reduction in smoke resulted in a 1% increase in total SW↓. Testing of the winter regression equation (on untransformed smoke data):

$$\text{URBAN Tr DEFICIT} = 2.13 + 0.04S \quad \ldots 7.3$$

yields a 0.4% increase in urban transmissivity with every 10 $\mu g\ m^{-3}$ of smoke decrease. Unfortunately, comparison of these figures with those of Monteith is difficult because they apply to different measures of short wave radiation. To obtain some form of comparison it is necessary to assume that urban-rural differences in diffuse radiation (q) are insignificant, a not unreasonable assumption in the case of

TABLE 7.6 Summary of Regression Analysis - Urban Tr Deficit (%) and Pollution Characteristics

	LOG POLLUTION (LOG^N, LOGS)				
DEPENDENT VARIABLE	NO. OBS	a	b	*r*	SIGNIF
Summer Urban Tr Deficit (%)	115	-2.6	4.1	0.24	0.05
Winter Urban Tr Deficit (%)	129	-1.88	4.3	0.55	0.01

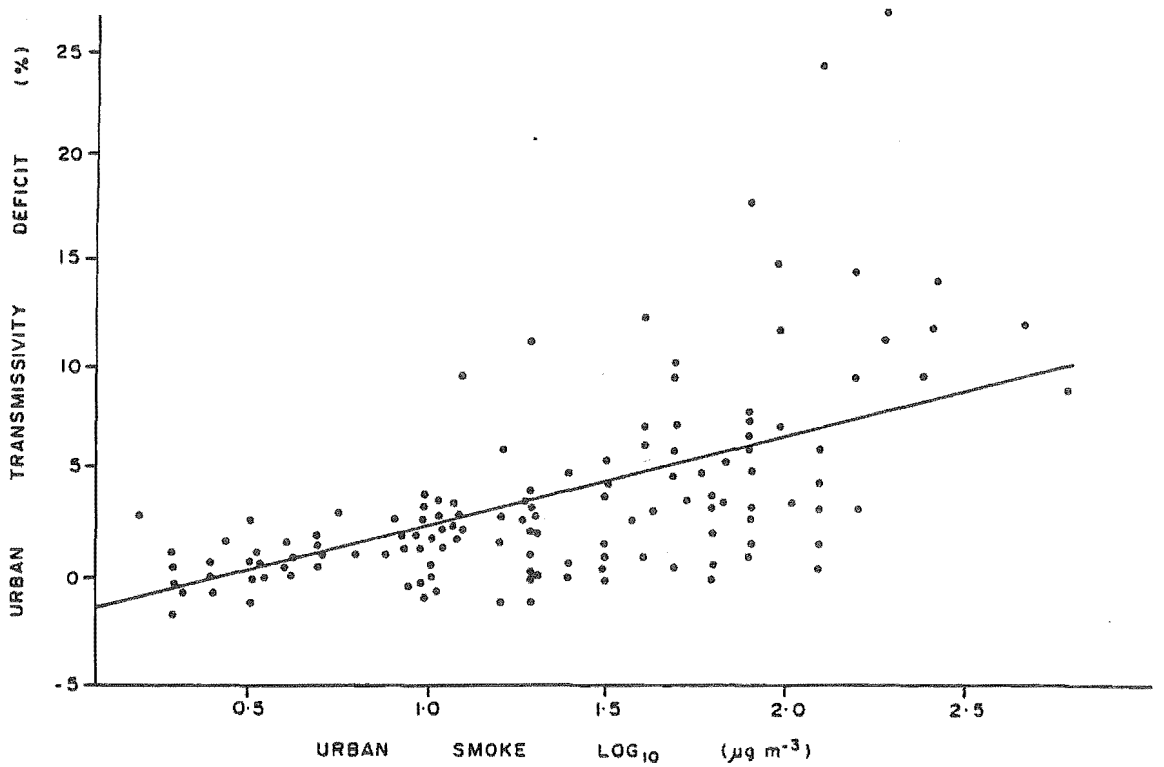

FIGURE 7.1 Relationship Between Urban Transmissivity Deficit and Log Urban Smoke Particulate.

Christchurch (Tapper, 1976 p. 54). From Equation 7.1 it can be seen that a given reduction in Tr will only be equivalent to a reduction in Q if the optical air mass term m = 1.0. For values of m > 1.0, corresponding reductions in Tr will be smaller than reductions in Q. Thus it appears that the effect of smoke pollution on short wave radiation in Christchurch is similar to that established for London by Monteith (given that m is always considerably > 1 during winter months).

Implicit in the loss of SW↓ at the surface in urban areas is absorption and backscatter in the pollution layer, in unknown proportions. Almost certainly absorption is causing some of the heating observed within the urban boundary-layer (Chapter 4), and thereby indirectly influencing IR↓.

INCOMING INFRA-RED RADIATION CHARACTERISTICS

Urban-Rural Differences in IR↓

Daily average IR↓ for each site computed from hourly radiation values are presented in Table 7.7. This table comprises 20 complete days and five further days with at least 12 h of continuous clear weather chosen from throughout the study period (550 hours of data represented). Table 7.7 indicates a clear seasonal variation in IR↓ for both representative sites, with IR↓ decreasing noticeably towards the winter half-year. In the absence of cloud, IR↓ in clear rural areas is dependent upon the bulk atmospheric temperature and emissivity (which is itself dependent upon the distribution of temperature, water vapour, carbon dioxide and other gaseous atmospheric constituents).

TABLE 7.7 Average Daily IR↓ By Site (Wm^{-2})

DATE	RURAL IR↓	URBAN IR↓	URBAN IR↓ EXCESS (%)	SIGNIFICANCE BY t-TEST
Feb 11/78	297	300	1.0	
Feb 22/78	313	323	3.1	
March 1/78*	323	325	0.6	0.01
Feb 24/79*	300	315	4.6	
Feb 27/79	325	330	1.5	
Summer $\bar{X}$	312	319	2.2	
April 3/79*	314	323	2.8	
April 14/79	256	271	5.5	
April 15/79	278	297	6.4	
April 16/79	280	302	7.3	0.01
April 22/79	310	323	4.0	
April 26/79	245	259	5.4	
April 27/79	243	257	5.4	
Autumn $\bar{X}$	275	290	5.2	
July 16/78*	243	247	1.6	
July 17/78	252	272	7.3	
Aug 5/78	258	271	4.8	
Aug 19/78	258	267	3.4	
Aug 20/78	259	270	4.1	
July 7/79	234	262	10.7	
July 8/79	237	266	10.9	0.01
July 10/79*	262	263	0.2	
July 21/79	235	270	12.9	
July 22/79	240	260	7.7	
Aug 3/79	250	276	9.4	
Aug 10/79	229	244	6.1	
Aug 16/79	218	242	9.9	
Winter $\bar{X}$	244	262	6.9	
Term $\bar{X}$	266	281	5.3	

* Incomplete day but generally at least ten consecutive hours.

This is described by the Stefan-Boltzmann Law (Equation 1.2). Summer conditions produce greater IR↓ because increased solar radiation raises atmospheric temperatures (directly contributing to IR↓), and these higher temperatures enable a considerable amount more water vapour to be absorbed into the atmosphere. In addition, the flux emissivities of certain atmospheric constituents become greater with warmer atmospheric temperatures (Staley and Jurica, 1970).

Distinct from the seasonal trend in IR↓, an urban-rural trend is also evident in Table 7.7. An urban excess IR↓ is evident in all seasons, with the excess relatively greater during the winter season. The urban-rural difference in hourly data by season is statistically significant at the 0.01 level by t-test. The average urban IR↓ excess on clear days over the study period was 5.3%, with the highest daily urban IR↓ excess of 12.9% occurring on July 21, 1979. The only comparable data obtaining in the literature is an 11% urban excess measured over 160 h in Hamilton, Ontario, by Rouse and McCutcheon (1972).

To more closely examine reasons for increased urban IR↓ the direct temperature dependence of radiation has been eliminated by considering the atmospheric apparent emissivity:-

$$\varepsilon a = IR\downarrow/\sigma T^4 \qquad \ldots 7.5$$

The ideal temperature input to Equation 7.5 would be a value for the bulk atmospheric temperature, but in the absence of radiosonde data on an hourly basis it has been necessary to substitute screen level temperature in this study. Table 7.8 indicates atmospheric apparent emissivities for the same data base employed in Table 7.7. A general decrease in apparent emissivities at both sites toward winter in line with reasons advanced previously for IR↓ is evident. Overall atmospheric

TABLE 7.8 Average Daily Emissivity By Site

DATE	RURAL EMISSIVITY	URBAN EMISSIVITY	URBAN EMISSIVITY EXCESS %
Feb 11/78	.7400	.7164	-3.2
Feb 22/78	.7388	.7331	-0.7
March 1/78*	.7513	.7406	-1.4
Feb 24/79*	.7773	.8294	6.3
Feb 27/79	.7760	.7850	1.1
Summer $\bar{X}$	.7567	.7609	0.6
April 3/79*	.8698	.8731	0.4
April 14/79	.7575	.7276	-4.1
April 15/79	.7946	.7970	0.3
April 16/79	.7736	.7946	2.6
April 22/79	.8039	.8287	3.0
April 26/79	.7190	.7148	-0.5
April 27/79	.7557	.7417	-1.8
Autumn $\bar{X}$	.7820	.7825	0.1
July 16/78*	.7582	.7479	-1.4
July 17/78	.7592	.8085	6.1
Aug 5/78	.7459	.7703	3.2
Aug 19/78	.7313	.7320	0.1
Aug 20/78	.7478	.7670	2.5
July 7/79	.7187	.7868	8.6
July 8/79	.7178	.8059	10.9
July 10/79*	.7487	.7250	-3.3
July 21/79	.7080	.8208	13.7
July 22/79	.7331	.7757	5.5
Aug 3/79	.7560	.7824	3.4
Aug 10/79	.7296	.7432	1.8
Aug 16/79	.6946	.7485	7.2
Winter $\bar{X}$	.7345	.7703	4.6
Term $\bar{X}$	.7522	.7718	2.5

* Incomplete day but at least ten consecutive hours.

apparent emissivities for the whole term are 0.7522 for the rural station and 0.7703 for the urban station, a mean urban excess emissivity of 2.5%. While the urban excess emissivity is quite small for the summer and autumn seasons, the urban excess is markedly larger (4.6%) during the winter.

Diurnal variations in clear weather IR↓ for individual sites and urban IR↓ excess from a data base of 599 hours are shown in Table 7.9. In both the summer/autumn and the winter season the diurnal variation of IR↓ at the rural site is relatively small and peaks near solar noon, a phenomenon common to other rural observations of IR↓ (Monteith and Szeicz, 1961; Sanderson, 1974). This is to be expected with the relative stability of the bulk atmospheric temperature and emissivity, neither of which fluctuate rapidly or widely during the day (Oke, 1979). Urban IR↓ similarly varies only slightly diurnally and also peaks during the middle of the day, but distinct trends in urban excess IR↓ are evident. The summertime trend in urban excess IR↓ shows a minor peak during the early morning (0600 - 0800 h), and a more significant and sustained excess overnight, particularly between 2000 and 0200 h ($\sim$ 7%). During the middle of the day urban excess IR↓ remains relatively low, generally below 4%. The wintertime trend in diurnal urban excess IR↓ shows a significant peak as high as 12% between 0600 and 0900 h following a sustained build up in urban excess IR↓ from 2100 h the previous evening. A minor peak urban excess IR↓ in winter also occurs between 1500 and 1700 h. The diurnal variation of urban excess IR↓ is discussed in more detail below.

TABLE 7.9 Seasonal Hourly IR↓ Values By Site (Wm^{-2})

	SUMMER/AUTUMN				WINTER			
TIME N.Z.S.T.	RURAL IR↓	URBAN IR↓	URBAN IR↓ EXCESS %	N	RURAL IR↓	URBAN IR↓	URBAN IR↓ EXCESS %	N
00-01	270	288	6.2	12	238	256	7.0	15
01-02	267	284	6.0	12	234	254	7.8	15
02-03	265	278	4.7	11	233	253	7.9	15
03-04	263	276	4.7	11	230	253	9.0	15
04-05	263	276	4.7	12	227	252	9.9	14
05-06	263	273	3.6	12	228	252	9.5	13
06-07	256	271	5.5	10	227	254	10.6	14
07-08	270	282	4.2	10	227	258	12.0	13
08-09	303	312	2.9	10	240	265	9.4	13
09-10	315	326	3.4	10	251	274	8.3	13
10-11	325	332	2.1	10	262	281	6.8	13
11-12	322	332	3.0	10	265	278	4.7	13
12-13	321	333	3.6	11	262	278	5.7	12
13-14	317	329	3.6	10	265	284	6.6	13
14-15	317	330	3.9	10	266	286	7.0	13
15-16	320	331	3.3	10	264	286	8.6	13
16-17	317	331	4.2	10	254	277	8.3	14
17-18	302	312	3.2	10	252	259	3.0	15
18-19	292	299	2.3	11	244	248	2.0	15
19-20	282	290	2.7	11	240	249	3.6	15
20-21	275	291	5.5	11	239	251	4.8	15
21-22	273	294	7.1	12	238	252	5.6	16
22-23	273	294	7.1	12	237	256	7.5	16
23-00	276	294	6.1	12	238	256	7.0	16

Rouse and McCutcheon (1972) report a maximum mean hourly urban excess IR↓ of 31% and an extreme maximum hourly excess of 66%, both recorded near solar noon. In this study the maximum mean hourly urban excess and extreme hourly excess were 12% and 22% respectively, both recorded between 0700 and 0900 h under winter conditions. The continuation of urban excess IR↓ into nighttime hours shown in Table 7.9 was not observed to the same extent by Rouse and McCutcheon (1972) or Rouse, Noad and McCutcheon (1973). However, Oke and Fuggle (1972), in a series of night-time observations in Montreal found an urban excess IR↓ of approximately 5%.

Removal of direct temperature influence on IR↓ to give the diurnal variation of atmospheric apparent emissivity (εa) yields Table 7.10. Because of the diurnal variation of vapour pressure (Table 5.1, page 146) and the temperature dependence of other gaseous emissions, emissivities would be expected highest during the middle of the day. Both urban and rural εa show a distinct diurnal trend in both seasons, with emissivities at a minimum overnight and highest during the day, although peaking somewhat earlier than expected (between 0800 and 1000 h). The most likely explanation for this phenomenon relates to the 'centre of gravity' of atmospheric emission concept, where early morning near-surface temperatures (for input into equation 7.5) considerably underestimate the bulk atmospheric temperature, hence overestimating εa. A diurnal variation of urban emissivity excess superimposed on the above pattern is also revealed in Table 7.10. Both seasons show an urban excess emissivity which peaks during the early morning (11.8% between 0800 and 1000 h in the winter case), and to a lesser extent overnight. Since temperature profiles over the urban site generally show weaker inversions (Chapter 4), urban-rural differences in the 'centre of

TABLE 7.10 Seasonal Hourly Emissivity By Site

	SUMMER/AUTUMN				WINTER			
TIME N.Z.S.T.	RURAL ϵa	URBAN ϵa	URBAN ϵa EXCESS (%)	N	RURAL ϵa	URBAN ϵa	URBAN ϵa EXCESS (%)	N
00-01	.7646	.7632	-0.2	12	.7340	.7750	5.3	15
01-02	.7618	.7580	-0.5	12	.7299	.7761	5.9	15
02-03	.7628	.7511	-1.5	11	.7248	.7898	8.2	15
03-04	.7581	.7527	-0.7	11	.7206	.7782	7.4	15
04-05	.7597	.7525	-0.9	12	.7203	.7832	8.0	14
05-06	.7619	.7485	-1.7	12	.7281	.7834	7.0	13
06-07	.7589	.7535	-0.7	10	.7303	.7994	8.6	14
07-08	.7938	.8090	1.9	10	.7332	.8221	10.8	13
08-09	.8136	.8588	5.3	10	.7570	.8551	11.5	13
09-10	.8401	.8510	1.3	10	.7867	.8544	7.9	13
10-11	.8269	.8227	-0.5	10	.7603	.8112	6.2	13
11-12	.7915	.8009	1.2	10	.7631	.7863	2.9	13
12-13	.7923	.7993	0.9	11	.7360	.7685	4.2	12
13-14	.7784	.7876	1.2	10	.7345	.7796	5.8	13
14-15	.7781	.7954	2.2	10	.7356	.7819	5.9	13
15-16	.7794	.7963	2.1	10	.7227	.7784	7.1	13
16-17	.7624	.7863	3.0	10	.7270	.7729	5.9	14
17-18	.7529	.7566	0.5	10	.7360	.7211	-2.0	15
18-19	.7458	.7281	-2.4	11	.7245	.7022	-3.2	15
19-20	.7391	.7116	-3.9	11	.7265	.7151	-1.5	15
20-21	.7302	.7283	-0.3	11	.7265	.7271	0.1	15
21-22	.7254	.7423	2.3	12	.7278	.7310	0.4	16
22-23	.7320	.7459	1.9	12	.7338	.7469	1.8	16
23-00	.7405	.7485	1.1	12	.7366	.7560	2.8	16

gravity' effect are unlikely a cause of the excess emissivity, suggesting that a non-meteorological variable such as atmospheric pollution may be at least partially responsible.

Simple plots of wintertime εa and relevant atmospheric variables at the urban and rural sites are shown in Figures 7.2a and b. Such plots are an initial step in understanding reasons for urban-rural differences in IR↓. In the rural case (Figure 7.2a) there is general agreement between the temperature/vapour pressure trends and that of εa, with higher daytime and lower night-time levels. As described above the 'centre of gravity' problem appears to be the major cause of εa peaking several hours before temperature and vapour pressure. Rural absolute humidities exhibit a minor peak shortly after sunrise (Chapter 5) due to moisture input to a stable atmosphere, but this is unlikely a significant cause. One mechanism previously invoked for anomalously large daytime atmospheric emission in rural areas has been the addition of natural aerosol matter to the lower atmosphere by solar induced turbulence (Idso *et al.*, 1969). Since stable conditions persist through most of the period of increased rural εa, this hypothesis is also unlikely.

The difficulty of defining the bulk atmospheric temperature also creates problems in relating wintertime urban εa to atmospheric variables (Figure 8.2b). The peak in urban εa after sunrise and the trough after sunset are at least partially related to the 'centre of gravity' concept described previously. The marked drop in urban εa at sunset is possibly related to aspects of the urban heat island described in Chapter 4. Near-surface urban warmth at a time when overall atmospheric temperatures are decreasing rapidly may be artificially lowering apparent urban emissivities. As a result εa

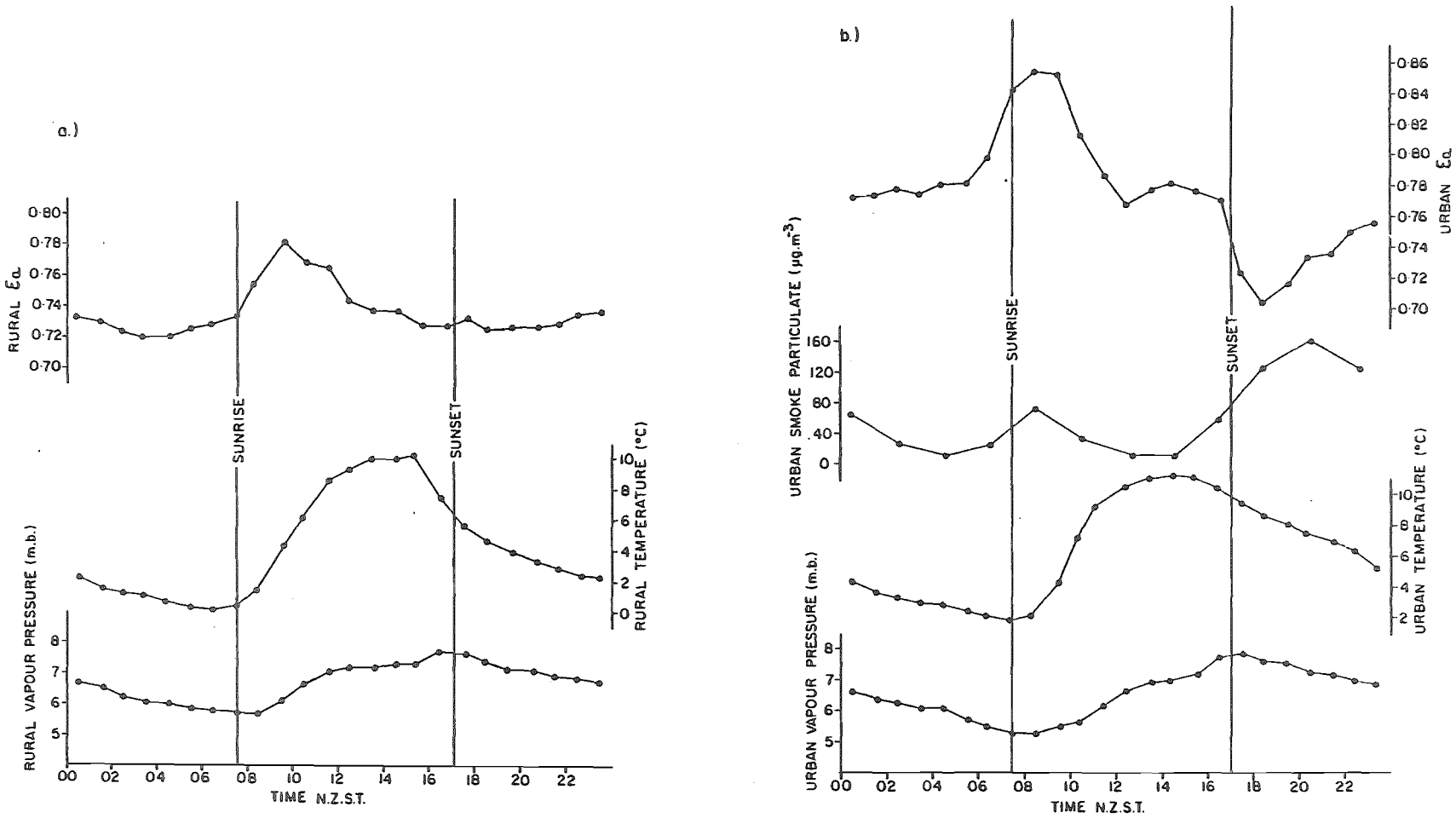

FIGURE 7.2 Relationship Between the Winter Diurnal Variation of Clear Sky Apparent Atmospheric Emissivity and that of Other Atmospheric Variables for, a) The Rural, and b) The Urban Representative Sites.

variation is largely a reflection of the difference between screen level and 'centre of gravity' temperature, with secondary influences of vapour pressure, atmospheric pollution and temperature.

Despite the fact that relationships may be masked by the 'centre of gravity' effect, there is little apparent variation of urban εa with temperature and vapour pressure. There do appear to be some slight pollution effects superimposed on the diurnal variation of εa shown in Figure 7.2b. The morning peak in urban εa is substantially higher, and the overall diurnal variation three times greater than that of rural εa. Urban-rural differences in the effect of the 'centre of gravity' problem are unlikely to be a major reason for the magnitude of this variation, and the presence of pollution at the urban site appears the probable cause. Peak urban εa is coincident with the highest daytime levels of pollution. There is also an increasing urban εa during the evening in line with smoke particulate, but this may relate to the recovery of εa from the early evening underestimate. In view of the several uncertainties it is not possible to elaborate further on this possible relationship here.

Plots of urban excess $IR\downarrow$ and εa with urban-rural variations in vapour pressure, temperature and air pollution appear in Figure 7.3a and 7.3b, the summer/autumn and the winter case respectively. Urban excess $IR\downarrow$ is independent of the 'centre of gravity' problem, and consideration of urban-rural differences in εa removes some of the problems associated with the use of εa at individual sites. Apparent relationships support the suggestions made above concerning possible causal mechanisms. Diurnal trends in urban excess vapour pressure and temperature are similar in both seasons, with a minimum excess mid to late morning and a maximum excess in the late evening. Theoretical considera-

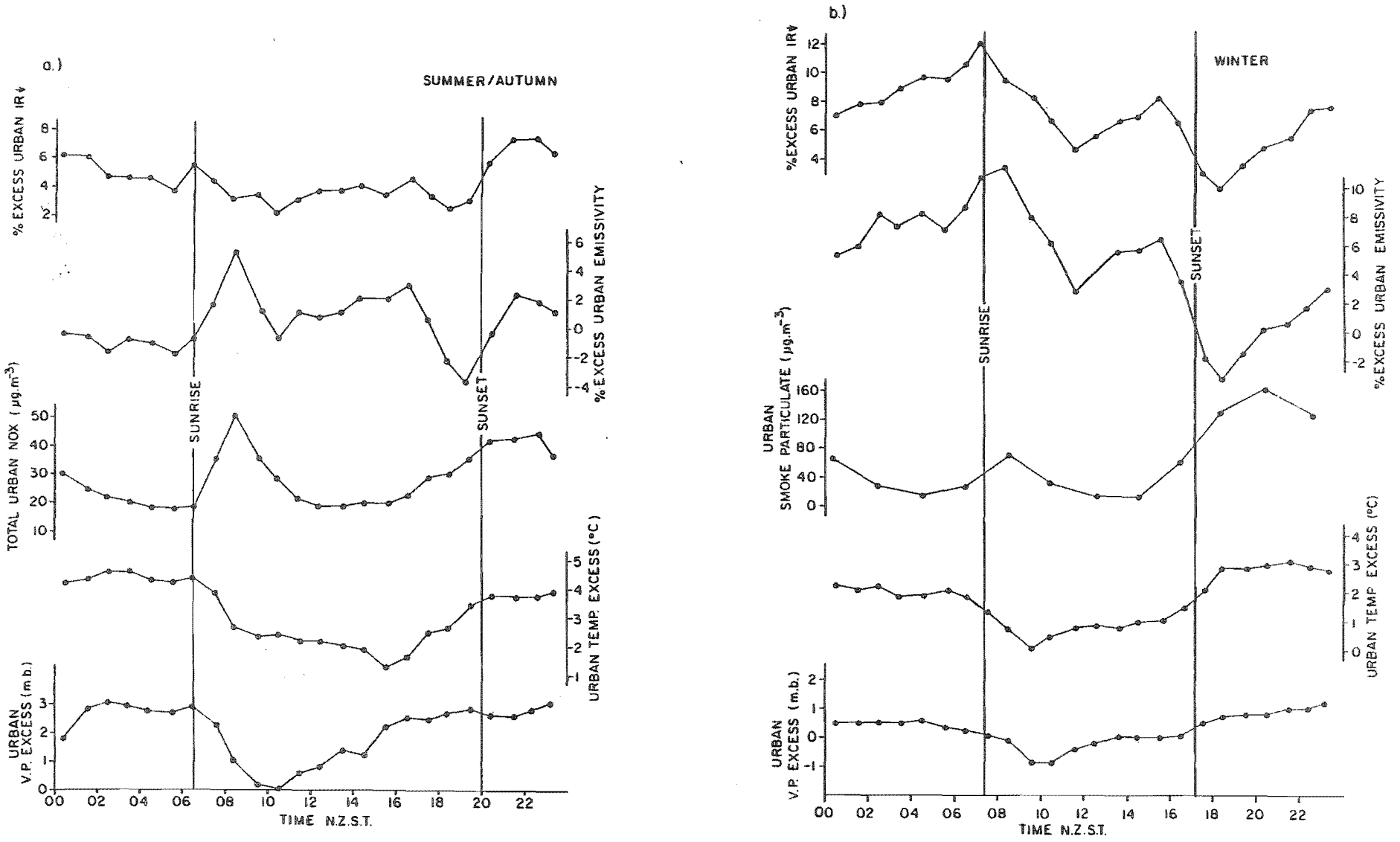

FIGURE 7.3 Relationship Between the Diurnal Variation of Clear Sky Urban Excess IR↓ and that of Other Atmospheric Variables Exhibiting Urban-Rural Differences, Showing a) the Summer/Autumn Case, and b) The Winter Case.

tions suggest that there should be a positive relationship between these variables and urban excess IR↓ and εa. Comparison of the respective plots, particularly in winter, implies in fact that the reverse applies. Examining the winter case (Figure 7.3b) in detail, at the time urban excess εa and IR↓ reach their peak shortly after sunrise, urban excess temperature and vapour pressure are dropping rapidly. The time of minimum urban excess εa and IR↓ (near 1800 h) is coincident with an increasing urban temperature and vapour pressure excess.

In comparison with the other variables, the diurnal trend in pollution levels suggest some variation in accord with radiation characteristics. For the summer/autumn case the general trends in urban excess IR↓ and urban pollution are similar, and the peak urban excess emissivity corresponds exactly with peak morning pollution levels. Similar trends apply in the winter case, although there is a marked divergence near sunset. Because the 'centre of gravity' problem is not relevant to IR↓ a further explanation must be sought to explain this marked drop in urban excess IR↓ (and εa) at this time. The loss of solar irradiation of the pollution layer is an obvious possible reason for the reduction of urban excess IR↓, despite generally increasing pollution levels. One further possibility would be the suggestion that with the cessation of daytime turbulence, aerosols settle out of the atmosphere thus lowering urban εa and IR↓, but consideration of near-surface pollution (Figure 7.3b) suggests that this is unlikely. Because of the stringent criteria applied to selection of sites, the phenomenon is unlikely related to physical characteristics of the sites. Similarly, the behaviour of rural IR↓ characteristics near sunset is quite different, suggesting that the observations are not an artifact created by instrumental problems. In the absence of

evidence to the contrary, the phenomenon appears to be real and related to peculiar characteristics of the urban atmospheric environment. The steady increase in winter urban excess IR↓ and εa after 0000 h and before the increase in pollution commencing after 0600 h, is due to a decrease in rural IR↓ and εa over that time, rather than significant differences in urban radiation characteristics.

Subsequent chapters establish relationships between atmospheric variables and infra-red radiational characteristics on a firmer basis than is possible with the preliminary treatment given here.

VARIATIONS IN INCOMING ALL-WAVE RADIATION AT THE REPRESENTATIVE SITES

The total impact of the urban atmospheric environment on the overall radiation regime of Christchurch can only be determined from an examination of all-wave (IR↓ + SW↓) radiation receipt at the urban and rural sites. Table 7.11 shows the total incoming radiation at each site for both seasons. The ratio of urban to rural total radiation is also shown. In both seasons there exists a marked urban nocturnal excess radiant energy income, while during daylight hours the ratio of total radiation for both sites is much closer (1.00 - 1.01 between 1000 and 1700 h in wintertime, and 0.98 - 1.01 between 0700 and 1900 h during the summer). Overall, a slight excess daily radiant income exists at the urban site (urban-rural ratio of 1.03 in summer and 1.05 in winter).

The observation that lowered urban SW↓ is almost completely balanced by increased IR↓ during the day supports the observations of Rouse *et al.* (1973) for Hamilton, Ontario. A balance of SW↓ attenuation with IR↓ increase implies an extra source of atmospheric energy. This

TABLE 7.11 Ratio of Urban-Rural Total Radiation (Energy units in Wm^{-2})

TIME N.Z.S.T.	URBAN IR↓ + SW↓	RURAL IR↓ + SW↓	URBAN-RURAL RATIO	URBAN IR↓ + SW↓	RURAL IR↓ + SW↓	URBAN-RURAL RATIO
00-01	256	238	1.08	288	270	1.07
01-02	254	234	1.08	284	267	1.06
02-03	253	233	1.09	278	265	1.05
03-04	253	230	1.10	276	263	1.05
04-05	252	227	1.11	276	263	1.05
05-06	252	228	1.10	273	263	1.04
06-07	254	227	1.12	271	256	1.06
07-08	271	255	1.06	305	307	0.99
08-09	299	285	1.05	489	489	1.00
09-10	441	415	1.06	669	666	1.00
10-11	597	595	1.00	821	841	0.98
11-12	694	689	1.01	976	980	1.00
12-13	748	736	1.00	1034	1035	1.00
13-14	741	731	1.01	1062	1049	1.01
14-15	684	675	1.01	989	995	0.99
15-16	569	562	1.01	901	919	0.98
16-17	401	402	1.00	766	781	0.98
17-18	282	287	0.98	545	564	0.97
18-19	248	244	1.02	511	513	1.00
19-20	249	240	1.04	453	421	1.07
20-21	251	239	1.05	364	319	1.14
21-22	252	238	1.06	294	273	1.08
22-23	256	237	1.08	294	273	1.08
23-00	256	238	1.08	294	276	1.07
			$\bar{X}$ 1.05			$\bar{X}$ 1.03

is because absorbed SW↓ energy in the atmosphere is converted to IR and is then emitted in all directions, rather than directly toward the surface. Rouse *et al.* (1973) ascribe this extra source of energy to an increased absorption of IR↑ from warm city surfaces by atmospheric pollution, with subsequent re-radiation. That this may also be the case for Christchurch is supported by the results of the energy balance model (Chapter 2 page 50) which show daytime values of sensible heat flux to be at a maximum over the central city area.

Computations reported by Fischer (1975) indicate approximate equivalence between heating rates in the short-wave and cooling rates in the transparent infra-red part of the spectrum in aerosol polluted environments. However, it was stated that whether this compensating effect in radiative flux divergence is the general case will only be established by comprehensive investigations of atmospheric physics.

In contrast to the results of Rouse *et al.* (1973), this study shows a substantial, true energy gain at night in all seasons, so that the daily total radiation receipt shows an urban energy excess. A gain in energy from this source has often been quoted as one cause of the urban heat island, but the observed energy excess here is unlikely to play anything but a small part in the production of observed temperature excesses.

CONCLUSIONS

Several major conclusions can be drawn from this investigation of aspects of the incoming radiation regime over Christchurch:-

(i) An average clear weather depletion of SW↓ at the urban site of 3.5% was observed over the study term, with individual daily depletions ranging as high as 10.3%. Depletion of the solar beam was observed to increase toward winter in line with increasing pollution levels and an increasing solar path.

(ii) Atmospheric transmissivities at both the urban and rural site showed an increase toward winter related to a decreasing atmospheric water vapour content. Urban transmissivity deficits showed an increase at lower solar elevations, both on a seasonal and daily basis and when atmospheric pollution was highest. Loss of solar radiation at the surface implied atmospheric heating with resultant effects on IR↓.

(iii) Regression analysis yielded a very clear relationship between urban transmissivity deficit and urban smoke pollution in winter. A 0.4% increase in urban transmissivity with every 10μg m^{-3} decrease in smoke was observed.

(iv) Clear weather urban IR↓ excess over the study period averaged 5.3%, with the excess reaching 6.9% during the winter term. Urban atmospheric apparent emissivities (εa) were also found to be higher than the rural case, particularly during the winter term.

(v) Simple plots of εa and atmospheric variables were handicapped by an inability to correctly specify the bulk atmospheric

temperature. Plots of urban excess IR↓ and urban excess temperature and vapour pressure were inconclusive but there was some evidence of a relationship with atmospheric pollution.

(iv) Daytime excess IR↓ at the urban site almost exactly balanced the SW↓ deficit, therefore daytime total energy receipt at the urban and rural sites was found to be in balance. A continuation of urban IR↓ excess into night-time hours results in a net excess of incoming radiant energy at the urban site at that time.

CHAPTER 8

PREDICTION OF ATMOSPHERIC IR↓ OVER CHRISTCHURCH : I. THE USE OF SCREEN-LEVEL DATA

INTRODUCTION

In the previous chapter, an urban-rural variation of IR↓ was identified and some potential causative mechanisms tentatively isolated. The purpose of the current chapter is to establish the mechanisms which produce increased IR↓ over urban Christchurch on a firmer base using screen-level data only. Two approaches are utilised here. Firstly, a statistical approach using simple and stepwise multiple correlation and analysis techniques on the large data base is used. Secondly, various semi-empirical predictive equations are used to establish systematic deviations of measured IR↓ flux from that predicted.

A STATISTICAL APPROACH : REGRESSION ANALYSIS

Introduction

This analysis concentrates on those variables which theoretically can contribute directly to differences in IR↓ across urban areas, namely temperature, vapour pressure and air pollution. As the investigation is primarily concerned with the explanation of

urban excess IR↓ (%), the independent variables are also expressed in terms of an urban excess. Because of the problems associated with establishing a 'centre of gravity' temperature of emission, analysis of atmospheric apparent emissivity derived from screen level temperature is omitted here. With the exception of atmospheric pollution, all parameters utilised in this study (urban excess IR↓, temperature and vapour pressure) could be considered normally distributed at the 0.05 level of significance using the Kolmargarov-Smirnov test. To normalise the pollution data (NOx in summer, smoke particulate in winter), a logarithmic transformation was performed on that data.

Several drawbacks of the use of regression techniques on these data should be mentioned at this point. Since much of the data is on an hourly basis, the observations are not independent of each other and some form of time series analysis would perhaps be more appropriate. Unfortunately time series analysis techniques generally require long continuous series of observations ($\sim$ 100 or more) and this is simply not available for clear weather data. Regression analysis on daily data, where possible, removes some of the problems, but this limitation should be remembered. One further point to emphasise is that a good correlation between two or more variables does not necessarily mean a cause and effect relationship exists unless there are sound theoretical reasons for believing this to be the case.

Relationships Between Urban Excess IR↓ and Atmospheric Variables - Simple Regression Analysis

Atmospheric Pollution

In clear, rural areas, the partial flux density of IR↓ due to aerosol and trace gas emitters is relatively insignificant beside

that due to H_2O, CO_2 and O_3. Under certain conditions the flux density of aerosol can conceivably exceed that of O_3 (Staley and Jurica, 1972). Robinson (1966) noted the potential importance of aerosol radiation, particularly over polluted urban areas, in adding to the total flux density of IR↓. Atwater (1971b) calculated an increased IR↓ with the introduction of a radiatively active aerosol and significant quantities of NO_2 (indirectly increasing IR↓ by increasing atmospheric heating rates). Paltridge and Platt (1976) summarise most of the important studies examining IR radiative effects of pollutants (non-natural quantities and types of aerosol and gases).

Correlation of up to 497 hourly observations of urban pollution ($\log_{10}$) and measured urban IR↓ excess produced the summary of regression shown in Table 8.1. Urban IR↓ excess shows a reasonably strong, positive correlation with atmospheric pollution, becoming progressively better toward winter and at night. This follows from the seasonal trend in atmospheric pollution that has been observed and also because two pollution measures (NOx and smoke) are included in the whole term data, a not entirely satisfactory situation given that NOx is there largely as a surrogate for pollutants that are radiatively active in the infra-red. The best correlation observed is for winter nocturnal urban IR↓ excess and log smoke pollution, with slightly more than 10% of the variance in the dependent variable explained. The relationship between urban excess IR↓ and pollution on a daily basis confirms the hourly relationship, but is less significant by virtue of the small sample numbers. Since atmospheric pollution shows a reasonable relationship with IR↓ characteristics, it would also be expected that meteorological factors responsible for variations in atmospheric pollution including windspeed and atmospheric

TABLE 8.1 Summary of Regression Analysis (Log Pollution)

DEPENDENT VARIABLE	NO. OBSERVATIONS	a COEFFICIENT	b COEFFICIENT	r	SIGNIFICANCE
Term Urban IR↓ Excess (hourly)	497	1.552	0.027	0.253	0.01
Winter Urban IR↓ Exesss (hourly)	339	1.471	0.035	0.316	0.01
Winter Nocturnal Urban IR↓ Excess (hourly)	222	1.650	0.034	0.320	0.01
Term Urban IR↓ Excess (Daily)	25	-	-	0.418	0.05
Winter Urban IR↓ Excess (Daily)	13	-	-	0.420	N.S.
Winter Urban IR↓ (hourly)	222	270.46	-7.148	-0.175	N.S.

stability, would also show a relationship with urban excess IR↓.

Consideration of pollution effects on winter IR↓ at the urban site (Table 8.1) shows a negative but insignificant relationship. It therefore seems likely that the variation of IR↓ at a point location is dependent more on other atmospheric variables potentially responsible for IR↓ variations (temperature and water vapour). This hypothesis is tested in later analyses. The negative relationship between urban IR↓ and smoke pollution (opposite to that expected) is related to the occurrence of peak air pollution at times of relatively low air temperature and high atmospheric stability.

Temperature

The relationship between IR↓ and temperature in urban areas is potentially complex, and some disagreement on this has appeared in the literature. Many early papers (Duckworth and Sandberg, 1954; Landsberg, 1956; Mitchell, 1962; Peterson, 1969) cite the apparently higher urban IR↓ produced by the blanketing effect of the urban pollution dome as contributing to the formation of the urban heat island. Oke and Fuggle (1972) called this viewpoint into question and suggested that IR↓ increases in urban areas are merely the result of urban temperature excess caused by factors other than atmospheric absorption of SW↓ and terrestrial IR↑ and subsequent re-radiation of IR↓. Other authors, for example Atwater (1971a, b) and Rouse Noad and McCutcheon (1973) believe that urban pollution can absorb both SW↓ and IR↑, with consequent increases in IR↓ from higher atmospheric temperatures and radiatively active pollutants. In this case urban-rural IR↓ differences would not necessarily be related to near surface temperatures.

A summary of regression of hourly screen temperature and IR↓ radiational characteristics is given in Table 8.2. From theoretical consideration in the Stefan-Boltzmann relation, it would be expected that there would be a positive relationship between higher temperatures and IR↓, both in terms of urban excess IR↓ and with IR↓ at the individual sites. Surprisingly, it is only data for the individual sites which yield the relationship expected. IR↓ at both the urban and rural sites has a strong positive correlation with screen level temperature. Presumably because of the interference effects of other variables at the urban site, the relationship is stronger at the rural site where more than 75% of the variance in the dependent variable is explained. The equation for the rural case:

$$IR\downarrow \text{ (rural)} = 226.88 + 4.232\ T\ (^{o}C) \qquad \ldots\ 8.1$$

yields a rate of IR↓ increase with temperature almost identical to that described by the Stefan-Boltzmann relation.

The apparent negative relation between urban excess IR↓ and urban temperature excess is puzzling and defys simple explanation. As is evident from the relationship between IR↓ and temperature at the individual sites, there is no physical reason for urban excess IR↓ to fall with increasing urban temperature excess. Rather, it appears that the negative relationship is an artifact of the technique, determined by the variation of urban excess IR↓ in phase with atmospheric pollution. As shown in Figure 7.3b, the strong diurnal cycle of pollution levels and possible influences of solar irradiation of the pollution layer during daytime may be masking any temperature effects on IR↓. The lag effect between heating and cooling at the urban site relative to the rural site (described in detail in Chapter 4) creates

TABLE 8.2 Summary of Regression Analysis (Temperature)

DEPENDENT VARIABLE	NO. OBSERVATIONS	a COEFFICIENT	b COEFFICIENT	r	SIGNIFICANCE
Term Urban IR↓ Excess (hourly)	497	2.769	-0.064	-0.168	0.05
Winter Urban IR↓ Excess (hourly)	339	2.391	-0.10	-0.322	0.01
Winter Nocturnal Urban IR↓ Excess (hourly)	222	2.733	-0.108	-0.367	0.01
Term Urban IR↓ Excess (daily)	25	-	-	-0.241	N.S.
Winter Urban IR↓ Excess (daily)	13	-	-	-0.361	N.S.
Winter Urban IR↓ (hourly)	222	247.96	2.521	0.490	0.01
Winter Rural IR↓ (hourly)	222	226.88	4.232	0.868	0.01

a minimum urban temperature excess during the morning at a time approximately that of highest urban IR↓ excess and highest daytime pollution levels. Although most noticeable in the early part of the day, the cycle of urban temperature excess remains somewhat out of phase with urban excess IR↓ throughout much of the rest of the day. The continued negative relationship between urban excess temperature and IR↓ on a daily basis suggests that the phenomenon is due to the dominance of pollution over any other effect.

Vapour Pressure

According to theory atmospheric moisture content is a further variable which should bear strong influence on IR↓ at the individual sites, and to a lesser degree urban-rural differences (large urban-rural differences of vapour pressure indeed would be required to significantly alter IR↓ excess). Table 8.3 is a summary of regression analysis for these two variables. In view of the close inter-relationship between vapour pressure and temperature, similarity with the regression analysis for temperature (Table 8.2) is not surprising. As with temperature, the relationship between urban IR↓ and urban vapour pressure excess is negative in all cases and becomes stronger toward winter. The same mechanism invoked in the previous section to explain the apparent negative relationship of urban excess temperature and IR↓ applies here.

Vapour pressure was also examined with respect to its possible effect on IR↓ at point locations (Table 8.3). The relationship is positive and significant for both representative sites, although it is stronger at the rural site where 52% of the variance of the dependent variable is explained. Because of the close relationship with temperature it is difficult to determine exact influences on IR↓.

TABLE 8.3 Summary of Regression Analysis (Vapour Pressure)

DEPENDENT VARIABLE	NO. OBSERVATIONS	a COEFFICIENT	b COEFFICIENT	r	SIGNIFICANCE
Term Urban IR↓ Excess (hourly)	497	0.556	-0.024	-0.118	N.S.
Term Urban IR↓ Excess (hourly)	339	0.426	-0.037	-0.252	0.01
Winter Nocturnal Urban IR↓ Excess (hourly)	222	0.567	-0.041	-0.315	0.01
Term Urban IR↓ Excess (daily)	25	-	-	-0.403	0.05
Winter Urban IR↓ Excess (daily)	13	-	-	-0.249	N.S.
Winter Urban IR↓ (hourly)	222	229.9	4.439	0.260	0.01
Winter Rural IR↓ (hourly)	222	155.5	13.28	0.719	0.01

To accomplish this it would be necessary to have a measure of actual atmospheric emissivity independent of temperature.

The Relative Importance of Variables in Determination of Urban IR↓ Excess - Stepwise Multiple Regression

Interrelationships between the three independent variables and urban IR↓ excess have been considered in a multiple correlation and stepwise regression analysis carried out on up to 497 hourly observations from throughout the study period. Analysis of up to 25 daily observations has also been performed.

Table 8.4a confirms the relationships already described. Of note is the strong, positive relationship between vapour pressure and temperature excess. The contribution of each independent variable to observed IR↓ excess throughout the study period is shown in Table 8.4b. Urban pollution levels explain 6.4% of variance in the dependent variable, with the other variables adding only a further 3.1%, despite the use of two different pollution measures at different times of the year. Although the negative relationship with IR↓ excess is contrary to expectation for reasons described previously, urban excess temperature is responsible for most of the explanation of variance after urban pollution. The contribution of excess vapour pressure is small by virtue of its strong dependence on temperature. The multiple correlation coefficient of 0.31, although low, is significant at the 0.01 level.

The data base represented in Table 8.4 has been stratified to show the contribution of the independent variables for the summer and winter case. A correlation matrix for summer data (Table 8.5a) shows a lack of relationship between urban NOx pollution and urban IR↓

TABLE 8.4 Multiple Regression Analysis - All Data (497 hours)

(a) Correlation matrix of urban excess IR↓ and emissivity and associated variables (values of r, Pearson product-moment correlation coefficient).

LOG URBAN POLLUTION	URBAN TEMPERATURE EXCESS	URBAN VAPOUR PRESSURE EXCESS	URBAN IR↓ EXCESS(%)	URBAN EMISSIVITY EXCESS (%)	
1.0	0.031	0.048	0.253**	0.269**	LOG URBAN POLLUTION
	1.0	0.704**	-0.168*	-0.504	URBAN TEMP. EXCESS
		1.0	-0.118	-0.359	URBAN VAPOUR PRESSURE EX.
			1.0	0.868**	URBAN IR↓ EXCESS (%)
				1.0	URBAN EMISS. EXCESS (%)

**Significant at the 0.01 level. *Significant at the 0.05 level.

(b) Contribution of the independent variables to urban IR↓ excess.

INDEPENDENT VARIABLE	TOTAL EXPLAINED VARIANCE (%)	VARIANCE EXPLAINED BY NEW VARIABLE (%)	F RATIO	SIGNIFICANCE
LOG URBAN POLLUTION	6.39	6.39	33.7	0.01
URBAN EXCESS TEMPERATURE	9.47	3.08	25.8	0.01
URBAN EXCESS VAPOUR PRESSURE	9.48	0.01	17.2	0.01

Coefficient of multiple R - 0.31

Multiple regression equation - IR↓ excess (%) = 3.44 - 0.43 T excess - 0.07 VP excess + 2.45 log pollution.

TABLE 8.5 Multiple Regression Analysis - Summer Data (158 hours)

(a) Correlation matrix of urban excess IR↓ and associated variables (values of r, Pearson product-moment correlation coefficient).

LOG URBAN NOX POLLUTION	URBAN EXCESS TEMPERATURE	URBAN EXCESS VAPOUR PRESSURE	URBAN IR↓ EXCESS(%)	
1.0	0.037	0.124	-0.044	LOG URBAN NOX POLLUTION
	1.0	0.567**	0.294**	URBAN EXCESS TEMPERATURE
		1.0	0.166*	URBAN EXCESS VAPOUR PRESSURE
			1.0	URBAN IR↓ EXCESS (%)

**Significant at the 0.01 level. *Significant at the 0.05 level.

(b) Contribution of the independent variables to summer urban IR↓ excess.

INDEPENDENT VARIABLE	TOTAL EXPLAINED VARIANCE (%)	VARIANCE EXPLAINED BY NEW VARIABLE (%)	F RATIO	SIGNIFICANCE
URBAN EXCESS TEMPERATURE	8.62	8.62	14.7	0.01
LOG URBAN NOX POLLUTION	8.92	0.3	7.6	0.01
URBAN EXCESS VAPOUR PRESSURE	8.93	0.01	4.3	0.01

Mult. R - 0.30

Summer urban IR↓ excess (%) = 4.76 + 0.66 T excess + 0.10 V.P. excess - 0.71 Log Nox.

excess, and a positive relationship of urban IR↓ excess with excess temperature and vapour pressure (as should be expected from theory). Consequently, urban excess temperature contributes most to the variance of urban IR↓ excess in summertime (Table 8.5b), with NOx pollution and vapour pressure excess adding only 0.3% more. Total variance of summertime urban IR↓ excess explained is small at 8.9%, although remains significant at the 0.01 level. It therefore appears that in summertime at least, the effect of urban excess temperature on IR↓ is not being masked by the diurnal variation of atmospheric pollution. This is probably related to the lower general pollution levels at this time and also possibly because the pollutants present in summertime (of which NOx is an indicator only) are less radiatively active in the infra-red.

The winter case (Table 8.6) again shows the relative importance of urban pollution as a determination of urban excess IR↓, although the variance contributed by urban excess temperature is also high (but negative as the multiple regression equation indicates). The coefficient of multiple correlation at 0.46 is higher than for both term and summertime only data. Subdividing the 339 hours of winter data into daytime and nightime data yields Tables 8.7 and 8.8. These analyses both confirm the importance of urban smoke pollution as the major controlling variable, particularly during daytime hours, where log urban smoke explains 18.3% of the variance of urban IR↓ excess, and the other two independent variables only 2.5% more. This probably reflects the effect of solar irradiation on the pollution layer during daytime hours, a hypothesis supported by examination of the respective multiple regression equations. The only significant difference between equations for the prediction of winter urban IR↓ excess is a much higher

TABLE 8.6 Multiple Regression Analysis - Winter Data (339 hours)

Contribution of the independent variables to winter urban excess IR↓

INDEPENDENT VARIABLE	TOTAL EXPLAINED VARIANCE (%)	VARIANCE EXPLAINED BY NEW VARIABLE (%)	F RATIO	SIGNIFICANCE
LOG URBAN SMOKE POLLUTION	10.35	10.35	38.9	0.01
URBAN EXCESS TEMPERATURE	20.61	10.26	43.6	0.01
URBAN EXCESS VAPOUR PRESSURE	20.63	0.02	29.0	0.01

Mult. R - 0.46

Winter urban excess IR↓ (%) = 3.77 - 1.0 T excess - 0.15 V.P. excess + 2.85 log smoke.

TABLE 8.7 Multiple Regression Analysis - Winter Days (117 hours)

Contribution of the Independent Variables to Winter Daytime IR↓ excess

INDEPENDENT VARIABLE	TOTAL EXPLAINED VARIANCE (%)	VARIANCE EXPLAINED BY NEW VARIABLE (%)	F RATIO	SIGNIFICANCE
LOG URBAN SMOKE POLLUTION	18.28	18.28	22.7	0.01
URBAN EXCESS TEMPERATURE	20.13	1.85	14.4	0.01
URBAN EXCESS VAPOUR PRESSURE	21.73	1.61	10.5	0.01

Mult. R - 0.47

Winter daytime IR↓ excess (%) = 2.82 - 0.84 T excess + 1.04 V.P. excess + 3.84 log smoke.

TABLE 8.8 Multiple Regression Analysis - Winter Nights (222 hours)

Contribution of the independent variables to winter nocturnal IR↓ excess

INDEPENDENT VARIABLE	TOTAL EXPLAINED VARIANCE (%)	VARIANCE EXPLAINED BY NEW VARIABLE (%)	F RATIO	SIGNIFICANCE
LOG URBAN SMOKE POLLUTION	13.46	13.46	34.2	0.01
URBAN EXCESS TEMPERATURE	23.00	9.53	32.7	0.01
URBAN EXCESS VAPOUR PRESSURE	23.87	0.87	22.8	0.01

Mult. R - 0.49

Winter urban nocturnal IR↓ excess (%) = 2.92 - 0.83 T excess - 1.12 V.P. excess + 3.12 log smoke.

TABLE 8.9 Multiple Regression Analysis - All Daily Data

Contribution of independent variables to daily IR↓ excess (N = 25)

INDEPENDENT VARIABLE	TOTAL EXPLAINED VARIANCE (%)	VARIANCE EXPLAINED BY NEW VARIABLE (%)	F RATIO	SIGNIFICANCE
LOG URBAN POLLUTION	13.44	13.44	3.4	N.S.
URBAN EXCESS VAPOUR PRESSURE	26.36	12.92	3.7	0.05
URBAN EXCESS TEMPERATURE	27.01	0.65	2.5	N.S.

Mult. R - 0.52

Daily IR↓ excess (%) = 1.56 - 0.20 T excess - 0.74 V.P. excess + 2.86 Log Pollution.

log smoke regression coefficient in the daytime equation, probably reflecting a solar heating effect.

Multiple regression of daily data (Table 8.9 and 8.10) again confirms the relative importance of pollution in determination of urban IR↓ excess, although the coefficients of multiple correlation are not significant by virtue of small sample numbers. The only significant relationship is for all daily data (Table 8.9), where the entry of urban excess vapour pressure after log urban pollution gives a relationship significant at the 0.05 level. Urban temperature excess again shows an apparent negative relationship with urban IR↓ excess.

Although appearing the dominant influence on urban-rural differences in IR↓, at least during wintertime, atmospheric pollution appears much less important in explaining variations in IR↓ at individual sites. Analysis of all winter data (Table 8.11) shows that the variation of IR↓ at both urban and rural representative sites is primarily determined by variations in atmospheric temperature. The true contribution of vapour pressure to IR↓ is masked to a certain extent by the co-variance of vapour pressure and temperature. The multiple correlation coefficient obtained for the rural site is higher than at the urban site, indicating that reasons for variations in IR↓ at the urban site are more complex. As the analysis indicates (Table 8.11(b) ii), the contribution of smoke pollution to IR↓ at the urban site is small, adding less than 2% to the explained variance of IR↓. The contribution of smoke is positive, as would be expected from theory.

To conclude; while regression analysis is a reasonable technique for identifying potential relationships amongst variables,

TABLE 8.10 Multiple Regression Analysis - Winter Daily Data

Contribution of independent variables
to winter daily IR↓ excess (N = 13)

INDEPENDENT VARIABLE	TOTAL EXPLAINED VARIANCE (%)	VARIANCE EXPLAINED BY NEW VARIABLE (%)	F RATIO	SIGNIFICANCE
LOG URBAN SMOKE	11.52	11.52	1.43	N.S.
URBAN EXCESS TEMPERATURE	22.45	10.93	1.45	N.S.
URBAN EXCESS VAPOUR PRESSURE	24.50	2.05	0.97	N.S.

Mult. R - 0.5

Winter daily IR↓ excess (%) = 2.57 - 1.7 T excess + 1.46 V.P. excess
+ 3.5 log smoke.

TABLE 8.11 Multiple Regression Analysis - Individual Site Winter IR↓ Data (339 hours)

(a) RURAL SITE

i) Correlation matrix of rural IR↓ and associated variables (values of r, Pearson product-moment correlation coefficient)

RURAL TEMPERATURE	RURAL VAPOUR PRESSURE	RURAL IR↓	
1.0	0.794**	0.868**	RURAL TEMPERATURE
	1.0	0.719**	RURAL VAPOUR PRESSURE
		1.0	RURAL IR↓

**Significant at the 0.01 level

ii) Contribution of the independent variables to rural IR↓

INDEPENDENT VARIABLE	TOTAL EXPLAINED VARIANCE (%)	VARIANCE EXPLAINED BY NEW VARIABLE (%)	F RATIO	SIGNIFICANCE
RURAL TEMPERATURE	75.43	75.43	583.2	0.01
RURAL VAPOUR PRESSURE	75.66	0.24	293.8	0.01

Mult. R - 0.87

Rural IR↓ = 218.6 + 3.92 T + 1.48 V.P.

TABLE 8.11 Multiple Regression Analysis - Individual Site
Winter IR↓ Data (339 hours) - Continued

(b) URBAN SITE

i) Correlation matrix of urban IR↓ and associated variables (values of r, Pearson product-moment correlation coefficient)

URBAN TEMPERATURE	URBAN VAPOUR PRESSURE	LOG URBAN SMOKE	URBAN IR↓	
1.0	0.792**	-0.417**	0.490**	URBAN TEMPERATURE
	1.0	-0.089	0.260**	URBAN VAPOUR PRESSURE
		1.0	-0.175*	LOG URBAN SMOKE
			1.0	URBAN IR↓

**Significant at 0.01 level. *Significant at 0.05 level.

ii) Contribution of the independent variables to urban IR↓

INDEPENDENT VARIABLE	TOTAL EXPLAINED VARIANCE (%)	VARIANCE EXPLAINED BY NEW VARIABLE (%)	F RATIO	SIGNIFICANCE
URBAN TEMPERATURE	24.00	24.00	60.0	0.01
URBAN VAPOUR PRESSURE	28.39	4.38	37.4	0.01
LOG URBAN SMOKE	30.27	1.88	27.2	0.01

Mult. R - 0.55

Urban IR↓ = 274.72 + 4.72 T - 7.71 V.P. + 6.85 log smoke.

it is a poor tool for quantifying relative effects on sound theoretical grounds. With such an approach, the actual mechanism of relationships between two or more variables must remain obscure.

A SEMI-EMPIRICAL APPROACH : PREDICTIVE EQUATIONS FOR IR↓

General

Some investigators seeking to isolate and identify reasons for the variation of IR↓ from that expected have used various semi-empirical equations which relate IR↓ at point locations to readily available meteorological observations. The approach has been used successfully in both mountain (Le Drew, 1975) and urban environments (Oke and Fuggle, 1972; Brazel and Osborne, 1976). Although such a method is a useful investigating tool, the most common usage is to generate IR↓ data in the absence of measurements. One such method, the Brutsaert equation, was used in the Christchurch energy balance model in such a capacity (Chapter 2).

The most common approach of investigators has been to relate empirically the atmospheric apparent emissivity, $\varepsilon a = IR\downarrow/\sigma T^4$, to atmospheric moisture content and/or temperature. The limitation of all predictive models of εa lies in the approximation of emissivity based on screen level observations of temperature and water vapour content (either implicitly or explicitly) to a 'centre of gravity' atmospheric emissivity. Since almost 60% of IR↓ originates within the lowest 100 m of the atmosphere and 99% within 4 km of the surface (Lettau and Davidson, 1957), and most applications are for daily (or longer) averages, this problem is not usually significant. The

'centre of gravity' problem can cause problems for short-term prediction of IR↓.

Many formulae have been developed to predict εa, although only three such methods are described and used here.

Empirical Formulae

THE BRUNT FORMULA. Brunt (1932) produced a formulation for atmospheric emissivity of clear skies:-

$$\varepsilon a = a + b\sqrt{e_s} \qquad \ldots 8.2$$

where a and b are regression coefficients, and e_s is screen level vapour pressure (mb). This has remained one of the most widely used formulae for the determination of IR↓. The regression statistics a and b in the Brunt relationship are not constants, but are variable coefficients dependent on the spatial variability of e with temperature (Swinbank, 1963). Values of a and b in the literature for various parts of the world range from 0.34 to 0.71 for a, and from 0.023 to 0.110 for b (Sellers, 1972). Sellers suggested a median of twenty-two evaluations of a = 0.605 and b = 0.048. These values are used in the present application.

THE IDSO-JACKSON FORMULA. The local specificity of empirical relations such as that of Brunt (1932) are an acknowledged problem. Swinbank (1963) in an attempt to overcome this problem established a strong relation between IR↓ and σT^4 exclusive of e, which appeared to have a wide degree of universality. While Brunt-type relationships provide for no temperature dependence of εa, except through that inherent in vapour pressure (e), the relation established by Swinbank (1963), as well as including temperature effects on IR↓, implicitly includes

vapour pressure through the nature of correlation of air temperature with vapour pressure. Idso and Jackson (1969) considered that Swinbank's formula fails on theoretical grounds at both very high and very low temperatures, considerably underestimating εa at temperatures below 0^{o} C. Using Swinbank's original data base as well as observations from extreme climatic environments, Idso and Jackson produced a formula deemed to be of more general validity:-

$$\varepsilon a = 1 - 0.261 \exp\left[- 7.77 \times 10^{-4} (273 - T_a)^2 \right] \quad \ldots 8.3$$

where T_a is screen temperature in ^{o}K.

A Derivable Formula - *THE BRUTSAERT RELATION*

Brutsaert (1975) in a significant advance, produced a derivable formula for prediction of IR↓ for clear days in a nearly standard atmosphere. By direct solution of the governing Schwarzschild equation for standard atmospheric conditions (using assumed profiles of temperature, pressure and water vapour) and using an algebraic relationship for the emissivity, Brutsaert produced an approximation of atmospheric emissivity:-

$$\varepsilon a = 1.24 \, (e_s/T_a)^{1/7} \quad \ldots 8.4$$

Brutsaert suggests that the variation of the coefficient 1.24 is relatively insensitive to variations in 'typical' values of atmospheric parameters. Although the assumed profiles represent actual vertical profiles for brief periods only, Brutsaert considers Equation 8.4 yields satisfactory results for representative weather conditions under clear skies. A major advantage in the derivation of Equation 8.4 over other more empirical formulae is that whereas the latter require at least one (Idso and Jackson, 1969) or more (Brunt, 1932) parameters to

be determined from radiation experiments (often of local applicability only), the Brutsaert relation requires no empirical parameters for its application. A significant advantage that the Brutsaert relation has over other formulae is that it may be adjusted in a simple manner to allow εa to reflect changes in climatic and atmospheric conditions. One slight disadvantage of the Brutsaert relation is the requirement of both screen temperature and vapour pressure input to determine εa in contrast to the other two formulae described which require only one or the other.

Evaluation of IR↓ Predictive Equations

The Diurnal Variability of Predictive Errors

Although most atmospheric emissivity formulae were developed originally for prediction of IR↓ over long periods, many workers have sought to apply them to the task of estimating the diurnal variation of IR↓, either for comparison with measured IR↓ (Paltridge, 1970; Idso, 1972; Oke and Fuggle, 1972; Brazel and Osborne, 1976; Arnfield, 1979) or as input into an energy balance simulation model (Outcalt, 1971, 1972a; Morgan *et al.*, 1977; Marks and Dozier, 1979). This section investigates the appropriatness of the expressions described above for estimating the diurnal variability of IR↓ at the urban and rural representative sites.

For each of the three formulae used, the mean hourly deviation between estimated and actual clear sky emissivity at the two sites has been plotted against time of the day (Figure 8.1). Also plotted are the results of Arnfield (1979) for a site in rural Ontario which will be referred to presently. The vertical axis indicates the percentage estimation error, calculated as the actual εa minus the estimated εa

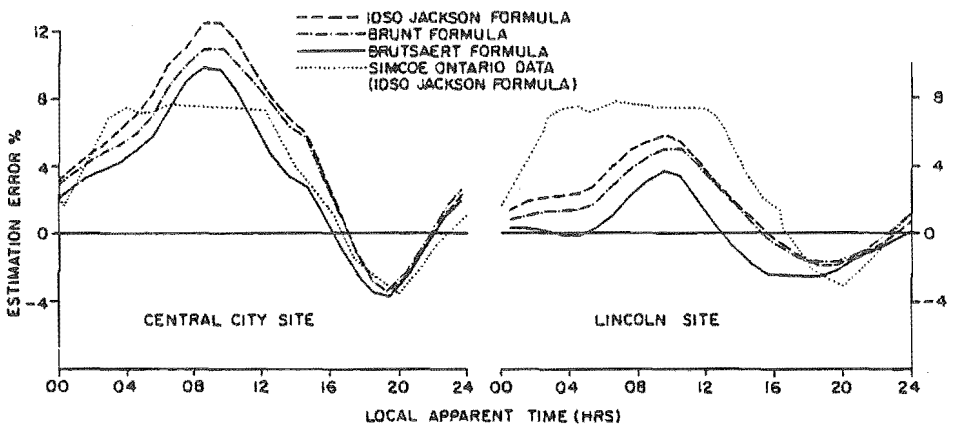

FIGURE 8.1 Diurnal Variation of Clear-Sky Apparent Atmospheric Emissivity Estimation Error (Various Formulae).

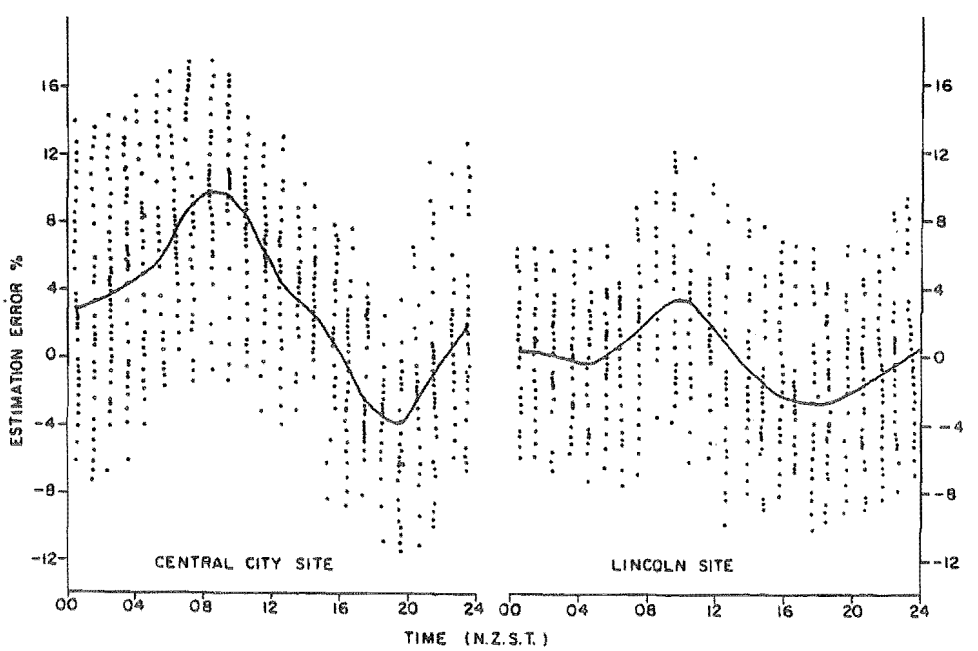

FIGURE 8.2 Diurnal Variation of Clear-Sky Apparent Atmospheric Emissivity Estimation Error (Brutsaert Formula), Showing Variability of the Individual Point Deviations.

expressed as a percentage of the actual value; therefore positive error values indicate a model underestimation. Four hundred and ninety-seven hourly observations at each site are included in Figure 8.1, and the plotted error curves join five hour running means. To give some measure of the variability of individual point deviations, Figure 8.2 shows the individual data points for the Brutsaert formula at each site.

Of immediate note at both sites and for all equations in Figure 8.1, is a non-random distribution of estimation error throughout the day. The diurnal variation is most marked at the urban site, where apart from a slight overestimation of εa in the late afternoon and early evening (maximum error 3 - 4%), there is a continuous but variable model underestimation. Model underestimation increases steadily throughout the evening, rising more abruptly to a peak underestimate of 10 - 12% at approximately 0900 h, following which it declines through the late morning - early afternoon period. Generally speaking, the Brutsaert formula appears to perform most satisfactorily, the underestimation being $\sim$ 3% less than the Idso-Jackson formula and 1 $\sim$ 3% less than the Brunt formula. All three models give similar overestimation during the late afternoon. The larger magnitude of model underestimation and the longer period during which this occurs are responsible for the overall tendency of all formulae to underestimate urban atmospheric emission. For the Brutsaert relation, the mean diurnal underestimate is 3.2%, and for the Brunt and Idso-Jackson relations, 4.7% and 5.1% respectively.

Diurnal variability at the rural site, although exhibiting the same pattern, is considerably reduced. Late afternoon εa overestimates of 2 - 3% are similar, but the magnitude of the early morning underestimate is only half that at the urban site (4 - 6%). Accordingly,

the overall daily performance of the predictive formulae is better for the rural site, with the Brutsaert formula underestimating daily emissivity by 0.05% only, and the other two formulae by less than 2%. Although the average hourly and daily performance of the formula is reasonable, it can be seen in Figure 8.2 that there is considerable scatter about the running-mean line, although the maximum hourly deviation observed was only 12%.

The differences between the urban and rural error curves are worth further comment here. Diurnal trends are quite similar, indicating that the basic mechanism promoting this behaviour is the same, but the effect at the urban site is either magnified, or more likely a purely urban influence is being superimposed upon the underlying mechanism. The time of maximum underestimate at the urban site (and the time of maximum divergence from the rural pattern) is near 0900 h, coincident with the measured peak urban excess $IR\downarrow$ and εa described in the previous chapter.

The most significant and remarkable point arising from the error curve exhibited in Figure 8.1 is the similarity with results of previous studies, indicating that the probable basic cause of the systematic deviation is not unique to the present study. Arnfield (1979) plotted a diurnal error curve for the Idso-Jackson formula for Simcoe, a rural site in southern Ontario. His curves are superimposed on the current error curves for the urban and rural sites. The units used in both studies are identical, therefore the curves are directly comparable. At the urban site, apart from the period 0600 - 1200 h, the degree of convergence is quite remarkable, while at the rural site the predictive formulae in the present study appear to operate more effectively, particularly during nightime hours. Figure 8.3 shows the

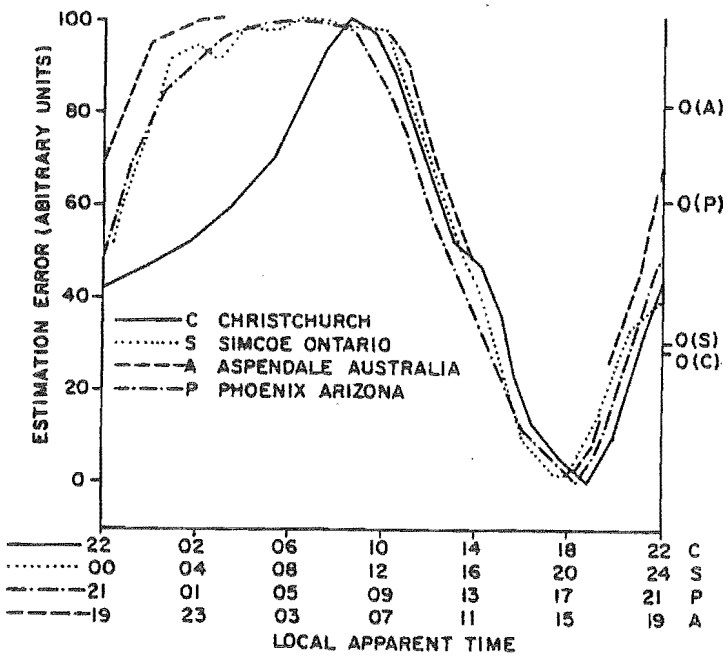

FIGURE 8.3 The Diurnal Variations of Clear-Sky Apparent Atmospheric Emissivity Estimation Error in Four Different Studies. The Zero Line (No Error) is Shown on the Right Hand Axis.

urban error curve of the Brutsaert formula used in this study, plotted with the results of Paltridge (1970), Idso (1972) and Arnfield (1979). This diagram has been plotted in a similar manner to one produced by Arnfield (1979), where each error curve has been standardised to the same daily range, and phase differences have been eliminated by employing separate time scales on the horizontal axis. Zero error lines for the individual studies have been plotted on the right vertical axis. As can be seen in Figure 8.3 the curve for Aspendale, Australia (Paltridge, 1970) precedes that of the Simcoe data by 5 h, and the curve of Phoenix, Arizona (Idso, 1972) and the present data precede the Simcoe curve by 3 and 2 h respectively. Apart from a nocturnal divergence of the Christchurch error curve, there is a close correspondence between all curves, this despite differences between studies in which they were obtained. Table 8.12 summarises the major differences between the individual studies. Reasons for the lack of a 'plateau' effect in the Christchurch error curve are unclear, but are not necessarily urban related, as the rural pattern is similar. Apart from this, the most significant difference between studies appears to be in the position of the zero line. The position of the zero line for the present study and that of Arnfield (1979) are well removed from those of Idso and Paltridge respectively. This in fact may be related to differences in equipment and instrumental technique, as Arnfield's study and the present one use almost identical equipment. Despite this, the trend evident in all error curves suggests that the common deviations observed are highly unlikely to be the result of instrumental techniques or entirely localized atmospheric radiative processes.

Anormalously large diurnal ranges of atmospheric emission have been reported previously and various mechanisms suggested. Idso

TABLE 8.12 Summary of Studies from which Error Curves in Fig. 8.3 were Obtained (after Arnfield, 1979)

STUDY	LOCATION	SEASON	FORMULA(E)	INSTRUMENTATION
Paltridge (1970)	Aspendale, Victoria, Australia	Summer-Autumn	Swinbank	Net pyrgeometer with unidirectional adaptor
Idso (1972)	Phoenix, Arizona, U.S.A.	Winter	Idso-Jackson	Unidirectional Fritschen-type net pyrradiometer, Eppley Pyranometer
Arnfield (1979)	Simcoe, Ontario, Canada	Summer-Autumn	Idso-Jackson	Funk-type net pyrradiometer with unidirectional adaptor; pyranometer -Funk-type radiometer with glass dome
This Study	Christchurch, New Zealand	Summer-Autumn and Winter	Brutsaert (Figure 8.3) Brunt, Idso-Jackson	Funk-type net pyrradiometer with unidirectional adaptor; Kipp and Zonen pyranometer with glass dome.

et al. (1969) cited the addition of aerosol into the lower atmosphere by turbulence, roughly in phase with the diurnal variability of IR↓, as one possibility in unpolluted rural areas. Idso (1975) also showed the effect of a desert dust storm on atmospheric ε_a. Brazel and Osborne (1976) relate an observed IR↓ excess over that predicted near noon for Hamilton, Ontario, to increased atmospheric emission due to urban pollution. The systematic trend exhibited in Figure 8.3 has been attributed by Paltridge (1970) and Idso (1972) to the problem inherent in the IR↓ predictive models of obtaining a representative 'centre of gravity' of emission. Paltridge suggests that the temperature of air at a height of 200 - 300 m would be more representative than screen level temperature and that since inversion conditions prevail at night and lapse conditions during the day, screen level temperature would underestimate the 'centre of gravity' temperature for atmospheric emission at night and over estimate it during the day. Because of the phase difference of his data, and the position of his zero line (implicit), Arnfield (1979) could not agree with the argument of Paltridge and Idso, but was unable to offer a further explanation. Criteria for agreement with Paltridge and Idso would appear to be a similar phase relationship and a zero error point at a time consistent with an isothermal lower boundary-layer (screen level temperature representative of the 'centre of gravity' of emission). With the Christchurch data there is little discrepancy on the first point, with the points of error curve inflexion coinciding closely (Figure 8.3), but the latter criterion is more difficult to resolve. Part of the problem for the position of the zero line may relate to instrumental techniques (note the similarity with the Simcoe curve), and could be due to calibration differences in equipment. An arbitrary upward movement of the zero line on the vertical axis for both the urban and rural error curves for Christchurch

would improve the explanation in terms of the Paltridge and Idso hypothesis. In the absence of evidence to the contrary, the hypothesis of Paltridge and Idso would appear to be the only explanation able to explain observed errors in prediction of IR↓.

In the case of the Christchurch urban data, pollution effects coincident with the early morning inversion conditions appear to be superimposed upon the model underestimate caused primarily by the inversion conditions. This more than doubles the quite modest model underestimate of εa observed at the rural site.

Performance Characteristics of Individual Equations

Data presented in the previous section suggests that of all IR↓ predictive formulae, the Brutsaert relation is most suitable for application in the Christchurch environment. To more fully evaluate the performance of individual formulae, regression analysis of predicted and measured atmospheric εa has been performed on up to 496 clear sky hourly observations for each representative site. A summary of this regression analysis is included in Table 8.13. Performance characteristics tabulated for each equation include the correlation coefficient (r) and per cent variance of actual emissivity explained (r^2), the coefficient of variation (v) calculated from the root-mean-square (r.m.s.) error, and the ratio of average estimated to average measured emissivity.

Two major points arise from Table 8.13. Firstly, all equations perform markedly better for rural than for urban data, and secondly, the Brutsaert relation appears superior to the other two more empirically based formulae in the prediction of εa, particularly for the rural site. The entries in Table 8.13 are ranked in order

TABLE 8.13 Performance Statistics - Predictive Formulae

			RURAL DATA				URBAN DATA			
DATA TYPE	NO.OBS	FORMULA	r COEFF	r^2(%)	V (%)	RATIO	r COEFF	r^2(%)	V (%)	RATIO
		Brutsaert	0.44**	19	7.4	0.9995	0.03	0.1	10.2	0.9680
All data	497	Brunt	0.43**	19	7.9	0.9875	0.04	0.2	9.2	0.9534
		Idso-Jackson	0.36**	12	8.3	0.9826	0.04	0.2	9.6	0.9457
		Brutsaert	0.55**	30	6.1	0.9987	0.21*	4.6	8.6	0.9470
Daytime data	178	Brunt	0.54**	29	6.3	0.9759	0.22*	4.9	8.5	0.9250
		Idso-Jackson	0.32**	10	7.1	0.9710	0.17*	1.3	9.1	0.9190
		Brutsaert	0.34**	12	8.0	0.9999	-0.05	0.3	10.1	0.9890
Nightime data	319	Brunt	0.34**	11	8.1	0.9991	-0.04	0.1	10.0	0.9818
		Idso-Jackson	0.26**	7	8.7	0.9943	-0.007	-	10.4	0.9788
		Brutsaert	0.48**	23	6.3	0.9987	-0.33**	11	10.2	0.9671
Winter data	339	Brunt	0.46**	21	6.6	0.9965	-0.33**	11	10.3	0.9598
		Idso-Jackson	0.37**	14	7.4	0.9878	-0.23**	5	10.5	0.9547

**Significant at 0.01 level. *Significant at 0.05 level.

of increasing r.m.s. error for each data type at the rural site. All relationships at the rural site show correlation coefficients significantly different from $r = 0$ at the 0.01 level of significance; this despite the systematic variation in predictive error indicated in Figure 8.1. The Brutsaert relation, apart from showing the best correlations and lowest coefficients of variation (v), also gives the best estimate of average rural εa under all conditions (less than a 1% under estimate indicated by predicted/measured ratios). The Brunt and Idso-Jackson formulae also show an average model underestimate for all data types, although the magnitude of the errors evident in the ratios is larger. The relatively good performance of the Brunt relation is quite surprising, especially considering that the a and b coefficients are medians of selected studies from around the world.

Regression relationships at the urban site are poor, with only the daytime and wintertime relationships being significant at the 0.05 level and 0.01 level respectively. The marked variability of the error curves exhibited in Figure 8.1 and the wide scatter of points about the line obviously has an adverse effect on the regression relationship. This variability is also reflected in the urban coefficient of variation (v) for each of the formulae. In addition, all formulae appear to heavily underestimate mean measured εa, although the Brutsaert relation again provides the lowest underestimate. The apparent negative relationship between predicted and measured εa for the winter data at the urban site (Table 8.13) is unexpected, but is probably related to the wintertime diurnal pollution cycle in phase with atmospheric temperature. As shown in Figure 7.2b, the time when atmospheric temperature and vapour pressure is lowest (hence low predicted εa) is coincident with high pollution levels under inversion

conditions (which appear to give high measured εa).

Given the relative poor performance of predictive formulae for IR↓ in the urban environment, it is not surprising that IR↓ prediction in the Christchurch energy balance model is unsatisfactory in urban areas. From the above analysis it would appear that the Brutsaert relation, with its greater universality, is probably the best predictive formula to use for Christchurch. However, its application in the urban environment appears to be severely limited by an inability to account for excess atmospheric emissivity produced by atmospheric pollution. That the Brutsaert relation is readily amenable to emissivity adjustments that reflect localized atmospheric conditions (Brutsaert, 1975) is a further reason for retaining the Brutsaert relation for use in the Christchurch urban environment.

CONCLUSIONS

In summary, this analysis of atmospheric IR↓ over Christchurch using statistical and semi-empirical techniques on surface based data has shown:-

(i) That atmospheric pollution is the dominant influence on urban IR↓ excess, at least during the winter term, and that this effect masks the influence of other variables potentially responsible for the variation of IR↓ across Christchurch.

(ii) In terms of variability of IR↓ at individual sites, the variation of temperature and vapour pressure is most important.

(iii) Three standard formulae used to predict atmospheric emissivity from screen level data (Brunt, Idso-Jackson and Brutsaert) each showed a non-random distribution of εa estimation error diurnally. Reasons for the systematic estimation error appeared related to an inability to correctly specify a 'centre of gravity' temperature for atmospheric emission.

(iv) Examination of performance characteristics for individual equations showed that prediction of εa was better for the rural location than for the urban location, and this appeared related to anomalous emissivity in the city environment not accounted for in the predictive equations. At both sites and in all conditions, the more theoretical Brutsaert relation gave improved results.

CHAPTER 9

PREDICTION OF ATMOSPHERIC IR↓ OVER CHRISTCHURCH : II. THE USE OF VERTICAL ATMOSPHERIC SOUNDINGS

INTRODUCTION

Techniques of IR↓ analysis used in the previous chapter, although simple in conception, suffer from their relative inflexibility. Neither the statistical approach nor the approach utilising predictive equations accounts for the influence of a full range of atmospheric variables, and a particular problem of such methods relates to an inability to account for the influence of meteorological variables at some distance above the surface. For this reason a more theoretical approach to the prediction of IR↓ utilising atmospheric soundings is used here. Such an approach requires the measurement or estimation of a wide range of atmospheric variables through multiple layers of the atmosphere, and the subsequent calculation of IR radiative transfer by numerical solutions of Schwarzschild's equation or chart methods. A similar approach has previously been used to determine reasons for observed IR↓ excess at a rural site in Britain (Dalrymple and Unsworth, 1978).

After a careful consideration of emissivity characteristics of the Christchurch atmosphere using the approach outlined above, an empirical reformulation of the Brutsaert relation to account for atmospheric pollution is suggested.

PREDICTION OF ATMOSPHERIC IR↓ FROM KYTOON AND RADIOSONDE PROFILES

General

Of all the methods of predicting IR↓ at the surface from vertical profiles of temperature and humidity, various forms of the emissivity or 'grey body' approximation method have been the most widely used and evaluated. These methods essentially comprise radiation chart procedures and the various numerical derivatives of that method. Sellers (1972), Komdratyev (1969) and Paltridge and Platt (1976) discuss in detail the principles involved in these methods. Essentially they all make use of empirical and/or theoretical relationships between the isothermal emissivity of a slab of radiating material and the optical thickness of that material. The major problem involved with this method is that of numerical integration over the line structure of the atmospheric absorption spectrum (Paltridge and Platt, 1976). The chart method and its derivatives use approximations to perform the integration once and for all. Effects of pressure on the width of absorption lines are included in the model, and more recently the variability of emissivity with temperature has also been included. Most emissivity approximation methods rely on pressure and temperature dependent emissivities of various atmospheric constituents (usually H_2O, CO_2 and sometimes O_3) derived originally from laboratory experiments. Accuracy of the various emissivity approximation methods has improved recently with the production of a new set of emissivity tables by Staley and Jurica (1970), which correct an error in the tables of Elsasser and Culbertson (1960).

The present analysis uses an improved numerical form of the scheme described by Robinson (1947, Table III). The improved

emissivity tables of Staley and Jurica (1970), which allow for temperature dependence of emissivity are also used. The method essentially involves dividing the atmosphere into homogeneous layers and calculating the product of the effective emissivity for each layer with the blackbody radiation at a mean layer temperature.

The Prediction Method - Assumptions and Procedures Used

For purposes of computation, it is convenient to express the total downward flux density IR↓ as:-

$$IR\downarrow = IR\downarrow(H_2O) + IR\downarrow(CO_2) + IR\downarrow(H_2O - CO_2 \text{ overlap}) + IR\downarrow(O_3) + IR\downarrow(\text{aerosol}) + IR\downarrow(\text{trace gases}) \quad \ldots 9.1$$

where the first two terms on the right represent the flux densities contributed by H_2O and CO_2 each in isolation of the other. The negative flux density contribution associated with overlap of the H_2O and CO_2 bands is represented by the third term. The contribution of ozone (assumed not to overlap the emission of the other gases) is represented by the fourth term, while the fifth and six terms account for the flux density contribution of aerosol and emitting gases respectively. When the individual flux density contributions are expressed in terms of integrations of black body flux density over emissivity (Staley and Jurica, 1972), the effective atmospheric emissivity becomes:-

$$\varepsilon a = \varepsilon a(H_2O) + \varepsilon a(CO_2) + \varepsilon a\ (\text{overlap}) + \varepsilon a(O_3) + \varepsilon a\ (\text{aerosol}) + \varepsilon a\ (\text{trace gases}) \quad \ldots 9.2$$

While it is reasonably straightforward to calculate atmospheric emissivity due to water vapour, carbon dioxide and ozone, the contribution

of aerosol and trace gases is yet poorly understood. Staley and Jurica (1972) state that while aerosol and trace gas emission is insignificant in unpolluted atmospheres, the contribution of aerosol under heavily polluted conditions can conceivably exceed that of O_3. When emissivities due to aerosol and trace gases are left out of the computation, this method therefore becomes a powerful tool for isolating and determining pollution effects on IR↓ in heavily polluted urban areas.

Errors involved in applying emissivities for homogeneous slabs to computations of the flux density of IR↓ have been discussed by Rodgers (1967) and Staley and Jurica (1972). Computational errors of H_2O emissivity appear small in the lower troposphere where most water vapour is to be found and where IR↓ is contributed mostly by layers near the surface having temperatures and pressures similar to surface values. For similar reasons and also because the temperature dependence of CO_2 emission is small, errors in applying slab emissivities to CO_2 are also small (Staley and Jurica, 1972). Such a method therefore appears suitable for application in the present study.

Calculation of IR↓ was carried out by a computer programme 'Finale' (see Appendix VI for listing and documentation). Detailed profiles of temperature and humidity up to 500 m obtained by the instrumented kytoon at the representative sites were used as input to 'Finale'. Above 500 m, and continuing to the tropopause at $\sim$ 11 km, the temperature and humidity profile was drawn from routine N.Z.M.S. radiosonde ascents made once or twice daily from Christchurch International Airport. In all cases, the radiosonde profile most closely approximating the time of kytoon ascent was used. Errors involved in using the radiosonde profile separated in time and space from the kytoon are unknown but believed small, this largely because atmospheric con-

ditions during periods under study were always synoptically stable and because ∿ 80% of atmospheric IR↓ is derived from below 500 m. (Lettau and Davidson, 1957). Robinson (1947) concluded that maximum errors in IR using complete profiles from rather distant sites were < 2% of total IR↓, so this figure is unlikely to be exceeded in the present study, where the introduced profile is only for above 500 m. In addition, any error involved would be applied equally at both representative sites so urban-rural differences would not be affected.

Division of the atmosphere into homogeneous slabs involved 20 m (∿ 2 mb) slabs to 200 m and 50 m (∿ 5 mb) slabs to the top of the kytoon profile at ∿ 500 m. Above the kytoon profile slabs were of 50 mb thickness to 800 mb (∿ 2000 m) and at 100 mb increments above that level to the tropopause at ∿ 250 mb. Since less than 1% of IR↓ is contributed from above that level, no account is made of emission from above the tropopause. Generally, about 25 homogeneous slabs were involved in the calculation for each profile. The bottom of the first slab at each site was adjusted to coincide with the height of the individual IR↓ sensors, so that full comparison of measured and predicted IR↓ could be made without error in the lowest layer (where a substantial portion of total IR↓ flux density originates).

At each layer 'Finale' calculates the mixing ratio and optical path length for water vapour, making a square root pressure correction (Robinson, 1947; Kondratyev, 1969; Dalrymple and Unsworth, 1978). Values for H_2O emissivity were determined by two dimensional linear interpolation from the tables of Staley and Jurica (1970), which are included within the program. Similarly, values for CO_2 emission, assuming a mean mixing ratio of 5×10^{-4} g g^{-1} throughout the atmosphere, were calculated at each layer. This CO_2 mixing ratio

is suggested by Staley and Jurica (1972) as a mean value near the earth's surface, and they state that extremely large variations away from the mean figure would produce only a 2% difference in CO_2 emissivity. Pressure scaling of CO_2 optical depths was performed according to Kondratyev (1969). At each layer a negative correction for H_2O - CO_2 overlap was also calculated. The method of summation of the individual contributions for each layer is as described by Robinson (1947) and Dalrymple and Unsworth (1978), but unlike those studies, the method here has been extended to CO_2.

Robinson and Dalrymple and Unsworth simply added a bulk contribution of CO_2 at screen level temperature at the end of their summation. This method of accounting for IR↓ flux density due to CO_2 involves an expression of the following nature:

$$IR\downarrow (CO_2) = b \sigma T^4 \quad \ldots 9.3$$

where b is a constant and T is the reference level temperature. This expression is based on the argument that CO_2 absorbs so strongly in the dominant 15 μm CO_2 band, that a thin atmospheric layer is a black body in this range. Elsasser (1942) indicated a value of 0.18 for b, while the most frequently quoted value is 0.185 (Robinson, 1974; Haltiner and Martin, 1957). Kondratyev (1969) argued that a fixed value of b of 0.185 is unrealistic and Staley and Jurica (1972) suggest that while most CO_2 IR↓ flux density originates in near surface layers, at least some is contributed by more distant layers, and their contribution is dependent on rate of change of temperature with CO_2 optical depth. Staley and Jurica conclude that no universal value of b can be obtained and that only computation can determine its magnitude and variability. For this reason the contribution of CO_2 has been

calculated in this study on a layer by layer basis.

The only contribution to surface IR↓ not calculated on a layer basis was that of O_3. In the manner advocated by Robinson (1947) for CO_2, 5% of blackbody radiation at screen level temperature was added to total IR↓ to account for O_3. An O_3 emissivity of 0.05 was suggested by Staley and Jurica (1972) for 0.30 cm of total ozone in the atmosphere. Total O_3 over New Zealand during the present study varied from an average 0.30 cm in summer, to 0.37 cm in winter (Ozone Data for the World), so the approximations of Staley and Jurica appear reasonable, particularly in view of the uncertainties they quote. Fortunately, because the total contribution of O_3 is small, errors involved are very slight and are equally applied at both representative sites. Many emissivity approximation methods do not even account for the influence of ozone.

An example profile for 0605 h 8 July, 1979 at the Central City Site is reproduced in Figure 9.1. For obvious reasons a complete profile cannot be produced here. For each layer, the mean temperature, pressure and specific humidity are shown (see lowest layer), as well as the resultant IR↓ emission. Only part of the total amount of information available from 'Finale' is included in Figure 9.1. The contribution of near surface layers can be seen to be dominant, with more than 25% of total IR↓ being contributed from the first layer alone, despite the fact that it is only 5 m deep. Note also that the summation begins at the 5 m level, the height of the IR↓ sensor at the Central City Site.

Of 82 kytoon profiles available for analysis at both sites by 'Finale', only 68 were eventually used. Most of the fourteen profiles discarded were those where measured IR↓ was not available

80m

	8.2° C	7.44 Wm^{-2}
LAYER 5	1012.0 mb	0.28 Wm^{-2}
	3.54 gm kg^{-1}	7.69 Wm^{-2}

60m

	5.6° C	9.16 Wm^{-2}
LAYER 4	1014.3 mb	0.39 Wm^{-2}
	3.102 gm kg^{-1}	9.52 Wm^{-2}

40m

	1.7° C	15.74 Wm^{-2}
LAYER 3	1016.6 mb	0.68 Wm^{-2}
	3.196 gm kg^{-1}	16.40 Wm^{-2}

20m

	-0.6° C	20.18 Wm^{-2}
LAYER 2	1018.3 mb	0.76 Wm^{-2}
	3.288 gm kg^{-1}	20.93 Wm^{-2}

10m

LAYER 1	Temperature	-1.3° C	H_2O IR↓ 54.87 Wm^{-2}
	Pressure	1019.1 mb	CO_2 IR↓ 1.27 Wm^{-2}
	Specific Humidity	3.103 gm kg^{-1}	TOTAL LAYER IR↓ 56.14 Wm^{-2}

5m

ALL LAYER

H_2O+CO_2 IR↓ 202.57 Wm^2

OZONE IR↓ 15.46 Wm^2

TOTAL IR↓ = 218.03 Wm^{-2}

FIGURE 9.1 EXAMPLE PROFILE FROM 'FINALE' - CENTRAL CITY SITE 0605 8.7.79

for comparison with that calculated, or where there were possible cloud effects. In the subsequent analysis the urban site is represented by 36 profiles (seventeen nocturnal) and the rural site by 32 profiles (nineteen nocturnal). Twenty-six profiles were able to be paired for use in assessing urban-rural $IR\downarrow$ difference. Because of higher winds and equipment failure relatively few summertime profiles were available for analysis.

In assessing the mechanisms involved in augmented urban $IR\downarrow$, the predictive model 'Finale' offers two important approaches. Firstly, it allows urban-rural differences to be examined once again in terms of the probable contributing factors discussed in the previous chapters; namely temperature, atmospheric water vapour and pollution effects. Secondly, at the individual sites, $IR\downarrow$ not accounted for in the predictive model can be examined in detail in terms of those variables not considered in the calculation of $IR\downarrow$ from atmospheric profiles, aerosol and trace gas emitters. Both of these approaches are considered in the following sections.

Prediction of Urban $IR\downarrow$ Excess From Paired Profiles

Detailed analysis of kytoon profiles in Chapters 4 and 5 indicated a marked nocturnal urban temperature and specific humidity excess extending approximately 300 m into the boundary-layer. Daytime temperature profiles revealed a slight urban excess only, while daytime specific humidities appeared reduced over urban Christchurch. Then, only guesses could be made at estimating the effect of these urban-rural differences on $IR\downarrow$. The analysis summarised in Table 9.1 attempts to quantify these influences.

TABLE 9.1 Measured Urban Excess IR↓ and Urban Excess IR↓ Calculated from Profiles

(a) NOCTURNAL

DATE	TIME (N.Z.S.T.)	MEASURED URBAN EXCESS IR↓ (%)	COMPUTED URBAN EXCESS IR↓ (%)	URBAN EXCESS IR↓ (%) UNACCOUNTED FOR
15.7.78	2200	0	1.8	-
16.7.78	2100	- 0.9	1.7	-
22.7.78	2145	13.6	1.3	12.3
19.8.78	2135	2.0	3.0	-
2.4.79	2305	8.8	1.3	7.5
5.4.79	2325	11.0	3.5	7.5
16.4.79	0520	0.8	- 0.4	1.2
23.4.79	0040	6.4	- 3.6	10.0
26.4.79	2315	7.4	1.8	5.6
7.7.79	2300	13.1	- 0.5	13.6
8.7.79	1930	2.9	0.9	2.0
10.7.79	2230	3.6	4.0	-
21.7.79	2220	15.6	5.8	9.8
3.8.79	2400	7.1	0.0	7.1
15.8.79	2200	13.4	5.6	7.8
16.8.79	0700	15.5	3.3	12.2
$\overline{X}$		7.5	1.8	5.7

(b) DAYTIME

DATE	TIME (N.Z.S.T.)	MEASURED URBAN EXCESS IR (%)	COMPUTED URBAN EXCESS IR (%)	URBAN EXCESS IR (%) UNACCOUNTED FOR
12.8.78	1300	9.9	- 5.4	15.3
20.8.78	0845	- 4.5	- 2.7	-
3.4.79	0845	5.0	3.2	1.8
16.4.79	1045	2.6	3.8	-
7.7.79	1335	10.8	0.9	9.9
10.7.79	1440	0.7	0.4	0.3
21.7.79	1405	10.9	1.3	9.6
22.7.79	1040	11.9	0.5	11.4
3.8.79	1330	10.3	0.4	9.9
10.8.79	1150	9.8	0.5	9.3
$\overline{X}$		6.7	0.3	6.4

Table 9.1 shows the proportion of measured urban excess IR↓ accounted for by profile characteristics for the 26 paired profiles. In the nocturnal case (Table 9.1a), the mean measured urban excess IR↓ at time of profiling is 7.5%, consistent with the urban excess reported in Table 7.9. The corresponding profiles predict an urban excess IR↓ of less than 2% due to urban excess temperature and humidity in the boundary-layer. This leaves almost 5.7% of urban excess IR↓ to be accounted for by other factors. The most likely source of excess radiation would be urban particulate and gaseous pollution. In the daytime case (Table 9.1b), small urban-rural profile differences result in only a small computed urban excess IR↓ of 0.3%. Of the average urban excess IR↓ measured during daytime fully 95% (6.4%) is left unaccounted for. The pattern described is not definitive, as it is likely that the rural site is at least sometimes under the influence of pollution originating from urban Christchurch with winds from the east and north-east. This would have the effect of reducing the apparent urban excess IR↓, as well as that unaccounted for in Table 9.1.

Excess IR↓ at the Representative Sites

General

The profile computed atmospheric apparent emissivity at the height of the IR↓ radiation sensor is $\varepsilon a(c) = IR\downarrow(c)/\sigma T^4$, where IR↓(c) is the computed IR↓ flux density and T(c) the temperature (^{o}K) at the instrument level. With both aerosol and gaseous pollution emission present, measured apparent emissivity would be:-

$$\varepsilon a = \varepsilon a(c) + f\bar{\varepsilon} = (IR\downarrow(c) + IR\downarrow(p)/\sigma T(c)^4) \qquad \ldots 9.4$$

where $f\bar{\varepsilon}$ is the effective emissivity of the atmosphere for pollution

and IR↓(p) is the flux density of infra-red radiation due to pollution. The fractional excess emissivity is then given by:-

$$\gamma = f\bar{\varepsilon}/\varepsilon a(c) \qquad \ldots 9.5$$

Results of profile analysis to derive values of $f\bar{\varepsilon}$ and γ are presented in Tables 9.2 through 9.5. For the analysis of nocturnal and daytime profiles at the urban site (Tables 9.2 and 9.3), profile identification data is presented along with other relevant variables, and summer data is separated from the winter data.

Nocturnal winter fractional excess emissivities (γ) at the urban site (Table 9.2) vary between 0.01 and 0.31 on individual occasions, with a mean of 0.13. The nocturnal summer case shows a slightly higher mean γ of 0.15, but the number of observations is small ($N = 6$). Daytime winter urban γ values (Table 9.3) are markedly higher, ranging between 0.06 and 0.35 ($\bar{X} = 0.22$), these higher values apparently reflecting effects of daytime solar irradiation on the pollution layer. Robinson (1947, p. 148) also noted the probable effect of sunlit smoke particles radiating at temperatures higher than that of surrounding air, and thus not being reflected in profile computations of IR↓.

Tables 9.4 and 9.5 summarise data from the rural representative site. Mean winter nocturnal and daytime values of γ at the rural site of 0.05 and 0.09 respectively are each considerably lower than those observed for the urban site. This may reflect sampling at different times of the day, as considerable diurnal variation would be expected. As with urban data, there is a significant day to day variability of γ.

TABLE 9.2 Summary of Profile Analysis - Central City Nocturnal Data

DATE	TIME	MEASURED IR↓ (Wm^{-2})	PROFILE IR↓ (Wm^{-2})	εa(Meas)	εa(Profile)	$f\bar{\varepsilon}$	γ	LOG_{10} * NEAR SURFACE POLLUTION ($\mu g\ m^{-3}$)	LOG_{10} * TOTAL WT POLLUTION ($\mu g\ m^{-2}$)
15.7.78	2200	230	219	0.6827	0.6500	0.0327	0.0503	2.32	4.1
16.7.78	2100	232	230	0.6860	0.6800	0.0060	0.0100	2.04	4.17
22.7.78	2145	294	231	0.8359	0.6568	0.1791	0.2727	2.69	4.09
31.7.78	2225	272	230	0.8259	0.6976	0.1283	0.1839	2.75	3.91
19.8.78	2135	250	223	0.7159	0.6386	0.0773	0.1210	2.41	4.21
20.8.78	0645	237	211	0.7427	0.6612	0.0815	0.1233	1.54	3.15
3.9.78	0045	279	228	0.8169	0.6676	0.1493	0.2236	2.58	3.70
7.7.79	2300	259	197	0.8086	0.6150	0.1936	0.3148	3.00	4.19
8.7.79	0605	256	218	0.8279	0.7050	0.1229	0.1743	2.38	3.69
8.7.79	1930	237	232	0.6682	0.6532	0.0150	0.0230	1.78	3.52
10.7.79	2230	253	244	0.7093	0.6840	0.0253	0.0370	1.84	3.73
21.7.79	1815	225	214	0.6592	0.6270	0.0322	0.0513	2.36	3.95
21.7.79	2010	239	209	0.7258	0.6347	0.0911	0.1435	2.46	4.10
21.7.79	2220	263	223	0.7998	0.6782	0.1216	0.1793	2.46	3.76
3.8.79	2400	253	235	0.7402	0.6875	0.0527	0.0766	2.3	3.70
15.8.79	2200	232	215	0.7119	0.6597	0.0513	0.0791	1.80	3.85
16.8.79	0700	239	211	0.7857	0.6936	0.0921	0.1328	2.18	3.51
2.4.79	2305	317	242	0.8810	0.6726	0.2084	0.3098	2.38	4.28
5.4.79	2325	310	258	0.8177	0.6805	0.1372	0.2016	1.68	4.60
14.4.79	2200	263	235	0.7245	0.6476	0.0769	0.1187	1.78	4.45
16.4.79	0520	253	246	0.7424	0.7218	0.0206	0.0285	1.48	-
23.4.79	0040	313	274	0.8529	0.7466	0.1063	0.1424	2.58	4.02
26.4.79	2315	256	227	0.7576	0.6718	0.0858	0.1277	2.58	4.44

*Smoke particulate in winter, total NOx in summer.

TABLE 9.3 Summary of Profile Analysis - Central City Daytime Data

DATE	TIME	MEASURED IR↓ (Wm^{-2})	PROFILE IR↓ (Wm^{-2})	εa(Meas)	εa(Profile)	$f\bar{\varepsilon}$	γ	LOG_{10} * NEAR SURFACE POLLUTION ($\mu g\ m^{-3}$)	LOG_{10} * TOTAL WT POLLUTION ($\mu g\ m^{-2}$)
17.7.78	1000	299	221	0.8794	0.6500	0.2294	0.3529	2.23	-
2.8.78	0815	295	221	0.8899	0.6667	0.2232	0.3348	2.18	3.20
5.8.78	1405	279	242	0.7373	0.6395	0.0978	0.1529	1.18	-
12.8.78	0945	296	235	0.7899	0.6272	0.1627	0.2594	1.60	3.28
12.8.78	1300	292	241	0.7700	0.6355	0.1345	0.2116	1.30	-
20.8.78	0845	243	219	0.7304	0.6582	0.0722	0.1097	1.00	3.08
3.9.78	1300	310	242	0.8192	0.6395	0.1797	0.2810	1.48	2.95
7.7.79	1335	286	224	0.7927	0.6208	0.1719	0.2769	1.78	-
8.7.79	0810	270	205	0.8684	0.6594	0.2090	0.3169	2.18	-
8.7.79	0930	280	222	0.8682	0.6884	0.1798	0.2611	2.11	3.89
8.7.79	1050	290	225	0.8283	0.6427	0.1856	0.2888	2.11	3.81
8.7.79	1500	275	233	0.7400	0.6270	0.1130	0.1802	1.40	-
8.7.79	1630	256	232	0.7107	0.6441	0.0666	0.1034	1.10	-
10.7.79	1440	277	261	0.7088	0.6679	0.0409	0.0612	1.00	3.33
21.7.79	1405	285	225	0.7768	0.6132	0.1636	0.2668	1.84	-
22.7.79	1040	252	203	0.7332	0.5906	0.1426	0.2414	1.81	2.91
3.8.79	1330	310	252	0.7878	0.6404	0.1474	0.2302	1.20	-
10.8.79	1150	255	217	0.7139	0.6075	0.1064	0.1751	1.30	-
16.8.79	1250	250	218	0.7161	0.6245	0.0916	0.1467	1.30	-
3.4.79	0845	318	247	0.8789	0.6827	0.1962	0.2873	2.0	4.19
15.4.79	0930	296	249	0.7955	0.6692	0.1263	0.1887	1.84	-
15.4.79	1135	324	255	0.8361	0.6580	0.1790	0.2707	1.69	-
16.4.79	1045	309	262	0.8018	0.6798	0.1220	0.1795	1.60	3.94

*Smoke particulate in winter, total NOx in summer.

TABLE 9.4 Summary of Profile Analysis - Lincoln Site Nocturnal Data

DATE	TIME	MEASURED IR↓ (Wm^{-2})	PROFILE IR↓ (Wm^{-2})	εa(Meas)	εa(Profile)	γ	WIND DIRECTION (^{o}) *
15.7.78	2200	230	215	0.6857	0.6410	0.0697	
16.7.78	2100	234	226	0.6966	0.6728	0.0354	
22.7.78	2145	254	228	0.7286	0.6540	0.1141	090 Surface
19.8.78	2135	245	215	0.6821	0.5985	0.1397	
7.7.79	1745	226	200	0.6909	0.6112	0.1304	000 Throughout
7.7.79	2300	225	198	0.6795	0.5980	0.1363	000 Throughout
8.7.79	1930	230	230	0.6493	0.6493	0.0000	
10.7.79	2230	244	234	0.7275	0.6977	0.0427	
21.7.79	2220	222	210	0.6833	0.6463	0.0572	000 Above 100 metres
3.8.79	1830	243	243	0.6756	0.6756	0.0000	
3.8.79	2000	238	234	0.6682	0.6569	0.0172	070 Above 200 metres
3.8.79	2400	235	235	0.6597	0.6597	0.0000	
15.8.79	2200	201	203	0.6317	0.6378	-0.0096	
16.8.79	0700	202	204	0.6603	0.6668	-0.0097	
2.4.79	2305	289	239	0.7977	0.6597	0.2092	040 Throughout
5.4.79	2325	276	249	0.7512	0.6777	0.1084	060 Above 100 metres
16.4.79	0520	251	247	0.6987	0.6876	0.0161	020 Above 200 metres
23.4.79	0040	293	284	0.7354	0.7128	0.0317	
26.4.79	2315	237	223	0.7158	0.6735	0.0628	040 Above 100 metres

*Wind direction reported when from over city.

TABLE 9.5 Summary of Profile Analysis - Lincoln Site Daytime Data

DATE	TIME	MEASURED IR↓ (Wm^{-2})	PROFILE IR↓ (Wm^{-2})	εa(Meas)	εa(Profile)	γ	WIND DIRECTION (°) *
12.8.78	1300	263	254	0.6729	0.6499	0.0354	
20.8.78	0845	254	225	0.7486	0.6631	0.1289	040 Above 100 metres
7.7.79	1335	255	222	0.7099	0.6180	0.1487	010 Throughout
7.7.79	1655	230	206	0.6769	0.6062	0.1166	000-010 Throughout
10.7.79	1440	275	260	0.7216	0.6822	0.0577	010 Throughout
21.7.79	1405	254	222	0.7052	0.6163	0.1442	000-020 Throughout
22.7.79	1040	221	202	0.6494	0.5936	0.0935	
3.8.79	1330	278	251	0.7045	0.6361	0.1075	100 to 200 metres
3.8.79	1700	243	243	0.6603	0.6603	0.0000	
10.8.79	1150	230	216	0.6588	0.6187	0.0648	
12.2.79	1445	331	300	0.8016	0.7266	0.1032	
3.4.79	0845	302	239	0.8419	0.6676	0.2610	040 Throughout
16.4.79	1045	301	252	0.7963	0.6666	0.1946	040-010 Throughout

*Wind direction reported when from over city.

Comparison with Previous Measurements

Similar previous studies include those of Robinson (1947, 1950), Staley and Jurica (1972) and Dalrymple and Unsworth (1978). Robinson (1947, 1950) made a detailed study of IR↓ at Kew, a site in suburban London. He found a variable component of 0 - 10% excess radiation above that computed by radiation chart and ascribed this excess radiation to particulate matter of urban origin in the atmosphere. Typical values of γ using his data would appear to be $\simeq 0.10$, with individual values considerably exceeding this. However, had he used in his computations the emissivities used in this study, his values for γ would have been lower.

Staley and Jurica (1972) also compared measured and calculated IR↓ for a rural desert environment near Tucson, Arizona. Their measurements suggested an excess atmospheric effective emissivity of about 0.03, which is approximately equivalent to a fractional excess emissivity of 0.04. Unfortunately their instrumentation required the assumption of a soil surface emissivity of 0.90 to recover the effective atmospheric emissivity, and this may have involved considerable error.

Dalrymple and Unsworth (1978), in the most comparable study available in the literature, found values of 0.045 and 0.083 for mean nocturnal and daytime γ in a study of IR↓ under cloudless skies in rural England and British Columbia. These results are almost identical to the rural results for the Christchurch study. Similarity of the present results with those of Dalrymple and Unsworth is remarkable considering slight differences in computational scheme, instrumentation, site, and the relatively few observations involved in both studies.

Origin of the Excess Emissivity

The papers of Robinson (1947, 1950) and Dalrymple and Unsworth (1978) each emphasise the effect of atmospheric aerosol, particularly within the more important'atmospheric window' ($8 \leq \lambda \geq 13$ μm), in contributing to excess radiation. The effect of this additional atmospheric constituent is that its absorption properties make the atmosphere more opaque within those wavelength regions which do not normally absorb strongly. Strong absorption at these wavelengths is related to characteristic bands associated with the main constituents or urban aerosol, particularly sulfates and organic compounds such as soot and other carbon-mixed polymerides (Fischer, 1975).

While Dalrymple and Unsworth (1978) noted a close relationship between γ and a measure of atmospheric turbidity derived from radiation measurements, a more soundly based analysis of this effect is possible here because of the availability of independently obtained pollution observations at and above the surface.

Tables 9.6 and 9.7 summarise winter and summer relationships between urban γ, $\overline{f\varepsilon}$ and pollution respectively. Initially, it was anticipated that variability of wintertime γ (and $\overline{f\varepsilon}$) would be related more closely to the total particulate loading of the atmosphere rather than simply the near surface particulate concentration. Accordingly, the pollution profiles relating to each individual observation of γ were digitised to give a total integrated particulate loading (μg m^{-2}) above the urban site (Tables 9.2 and 9.3). Results of the regression analysis of $\log_{10}$ total particulate loading and nocturnal γ were poor, with $\log_{10}$ total particulate loading explaining less than 3% of variance in γ (Table 9.6a). Surprisingly, $\log_{10}$ near surface particulate produced a considerably better relationship, explaining 67% of variance in

TABLE 9.6 Summary of Regression Analysis - Winter C.C.S. Emissivity and Particulate Concentration (Log Smoke)

(a) NOCTURNAL DATA

DEPENDENT VARIABLE	INDEPENDENT VARIABLE	NO. OBSERVATIONS	a COEFFICIENT	b COEFFICIENT	r	SIGNIFICANCE
Fractional excess emissivity γ	Log_{10} Total Particulate Weight ($\mu g\ m^{-2}$)	17	0.1058	0.000003	0.17	N.S.
Fractional excess emissivity γ	Log_{10} Near surface Particulate ($\mu g\ m^{-3}$)	17	-0.2775	0.177	0.821	0.01
Pollutant effective emissivity $\overline{f\epsilon}$	Log_{10} Near surface Particulate ($\mu g\ m^{-3}$)	17	-0.1754	0.114	0.810	0.01

TABLE 9.6 Summary of Regression Analysis - Winter C.C.S. Emissivity and Particulate Concentration (Log Smoke)

CONTINUED

(b) DAYTIME DATA

DEPENDENT VARIABLE	INDEPENDENT VARIABLE	NO. OBSERVATIONS	a COEFFICIENT	b COEFFICIENT	r	SIGNIFICANCE
Fractional excess emissivity γ	Log_{10} near Surface particulate ($\mu g\ m^{-3}$)	19	-0.027	0.1599	0.873	0.01
Pollutant effective emissivity $f\bar{\varepsilon}$	Log_{10} near Surface particulate ($\mu g\ m^{-3}$)	19	-0.023	0.1059	0.881	0.01

TABLE 9.7 Summary of Regression Analysis - Summer C.C.S. Emissivity (Nocturnal) and Nitrogen Oxides Concentration (Log NOx)

DEPENDENT VARIABLE	INDEPENDENT VARIABLE	NO. OBSERVATIONS	a COEFFICIENT	b COEFFICIENT	r	SIGNIFICANCE
Fractional excess emissivity γ	Log_{10} Total NOx Weight ($\mu g\ m^{-2}$)	6	0.190	-0.0000004	0.056	N.S.
Fractional excess emissivity γ	Log_{10} Near Surface NOx ($\mu g\ m^{-3}$)	6	-0.0092	0.079	0.41	N.S.
Pollutant effective emissivity $\overline{f\varepsilon}$	Log_{10} Near Surface NOx ($\mu g\ m^{-3}$)	6	-0.0124	0.0569	0.44	N.S.

wintertime nocturnal γ at the urban site and 66% of the variance in $f\bar{\varepsilon}$. Subsequent regression analysis between 22 observations of $\log_{10}$ near surface particulate and $\log_{10}$ total particulate loading showed a statistically insignificant relationship, with only 12% of the variability in total particulate explained by near surface particulate. The significance of these results for IR$\downarrow$ appears to be that layers of particulate matter quite near to the ground are contributing most to excess emissivity, a particularly useful result considering the ready availability of pollution data from instrumentation at ground level.

The winter daytime relationship of γ and $f\bar{\varepsilon}$ with near surface particulate (Table 9.6b) also shows a strong, positive correlation. Analysis of summer emissivity characteristics and pollution was less successful (Table 9.7), partly becasue of small sample numbers and also because oxides of nitrogen have relatively little bearing on emissivity variation, even though they could be considered a surrogate for pollutants such as O_3 which may have an effect. No regression analysis was performed on summer daytime data as the number of observations was too few (N = 4).

Figure 9.2 is a plot of the relationship between winter fractional excess emissivity and $\log_{10}$ smoke particulate concentrations. Apart from the obvious strength of the relationships shown, two points are worth further discussion. Firstly, there is a significant difference between the position of daytime and night-time data on the vertical axis, with a given particulate level associated with higher γ during the day than at night. As described previously, this appears related to solar heating of the pollution layer. Secondly, while the intercept for the daytime data is not significantly different from zero, that of the nocturnal data is well removed. Since the daytime intercept is

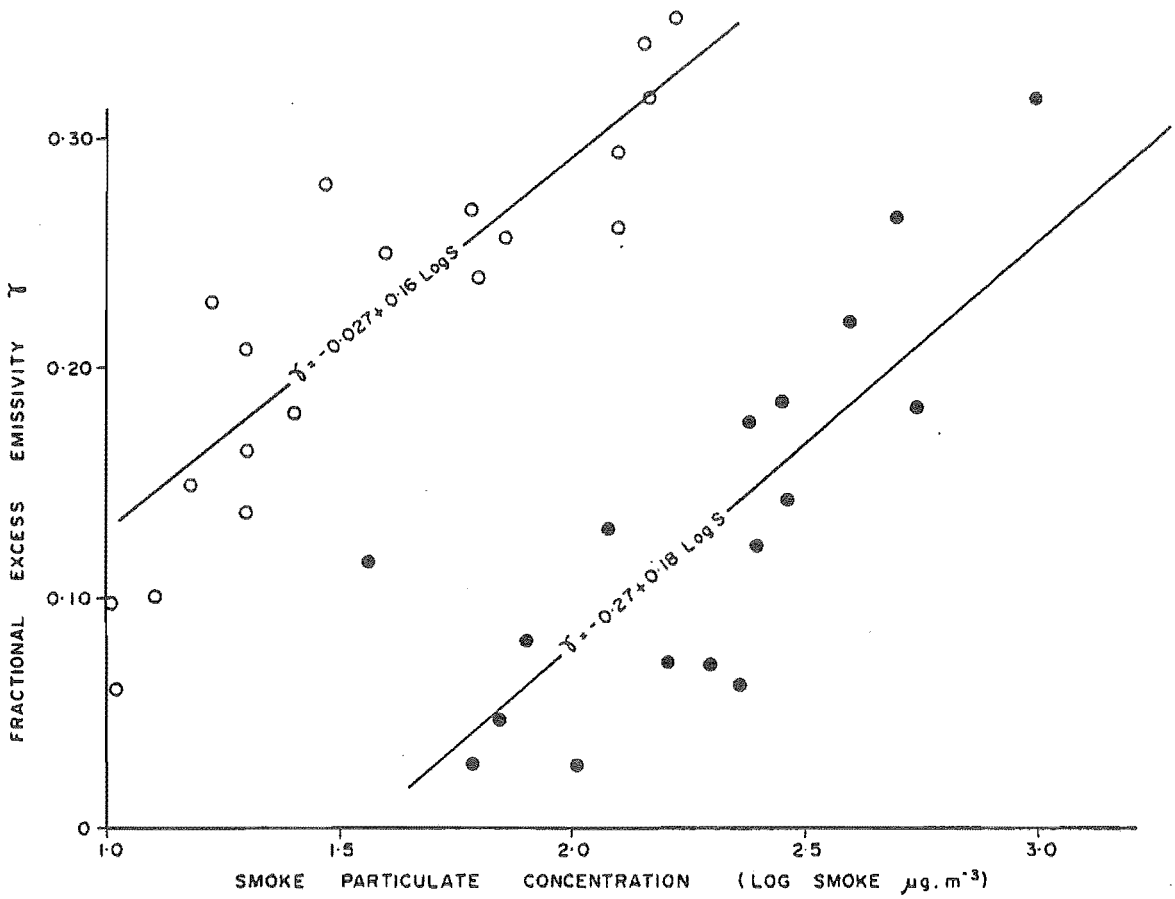

FIGURE 9.2 Plot of Winter Time Fractional Excess Emissivity and Log_{10} Smoke Particulate Concentrations (Open Circles Show Daytime Relationship and Solid Circles the Nocturnal Relationship).

reasonable the problem does not appear to be instrumental, but rather appears to be related to sampling problems. There is a marked paucity of nocturnal observations with pollution concentrations below 40 $\mu g\ m^{-3}$ (1.6 $\log_{10}$), a situation difficult to remedy in the Christchurch nocturnal case where winter clear sky conditions are always associated with high levels of particulate pollution.

In their study Dalrymple and Unsworth (1978) observed a daytime relationship between γ and aerosol turbidity similar to that revealed for the Christchurch data in Figure 9.2. Their night-time data however, showed no systematic variation with nocturnal aerosol turbidity (estimated crudely as the mean value of the last turbidity measurement of the evening and the first of the following morning), a fact they ascribed to sedimentation of aerosols kept aloft by convection during daytime hours. In the Christchurch case it appears that radiatively active particulate matter is effective throughout the evening.

Since observations of γ at the rural site in this study were unaccompanied by atmospheric pollution measurements, analysis for this site is somewhat constrained. Slightly higher values of γ during the day than at night are indicated in Tables 9.4 and 9.5. These differences could possibly be related to convective influences on natural aerosol (Dalrymple and Unsworth, 1978), but are more likely related to solar radiation effects on residual urban air pollution. If night-time and daytime data from the rural Lincoln site is stratified according to whether airflow (determined from kytoon wind profiles) is from over the urban area or from unpolluted rural areas, statistically significant differences in γ are obtained (Table 9.8). With winds from over urban Christchurch (000° - 090°), the mean nocturnal value of γ is 0.0946, while that for all other wind directions is 0.030 (Table 9.8a). The

TABLE 9.8 Fractional Excess Emissivity (γ) at Lincoln Site with Wind Direction

(a) NOCTURNAL DATA

γ (Wind 000°-090°)	γ (Wind all other Directions)	
0.1141	0.0697	
0.2092	0.0354	
0.1084	0.1397	
0.0161*	0.0317	
0.0628	0.0000	
0.1304	0.0427	
0.1363	0.0000	
0.0572	0.0000	
0.0172*	-0.0096	
	-0.0097	
$\bar{X}$ 0.0946	0.0300	t = 3.636
		significant at 0.01 level

with * removed (16.4.79 and 3.8.79 - days with very low city pollution)

$\bar{X}$ 0.1169

(b) DAYTIME DATA

γ (Wind 000°-090°)	γ (Wind all other Directions)	
0.1289	0.0354	
0.2610	0.1032	
0.1946	0.0935	
0.1487	0.0000	
0.1166	0.0648	
0.0577		
0.1442		
0.1075		
$\bar{X}$ 0.1449	0.0590	t = 2.728
		significant at 0.025 level

difference becomes even more significant with the removal from the 000^{o} - 090^{o} data base of two days of very low city pollution. A similar pattern emerges in Table 9.8b for daytime data. Thus it appears that even at the Lincoln site, selected in this study for its relative isolation from urban influences, radiative effects of urban pollution are felt. Therefore, actual urban-rural differences in IR↓ may be even larger than identified in Chapter 8.

From the above analysis it is clear that wintertime γ and $\overline{f\varepsilon}$ is closely and linearly related to the logarithim of atmospheric smoke particulate concentration over Christchurch and surrounding areas. To attempt to quantify the relative effects of particulate pollution and identify other possible contributing factors it is necessary to examine more closely the mechanism of particulate radiation. Table 9.9 gives the size distribution of particulate matter collected over Christchurch during the winters of 1978 and 1979. Samples were gathered by an Anderson particle fractionating sampler consisting of six stages and one filter. Over 20% of particulates would appear to be radiatively active in the infra-red and a relatively large proportion of these in the crucial 'atmospheric window' region. The substantial proportion of relatively large particles in the Christchurch urban atmosphere is due mainly to incomplete combustion of solid fossil fuels, and also possibly dust produced by strong north-westerly winds (pers. comm. D. Pullen, Air Pollution Section, Department of Health). The latter effect is only likely to be important during spring and summer.

It is possible to make a theoretical approximation of the likely effect of Christchurch aerosol on atmospheric emissivity. Aerosols are only likely to influence IR↓ at ground level in the atmospheric window region, 8 - 12 μm (λ_1 to λ_2). The flux density

TABLE 9.9 Size Distribution of Christchurch Winter Particulate Matter

Size (μm)	Percent Occurrence
> 8	9.1
6 - 8	4.2
4 - 6	8.3
2 - 4	3.7
1 - 2	6.1
0.6 - 1	6.4
< 6	62.2

21.6% particulate > 4 μm

78.4% particulate < 4 μm

of radiation emitted by a layer of aerosol at temperature T is given by:

$$IR\downarrow \text{ (aerosol)} = \int_{\lambda_1}^{\lambda_2} \varepsilon(\lambda)\ B(\lambda,T)d\lambda \qquad \ldots 9.6$$

where ε (λ) is the emissivity of the layer, B (λ,T) the Planck distribution and d the depth of the layer. Since for aerosol at low levels the term $\int_{\lambda_1}^{\lambda_2} B\, d(\lambda)$, expressed as a fraction, f of black body radiation is almost independent of air temperature, T, Equation 9.6 may be rewritten:

$$IR\downarrow \text{ (aerosol)} = \frac{\int B\, d\lambda}{\sigma T^4} \quad \frac{\int \varepsilon(\lambda)\, d\lambda}{\int d\lambda} \quad \sigma T^4 \qquad \ldots 9.7$$

$$= f\bar{\varepsilon} \text{ (aerosol)}\ \sigma T^4$$

where integrals are from λ_1 to λ_2 and $\bar{\varepsilon}$ is the mean emissivity of aerosol averaged over the atmospheric window. $f\bar{\varepsilon}$ (aerosol) = IR$\downarrow$ (aerosol)/σT^4, is the effective emissivity of the atmosphere for particles. Values for f range from 0.31 to 0.33 in the temperature range 10 to 30^{o} C (Dalrymple and Unsworth, 1978). In order to evaluate Equation 9.7 it is necessary to determine $\varepsilon(\lambda)$ which from Kirchoff's Law is identical to the absorptivity, $a(\lambda)$. Neglecting scattering effects (which will likely produce some error in terms of the size distribution of particles and wavelength considered here), $\varepsilon(\lambda) = a(\lambda) \simeq 1 - t(\lambda)$, where $t(\lambda)$ is the transmissivity of an aerosol layer. Transmissivity of the aerosol layer is given by a derivation of Beer's Law:

$$t(\lambda) = \exp\ (-\ Ka\ (\lambda)\ Mz) \qquad \ldots 9.8$$

where Ka (λ) is the mass absorption coefficient (m^2kg^{-1}), M the mass concentration of aerosol (kg m^{-3}) and z the aerosol layer depth (m).

Full evaluation of Equation 9.8 is precluded by the lack of measurements of mass absorption coefficients of various types of

aerosol. Volz (1972) and Fischer (1975) identified mass absorption indices for various types of aerosol, and their mean value for urban aerosol collected over Mainz, Germany, was Ka (8 - 13 μm) ≃ 100 m^2 kg^{-1}. This value for Ka has been used as a starting point for the construction of a diagram relating the effective atmospheric emissivity for particles, $f\bar{\varepsilon}$ (aerosol), to particulate concentration through a fixed depth z (Figure 9.3). As illustrated in Chapter 6, the distribution of aerosol with height over Christchurch is quite variable, but most urban aerosol could be considered to be confined below 150 m. Dalrymple and Unsworth (1978) assumed a uniform distribution of aerosol through the layer (z) to make an estimate of the emissivity of aerosol. Similarly, a uniform concentration of aerosol to 150 m has been assumed in Figure 9.3.

Mean winter nocturnal values of the effective emissivity of the atmosphere for pollution, $f\bar{\varepsilon}$, in central Christchurch are in the order of 0.085 with a maximum ≃ 0.190. Equivalent particulate concentrations are ≃ 200 μg m^{-3} and 1000 μg m^{-3} respectively. Consideration of Figure 9.3 indicates that given the assumed urban mass absorption coefficient and apparent observed aerosol mixing depths and concentrations, calculated aerosol emissivity falls well short of providing all of the apparent pollution effective emissivity. There are several possible sources of this discrepancy, some relating to computational and measurement error and some to possible extra radiation sources. These will be examined in turn.

Errors in application of the aerosol transmissivity equation

There is no reason to question the theoretical basis of Equation 9.8. However, the derivation of terms for its application in Christchurch may well be in error. Since the technique for deriving values of Ka for different types of aerosol is very specialized,

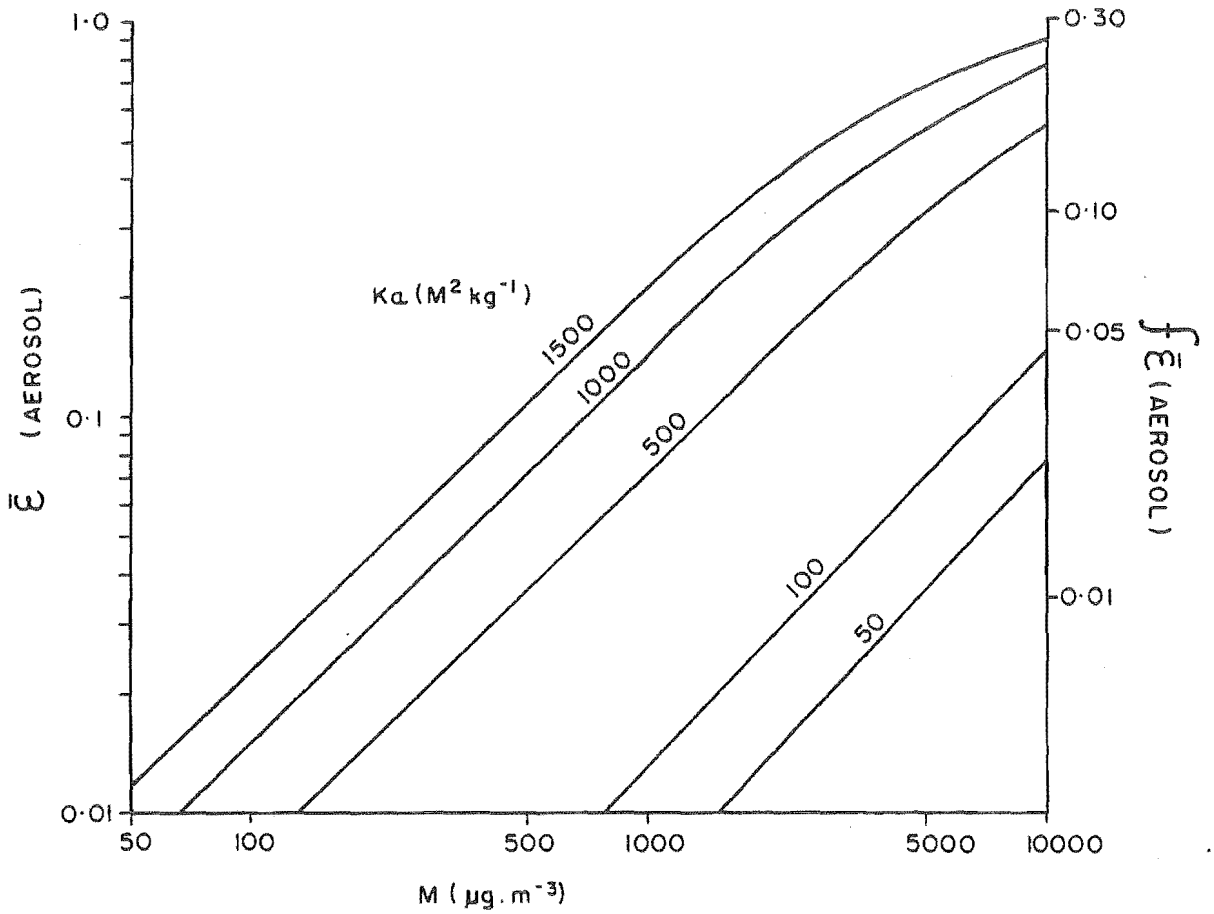

FIGURE 9.3 Dependence of the Mean Emissivity, $\bar{\varepsilon}$, of Aerosol in the Atmospheric Window and of the Effective Emissivity, $f\bar{\varepsilon}$, of the Atmosphere for Particles, on the Mass Absorption Coefficient, Ka, and on Aerosol Mass Concentration, M. Depth of Aerosol layer z is 150 m.

it has not been possible to even approximate a value for Christchurch, so the value for aerosol over Mainz, Germany (Fischer, 1975) has been accepted. Mass absorption indices for certain radiation wavelengths are determined in part by the interference of the beam by various mineral constituents and by other physical properties of the aerosol including its mass and area. The high proportion of very large particulate matter in Christchurch aerosol (Table 9.9) suggests that Ka would be high, but unfortunately Volz (1972) and Fischer (1975) do not publish the size distribution of their aerosol. The exact nature of Ka for Christchurch aerosol must therefore remain uncertain.

Mass concentrations (M) and aerosol depth (z) for input to Equation 9.8 may also be in error. The OECD Filter soiling method used to determine smoke concentrations in this study is known to be size selective and to exclude particulate matter > 5.0 μm and < 0.3 μm. As can be seen from Table 9.9, much of Christchurch particulate matter would therefore escape detection, a substantial portion of that undetected being radiatively active in the infra-red. In addition, other aerosols not able to be detected by the filter soiling method because of colour may be present in large quantities in the Christchurch atmosphere (pers. comm. D. Pullen, Air Pollution Section, Department of Health). This aerosol would include marine salts, greywacke rock dust (sodium aluminium silicate) and pollen. The latter two aerosols are unlikely to be important in winter, but may be important at both the urban and rural sites in summer. Dalrymple and Unsworth (1978) suggested that an important factor in determining γ at their rural site in England was pollen (typical diameter 30 μm) and spores (10 μm), since they had a high ratio of particle circumference to wavelength and were present in high concentrations (> 400 μg m^{-3}). Although no

measurements of pollen concentrations over Christchurch are available, pollen and spore levels are known to be very high at certain times of the year. Licitus (1953), in a study of pollen fall-out from the atmosphere at five New Zealand stations, found that Christchurch had easily the largest quantities of airborne pollen and spores. Marine aerosol, comprising mainly NaCl and KCl salts appear to be present throughout the year (D. Pullen, pers. comm.) but since absorption of this aerosol is weaker than typical urban aerosol (Fischer, 1975), its contribution to $f\bar{\varepsilon}$ would be slight.

Finally, while the assumption of an aerosol depth of 150 m appears generous in relation to pollution stratification indicated in Chapter 6, it is entirely possible that some pollution concentrations exist above the top of the kytoon pollution profile. Short of more detailed observations with a different pollution measurement system, this possibility cannot be verified.

Errors in instrumentation

Since the radiosonde used to derive the temperature and humidity profile was tested rigorously (Figure A.3) and individually calibrated before each flight, it is unlikely that this is a source of error in calculating IR↓. Radiometers used to measure IR↓ were carefully calibrated initially and were recalibrated during the measurement period, so no systematic trend in error from this source is likely. Considerable efforts were made to ensure that radiometer domes were kept free of dust and moisture. However, relatively small differences in absolute calibration could have significant effects on apparent $f\bar{\varepsilon}$ at both representative sites. Figure 8.3 indicated that IR↓ radiometers used in this study were possibly measuring too high, and this could result in some of the apparent $f\bar{\varepsilon}$, but two points suggest that

measurement error, if present, is relatively small. First, observed $f\bar{\varepsilon}$ is comparable with observations of previous investigators, including Dalrymple and Unsworth, who were working in a less polluted environment. Second, the intercept in the regression analysis (Figure 9.2) does not indicate an excess $\gamma(f\bar{\varepsilon})$ with zero measured pollution (which would point to an overestimate of measured IR↓). In fact the opposite is apparent for reasons outlined previously.

Errors in emissivity approximation method for predicting IR↓

A further possible cause of apparent $f\bar{\varepsilon}$ is underestimation of IR↓ by 'Finale'. As water vapour emission is dominant, it is important that the emissivities used are as accurate as possible. The use of the water vapour emissivities of Staley and Jurica (1970) in comparison with other published emissivities (Robinson, 1947; Elsasser and Culbertson, 1960), has the effect of reducing apparent emissivity for pollutants, $f\bar{\varepsilon}$. In addition the tables of Staley and Jurica are derived from careful and accurate laboratory procedures so their use appears appropriate. Variations of CO_2 and O_3 concentrations from those assumed could cause some small error and this will be discussed presently. IR↓ emission from above the tropopause has been ignored in 'Finale', but this would reduce $f\bar{\varepsilon}$ only by approximately 0.006.

The small errors in applying emissivities for homogeneous layers have already been discussed. Calculations of Sasamori (1968) using a similar method to that of 'Finale' to calculate atmospheric cooling, found good agreement with the results of Rodgers and Walshaw (1966), who used a much more rigorous computational method.

It is therefore unlikely that the observed discrepancy is due to significant errors in the computational scheme used here to predict IR↓.

Unidentified high cloud and anomalous water vapour effects

The presence of tenuous high cloud is one possible extra radiation source. Data in this study was carefully screened to ensure freedom of IR↓ from the influence of cloud, but the possibility of some unobserved cloud being present exists. Nevertheless, observed trends of $f\bar{\varepsilon}$ and γ diurnally and with particulate pollution, suggest that they are unlikely to be related to variations in cloud density.

Several field studies of vertical profiles of IR↓ (Houghton and Lee, 1974; Cox, 1973; Kano and Miyauchi, 1977) have ascribed discrepancies between observed and computed fluxes, particularly in the lower atmosphere, to the contribution of vapour pressure broadened continuum absorption (water dimer molecules). Bignell (1970) demonstrated that there was a component of water vapour absorption in the 11 μm - 20 μm region which increased markedly with partial water vapour pressure. Burroughs *et al.* (1971) further inferred the existence of water dimer molecules from physical measurement, but it has been only recently that direct observations of the species have been made using sophisticated techniques (Dyke *et al.*, 1977). The concentration of water dimer molecules is dependent on atmospheric vapour pressure and temperature. Since the formation of dimers depends on collisions between pairs of water molecules, their concentration is proportional to the square of water vapour pressure (Burroughs, 1979). A low binding energy between the two water molecules means that the concentration of dimers increases rapidly with temperature, a fact that Burroughs states gives them considerable potential importance over

tropical oceans.

A positive correlation between vapour pressure and $f\bar{\varepsilon}$ would therefore help explain part of the discrepancy. Correlation with winter nocturnal vapour pressure at both the urban and rural sites showed no significant relationship ($r = 0.06$, $r = 0.08$ respectively), indicating that at least for the temperatures and vapour pressures involved, effects of water dimers are minimal.

Gaseous emission

Table 9.10 outlines atmospheric gases known to absorb to varying degrees in the infra-red and all of which are present to some extent in an urban atmosphere. Except for water vapour, carbon dioxide and ozone, little is known about emission characteristics of individual gases and for some of them not much about their concentrations in urban areas.

Carbon dioxide and ozone were assigned mean concentrations in 'Finale' computations, although emissivity of CO_2 was varied by pressure scaling and accounting for its temperature dependence. Because it is relatively harmless, little is known of concentrations of CO_2 in urban areas. Since CO_2 is produced both by vegetation and industrial activity, urban-rural differences in its concentration may not be very large. An increase in the assumed mixing ratio of CO_2 in 'Finale' would decrease apparent $f\bar{\varepsilon}$, but effects would appear to be quite small. Staley and Jurica (1972, Figure 1) show that an increase in CO_2 mixing ratio throughout the profile from 0.5 g kg^{-1} to 0.8 g kg^{-1} would increase effective atmospheric emissivity only by approximately 0.01. Similarly, an increase in assumed ozone optical depth would account for some $f\bar{\varepsilon}$ as it is a strong absorber in the atmospheric

TABLE 9.10 Gaseous Absorbers in the Infra-Red Showing Wave Length (μm) at the Centre of the Absorption Band. Underlined Values indicate strong absorption.

GAS	WAVE LENGTH NEAR BAND CENTRE (μM)
WATER VAPOUR	0.9, 1.1, <u>1.4</u>, <u>1.9</u>, <u>2.7</u>, 3.2, <u>6.3</u>, > <u>15.0</u>[1]
CARBON DIOXIDE	1.4, 1.6, <u>2.0</u>, <u>2.7</u>, <u>4.3</u>, 4.8, 5.2, <u>14.8</u>[1]
OZONE	< <u>0.35</u>, 0.6, <u>9.6</u>[1,3]
CARBON MONOXIDE	<u>4.67</u>[2]
METHANE	6.43, <u>7.66</u>[2]
NITROUS OXIDE	<u>4.5</u>[3]
SULFUR DIOXIDE	0.29, 7.43[3]

1. Handbook of Geophysics (1960)
2. Burch *et al.* (1962)
3. Leighton (1961)

window. Staley and Jurica (1972) state that natural variations in ozone optical path would account for a change in atmospheric emissivity of ± 0.02 only. Farkas (1978) has made the only detailed survey of surface ozone in the Christchurch area. During a four month summer period in 1978, the highest concentration of ozone recorded was 7.5 p.p.h.m., which would only increase atmospheric emissivity by about 0.001.

Other urban gaseous pollutants have absorption bands generally outside of the 'atmospheric window' and therefore, even in high concentrations, will have only limited effects on IR↓. Measurements of carbon monoxide throughout the winter of 1979 by the Air Pollution Section, Department of Health, showed very low levels of CO pollution in Christchurch, with a maximum observed hourly reading of 34 $\mu g\ m^{-3}$. Since its absorption band is in the very near infra-red, CO pollution over Christchurch is unlikely to be an important influence. Sulphur-dioxide is present in the Christchurch atmosphere in approximately the same concentrations as smoke particulate, but since it has only a weak absorption band in the infra-red is also unlikely to influence atmospheric emissivity to any great extent. Influence of methane and nitrous oxide on atmospheric emissivity in Christchurch is unknown, but believed very small.

Although the combined effect of gaseous constituents of the urban atmosphere would be to increase atmospheric emissivity, it would appear that any such increase would be less than 0.03.

REFORMULATION OF THE BRUTSAERT RELATION FOR URBAN CHRISTCHURCH

The foregoing analysis indicates that particulate matter, in probable association with relatively smaller contributions from gaseous emission and from above the tropopause (approximately 0.006 together), accounts for most of observed $f\bar{\varepsilon}$ over Christchurch. Therefore it seems possible to use urban smoke particulate in an adjustment to the Brutsaert relation to correct predicted atmospheric apparent emissivities (εa) over Christchurch both on an hourly (diurnal), and daily basis. Smoke particulate matter used in this way also acts as a surrogate for other urban pollutants which would be expected to show a similar hourly and daily variation.

From Table 9.6, it can be seen that nocturnal and daytime $f\bar{\varepsilon}$ is predicted by log near surface smoke to a reasonable degree of accuracy (r^2 - 66% and 78% respectively). With hourly pollution data available, an adjusted Brutsaert relation for Christchurch would be expressed simply as $\varepsilon a = 1.24\ (e_s/T_a)^{1/7} + f\bar{\varepsilon}$, where wintertime $f\bar{\varepsilon}$ is given by $f\bar{\varepsilon}$ (nocturnal) = 0.114 logS - 0.175 and $f\bar{\varepsilon}$ (daytime) = 0.106 logS - 0.023. Such an adjustment on an hourly basis will of course make no difference to the systematic prediction error that has been identified in the previous chapter, but is able to considerably improve prediction of εa for urban Christchurch. Figure 9.4 shows the substantial improvement to wintertime hourly predicted εa in central Christchurch. A summary of regression analysis for this and for stratified daytime and night-time data is given in Table 9.11. Performance of the Brutsaert relation is improved in every respect. The apparent negative relationship between observed and predicted εa (due to the phase similarity of temperature and air pollution described

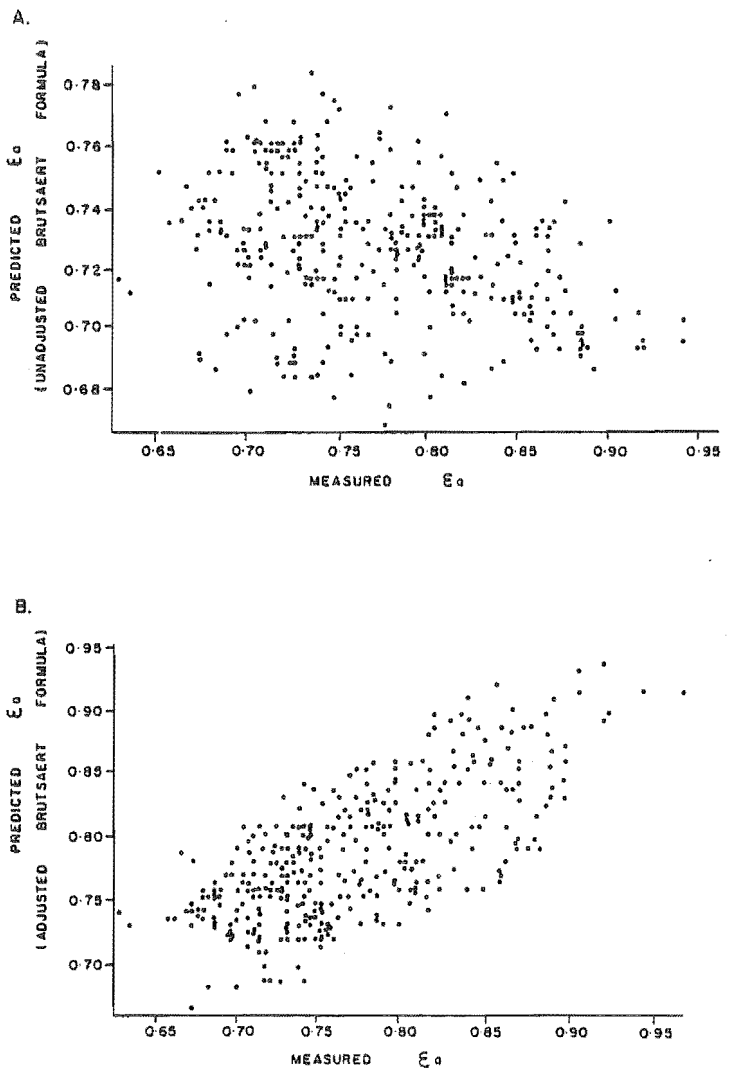

FIGURE 9.4 Prediction of Atmospheric Emissivity in Central Christchurch using, a) the Unadjusted, and b) The Pollution-adjusted Brutsaert Formula.

TABLE 9.11 Improvement to Brutsaert Relation at Urban Site with Emissivity Adjustment for Pollution

		UNADJUSTED BRUTSAERT EQUATION				ADJUSTED BRUTSAERT EQUATION			
DATA	NO. OBS	r coeff	r^2 (%)	V (%)	RATIO	r coeff	r^2 (%)	V (%)	RATIO
All winter (hourly)	339	-0.33	11	10.2	0.9671	0.69	48	5.9	1.007
Winter Daytime (hourly)	117	-0.36	13	10.6	0.9418	0.72	52	5.6	1.009
Winter Nightime (hourly)	222	-0.35	12	10.8	0.9873	0.63	40	6.2	1.004
Winter Daily	14	-0.23	5	6.0	0.9510	0.73	54	2.5	1.053

previously) is removed, and the explanation of measured by predicted εa improved markedly. In each case the coefficient of variation (v) is reduced by approximately 50%. From substantial and consistent underestimate of measured εa by 2 - 6%, the adjusted hourly relationships give a very slight overestimate of εa (< 1%) in each case.

Since predictive equations such as the Brutsaert relation were originally developed for use on a longer time scale than used here, the technique has also been applied on a daily basis to winter data. Using combined nocturnal and daytime data from Tables 9.2 and 9.3, regression analysis yields the equation $f\bar{\varepsilon}$ (winter daily) = 0.026 logS + 0.06. Although this relationship underestimates daytime $f\varepsilon$ and overestimates nightime $f\varepsilon$, on a daily basis errors would appear to even out. The improvement of this correction procedure to estimates of daily emissivity is also outlined in Table 9.11, and essentially parallels the improvement noted previously for hourly data. An apparent overestimate of adjusted daily εa (5%) appears related to the equal weighting afforded daytime data (when pollution levels are lower and wintertime hours are less).

To determine its suitability for reconstitution into the Christchurch energy balance model, it is necessary to consider the improvement to hourly IR↓ prediction following pollution adjustment of the Brutsaert relation. Figure 9.5 shows the diurnal variability of mean winter clear sky measured IR↓, and that predicted by the adjusted and unadjusted Brutsaert relation. The unadjusted form shows substantial underestimate (up to 35 Wm^{-2}), except for a short period of overestimate during late afternoon and early evening. Reasons for this systematic variation have been described previously. Pollution adjustment of the Brutsaert formula improves the relationship

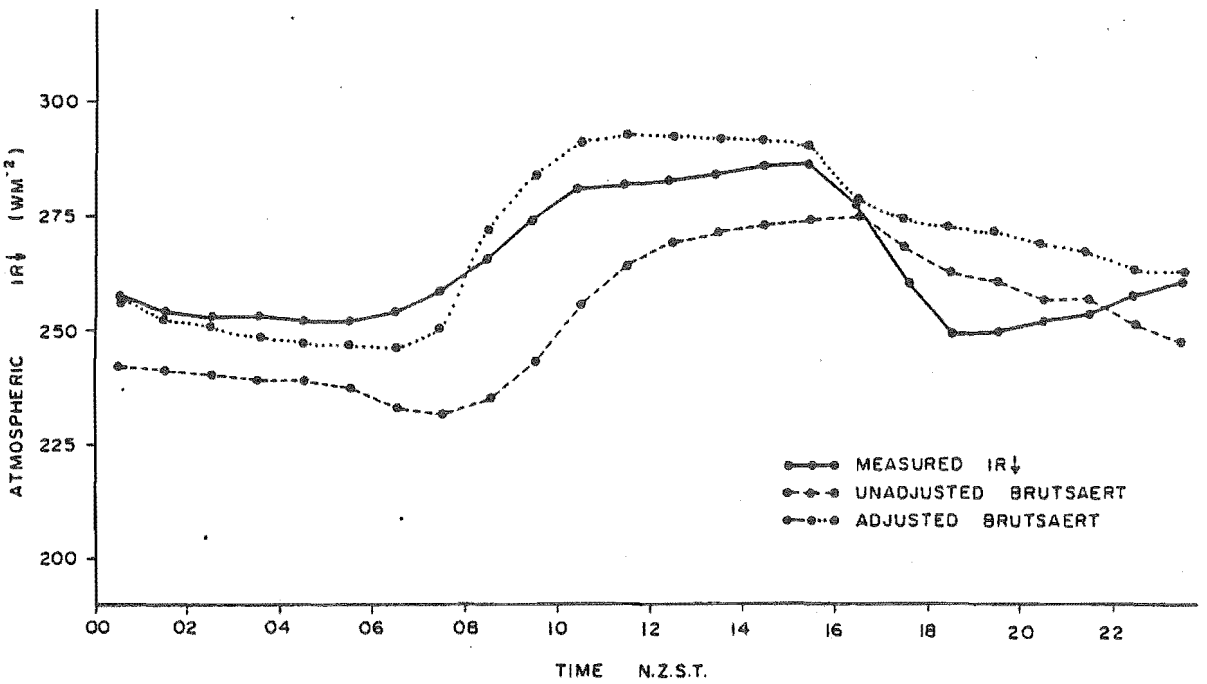

FIGURE 9.5 Prediction of the Diurnal Variability of Atmospheric Infra-red Radiation in Central Christchurch Using the Unadjusted and the Pollution-adjusted Brutsaert Formula.

markedly, particularly between 2300 and 1700 h when estimation error is within ± 10 Wm^{-2}. For a brief period in the evening, the systematic overestimate of IR↓ is exaggerated by the inclusion of extra atmospheric emissivity due to pollution. Despite the continuing problem of systematic variation, the adjusted Brutsaert formula appears a worthwhile inclusion in any revised energy balance model. The difficulty of all IR↓ prediction models utilising surface meteorological data as input is in accounting for the 'centre of gravity' of atmospheric emission. This is a problem requiring further investigation. Present alternatives are much too complicated for use in what is basically a simple energy balance model.

CONCLUSIONS

A prediction model for IR↓ over Christchurch utilising vertical atmospheric soundings has proven especially useful in establishing on a firmer basis those relationships tentatively suggested in previous chapters. Important points arising from this analysis may be summarised as follows:-

(i) The emissivity approximation model indicated that only a small proportion of observed urban-rural IR↓ difference in Christchurch could be accounted for by variations in temperature and water vapour.

(ii) Profile analysis at individual sites revealed a component of atmospheric emissivity which was unaccounted for by the temperature and water vapour profile. This excess emissivity was observed to be higher at the urban site and during daytime.

(iii) Careful consideration of possible causes of the excess emissivity at the urban site indicated the probable importance of particulate emission, and to a lesser degree emission by gaseous pollutants. Excess emissivity at the rural site appeared determined by direction of airflow in relation to the polluted Christchurch urban area.

(iv) An empirical relationship was derived between excess emissivity and smoke particulate pollution over Christchurch, and an emissivity adjustment incorporated into the Brutsaert formula for prediction of winter daytime and night-time $IR\downarrow$ on an hourly basis. The relationship was extended to the prediction of $IR\downarrow$ on a daily basis. In all cases adjustment of the Brutsaert formula resulted in significant improvements to prediction of $IR\downarrow$ in central Christchurch.

CHAPTER 10

CONCLUSION

SUMMARY OF CONCLUSIONS

This investigation of atmospheric infra-red radiation over Christchurch attempts a better understanding of the urban climate of the city in terms of causal mechanisms. Two major research objectives were identified; to relate spatial and temporal variations of IR↓ in Christchurch to peculiar attributes of the urban atmospheric environment, and to determine the relative role of IR↓ in contributing to the urban heat island. The following conclusions were reached.

An energy balance model, making no direct allowance for IR↓ variation across the city, predicted Christchurch's nocturnal heat island with a reasonable degree of success. This simulation of surface temperature variations over Christchurch indicated that surface characteristics such as roughness, thermal properties and evaporative fraction had a greater influence on heat island occurrence than atmospheric effects on radiation. In the model warmer temperatures over the city generate slightly higher IR↓, but this results largely from the influence of other factors and does not appear a direct cause of the urban heat island. There is a degree of feedback between IR↓ and ΔTu-r in the model however which is difficult to assess. All that can be reasonably stated is that urban IR↓ excess appears less important in determining ΔTu-r than other energy transfers related more especially to surface boundary parameters (sensible, substrate and evaporative heat flux).

A major contribution of the energy balance model was in identifying inadequacies of standard prediction methods for IR↓, particularly over urban areas, leading to a detailed investigation of potential causative mechanisms for this and for the observed urban excess IR↓ compared with outlying rural areas.

The surface heat island identified during the modelling exercise was confirmed by continuous observations at representative urban and rural sites. Heating and cooling curves from these sites indicated basic differences in site characteristics, particularly related to the thermal properties of surfaces. The urban temperature excess evident in the horizontal was also identified in the vertical, where warmer temperatures were consistently observed to approximately 300 m. The phenomenon was most marked at night and under low wind-speeds.

Atmospheric moisture regimes at the representative sites also showed distinctive urban and rural characteristics. The general pattern showed diurnal variations of absolute humidity, with a nocturnal urban moisture excess extending approximately 350 m into the boundary-layer, and a daytime urban deficit existing to about 200 m. The nocturnal moisture excess appeared to be related to enhanced vertical mixing, continued evapotranspiration and reduced dewfall over the city, while the daytime deficit appeared to be related to reduced urban evapotranspiration. In addition, large urban-rural differences in air quality were observed. Measurements at the rural site indicated levels of atmospheric contaminent at or below the level of detection, while levels above the urban site were shown to be high, especially during winter. Vertical soundings of pollution over the urban site clearly showed the low level character of atmospheric pollution over

Christchurch, determined largely by emission sources and the intensity and height of local inversions.

Detailed investigation of urban-rural differences in incoming radiation revealed an average clear weather depletion of SW↓ at the urban site of 3.5%, with individual daily depletions ranging above 10%. A very clear relationship with levels of atmospheric pollution was evident. The urban SW↓ deficit appeared to be more than compensated for by an urban excess IR↓ averaging 5.3% over the whole study period and substantially more during winter and at certain times of the day. Daytime excess IR↓ at the urban site was almost exactly balanced by the SW↓ deficit, but a continuation of urban IR↓ excess into night-time hours resulted in a net excess of incoming radiant energy at the urban site at that time. Overall urban radiant energy excess did not appear sufficient to account for the observed urban temperature excess, this supporting inferences made from the modelling exercise.

A simple statistical approach to the problem of establishing a relationship between atmospheric variables and IR↓ indicated that atmospheric pollution was the dominant influence on urban IR↓ excess, at least during the winter term, and that this effectively masks the influence of the other variables potentially responsible. In terms of the variability of IR↓ at individual sites however, atmospheric pollution had minimal influence compared to atmospheric temperature and moisture. A more theoretical approach using predictive equations for IR↓ indicated an anomalous urban atmospheric emissivity not accounted for by temperature and moisture variations, but explanation was limited by a systematic diurnal estimation error related to the centre of gravity of atmospheric emission. Neither of these approaches adequately accounted for mechanisms responsible for increased urban IR↓.

Use of a theoretically derived emissivity approximation model utilising atmospheric soundings showed that only a small proportion of the observed urban-rural IR↓ difference in Christchurch could be accounted for by variations in atmospheric temperature and water vapour across the city. Further detailed profile analysis at individual sites revealed a substantial component of atmospheric emissivity unaccounted for by profile characteristics. The excess emissivity was observed to be higher at the urban site and during daytime. Theoretical consideration of possible causes of the excess emissivity at the urban site indicated the probable importance of particulate emission, and to a lesser degree emission by gaseous pollutants.

On the basis of information gathered it is possible to formulate a mechanism to account for urban IR↓ excess observed over Christchurch. During daytime, part of SW↓ entering the polluted urban atmosphere is reflected off the polluted layer, part is absorbed and most is transmitted as direct or scattered diffuse beam solar radiation. For the Christchurch urban area, the proportion of attenuated SW↓ reflected or absorbed is unknown. Energy absorbed by the pollution layer is re-radiated in the infra-red in all directions, the downward component being the source of part of the observed urban IR↓ excess. Since the daytime increase in urban IR↓ balances the SW↓ deficit in this study, there must be an extra source of atmospheric energy. The source of this energy would appear to be the absorption, largely by particulate matter, of terrestrial infra-red radiation from warm city surfaces with subsequent counter-radiation. The continued presence

of pollutants at night, with resultant higher atmospheric emissivity, is responsible for the continuation of urban IR↓ excess into the evening. At night, in the absence of SW↓, the major source of excess IR↓ would again appear to be re-radiated terrestrial infra-red radiation. Also of some importance at night is the general warming and moistening of the urban boundary-layer due largely to the output of urban sensible heat and moisture. As evidenced by the presence of an elevated 'cross over' effect, some of the warming may be due to radiative effects of pollutants. Irrespective of the source of the urban warmth, profile analysis indicates most of the excess urban IR↓ is due to direct radiative effects of pollutants, particularly within the atmospheric window, where they are important absorbers of terrestrial infra-red radiation.

Overall evidence therefore suggests that urban excess IR↓ in Christchurch is largely a result of aerosol emission and partly an effect of the urban heat island (at least during night-time), but is unlikely a major cause of the urban heat island. Conclusions about the origins of excess urban IR↓ in this thesis therefore follow the hypotheses of Rouse *et al.* (1973) and Brazel and Osborne (1976) rather more closely than that of Oke and Fuggle (1972) who ascribed excess urban IR↓ to the heat island.

Suggestions for Further Research

During this study, a number of problems and areas for possible future research were recognized as follows.

The energy balance model used in this thesis is yet at an early stage of development and certain improvements can be incorporated

into a future model with varying degrees of difficulty. Arbitrary designation of surface evaporative fraction without accounting for dew fall was a significant factor in over prediction of C.B.D. temperatures in the model, and could be remedied relatively easily. Incorporation of the diurnal variation of artificial heat generation into the model would also be quite straightforward, while inclusion of advective effects would be more difficult. Of most significance in terms of this thesis would be incorporation of the emissivity correction factor to the Brutsaert equation for calculation of IR↓ over the Christchurch urban area. Simplest application would be on a daily basis (as with the Tr value in the energy balance model) using an average daily particulate value. With slightly more difficulty the emissivity correction factor could be employed on an hourly basis.

The most pressing need in any further investigation of IR↓ over Christchurch is a much more detailed understanding of the nature of Christchurch's urban particulate; particularly its size distribution, optical properties and actual concentration throughout the boundary-layer. It has been apparent that the method used for particulate detection in this study is not efficient for all types of matter, or for the particle size range so important in the infra-red. This would lead to substantial underestimates of total particulate and should be remedied in any future collection system. In addition, detailed analysis of the optical properties of Christchurch particulate matter should be undertaken, particularly to evaluate mass absorption indices. Observations of this type are essential for determining aerosol radiative effects in both the short-wave and infra-red portions of the energy spectrum, hence are necessary to further detail the mechanism for augmented urban IR↓ suggested above.

While the data base used in this study is extensive and will continue to be invaluable for further consideration of mechanisms of urban climate, it has been limited in some directions for various reasons. High summertime winds resulted in a lack of kytoon profiles for use in conjunction with surface radiation data in that season. Consequently, detailed profile analyses were confined almost exclusively to the winter case and future investigations could seek to rectify this problem. Since this study concentrated only on clear weather data where it could be assumed urban-rural differences are maximised, it could also be useful to consider the variation of incoming radiation under all weather types. Further, instrumental and operational considerations precluded the operation of more than two representative sites in this study where a number of stations scattered over different landuses would have been preferable. In addition, sensors mounted some distance away from the surface could be usefully employed to determine IR↓ and IR radiative divergence through the polluted urban boundary-layer, and may be a more appropriate data base than the near-surface measurements of IR↓ utilised here.

Finally, while the reasons for urban-rural variations in IR↓ have been identified here, the question of the relative effect of urban IR↓ excess on the urban heat island still awaits a definitive answer. Evidence presented here suggests that its role is relatively minor, but it is doubtful if a definitive answer can be provided satisfactorily by a purely modelling approach. The problem can probably only be fully answered with a full and detailed field program incorporating measurement of all relevant energy transfers at the interface and within the canopy and boundary-layer. As Geiger (1972)

states, "a real understanding of micrometeorological processes can only be achieved when all factors in the heat balance are followed quantitatively through their sphere of influence." The major contribution of this study has been in determining those attributes of the urban environment, both near the surface and in the boundary-layer responsible for the variation of $IR\downarrow$.

REFERENCES

ACKERMAN, T.P., LIOU, K. and LEOVY, C.B. 1976. Infrared radiative transfer in polluted atmospheres. J. App. Met. 15: 28-35.

ACTON, F.S. 1970. Numerical methods that work. Harper and Row, New York, 541 pp.

AHLQUIST, N.C. and CHARLSON, R.J. 1968. Measurement of the vertical and horizontal profile of aerosol concentration in urban air with the integrating nepholometer. Envir. Sci. Tech. 2(5): 363-366.

ANFOSSI, D., BACCI, P., and LONGHETTO, A. 1976. Forecasting of vertical temperature profiles in the atmosphere during nocturnal radiation inversions from air temperature trend at screen height. Quart. J. R. Met. Soc. 102: 173-180.

ANGELL, J.K., HOECKER, W.H., DICKSON, C.R. and PACK, D.H. 1973. Urban influence on a strong daytime airflow as determined from tetroon flights. J. Appl. Met. 12: 924-936.

ANGELL, J.K., PACK, D.H., DICKSON, C.R. and HOECKER, W.H., 1971. Urban influence on night-time airflow estimate from tetroon flights. J. App. Met. 10: 194-204.

ANGELL, J.K., PACK, D.H., HASS, W.A. and HOECKER, W.H. 1968. Tetroon flights over New York city. Weather 23: 184-191.

ANGSTRÖM, A. 1916. Über die Gegenstrahlung der Atmosphöre. Meteorol. Z. 33: 529-38.

ARNFIELD, A.J. 1979. Evaluation of empirical expressions for the estimation of hourly and daily totals of atmospheric longwave emission under all sky conditions. Quart. J. R. Met. Soc. 105: 1041-1052.

ATWATER, M.A. 1971a. The radiation budget for polluted layers of the urban environment. J. App. Met. 10(2): 205-214.

ATWATER, M.A. 1971b. Radiative effects of pollutants in the atmospheric boundary layer. J. Atmos. Sci. 28(8): 1367-1373.

ATWATER, M.A. 1975. Thermal Changes Induced by Urbanization and Pollutants. J. App. Met. 14:1061-1071.

AUER, A.H. and DIRKS, R.A. 1974. Contributions to an urban meteorological study: METROMEX. Bull. Amer. Met. Soc. 55: 106-110.

BACH, W. 1971. Variations of solar attenuation with height over an urbanised area. J. Air Poll. Cont. Assoc. 21: 621-628.

BACH, W. 1973. Solar radiation and atmospheric pollution. Arch. Met. Geophys. Biokl. Ser. B. 21: 67-75.

BACH, W. and PATTERSON, W. 1969. Heat budget studies in greater Cincinnati. A.A.G. Proceedings 1: 7-11.

BAUMGARTNER, A. 1956. Untersuchangen uber den Warme-und Wasserhousalt eines jungen Waldes. Ber. Deut. Wetterd. 5(8): 53.

BIGNELL, J.J. 1970. The water vapour infrared continuum. Quart. J. R. Met. Soc. 96: 390-403.

BORNSTEIN, R.D. 1968. Observations of the urban heat island effect in New York City. J. App. Met. 7(4): 575-582.

BORNSTEIN, R.D., LORENZEN, A. and JOHNSON, D.S. 1972. Recent observations of urban effects on winds and temperatures in and around New York City. In: Preprints of Conference on Urban Environment and Second Conference on Biomet. A.M.S.

BORNSTEIN, R.D. and OKE, T.R. 1979. Influence of pollution and urbanization on urban climates. In: Pfefflin, J.R. and Zeigler, E.N. (eds), Advances in Environmental Science and Engineering, Vol. 2. Gordon and Breach, New York.

BRAUN, R.C. and WILSON, M.J.G. 1961. The variation of atmospheric sulphur dioxide concentration with altitude. Int. J. Air Water Poll. 5(1): 1-13.

BRAZEL, A.J. and OSBORNE, R. 1976. Observations of atmospheric thermal radiation at Windsor, Ontario, Canada. Arch. Met. Geophys. Biokl., Ser. B. 28: 101-113.

BRIDGMAN, H.A. 1980. Diurnal variations in the spectrum of direct beam visible radiation at urban and rural locations at Milwaukee. Arch. Met. Geophys. Biokl., Ser. B. 28: 101-113.

BROOKS, C.E.P. 1952. Selective annotated bibliography on urban climate. Met. Abstracts and Bibliog. 3: 734-773.

BRUNT, D. 1932. Notes on radiation in the atmosphere, I. Quart. J. R. Met. Soc. 58: 389-418.

BRUNT, D. 1941. Physical and dynamical meteorology. Cambridge University Press, London. 428 pp.

BRUTSAERT, W. 1975. On a derivable formula for long-wave radiation from clear skies. Water Resour. Res. 11(5): 742-744.

BURCH, D. *et al.*, 1962. Infra-red Absorbtion by Carbon Dioxide, Water Vapour and Minor Atmosphere Constituents. AFCRL-62-698, 316 pp.

BURROUGHS, W.J. 1979. The water dimer: a meteorologically important molecular species. Weather 34(6): 233-237.

BURROUGHS, W.J., HARRIES, J.E., CHAMBERLAIN, J. and GEBBIE, H.A.G. 1971. Some effects of dimers of the water molecule in the atmosphere. In: Mesopheric Models and Related Experiments, pp. 292-298. D. Reidel Publishing Company.

CAMUFFO, D. 1979. Solar radiation at Rome, Italy, and its environment. Arch. Met. Geophys. Biokl, Ser. B. 27: 205-212.

CHANDLER, T.J. 1962a. London's urban climate. Geog. J. 127: 279-302.

CHANDLER, T.J. 1962b. Temperature and humidity traverses across London. Weather 17: 235-242.

CHANDLER, T.J. 1965. The Climate of London. Hutchinson and Co., London. 292 pp.

CHANDLER, T.J. 1967a. Night time temperatures in relation to Leicesters urban farm. Met. Mag. 96: 244-250.

CHANDLER, T.J. 1967b. Absolute and relative humidity in towns. Bull. Am. Meteorol. Soc. 48: 394-399.

CHANDLER, T.J. 1968. Selected Bibliography on Urban Climate. Compiled for W.M.O. Symposium on Urban Climates and Building Climatology. 289 pp.

CHRISTHURCH AIR POLLUTION ADVISORY COMMITTEE. 1966. Report. D.S.I.R. Information Series 55.

CLARKE, J.F. 1969. Nocturnal urban boundary layer over Cincinnati, Ohio. Man Wea. Rev. 97: 582-589.

CLARKE, J.F. 1972. Some effects of the urban structure on heat mortality. Environ. Res. 5: 76-84.

CLARKE, J.F. and PETERSON, J.T. 1973. An empirical model using eigenvalues to calculate the temporal and spatial variations of the St Louis heat island. J. App. Met. 12: 195-210.

COUNIHAN, J. 1975. Adiabatic atmospheric boundary layers: a review and analysis of data from the period 1880-1972. Atmos. Environ. 9: 871-905.

COX, S.K. 1973. Infa-red heating calculation with a water vapour pressure-broadened continuum. Quart. J. R. Met. Soc. 99: 669-679.

CRAIG, C.D. and LOWRY, W.P. 1972. Reflections on the urban albedo. In: Conference on Urban Environment and Second Conference on Biometeorology. Am. Met. Soc., Boston, pp. 159-164.

DALRYMPLE, G.J. and UNSWORTH, M.H. 1978. Longwave radiation at the ground: IV. Comparison of measurement and calculation of radiation from cloudless skies. Quart. J. R. Met. Soc. 104: 989-997.

DAVIDSON, B. 1967. A summary of the New York urban air pollution dynamics research program. J. Air Poll. Control. Assoc. 17: 154-158.

De BOER, H.J. 1966. Attenuation of solar radiation due to air pollution in Rotterdam and its surroundings. Koninkligk Nederlands Meteorologisch Instituten, Weterschappeligtz Rapport W.R. 66-1, 36 pp.

De LISLE, J.F. 1969. The climate and weather. In: Knox, G.A. (ed.), Natural History of Canterbury, pp. 68-70. Reed, Wellington.

De MARRAIS, G.A. 1961. Vertical temperature difference observed over an urban area. Bull. Am. Meteorol. Soc. 42: 548-554.

DIRKS, R.A. 1974. Urban atmosphere: warm dry envelope over St Louis. J. Geophys. Res. 79(24): 34-73.

DOZIER, J. and OUTCALT, S.I. 1979. An approach toward energy balance simulation over rugged terrain. Geog. Anal. 11: 65-82.

DRUMMOND, A.J. 1955. On the measurement of sky radiation. Arch. Met. Geophys. Biokl. Ser. B. 7: 413-436.

DUCHÊNE-MARULLAZ, P. 1976. Structure du vent an zone suburbaire rugosité et corrélation latérale. Report EN, CLI 76-2, Centre Scientif. Tech. Batiment, Nartes.

DUCKWORTH, F.S. and SANDBERG, J.S. 1954. The effect of cities on horizontal and vertical temperature gradients. Bull. Am. Met. Soc. 35(5): 198-207.

DURANT, R. 1979. An investigation into possible urban modification of rainfall over the Christchurch urban area. Unpub. M.A. thesis, Dept of Geog., Univ. Cant., N.Z.

DYKE, T.R., MACK, K.M. and MUENTER, J.S. 1977. The structure of the water dimer from molecular beam electric resonance spectroscopy. J. Chem. Phys. 66: 498-510.

EAST, J.J.C. 1968. Comparison of solar radiation in town and country. Cahiers de Geographie de Quebec 12(25): 81-89.

ELSASSER, W.M. 1942. Heat transfer by infrared radiation in the atmosphere. Harvard Meteorological Studies, No. 6.

ELSASSER, W.M. and CULBERTSON, M.F. 1960. Atmospheric radiation tables. Met. Mon. 4(23).

EMSLIE, J.H. 1964. The reduction of solar radiation by atmospheric pollution at Toronto, Canada. Canadian Dept of Tpt. Met. Branch Circular 4094, 3 pp.

ESTOQUE, M.A. 1961. A theoretical investigation of the sea breeze. Quart. J. R. Met. Soc. 87: 136-146.

ESTOQUE, M.A. 1963. A numerical model of the atmospheric boundary layer. J. Geophys. Res. 68: 1103-13.

ESTOQUE, M.A. and BHUMRALKAR, C.M. 1969. Flow over a localized heat source. Mon Weather Rev. 97: 850-859.

FARKAS, E. 1978. Surface ozone variations in Christchurch, January-April 1978 and motor vehicle air pollution. Proc. N.Z.M.S. Symposium on Meteorology and Transport, pp. 89-106.

FISCHER, K. 1975. Mass absorption indices of various types of meteorological aerosol particles in the infrared. Appl. Optics. 14: 2851-2856.

FITZHARRIS, B.B. 1974. Land-use change and the water balance - an example of an evaporation simulation model. J. Hydrol. (N.Z.) 13: 98-114.

FREDERICK, R.H. 1964. On the representativeness of surface wind observations using data from Nashville, Tennessee. Int. J. Air Water Poll. 8: 11-19.

FUGGLE, R.F. and OKE, T.R. 1970. Infra-red flux divergence and the urban heat island. In: Urban Climates. W.M.O. Tech. Note No. 108, pp. 70-78.

FUNK, J.P. 1959. Improved polythene shielded net radiometer. J. Sci. Instruments 36: 267-270.

FUNK, J.P. 1962a. A net radiometer designed for optimum sensitivity and a ribbon thermopile used in a miniaturized version. J. Geophys. Res. 67: 2753-2760.

FUNK, J.P. 1962b. A ribbon thermopile. J. Sci. Instruments 39: 32.

FUNK, J.T. 1962c. Transient responses of net radiometers. Arch. Met. Geophys. Biokl. Ser. B. 10: 228-231.

FUNK, J.T. 1962d. Measured radiative flux divergence near the ground at night. (Discussion of ....). Quart. J. R. Met. Soc. 88: 440-442.

GARNETT, A. and BACH, W. 1965. An estimation of the ratio of artificial heat generation to natural radiation heat in Sheffield. Mon. Weather Rev. 93: 383-385.

GARNIER, B.J. 1958. The Climate of New Zealand: a Geographical Survey. Edward Arnold, London. 191 pp.

GARSTANG, M., TYSON, P.D. and EMMITT, G.D. 1975. The structure of heat islands. Rev. Geophys. Space Phys. 13: 139-165.

GARTRELL, F.E. and CARPENTER, S.B. 1955. Aerial sampling by helicopter: a method for study of diffusion patterns. J. Met. 12: 215-19.

GEIGER, R. 1973. The Climate Near the Ground. 4th ed. Harvard Univ. Press. 611 pp.

GEORGII, H.W. 1970. The effects of air pollution on urban climates. Urban Climates, W.M.O. Tech. Note 108, pp. 214-237.

GIOVANARDI, A., GROSSE, E. and de FRAJA FRANGIPANE, E. 1959. Researches on the atmospheric pollution of the City of Milan. Int. Clean Air Conf. London. Paper IV, 38 pp.

GRAHAM, J.R. 1968. An analysis of turbulence statistics at Fort Wayne, Indiana. J. App. Met. 7: 90-93.

GRIFFITHS, J.F. and GRIFFITHS, M.J. 1974. Bibliography of the Urban Modification of the Atmospheric and Hydrologic Environment. NOAA Tech. Mem. EDS 21: U.S. Dept of Commerce.

HAGE, K.D. 1975. Urban-rural humidity differences. J. Appl. Met. 14: 1277-1283.

HANDBOOK OF GEOPHYSICS, 1980. The Macmillan Co., New York, 16-1 to 16-32.

HALSTEAD, M.H., RICKMAN, W., COVEY, W. and MERRYMAN, J.D. 1957. A preliminary report on the design of a computer for micrometeorology. J. Met. 14: 308-25.

HALTINER, G.J. and MARTIN, F.L. 1957. Dynamical and Physical Meteorology. McGraw-Hill, New York, 470 pp.

HAND, T.F. 1943. Transmission of total and the infra-red component of solar radiation through a smoky atmosphere. Bull. Am. Met. Soc. 24: 201-204.

HASTIE, W.J. 1979. A nocturnal energy balance model for Christchurch. Unpub. Hons. Research Project. 10 pp. Dept. Geog., Univ. Canterbury.

HEWSON, W.E. and GILL, G.C. 1943. Meteorological investigations in Columbia River Valley. U.S. Bur. Mines Bull. 453, Part II.

HOCKEY, J.B., OWENS, I.F. and TAPPER, N.J. 1980. Water Temperature in the Hurunui River. Report to Soil and Water Division, N.Z. Ministry of Works and Development, Christchurch. 44 pp.

HOCKEY, J.B., OWENS, I.F. and TAPPER, N.J. 1981. Empirical and theoretical models to isolate the influence of discharge on summer water temperatures in the Hurunui River. Appearing in N.Z. J. Hydrol.

HOUGHTON, S.T. and LEE, A.C.L. 1972. Atmospheric transmission in the 10-12 μm window. Nature 238: 117-118.

HOWARD, L. 1833. Climate of London deduced from meteorological observations. 3rd Ed. Harvey and Darton, London.

IDSO, S.B. 1972a. Radiation fluxes during a dust storm. Weather 27: 204-208.

IDSO, S.B. 1972b. Systematic deviations of clear sky atmospheric thermal radiation from predictions of empirical formulae. Quart. J. R. Met. Soc. 96: 765-767.

IDSO, S.B. 1974. Thermal blanketing: a case for aerosol-induced climatic alteration. Science 186: p. 318-320.

IDSO, S.B. 1975. Low-level aerosol effects on earth's surface energy balance. Tellus XXVII 3: 318-320.

IDSO, S.B., BAKER, D.G. and BLAD, B.L. 1969. Relations of radiation fluxes over natural surfaces. Quart. J. R. Met. Soc. 95: 244-257.

IDSO, S.B. and JACKSON, R.D. 1969. Thermal radiation from the atmosphere. J. Geophys. Res. 74(23): 5397-5403.

INGERSOLL, L., ZOBEL, R.J. and INGERSOLL, A.C. 1948. Heat conduction. McGraw Hill, New York. 278 pp.

JAMIESON, P.D. 1979. Relationships beteen net and solar radiation received by pastures at Lincoln, New Zealand. N.Z. J. Sci. 22: 245-247.

JAMIESON, P.D. and HEINE, R.W. 1976. Measurement of evaporation under north-east and north-west winds in Canterbury. Proc. Soil and Plant Water Symposium. Palmerston North, 25-27 May, 1976. pp. 180-185.

KALMA, J.D. 1974. An advective boundary-layer model applied to Sydney, Australia. Boundary-Layer Meteorol. 3(4): 351-61.

KANO, M. and MIYAUCHI, M. 1977. On the comparison between the observed vertical profiles of longwave radiative fluxes and the computed ones in Japan. Papers in Met. and Geophys. 28: 1-8.

KASTEN, F. 1966. A new table and approximation formula for the relative optical air mass. Archiv. Met. Geophys. Biokl. Ser. B. 14: 206-23.

KENNEDY, A.M. et al. 1974. Survey of fuel and energy usage in the Christchurch urban area, 1966-1973. Dept Chem. Eng., University of Canterbury. 71 pp.

KINGHAM, H.H. 1969. Surface temperature pattern in Christchurch at night. N.Z. Geographer 25: 16-22.

KLEIN, G.L. 1969. The Canadian low level sounding system. In: Proc. W.M.O. Technical Conference on Upper Air Instruments and Observations, Paris.

KONDRATYEV, K. Ya. 1969. Radiation in the atmosphere. Academic Press, London.

KOPEC, R.J. 1973. Daily spatial and secular variations of atmospheric humidity in a small city. J. App. Met. 12: 639-648.

KRATZER, P.A. 1956. The Climate of Cities (Translation). Friedr. Vieweg and Sohn, Brauraschweig. 221 pp.

KUNG, E.G., BRYSON, R.A. and LENSCHOW, P.D. 1964. Study of a continental surface albedo on the basis of flight measurements. Mon. Weather Rev. 92: 543-564.

LAMB, P.J. 1970. An Investigation of the Canterbury "Nor'wester". Unpubl. M.A. thesis, University of Canterbury. 95 pp.

LANDSBERG, H.E. 1956. The climate of towns. In: Thomas, W.C. (ed.), Mans Role in Changing the Face of the Earth, pp. 584-606. University of Chicago Press.

LANDSBERG, H.E. 1958. Physical climatology. Gray, Du Bois, Pa. 446 pp.

LANDSBERG, H.E. and MAISEL, T.N. 1972. Micro-meteorological observations in an area of urban growth. Bouundary Layer Met. 2: 365-370.

LEAHEY, D.M. 1969. An urban heat island model. Report TR-69-11, Dept of Meteorology and Oceanography, New York University. 70 pp.

LEAHEY, D.M. and FRIEND, J.P. 1971. A method for predicting the depth of the mixing layer over an urban heat island with application to New York city. J. App. Met. 10: 1162-1173.

LE DREW, E.F. 1975. The estimation of clear sky atmospheric emittance at high altitude. Arctic and Alpine Res. 7(3): 227-236.

LEIGHTON, P.A. 1961. Photochemistry of Air Pollution, Academic Press, N.Y. 300 pp.

LETTAU, H.H. 1951. Theory of surface-temperature and heat transfer oscillations near a level ground surface. Trans. Am. Geophys. Union 32: 189-200.

LETTAU, H.H. 1969. Note on the aerodynamic roughness-parameter estimation on the basis of roughness-element description. J. App. Met. 8: 828-832.

LETTAU, H.H. and DAVIDSON, B. (eds). 1957. Exploring the atmosphere's first mile. Vol. II. Pergamon Press Inc., New York.

LETTAU, H. and LETTAU, K. 1969. Short-wave radiation climatonomy. Tellus 21(3): 308-330.

LEVAGGI, D.A., SIU, W. and FIELDSTEIN, M. 1973. A new method for measuring average 24 hour nitrogen dioxide concentrations in the atmosphere. J. Air. Poll. Cont. Assoc. 23(1): 30-33.

LEWIS, J.E., OUTCALT, S.T. and PEASE, R.W. 1976. Urban surface thermal response associated with land use. Climatological Bull. 19.

LICITUS, R. 1953. Airborne pollen and spores sampled at five New Zealand stations, 1951-52. N.Z. J. Sci. Tech. Sec. B. 34: 289-316.

LOOSE, T. and BORNSTEIN, R.D. 1976. Observation of mesoscale effects on frontal movement through an urban area. Final Report, Vol. 4, Contract GA041886, San Jose State Univ., San Jose.

LOWRY, W.P. 1970. Weather and Life: an Introduction to Biometeorology. Academic Press, New York. 305 pp.

LOWRY, W.P. 1977. Empirical estimation of urban effects on climate: a problem analysis. J. App. Met. 16: 129-135.

LUDWIG, F.L. 1970. Determination of mixing depths for use with synoptic model. Proc. Symposium Multi-source Urban Diff. Models. U.S.E.P.A. Research Triangle Park 5: 33-5.

McBOYLE, G.R. 1970. Observations on the effect of a city's form and functions on temperature patterns. N.Z. Geog. 26(2); 145-150.

McCORMICK, R.A. and BAULCH, D.M. 1962. The variation with height of the dust loading over a city as determined by atmospheric turbidity. J. Air Poll. Cont. Assoc. 12: 492-496.

McCORMICK, R.A. and KURFIS, K.R. 1966. Vertical diffusion of aerosols over a city. Quart. J. R. Met. Soc. 92: 393-396.

MacDOWALL, J. 1954. A total radiation flux meter. Met. Res. Cttee, Air Ministry, London, M.R.P. No. 858.

MACHALEK, A. 1974. Das vertikale temperativprofil über der Stadt Wein. Wetter und Leben, Ser. B. 23: 127-136.

MALKUS, J.S. and STERN, M.E. 1953. The flow of a stable atmosphere over a heated island. Part I. J. Met. 10: 30-41.

MANES, A. GOLDREICH, Y., RINDSBERGER, M. and GUETTA, D. 1975. Inadvertent modification of the solar radiation climate at Bet-Dagan. In: Urban Effects on Local Climate at the Greater Tel Aviv Area. Israel Met. Service. Bet. Dagan.

MARKS, D. and DOZIER, J. 1979. A clear-sky longwave radiation model for remote alpine areas. Archiv. Met. Geophys. Biokl. Ser. B. 27: 159-187.

MATEER, C.L. 1961. Note on the effects of the weekly cycle of air pollution on solar radiation at Toronto. Int. J. Air Water Poll. 4: 52-57.

MILLER, E.L., JOHNSTON, R.E. and LOWRY, W.P. 1972. The case of the muddled meteoromodel. Preprints, A.M. Met. Soc. Conference on Urban Environment, Philadelphia, YY-82.

MITCHELL, J.M. 1961. The temperature of cities. Weatherwise 14: 224-229.

MITCHELL, J.J.M. 1962. The thermal climate of cities. In: Symposium: Air Over Cities, pp. 131-145. S.E.C. Tech. Rept A625.

MOLLER, F. 1951. Long wave radiation. In: Compedium of Meteorology, pp. 34-49. Am. Met. Soc., Boston.

MONTEITH, J.L. 1962. Attenuation of solar radiation: a climatological study. Quart. J. R. Met. Soc. 88: 508-521.

MONTEITH, J.L. 1966. Local differences in the attenuation of solar radiation over Britain. Quart. J. R. Met. Soc. 92(392): 254-262.

MONTEITH, J.L. and SZEICZ, G. 1961. The radiation balance of bare soil and vegetation. Quart. J. R. Met. Soc. 87: 159-170.

MORAN, R. 1971. Soil heat flow investigations in the Chilton Valley. Unpub. M.A. thesis, Dept of Geog., University of Canterbury.

MORGAN, D.L. and BASKETT, R.L. 1974. Comfort of man in the city: an energy balance model of man-environment coupling. Int. J. Biomet. 18: 184-198.

MORGAN, D.L., MYRUP, L. RODGERS, D. and BASKETT, R. 1977. Microclimate within an urban area. Annals Assoc. Am. Geog. 67: 55-65.

MORRIS, A.L., CALL, D.B. and McBETH, R.B. 1975. A small-tethered balloon sounding system. Bull. Am. Met. Soc. 56: 964-9.

MUNGER, H.P. 1951. Techniques for study of air pollution at low altitudes. Chem. Eng. Prog. 47: 436-439.

MUNN, R.E. 1966. Descriptive micrometeorology. Academic Press, New York. 245 pp.

MUNN, R.E. 1968. Annotated bibliography for air pollution meteorology. J. Air Poll. Cont. Assoc. 18: 449-453.

MUNN, R.E. and STEWART, I.M. 1967. The use of meteorological towers in urban air pollution programming. J. Air Poll. Cont. Assoc. 17: 98-101.

MYRUP, L.O. 1969. A numerical model of the urban heat island. J. App. Met. 8: 908-18.

MYRUP, L.O. 1970. A corrigendum. J. App. Met. 9: p. 541.

NEWBERRY, C.W. and EATON, K.J. 1974. Wind loading handbook. Build. Res. Estab. Report. Dept Envir. H.M.S.O., London, 74 pp.

NEW ZEALAND OFFICIAL YEAR BOOK. 1980. 85th Annual Edition. Dept of Statistics, Wellington. 1027 pp.

NISHIZAWA, T. and YAMASHITA, S. 1967. On attenuation of solar radiation in the large cities. Japanese Prog. in Climatology, Nov. 1967, pp. 66-70.

NKEMDIRIM, L.C. and LUNN, G.R. 1975. Pollutant concentration and stratification in urban heat island. Water, Air and Soil Pollution 4: 113-126.

NUNEZ, M. and OKE, T.R. 1977. The energy balance of an urban canyon. J. App. Met. 16: 11-19.

OKE, T.R. 1968. Some results of a pilot study of the urban climate in Montreal. Climat. Bull. (McGill Univ.) 5: 1-20.

OKE, T.R. 1973. City size and urban heat islands. Atm.Environment 7(8): 769-779.

OKE, T.R. 1974. Review of urban climatology 1968-1973. W.M.O. Tech. Note No. 134. Geneva, Switzerland.

OKE, T.R. 1976. The distinction between canopy and boundary layer urban heat islands. Atmosphere 14(4): 268-277.

OKE, T.R. 1978. Boundary layer climates. Methuen and Co. Ltd, London. 372 pp.

OKE, T.R. 1979. Review of urban climatology 1973-1976. W.M.O. Tech. Note 169.

OKE, T.R. and EAST, C. 1971. The urban boundary layer in Montreal. Boundary Layer Met. 1: 411-437.

OKE, T.R. and FUGGLE, R.F. 1972. Comparison of urban/rural counter and net radiation at night. Boundary-Layer Met. 2: 290-308.

OKE, T.R. and HANNELL, F.G. 1968. The form of the urban heat island in Hamilton, Canada. Proc. W.M.O. Symposium on Urban Climates. W.M.O. Tech. Note No. 108, pp. 113-126.

OKE, T.R. and MAXWELL, G.B. 1975. Urban heat island dynamics in Montreal and Vancouver. Atmos. Envir. 9: 191-200.

OKE, T.R., YAP, D. and FUGGLE, D.F. 1972. Determination of urban sensible heat fluxes. In: International Geography 1972, pp. 176-178. Univ. Toronto Press.

OLSSON, L.E., PERSSON, C., HÅGÅRD, A., OTTERSTEN, H., GRANAT, L. and TRÅGÅRDH, C. 1974. Measurements of meteorological parameters and air pollution spread over Stockholm, Sweden, by means of remote sensing and airborne instrumentation. W.M.O. 368: 545-556.

OUTCALT, S.I. 1971. A numerical surface climate simulator. Geog. Anal. 3: 379-393.

OUTCALT, S.I. 1972a. The development and application of a single digital surface climate simulator. J. App. Met. 11: 629-636.

OUTCALT, S.I. 1972b. A reconnaissance experiment in mapping and modelling the effect of land use on the urban thermal regime. Arch. Met. Geophys. Biokl. Ser. B. 20: 253-260.

OWENS, I.F. and TAPPER, N.J. The influence of meteorological factors on air pollution occurrence in Christchurch. N.Z. Geographical Society Proc. of the 9th Geog. Conference 1977. Dunedin, pp. 33-35.

OZONE DATA FOR THE WORLD - VOLS 19 and 20. Atmospheric Environment Service, Downsview, Ontario, Canada.

PAINTER, H.E. 1970. The tethered radiosande. Met. Mag. 99: 93-8.

PALTRIDGE, G.W. 1970. Day-time longwave radiation from the sky. Quart. J. R. Met. Soc. 96: 645-653.

PALTRIDGE, G.W. and PLATT, C.M.R. 1976. Radiative processes in meteorology and climatology. Elsevier Scientific Publishing Company, Amsterdam, 318 pp.

PATERSON, R.M. and PULLEN, D.R. 1979. Air pollution survey Christchurch: 1974-1976. Report to Canterbury Regional Planning Authority, 15 pp.

PENWARDEN, A.D. and WISE, A.F.E. 1975. Wind environment around buildings. Build. Res. Estab. Report, Dept Environ., H.M.S.O., London, 52 pp.

PERROUD, P., SYLVESTRE-BARON, M., PLEYBER, G., PERILHON, P., FAIURE-PIERRET, R., CLOSSON, A. and NICOTRA, C. 1973. Measurement of pollution in the lower layers of the atmosphere. In: Commisariat a l'Energie Atomique, 23 pp. Grenoble.

PETERSON, J.T. 1969. The climate of cities: a survey of recent literature. NAPCA Pub. No. AP-59. U.S. Govt Printing Office, Washington, D.C., 48 pp.

PETERSON, J.T. 1973. The climate of cities: a survey of recent literature. In: McBoyle, G. (ed.), Climate in Review, pp. 264-285. Houghton Mifflin, Boston.

PETERSON, J.T., FLOWERS, E.C. and RUDISILL, J.H. 1978. Urban-rural solar radiation and atmospheric turbidity measurement in the Los Angeles basin. J. App. Met. 17: 1595-1609.

POOLER, F. 1963. Airflow over a city in terrain of moderate relief. J. App. Met. 2: 446-456.

PRESTON-WHYTE, R.A. 1970. A spatial model of the urban heat island. J. App. Met. 9: 571-573.

PROBALD, F. 1972. Deviations in the heat balance, the basis of Budapest urban climate. In: Adams, W.P. and Helleiner, F.M. (eds), Int. Geog. 1972, pp. 184-186. University of Toronto Press.

PULLEN, D. 1970. Air pollution in the Christchurch metropolitan area. Proc. N.Z. Ecol. Soc. 17: 66-69.

PUESCHEL, R.F. and KUHN, P.M. 1975. Infra-red absorption of tropospheric aerosols: urban and rural aerosols of Phoenix, Arizona. J. Geophys. Res. 80(21): 2960-62.

RANDERSON, W. 1970. A comparison of the spectral distribution of solar radiation in a polluted and clear air mass. J. Air Poll. Cont. Assoc. 20: 546.

R.C.A. CORPORATION. 1978. R.C.A. Integrated Circuits. Somerville, N.J. 735 pp.

RECK, R.A. 1975. Influence of aerosol cloud height on the change in the atmospheric radiation balance due to aerosols. Atm. Envir. 9: 89-99.

ROBINSON, G.D. 1947. Notes on the measurement and estimation of atmospheric radiation: 1. Quart. J. R. Met. Soc. 73: 127-150.

ROBINSON, G.D. 1950. Notes on the measurement and estimation of atmospheric radiation: 2. Quart. J. R. Met. Soc. 76: 37-51.

ROBINSON, G.D. 1962. Absorption of solar radiation by atmospheric aerosol as revealed by measurements at the ground. Arch. Met. Geophys. Biokl. Ser. B. 12: 19-40.

ROBINSON, G.D. 1966. Some determinations of atmospheric absorption by measurement of solar radiation from aircraft and at the surface. Quart. J. R. Met. Soc. 92: 263-269.

ROBINSON, G.D. 1977. Book review - radiative processes in meteorology and climatology. Quart J. R. Met Soc. 103: 527-528.

RODGERS, C.D. 1967. The use of emissivity in atmospheric radiation calculations. Quart. J. R. Met. Soc. 93: 43-54.

RODGERS, C.D. and WALSHAW, C.D. 1966. The computation of infrared cooling rate in planetary atmospheres. Quart. J. R. Met. Soc. 92: 67-92.

ROUSE, W.R. and BELLO, R.L. 1979. Shortwave radiation balance in an urban aerosol layer. Atmosphere-Ocean 17: 157-168.

ROUSE, W.R. and McCUTCHEON, J. 1972. The diurnal behaviour of incoming solar and infra-red radiation in Hamilton, Canada. In: Adams, P.J. and Helleinin, S.R. (eds), Int. Geog. 1972, pp. 191-196. University of Toronto Press.

ROUSE, W.R., NOAD, D., McCUTCHEON, J. 1973. Radiation, temperatures and atmospheric emissivities in a polluted urban atmosphere at Hamilton, Ontario. J. App. Met. 12(5): 798-807.

RYAN, A.P. 1975. Low level airflow patterns in Christchurch on nights of high air pollution potential. In: Proceedings 1975 Clean Air Conference, pp. 403-420. Rotorua, New Zealand.

SANDERSON, M. 1974. A preliminary radiation climatology of Windsor, Ontario. McGill Univ. Climat. Bull. 16: 1-12.

SANDERSON, M., KUMANAN, I., TANGUAY, T. and SCHERTZER, W. 1973. Three aspects of the urban climate of Detroit-Windsor. J. App. Met. 12(6): 629-638.

SASAMORI, T. 1968. The radiative cooling calculation for application to general circulation experiments. J. App. Met. 7: 721-729.

SCORER, R.S. 1958. Natural aerodynamics. Pergamon Press, London. 312 pp.

SELLERS, W.D. 1969. A global climatic model based on the energy balance of the earth-atmosphere system. J. App. Met. 8: 392-400.

SELLERS, W.D. 1972. Physical climatology. Univ. of Chicago Press. 272 pp.

SEVELLE, F. 1969. The effect of the Southern Alps on the dynamic climatology of New Zealand. Unpublished M.A. Thesis, University of Canterbury, Christchurch.

SHAM, S. 1968. The analysis of temperatures in Christchurch in relation to the heat island effect. Unpub. M.Sc. Thesis, Dept of Geog., University of Canterbury, Christchurch.

SHEPPARD, P.A. 1958. The effect of pollution on radiation in the atmosphere. Int. J. Air Water Poll. 1: 31-47.

SHKLYAREVICH, D.B. 1974. Peculiarities of vertical wind distribution and temperature under city cond-tions. Meteorol. Hydrol. 7: 42-46.

S.M.I.C. 1971. Inadvertent Climate Modification. M.I.T. Press, 308 pp.

SPANGLER, T.C. and DIRKS, R.A. 1974. Meso-scale variations of the urban mixing height. Boundary-Layer Meteorol. 6: 423-441.

SPRIGG, W.A. and REIFSNYDER, 1972. Solar-radiation attenuation through the lowest 100 metres of an urban atmosphere. J. Geophys. Res. 77: 6499-6507.

STALEY, D.O. and JURICA, G.M. 1970. Flux emissivity tables for water vapour, carbon dioxide and ozone. J. App. Met. 9: 365-372.

STALEY, D.O. and JURICA, G.M. 1972. Effective atmospheric emissivity under clear skies. J. App. Met. 11:349-356.

STEWART, N.G., GALE, H.J. and CROOKS, R.N. 1958. The atmospheric diffusion of gases discharged from the chimney of the Harwell Reactor BEPO. Int. J. Air Poll. I: 87-102.

STURMAN, A.P. and TYSON, P.D. 1981. Sea breezes along the Canterbury coast in the vicinity of Christchurch, New Zealand. Journal of Climatology (Royal Met. Soc.). In press.

SUMMERS, P.W. 1965. An urban heat island model; its role in air pollution problems, with applications to Montreal. Proc. of the First Canadaian Conference on Micro-meteorology, Toronto. 22 pp.

SUNDBORG, A. 1951. Climatological studies in Uppsala, with special regard to the temperature conditions in the urban area. Geographica, No. 22, Universitet Geogrogiska Instituten, Uppsola, 111 pp.

SWINBANK, W.C. 1963. Longwave radiation from clear skies. Quart. J. R. Met. Soc. 89: 339-348.

TANNER, C.B. 1967. Basic instrumentation and measurements for plant environment and micrometeorology. University of Wisconsin, Dept of Soil Science Bulletin No. 6.

TAPPER, N.J. 1976. An investigation of incoming short and longwave radiation over Christchurch. Unpub. M.A. Thesis, University of Canterbury, Christchurch. 123 pp.

TAPPER, N.J. 1977. Christchurch solar radiation depletion in summer. Unpub. Report to Air Pollution Section, Dept of Health. 13 pp.

TAPPER, N.J. and OWENS, I.F. 1976. Radiation transfers in the Christchurch area with special reference to the effect of pollution. Proc. N.Z.M.S. Symposium on Meteorology and Air Pollution, pp. 113-121.

TAPPER, N.J. and STURMAN, A.P. 1980. A modified radiosonde for use in the boundary layer. N.Z. J. Sci. 23: 319-322.

TAPPER, N.J., TYSON, P.D., OWENS, I.F., HASTIE, W.J. 1981. Modelling the winter urban heat island over Christchurch, New Zealand. Appearing in J. App. Met.

TERJUNG, W.H. and LOUIE, S. 1973. Solar radiation and heat islands. Annals Assoc. Am. Geog. 63: 181-207.

TERZAGHI, K. 1952. Permafrost. J. Boston Soc. Civil Eng. 39: 319-68.

THOM, A.S. 1975. Momentum, mass and heat exchange of plant communities. In: Monteith, J.L. (ed.), Vegetation and the Atmosphere, Vol. 1, Principles, pp. 57-109. Academic Press, London.

TULLER, S.E. 1977. Some aspects of urban climate in Christchurch. N.Z. J. Geog. 63: 9-19.

TYSON, P.D., DU TOIT, W.J.F. and FUGGLE, R.F. 1972. Temperature structure above cities: Review and preliminary findings from the Johannesburg urban heat island project. Atmos. Environ. 6: 583-542.

TYSON, P.D., GARSTANG, M. and EMMITT, G.D. 1973. The structure of heat islands. Environmental Studies Occ. Paper No. 12, Dept Geog. Envir. Studies, University of the Witwatersrand, S.A.

U.S. COMMITTEE ON THE EXTENSION OF THE STANDARD ATMOSPHERE. 1962. U.S. Standard Atmosphere, 1962. U.S. Govt Printing Office, Washington, D.C. 278 pp.

VDOVIN, B.I. 1973. Peculiarities of temperature stratification in the lowest 1 km layer of air over Leningrad according to helicopter measurements. Trudy glavinia Geofriz. Observ. 293: 201-208.

VISKANTA, R. and DANIEL, R.A. 1980. Radiative effects of elevated pollutant layers on temperature structure and dispersion in an urban atmosphere. J. App. Met. 19: 64-70.

VOLZ, F.E. 1972. Infra-red absorption by atmospheric aerosol substances. J. Geophys. Res. 77: 1017-1031.

VON GOGH, 1979. A note on the Pretoria urban heat island of 15-16 June, 1977. South African Geog. J. 61: 29-34.

WAGNER, N.D. and YU, T. 1972. Heat island formation: a numerical experiment. Preprints, Am. Met. Soc. Conference on Urban Environment, Philadelphia, pp. 83-88.

WHITE, J.M., EATON, F.D. and AUER, A.H. 1978. The net radiation budget of the St Louis Metropolitan area. J. App. Met. 17: 593-599.

W.H.O. 1976a. Selected methods of measuring air pollutants. W.H.O. publ. No. 24, 1976. Geneva. 112 pp.

W.H.O. 1976b. Manual on Urban Air Quality Management. W.H.O. Regional Publications, European Series No. 1, Copenhagen. 200 pp.

WRIGHT, J.L. and LEMON, E.R. 1962. The energy budget at the earth's surface. Interim Report No. 62-7, 36 pp. N.Y. State College of Agriculture, Cornell University, N.Y.

YAMASHITA, S. 1970. An urban-climatological study of the attenuation of solar radiation by air pollution in Tokyo. Geog. Review Japan 43: 285-296.

YAMASHITA, S. 1973. Air pollution study from the measurement of solar radiation. Arch. Met. Geophys. Biokl. Series B. 21: 247-253.

YAMASHITA, S. 1979. Shortwave radiation climatology of the urban atmosphere in Toronto. Arch. Met. Geophys. Biokl. Ser. B. 27: 193-203.

YAP, D.H. 1973. Sensible heat fluxes measured in and near Vancouver. Unpublished Ph.D. Thesis, University British Columbia, 174 pp.

YAP, D. and OKE, T.R. 1974. Sensible heat fluxes over an urban area - Vancouver, B.C. J. App. Met. 13(8): 880-890.

APPENDIX I

PROGRAMME LISTING OF HEATIS

The Christchurch energy balance model HEATIS was written in Fortran IV for use on the University of Canterbury's Burroughs B6700 computer. Full documentation is provided in the comment cards at the beginning of the programme and wherever necessary in the body of the programme.

```
C     MAIN PRLGRAMME FOR HEATIS2                                        C  000:0000:5
C     HEATISLAND INPUT DESCRIPTION                                      C  000:0000:5
C     CARD 1(20A4)                                                      C  000:0000:5
C     ID = ANY IDENTIFICATION                                           C  000:0000:5
C     CARD 2(F10.2)                                                     C  000:0000:5
C     XLAT = LATITUDE                                                   C  000:0000:5
C     CARD 3(2I4,F10.1)                                                 C  000:0000:5
C     MO =MONTH                                                         C  000:0000:5
C     ID1 = DAY                                                         C  000:0000:5
C     P = PRESSURE(DEFAULT=1013.0)                                      C  000:0000:5
C     CARD 4(6F8.2,3F10.4,I2)                                           C  000:0000:5
C     TMAX = MAX. TEMP(C)                                               C  000:0000:5
C     TMIN = MIN. TEMP(C)                                               C  000:0000:5
C     ESCR = SCREEN VAP. PRESSURE(MB)                                   C  000:0000:5
C     ZA = HEIGHT OF REF. LEVEL(CM)                                     C  000:0000:5
C     TA = REF. LEVEL TEMP. (C)                                         C  000:0000:5
C     UA = REF. LEVEL WIND SPEED(CM/SEC)                                C  000:0000:5
C     QA = REF. LEVEL SPECIFIC HUMIDITY (GM/GM)                         C  000:0000:5
C     DT = TIME INTERVAL (SECS)                                         C  000:0000:5
C     DZ = DEPTH INTERVAL IN SOIL(CM)                                   C  000:0000:5
C     NODES = NO OF SOIL DEPTHS                                         C  000:0000:5
C     CARD GROUP 5 - I=1,NODES(3F10.4)                                  C  000:0000:5
C     POR(I) = POROSITY                                                 C  000:0000:5
C     CON(I) = CONDUCTIVITY                                             C  000:0000:5
C     TI(I) = INITIAL SOIL TEMPERATURE                                  C  000:0000:5
C     CARD GROUP 6 PROPERTIES VARYING OVER SPACE (7F10.4)               C  000:0000:5
C     BLOCK = BLOCK NUMBER                                              C  000:0000:5
C     IF BLOCK=0 (BLANK CARD) RETURN TO CARD 3 (NEW DATE)               C  000:0000:5
C     IF BLOCK>999(9 IN FIRST 6 COLS) RETURN TO CARD 1(NEW ID)          C  000:0000:5
C     Z0 = SURFACE ROUGHNESS(M)                                         C  000:0000:5
C     GD = SOIL THERMAL CAPACITY(CGS)                                   C  000:0000:5
C     ALBEDO = ALBEDO                                                   C  000:0000:5
C     ARHF = REL. HUMIDITY AS % WET FRACTION                            C  000:0000:5
C     GC = SOIL CONDUCTIVITY (CGS)                                      C  000:0000:5
C     TR =TRANSMISSIVITY                                                C  000:0000:5
C     CONVERSION TO W/M2                                                C  000:0000:5
                                                                  START OF SEGMENT 002
                                                          FORMAT SEGMENT IS 00CC LONG
      CW(X)=X*0.6975                                                    C  002:0000:6
      DIMENSION T(21),POR(21),CON(21),BAL(20),TGUS(20),ID(20),IDL(8)    C  002:0002:2
     1,TI(8)                                                            C  002:0002:2
C     READ MAIN HEADING                                                 C  002:0002:2
    5 READ(5,1001)(ID(K),K=1,20)                                        C  002:0002:2
                                                                  FIB IS 0006 LONG
 1001 FORMAT(20A4)                                                      C  002:000F:2
   10 READ(5,1002)XLAT                                                  C  002:000F:2
 1002 FORMAT(F10.2)                                                     C  002:0016:2
   20 READ(5,1003)MO,ID1,P                                              C  002:0016:2
C     MO = MONTH                                                        C  002:0021:2
C     ID1=DAY                                                           C  002:0021:2
C     P=PRESSURE                                                        C  002:0021:2
 1003 FORMAT(2I4,F10.1)                                                 C  002:0021:2
      CALL EPHEM(MO,ID1,DEC,R)                                          C  002:0021:2
      WRITE(6,50)(ID(K),K=1,20),XLAT                                    C  002:0024:2
                                                                  FIB IS 0006 LONG
   50 FORMAT(1H1,20X,"ENERGY BALANCE SIMULATION FOR: ",20A4/1H0,20X,"LAT C  002:0031:2
     1ITUDE  ",F8.2)                                                    C  002:0031:2
      WRITE(6,51)MO,ID1,DEC,R,P                                         C  002:0031:2
   51 FORMAT(1H0,"MONTH  ",I3/1H0,"DAY  ",I4/1H0,"SOLAR DECLINATION = "  C  002:003E:2
     1,F6.2/1H0,"RADIUS VECTOR = ",F8.4/1H0,"PRESSURE(MB) = ",F8.1)     C  002:003E:2
C    READ OTHER PARAMETERS NOT VARYING WITH BLOCK                       C  002:003E:2
      READ(5,59)TMAX,TMIN,ESCR,ZA,TA,UA,QA,DT,DZ,NODES                  C  002:003E:2
   59 FORMAT(6F8.2,3F10.4,I2)                                           C  002:0057:2
      DO 60 I=1,NODES                                                   C  002:0057:2
   60 READ(5,61)POR(I),CON(I),TI(I)                                     C  002:0058:3
   61 FORMAT(3F10.4)                                                    C  002:0068:3
   30 READ(5,62)BLOCK,Z0,GD,ALBEDO,ARHF,GC,TR                           C  002:0068:3
   62 FORMAT(7F10.4)                                                    C  002:007B:2
      IBLOCK=INT(BLOCK)                                                 C  002:007B:2
      Z0=Z0*100.                                                        C  002:007C:2
C    PROCEED ACCORDING TO VALUE OF IBLOCK                               C  002:007D:4
C        IBLOCK=0 (BLANK CARD) = NEW DATE                               C  002:007D:4
```

```
C          IBLOCK GREATER THAN 999 = NEW LOCATION                                C 002:007D:4
      IF(IBLOCK.EQ.0)GO TO 20                                                    C 002:007D:4
      IF(IBLOCK.GT.999)GO TO 5                                                   C 002:007E:5
      WRITE(6,52)IBLOCK,TMAX,TMIN,ESCR,ALBEDO,Z0,TR                              C 002:0080:2
      WRITE(6,53)ZA,UA,QA,TA                                                     C 002:0090:2
   52 FORMAT(1H1,10X,"BLOCK NO: ",I6/1H ,10X,9(1H=)/1HO,"MAX.TEMP.(C) =          C 002:0098:2
     1 ",F6.1,"  MIN.TEMP.(C) = ",F6.1/1HO,"VAPOUR PRESS.(MB) = ",F6.1/1       C 002:0095:2
     2HO,"ALBEDO = ",F6.4/1HO,"SURFACE ROUGHNESS(CM) =",F6.1/1HO,"TRANSM        C 002:0098:2
     3ISSIVITY = ",F6.4)                                                        C 002:009B:2
   53 FORMAT(1HO,"HEIGHT OF REFERENCE LEVEL(CM) =",F10.2/1HO,"REFERENCE          C 002:009B:2
     1 WIND SPEED(CM/SEC) =",F10.2/1HO,"REFERENCE SPECIFIC HUMIDITY(GM/GM       C 002:009B:2
     1) = ",F6.4/1HO,"REFERENCE LEVEL TEMP.(C) = ",F5.1)                        C 002:009B:2
      WRITE(6,58)ARHF,GD,GC,DT,DZ                                               C 002:009B:2
   58 FORMAT(    1HO,"RELATIVE HUMIDITY AS WET FRACTION (%) =",F6.2/1HO,       C 002:00A4:2
     1"SOIL DIFFUSIVITY(CM**2/SEC) =",F8.4/1HO,"SOIL CONDUCTIVITY(CAL/CM       C 002:00A6:2
     4/SEC/C) =",F8.4/1HO,"TIME INTERVAL(SECS) =",F8.1,"    DEPTH INTERV        C 002:00A8:2
     5AL IN SOIL(CM) =",F6.2)                                                   C 002:00A8:2
      WRITE(6,54)                                                               C 002:00AB:2
   54 FORMAT(1HO,10X,"INITIAL SOIL PROPERTIES"/1H ,10X,23(1H=)/1HO,4X,"D        C 002:00AC:2
     1EPTH  POROSITY  CONDUCTIVITY  TEMP(C)"/1H ,42(1H=))                        C 002:00AC:2
      IDZ=DZ                                                                    C 002:00AD:2
      DO 55 K=1,NODES                                                           C 002:00AE:0
      IID=IDZ*K-IDZ                                                             C 002:00B0:0
      IDD(K)=IID                                                                C 002:00B1:4
      T(K)=TI(K)                                                                C 002:00B4:0
      CON(K)=GC                                                                 C 002:00B5:4
      WRITE(6,56)IID,PUR(K),CON(K),T(K)                                         C 002:00C3:2
   55 CONTINUE                                                                  C 002:00C5:3
   56 FORMAT(1HO,I6,4X,F8.3,4X,F9.4,F8.1)                                       C 002:00C5:3
      WRITE(6,57)(IDD(J),J=1,NODES)                                             C 002:00D1:2
   57 FORMAT(1H ,42(1H=)/1HO,80X,'SOIL TEMPERATURES(C)'/1H ,' HOUR   SRN        C 002:00D1:2
     1     LWU      LWD      NLW       RN         S          H          LE     H/LE  C 002:00D1:2
     2AH       K =  ,I4,7I6)                                                    C 002:00D1:2
      WRITE(6,63)                                                               C 002:00D5:2
   63 FORMAT(1H ,125(1H=))                                                      C 002:00D6:2
      GK=CON(1)                                                                 C 002:00D6:3
      IL=(24.*3.6E3)/DT                                                         C 002:00DA:2
      IL2=2*IL+1                                                                C 002:00DB:0
      DO 1 I=1,IL2                                                              C 002:00DE:3
      IF(I.LE.IL)HR=(FLOAT(I-1)/FLOAT(IL))*24.                                  C 002:00E2:3
      IF(I.GT.IL)HR=(FLOAT(I-1)/FLOAT(IL))*24.-24.                              C 002:00E6:4
      CALL SOL(HR,XLAT,DEC,R,TR,ALBEDO,SRN)                                     C 002:00E7:4
      TS=T(2)                                                                   C 002:00E9:0
      TM10=TA-7.                                                                C 002:00EA:2
      TP10=TA+7.                                                                C 002:00EB:4
      TT=HR-9.                                                                  C 002:00ED:4
      IF(TT.LT.0.)TT=TT+24.                                                     C 002:00EF:5
      IF(TT.GT.24.)TT=TT-24.                                                    C 002:00F0:3
      TSCR=(TMAX+TMIN)/2.+0.5*(TMAX-TMIN)*SIN(.2618*TT)                         C 002:00F7:3
      CALL BALA(TP10,TA,TS,P,ZA,Z0,UA,SRN,GK,TSCR,ESCR,ARHF,QA,DZ,RN,           C 002:00FF:3
     1XLWU,XLWD,RNL,S,H,XLE,BAL1,AH)                                            C 002:0103:4
      CALL BALA(TM10,TA,TS,P,ZA,Z0,UA,SRN,GK,TSCR,ESCR,ARHF,QA,DZ,RN,           C 002:0108:4
     1XLWU,XLWD,RNL,S,H,XLE,BAL2,AH)                                            C 002:010F:5
      BAL(1)=BAL1                                                               C 002:0111:0
      BAL(2)=BAL2                                                               C 002:0112:1
      TGUS(1)=TP10                                                              C 002:0113:2
      TGUS(2)=TM10                                                              C 002:0114:3
      DO 3 K=3,20                                                               C 002:0116:3
      CALL SECANT(K,BAL,TGUS)                                                   C 002:0116:0
      TEQ=TGUS(K)                                                               C 002:011A:0
      T(1)=TEQ                                                                  C 002:011B:1
      CALL BALA(TEQ,TA,TS,P,ZA,Z0,UA,SRN,GK,TSCR,ESCR,ARHF,QA,DZ,RN,           C 002:0123:1
     1XLWU,XLWD,RNL,S,H,XLE,BALK,AH)                                            C 002:0127:2
      BAL(K)=BALK                                                               C 002:0129:0
      TEST=ABS(BAL(K))                                                          C 002:012A:5
      IF(TEST.LT.1.)GO TO 4                                                     C 002:012B:4
      IF(K.GT.18)GO TO 99                                                       C 002:012D:0
    3 CONTINUE                                                                  C 002:012F:1
   99 CONTINUE                                                                  C 002:012F:1
    4 CONTINUE                                                                  C 002:012F:1
      IF(I.LE.IL)GO TO 6                                                        C 002:0130:3
      Y=AINT(HR+0.5)                                                            C 002:0132:5
      YY=ABS(Y-HR)                                                              C 002:0134:1
      IF(YY.GT.0.01)GO TO 6                                                     C 002:0136:4
      SRN=CN(SRN)                                                               C 002:0138:1
      XLWU=CN(XLWU)                                                             C 002:0139:4
      XLWD=CN(XLWD)                                                             C
```

```
      RNL=CM(RNL)                                                       C  002:013B:1
      RN=CM(RN)                                                         C  002:013C:4
C     ADJUSTS SIGN OF HEAT BALANCE COMPONENTS                           C  002:013E:1
      S=CM(S)*(-1.)                                                     C  002:013E:1
      H=CM(H)*(-1.)                                                     C  002:0140:1
      XLE=CM(XLE)*(-1.)                                                 C  002:0142:1
      AH=CM(AH)                                                         C  002:0144:1
      B=H/XLE                                                           C  002:0145:4
      WRITE(6,7)HR,SRN,XLWU,XLWD,RNL,RN,S,H,XLE,B,AH,K,(T(J),J=1,NODES) C  002:0147:0
    7 FORMAT(1H ,F5.1,8F8.2,2F5.1,I6,8F6.1)                             C  002:0165:2
    6 CONTINUE                                                          C  002:0165:2
      CALL SOILD(NODES,DZ,DT,CON,POR,T,GU)                              C  002:0165:2
    1 CONTINUE                                                          C  002:016A:0
      GO TO 100                                                         C  002:016C:1
  100 CONTINUE                                                          C  002:016C:4
      WRITE(6,63)                                                       C  002:016C:4
      GO TO 30                                                          C  002:0170:2
  900 CONTINUE                                                          C  002:0170:5
      STOP                                                              C  002:0170:5
      END                                                               C  002:0171:4
                                                                  SEGMENT 002 IS 0199 LONG

                                                                  START OF SEGMENT 007
      SUBROUTINE TRIMP(NF,NL,A,B,C,D,T)                                 C  007:0000:0
      DIMENSION A(101),B(101),C(101),D(101)                             C  007:0000:0
      DIMENSION BETA(101),GAMMA(101),T(101)                             C  007:0000:0
      N1=NF+1                                                           C  007:0001:2
      N2=NF+2                                                           C  007:0002:5
      M1=NL-1                                                           C  007:0004:1
      M=NL-2                                                            C  007:0005:4
      GAMMA(NF)=T(NF)                                                   C  007:0008:3
      BETA(NF)=0.                                                       C  007:000A:0
      GAMMA(N1)=(D(N1)-A(N1)*T(NF))/B(N1)                               C  007:0011:5
      BETA(N1)=C(N1)/B(N1)                                              C  007:0016:2
      DO 1 L=N2,M1                                                      C  007:0018:0
      DENOM=B(L)-A(L)*BETA(L-1)                                         C  007:001D:0
      GAMMA(L)=(D(L)-A(L)*GAMMA(L-1))/DENOM                             C  007:0023:2
    1 BETA(L)=C(L)/DENOM                                                C  007:0026:5
      DO 2 K=1,M                                                        C  007:002A:0
      L=NL-K                                                            C  007:0026:3
    2 T(L)=GAMMA(L)-BETA(L)*T(L+1)                                      C  007:0033:0
      RETURN                                                            C  007:0033:3
      END                                                         SEGMENT 007 IS 003B LONG

                                                                  START OF SEGMENT 008
      SUBROUTINE SECANT(K,BAL,TGUS)                                     C  008:0000:0
      DIMENSION BAL(20),TGUS(20)                                        C  008:0000:0
      F1=BAL(K-2)                                                       C  008:0000:0
      F2=BAL(K-1)                                                       C  008:0002:1
      T1=TGUS(K-2)                                                      C  008:0004:2
      T2=TGUS(K-1)                                                      C  008:0006:3
      TGUS(K)=T2-(((T2-T1)*F2)/(F2-F1))                                 C  008:0008:4
      RETURN                                                            C  008:000D:1
      END                                                               C  008:000D:4
                                                                  SEGMENT 008 IS 0014 LONG

                                                                  START OF SEGMENT 009
      SUBROUTINE EPHEM(MO,IDAY,DEC,RV)                                  C  009:0000:0
      DIMENSION ID(12)                                                  C  009:0000:0
      DATA ID/0,31,59,90,120,151,181,212,243,273,304,334/               C  009:0000:0
      D=ID(MO)+IDAY                                                     C  009:0000:0
      DEC=SIN(((D-173.)*360./365.+90.)/57.3)*23.45                      C  009:0002:0
      RV=SIN(((D-186.)*360./365.+90.)/57.3)*0.01671+1.                  C  009:0009:4
      RETURN                                                            C  009:0011:0
      END                                                               C  009:0011:3
                                                                  SEGMENT 009 IS 001C LONG
```

```
                                                                        START OF SEGMENT 00A
      SUBROUTINE SOILD(N,DZ,DT,CON,POR,T,GD)                          C  00A:0000:0
C     READJUSTS TEMPERATURE PROFILE BY IMPLICIT SOLUTION OF           C  00A:0000:0
C     HEAT FLOW EQUATION(OUTCALT AND CARLSON,1975).                   C  00A:0000:0
C                                                                     C  00A:0000:0
C     INPUT--                                                         C  00A:0000:0
C     N NUMBER OF NODES                                               C  00A:0000:0
C     DZ NODE SPACING                                                 C  00A:0000:0
C     DT TIME STEP                                                    C  00A:0000:0
C     CON ARRAY OF THERMAL CONDUCTIVITY VALUES                        C  00A:0000:0
C     POR ARRAY OF POROSITY VALUES                                    C  00A:0000:0
C     T ARRAY OF TEMPERATURE VALUES AT BEGINNING OF TIME STEP         C  00A:0000:0
C                                                                     C  00A:0000:0
C     OUTPUT--                                                        C  00A:0000:0
C                                                                     C  00A:0000:0
C     T ARRAY OF TEMPERATURE VALUES AT END OF TIME STEP               C  00A:0000:0
C                                                                     C  00A:0000:0
      DIMENSION CON(N),POR(N),T(N),XW(21),XI(21),A(21),B(21),C(21),D(21)  C  00A:0000:0
      XLHF=80.                                                        C  00A:0000:0
      FO=DT/(DZ*DZ)                                                   C  00A:0000:5
      DO 400 L=1,N                                                    C  00A:0002:3
      IF(T(L).GE.273.16)GO TO 100                                     C  00A:0004:0
      TC=T(L)- 273.16                                                 C  00A:0007:4
      IF(TC.LT.-5.0)GO TO 200                                         C  00A:000B:4
      V1=TC-1.0                                                       C  00A:000C:5
      V2=TC+1.0                                                       C  00A:000E:0
      IF(V1.GT.0.)V1=0.                                               C  00A:000F:1
      X1=POR(L)*EXP(.5*V1)                                            C  00A:0011:0
      X2=POR(L)*EXP(.5*V2)                                            C  00A:0016:2
      HCAP=ABS((X2-X1)*(V2-V1))*XLHF                                  C  00A:001B:2
      XW(L)=POR(L)*EXP(.5*T(L))                                       C  00A:001E:1
      XI(L)=POR(L)-XW(L)                                              C  00A:0025:1
      GO TO 300                                                       C  00A:0029:1
  100 XW(L)=POR(L)                                                    C  00A:0029:4
      XI(L)=0.0                                                       C  00A:002C:3
      HCAP=0.0                                                        C  00A:002E:0
      GO TO 300                                                       C  00A:002E:4
  200 HCAP=0.0                                                        C  00A:002F:1
      XW(L)=0.0                                                       C  00A:002F:5
      XI(L)=POR(L)                                                    C  00A:0031:2
  300 CAP=0.46*(1.-POR(L))+XW(L)+.5*XI(L)+HCAP                        C  00A:0034:1
      CAP=CAP                                                         C  00A:0036:2
      F=FO*CON(L)/CAP                                                 C  00A:003E:1
      A(L)=-F                                                         C  00A:0041:1
      B(L)=1.+2.*F                                                    C  00A:0043:0
      C(L)=-F                                                         C  00A:0045:3
      D(L)=T(L)                                                       C  00A:0047:2
  400 CONTINUE                                                        C  00A:004A:1
      CALL TRIMP(1,N,A,B,C,D,T)                                       C  00A:004C:2
      RETURN                                                          C  00A:0051:1
      END                                                             C  00A:0051:4
                                                                        SEGMENT 00A IS 005E LONG
```

```
                                                                                START OF SEGMENT 00C
      SUBROUTINE BALA(T,TA,TS,P,ZA,ZO,UA,SRN,GK,TSCR,ESCR,ARHF,QA,DZ,RN,     C  00C:0000:0
     1XLHO,XLHD,RNL,S,H,XLE,BAL,AH)                                             C  00C:0000:0
C     COMPUTES ENERGY BALANCE COMPONENTS,BAL=RN+S+LE+H                          C  00C:0000:0
C     BAL=0 WHEN EQUATION BALANCED                                              C  00C:0000:0
C     STATEMENT FUNCTIONS                                                       C  00C:0000:0
      ZTK(TC)=TC+273.16                                                         C  00C:0000:0
      BB(TK)=5.14E-8*(TK**4)                                                    C  00C:0002:2
      AK2=0.1444                                                                C  00C:0005:2
      AC=0.24                                                                   C  00C:0007:3
C  THE NEXT STATEMENT IS INSERTED TO GIVE                                       C  00C:0009:3
C   A CONSTANT ARTIFICIAL HEAT VALUE                                            C  00C:0009:3
      AH=5.6                                                                    C  00C:0009:3
      IF(ARHF.GE.80.)AH=0                                                       C  00C:000B:3
      F=6.E4                                                                    C  00C:000E:3
      DRYADB=1.0E-4                                                             C  00C:0010:3
C     CONVERT TO DEGREES K                                                      C  00C:0010:3
      TAK=ZTK(TA)                                                               C  00C:0010:3
      TSK=ZTK(TS)                                                               C  00C:0012:0
      TSCRK=ZTK(TSCR)                                                           C  00C:0013:3
      TK=ZTK(T)                                                                 C  00C:0015:0
      ADEN=0.34838*((P*2.)/(TK*TAK))*1.E-3                                      C  00C:0016:3
      XLH=597.-0.6*T                                                            C  00C:001C:4
      XLHO=BB(TK)                                                               C  00C:0020:1
      XLHD=1.24*(ESCR/TSCRK)**.1428571*BB(TSCRK)                                C  00C:0021:4
      RNL=XLHL-XLHD                                                             C  00C:0027:5
      RN=SRN+RNL                                                                C  00C:0029:1
      S=(GK/DZ)*(TSK-TK)*F                                                      C  00C:002A:3
      WO=(3.74+2.64*(T/10)**2)*0.00001*ARHF                                     C  00C:0020:2
      XA=(XK2*UA*ADEN)/(ALOG(ZA/ZO)**2)                                         C  00C:0035:1
      RI=(G/TA)*((TA-T)*(ZA-ZO))/(UA*UA)                                        C  00C:0039:0
      IF(RI)15,10,5                                                             C  00C:003D:1
    5 A=XA*(1.-5.*RI)**2                                                        C  00C:003F:1
      GO TO 20                                                                  C  00C:0041:4
   15 X=XA*(1.-16.*RI)**0.75                                                    C  00C:0042:1
      GO TO 20                                                                  C  00C:0046:4
   10 X=XA                                                                      C  00C:0047:1
   20 XLE=X*(QA-QO)*XLH*F                                                       C  00C:0048:0
      H=X*(TA-T)*AC*F                                                           C  00C:004A:5
      BAL=S+H+XLE+RN+AH                                                         C  00C:004D:4
      RETURN                                                                    C  00C:0050:3
      END                                                                       C  00C:0051:0
                                                                              SEGMENT 00C IS 007A LONG
```

```
                                                                                START OF SEGMENT 00F
      SUBROUTINE SOL(HR,XLAT,DEC,R,TR,ALBEDO,SRN)                               C  00F:0000:0
      DEGRAD=3.1416/180.                                                        C  00F:0000:0
      RLAT=XLAT*DEGRAD                                                          C  00F:0003:0
      RDEC=DEC*DEGRAD                                                           C  00F:0004:2
      HRAD=(HR*15.-180.)*DEGRAD                                                 C  00F:0005:4
      COSZ=SIN(RLAT)*SIN(RDEC)+COS(RLAT)*COS(RDEC)*COS(HRAD)                    C  00F:0008:0
      IF(COSZ.LT.0.)GO TO 10                                                    C  00F:000E:1
      XM=1./(COSZ+0.15*(90.-ARCOS(COSZ)*(1./DEGRAD)+3.885)**(-1.253))           C  00F:000F:0
      SRN=(1.-ALBEDO)*(2000./R**2)*COSZ*TR**XM                                  C  00F:0019:1
      GO TO 20                                                                  C  00F:001E:1
   10 SRN=0.                                                                    C  00F:001E:4
   20 CONTINUE                                                                  C  00F:001F:2
      RETURN                                                                    C  00F:001F:2
      END                                                                       C  00F:001F:5
                                                                              SEGMENT 00F IS 002D LONG
```

APPENDIX II

EQUIPMENT CALIBRATION PROCEDURES AND RESULTS

The matching of sensors from respective sites was of prime importance in this study and was dealt with by detailed linear regression analysis. Absolute errors were minimised by using the output from sensors most recently calibrated by manufacturers as the independent variable (in this case sensors employed at the urban site). Two calibration periods were undertaken each over two week periods at the Lincoln Site, the relevant sensors set up in pairs, at the same height and exposure, and connected to the usual recording system. For each sensor the manufacturer's calibration coefficient was applied initially to give an energy value which was then used in regression analysis. Calibration was over hourly periods for the full day, excluding only partly cloudy days which are difficult to integrate accurately. Such an omission is acceptable as the present study concentrates on clear-sky conditions.

A summary of regression analysis for the two calibration periods is given in Table A.1 and A.2 (note that only one calibration has been performed for the net all-wave radiometers). For both calibrations correlation between all paired sensors is high, with IR↓ poorest at 97% of variance explained. In both calibrations IR↓ requires the most substantial adjustment, in this case upward for the Lincoln Site IR↓. It should be noted that the solar radiation and

TABLE A.1 Summary of Radiation Instrument Calibrations
October, 1978

SENSOR (X VARIABLE FIRST)	a COEFF.	b COEFF.	r^2	S.E.E. (Wm^{-2})	$\overline{X}$ (Wm^{-2})	% ACCURACY	NO. OBS
Lincoln IR↓ (CSIRO 6924)							
+	20.103	0.963	0.972	8.601	295	2.9	24
City IR↓ (CSIRO 6917)							
Lincoln SW↓ (K.Z. 742213)							
+	9.871	0.949	0.991	17.59	386	4.5	26
City SW↓ (K.Z. 721313)							
Lincoln Diffuse SW↓ (K.Z. 721340)							
+	-3.642	0.901	0.990	3.802	85	4.5	26
City Diffuse SW↓ (K.Z. 721340)							
Lincoln Cavity Temp (Diode No. 2)							
+	0.680	0.856	0.987	0.271°C	11.6°C	2.3	24
City Cavity Temp (Diode No. 1)							

TABLE A.2 Summary of Radiation Instrument Calibrations
November, 1979

SENSOR (X VARIABLE FIRST)	a COEFF.	b COEFF.	r^2	S.E.E. (Wm^{-2})	$\bar{X}$ (Wm^{-2})	% ACCURACY	NO. OBS
Lincoln IR↓ (CSIRO 6924)							
+	25.152	0.951	0.968	9.852	321	3.0	45
City IR↓ (CSIRO 6917)							
Lincoln SW↓ (K.Z. 742213)							
+	8.859	0.952	0.996	20.957	454	4.3	36
City SW↓ (K.Z. 721313)							
Lincoln Diffuse SW↓ (K.Z. 721340)							
+	-7.238	0.899	0.992	5.366	112	4.5	38
City Diffuse SW↓ (K.Z. 744065)							
Lincoln N.R. (CSIRO 6925)							
+	6.356	0.989	0.987	10.431	250	4.2	10
City N.R. (CSIRO 6918)							
Lincoln Cavity Temp (Diode No. 2)							
+	0.792	0.842	0.980	0.350°C	12.5°C	2.7	45
City Cavity Temp (Diode No. 1)							

black body cavity temperature input as used in Equations 3.1 and 3.2 for each of the infra-red sensors, is derived from the relevant rural or urban site instruments. Errors involved in the correction of this data are therefore included in the computation of IR↓, hence the lower correlation for that data. Also included in the relative error of all paired data is error resulting from the different modes of integration.

From the standard error of estimate (S.E.E.) in Tables A.1 and A.2, it is possible to estimate the accuracy of individual radiation parameters after adjustment in terms of the mean radiation during calibration. None of the data has an apparent accuracy worse than 4.5%, and in the case of IR↓ is 3% or better. This low calculated percentage error for IR↓ is related to the method of calculating the S.E.E. where S.E.E. $y.x = Sy\sqrt{1 - r^2}$, where S is the standard deviation of the y variable and r^2 is the coefficient of determination. The range of data in the independent variable therefore has an important bearing on the resultant S.E.E., with the naturally smaller range in IR↓ resulting in a lower calculated error. It should be remembered that the same S.E.E. represents a greater relative error at low energy values, an important point considering both calibrations were in spring and early summer. This problem may be partially corrected for in that this study concentrates on clear sky data (relatively higher energy values), whereas cloudy sky data was included in the calibration. Typical low values of IR↓ in Christchurch, $\sim$ 180 Wm^{-2} (Tapper 1976) suggest that this problem is minimal for IR↓, with calibration data indicating that at these values maximum errors would be only slightly greater than 5%.

Table A.3 shows calibration data for substrate heat flux plates used in this study. The two plates used in this study were compared with a standard (comprising three Middleton CN8 flux plates connected in series) loaned by D.S.I.R. Crop Research Division. All flux plates were buried in moist sand at a depth of 2 cm and the millivolt output monitored over a forty hour period. Accuracy of the two locally made flux plates was better than 2.5% over the calibration period, and the derived sensitivity values were subsequently used in this study.

TABLE A.3 Summary of Flux Plate Calibrations

SENSOR (X VARIABLE FIRST)	a COEFF.	b COEFF.	r^2	S.E.E. (MV)	$\overline{X}$ (MV)	% ACCURACY	NO. OBS
Standard + Flux Plate GN (Lincoln site)	-0.014	0.305	0.998	0.046	2.908	1.6	40
Standard + Flux Plate GS (City site)	0.056	0.243	0.994	0.070	2.908	2.4	40

Sensitivity - D.S.I.R. Standard (3 Middleton CN81N series) 0.0558 MV/Wm^{-2}

Derived Sensitivity Flux Plate GN 0.0171 MV/Wm^{-2}

Derived Sensitivity Flux Plate GS 0.0136 MV/Wm^{-2}

APPENDIX III

DETAILS OF THE INSTRUMENTED KYTOON SYSTEM

KYTOON LIFT CHARACTERISTICS

Figure A.1 outlines the aerostatic lift characteristics of the helium inflated Follmer 115 kytoon in terms of ambient air density in the U.S. Standard Atmosphere (1962). For heights of less than 5000 m the relationship can be expressed as,

$$M_L \simeq 1.056\ V_b \exp(-9.8 \times 10^{-5} z) - M_b \qquad \ldots\ldots \text{A.1}$$

where, M_L - total suspended mass able to be supported by aerostatic lift (kg), V_b - volume of kytoon (m^3), z - altitude above mean sea level (m), and M_b - mass of kytoon (1.5 kg).

The length of the tether line a kytoon can support in relation to the payload in aerostatic conditions is given by,

$$L = (M_L - M_p)/Ml \qquad \ldots\ldots \text{A.2}$$

where, M_p - mass of payload (gm), and Ml - mass of a unit length of tether line ($g\ m^{-1}$).

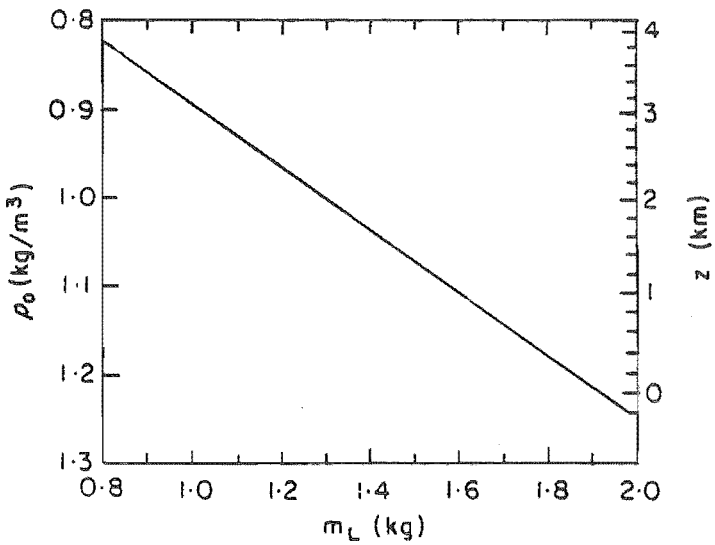

After Morris et al.

FIGURE A.1 Aerostatic Lift Characteristics of a Helium Inflated Follmer 115 Kytoon.

THE MODIFIED RADIOSONDE

In this study, a switching device independent of pressure was required for use with the Plessey radiosonde, so an integrated circuit timer (type 555) was chosen. The circuit (Figure A.2) was designed to allow the timer to connect each channel alternately to the transmitter, the duration of the signal for each channel (dependent on the values of R1, R2 and C2) being determined using equations given in R.C.A. (1978, p. 42-45). The timer is connected to the existing radiosonde circuitry so that it 'sinks' through the existing relay (i.e. it acts as a current sink rather than a source). With no output from the timer, the temperature sensor is connected to the transmitter, while when the timer activates the relay, the humidity sensor is connected.

Radiosonde Operation and Accuracy

The mode of operation of the system is quite straightforward, and that part of the operation involving the establishment of a reference signal and the evaluation of subsequent signals is identical to that followed by the New Zealand Meteorological Service (N.Z.M.S.) in their standard radiosonde flights. With practice the whole operation can be managed by one individual.

Before each flight a reference signal of the unmodulated frequency was used to check the transmitter stability. The modulated frequency associated with the screen level temperature and humidity was also noted. Temperature and humidity measurements were made simultaneously using an Assman aspirated psychrometer.

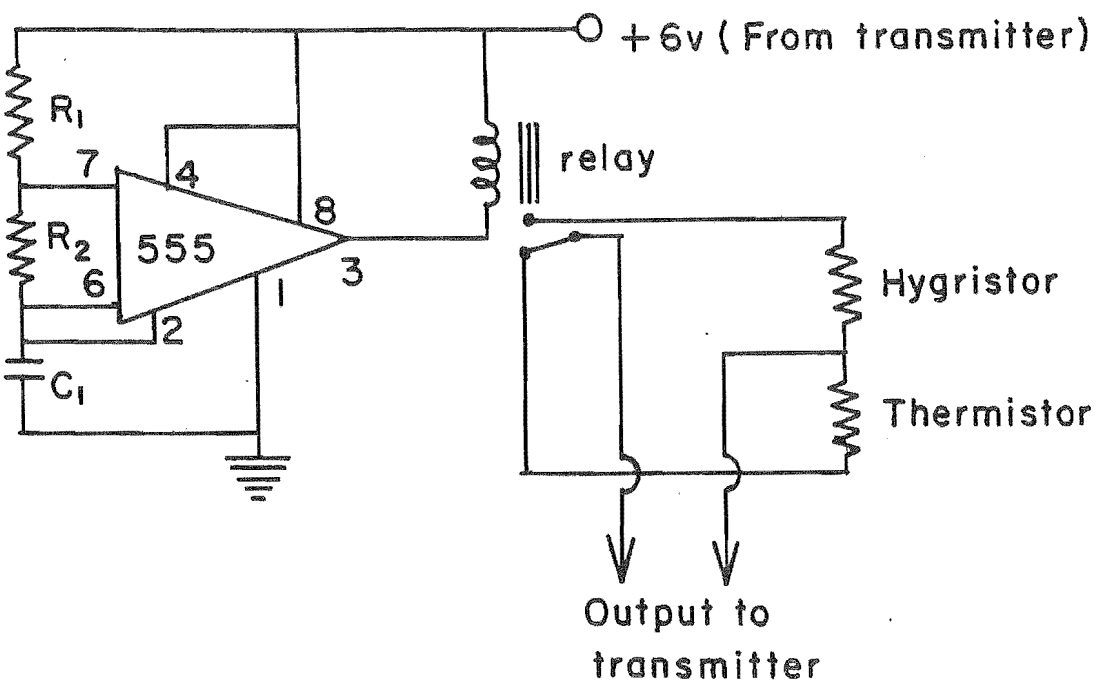

FIGURE A.2 Circuit Diagram of Radiosonde Timing Mechanism.

The kytoon and sensor package were then elevated to 100 m in 10 or 20 m increments, with the radiosonde temperature and humidity frequency readings taken at each stop. A fifteen second pause before reading has been found necessary for stability of signal. After 100 m the radiosonde was returned to the ground for a reference check and then returned to 100 m. Readings were then taken at 120, 140 ..... 200, 250, 300 ..... 500 m. On return to the ground, the unmodulated reference frequency and the modulated temperature and humidity frequency were once again checked. The entire operation was usually accomplished in 30 to 40 minutes.

Interpretation of the data involved establishing a baseline relationship between the initial actual temperature and humidity and their modulated frequencies, so that using the standard slide rules supplied by the radiosonde manufacturer, temperature and humidity could be derived from subsequent frequency values.

As the mode of operation of the boundary-layer radiosonde is almost identical to that of the N.Z.M.S., there is no reason to believe that it is any less effective. In the present study use of the radiosonde was confined largely to short, night-time flights under reasonably ventilated conditions, therefore errors through self-heating and radiant heating are thought to be minimal. If the radiosonde were to be used for prolonged periods of daytime operation, it would probably be necessary to use forced ventilation of the sensors.

In order to assess absolute errors in radiosonde temperature and humidity under adverse daytime and near unventilated conditions (windspeed < 1.5 m s^{-1}), a check was undertaken using the radiosonde operating continuously alongside an Assman psychrometer at ground level.

The equipment was operated for a three hour period, much longer than the typical period of continuous operation. Figure A.3 shows a mean temperature error of 0.2° C (maximum error 0.4° C) and a mean humidity error of 3% R.H. (maximum error 9% R.H.) over that time period. Actual humidity at the time of maximum humidity error (1530 h) appears anomalous in terms of the rest of the record, so the magnitude of this error may be smaller than suggested. For purposes of this project it is considered that radiosonde temperature and humidity are accurate to 0.5° C and 5% R.H. respectively.

DETERMINATION OF WINDSPEED ALOFT

To enable estimates of windspeed aloft a series of controlled experiments were made relating measured windspeed to kytoon aerodynamic lift. Lift in kilograms was determined using a Salter spring balance (10 kg maximum) attached at ground level to a loop in the tether line, while windspeed at kytoon level was independently determined using a tethered aerodynamically lifting anemometer (TALA, manufactured by Approach Fish, Inc. Va; U.S.A.) Accuracy of windspeed determined using this tethered kite anemometer is quoted by the manufacturer at better than 2%, and measurements are possible at any level to 300 m in windspeeds of up to 40 m s^{-1}. Apparent windspeed was controlled for by selecting a completely calm early morning and towing the kytoon and kite anemometer at varying speeds along the runway at R.N.Z.A.F. Base Wigram. As windspeed determination was to be made during normal radiosonde equipped flights, the light grade tether line and radiosonde package were fitted during the calibration procedure.

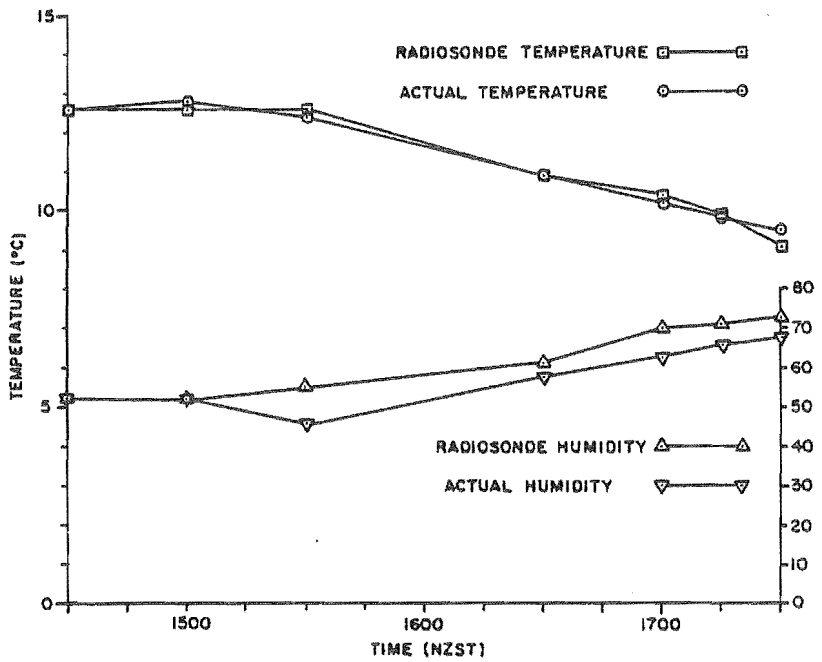

FIGURE A.3 Plot of Radiosonde Temperature and Humidity Errors.

Windspeeds from 0 to 13 m s^{-1} at heights varying between 100 and 300 m were simulated and the results are plotted in Figure A.4. The weight of relative lengths of suspended tether line has been accounted for in a corresponding addition to kytoon lift, included in Figure A.4. The relationship between measured windspeed and kytoon lift is reasonable, with the lack of systematic errors over this height range suggesting wind drag effects on line of varying lengths are minimal. This plot has therefore been used to determine windspeed from measured lift to an accuracy of approximately ± 1.0 m s^{-1}, an accuracy considered consistent with the importance of wind characteristics in this project.

DETERMINATION OF ATMOSPHERIC POLLUTION ALOFT

a) Smoke

Smoke was determined aloft by adapting the O.E.C.D. filter soiling method which is accepted as standard by the World Health Organisation (W.H.O., 1976a). Normally with this method, a metered volume of air is drawn through a standard filter paper on which the particulate is deposited. The soiling of the filter paper is determined using a reflectometer as described previously, and the measured reflectance is converted to an equivalent weight using a smoke evaluation chart. The final step involves dividing by the total air flow over the exposure period to determine a mean smoke concentration.

Figure A.5 is a diagram of the adapted apparatus used in this study for smoke determination. Plate A.1 shows the apparatus in its dismantled state. The apparatus consists of a 120 m length of plastic

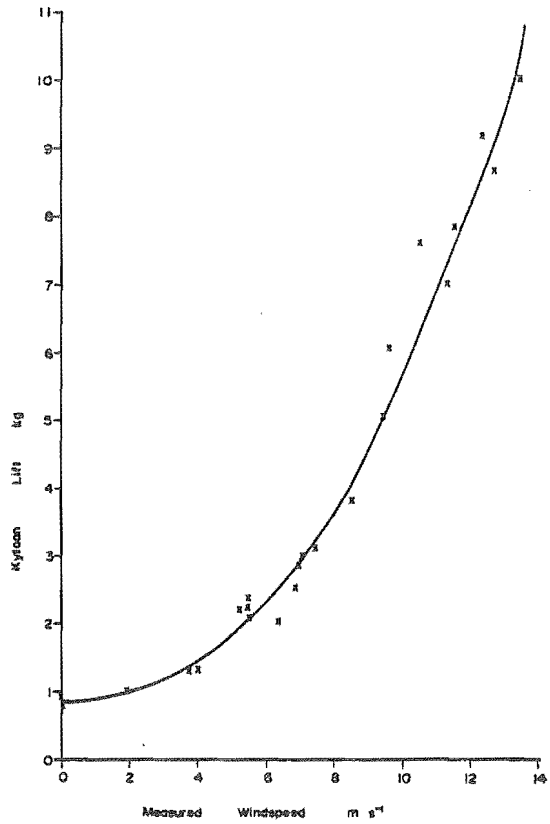

FIGURE A.4 Relationship Between Measured Windspeed and Kytoon Lift.

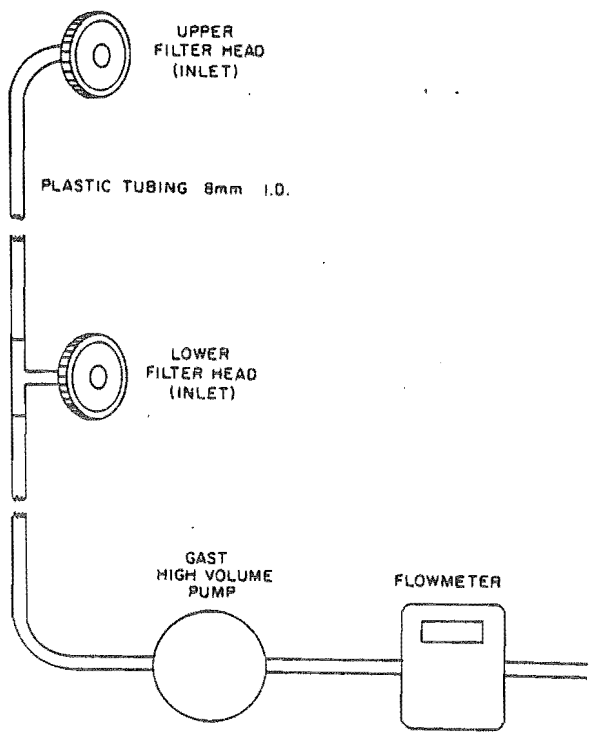

FIGURE A.5 Equipment for Determination of Smoke Particulate at Altitude (O.E.C.D. Method)

PLATE A.1 Kytoon Smoke Sampling Apparatus Showing Pump, Meter, Plastic Tubing and Filter Head.

tubing (8 mm internal diameter) with two filter head inlets, one at the top of the tubing and the other 30 m below the top. Frictional effects within the tubing confirmed the 8 mm I.D. tubing as the lightest grade able to be used without lowering air flow below that necessary to obtain smoke soiling of filters during a standard 30 minute flight. A Gast high volume air pump located at ground level provided air flow through the filters, while an accurate flow meter situated after the pump to remove vacuum effects, measured total air flow.

Plate A.2 shows a disassembled filter head, which for purposes of lightness was specially constructed of plastic and aluminium. The filter paper (Whatman No. 1 type) is clamped tightly between two aluminium discs, exposing a 25 mm diameter section of filter to the air flow. Gauze mesh prevents the filter from becoming distorted or ripped by air flow. As it was considered that there would be lower pollution concentrations at the level of the higher inlet, a flow restrictor was inserted behind the lower filter head to increase air flow at the higher level. This arrangement resulted in a 0.7 $m^3\ hr^{-1}$ flow through the upper filter and 0.34 $m^3\ hr^{-1}$ flow through the lower filter. After exposure, each filter paper was evaluated in the standard way and mean concentrations for each level determined.

Weight of the apparatus restricted the height of sampling of the upper filter to about 80 m (lower filter 50 m) in calm conditions, although sampling was possible above 100 m with wind assisted lift. Ground level smoke concentrations were obtained for each kytoon sampling period from the adjacent continuous paper tape sampler at the Central City Site. A 20 to 30 minute sampling period was usually sufficient to determine pollution concentrations, although longer periods were employed in low pollution conditions.

PLATE A.2 Dismantled Filter Head Showing Filter Paper and Retaining Rings.

b) Nitrogen Oxides

Nitrogen oxide (NO) and nitrogen dioxide (NO_2) concentrations aloft were determined with an adaptation of the Modified Saltzman Method, a procedure accepted as standard by the United States Environmental Protection Agency. The procedure is a wet chemical method and follows that originally described by Levaggi *et al.* (1973). In general terms, the method involves the use in the one sampling train of two solutions of an extremely efficient organic absorber of NO_2, triethanolamine. NO_2 in ambient air is absorbed into one of the solutions, while NO after being oxidised into NO_2 by potassium permanganate is absorbed into the other. Each solution is developed colorimetrically to determine quantities of NO_2 absorbed and a flow rate is applied to calculate pollutant concentrations over sampling periods.

Plate A.3 shows the nitrogen oxides sampling apparatus used in kytoon operations. The apparatus differs from the standard method in the use of lightweight plastic bubblers and tubing in place of glass, and the use of small self-contained pumps powered by rechargeable nickel cadmium batteries instead of mains powered aquarium pumps. The portable pumps used easily provide the necessary consistent flow rate of at least 200 cm^3 min^{-1} over the sampling period, which usually lasted approximately two hours. Flow rate data and consistency of flow for all pumps used is given in Figure A.6.

Accuracy of the standard method for nitrogen oxides determination is quoted as being excellent (Levaggi *et al.*, 1973). Use of plastic materials and an estimated average flow rate introduces unknown errors, but these are believed to be slight as ground level comparisons with oxides of nitrogen recorded continuously by the nearby

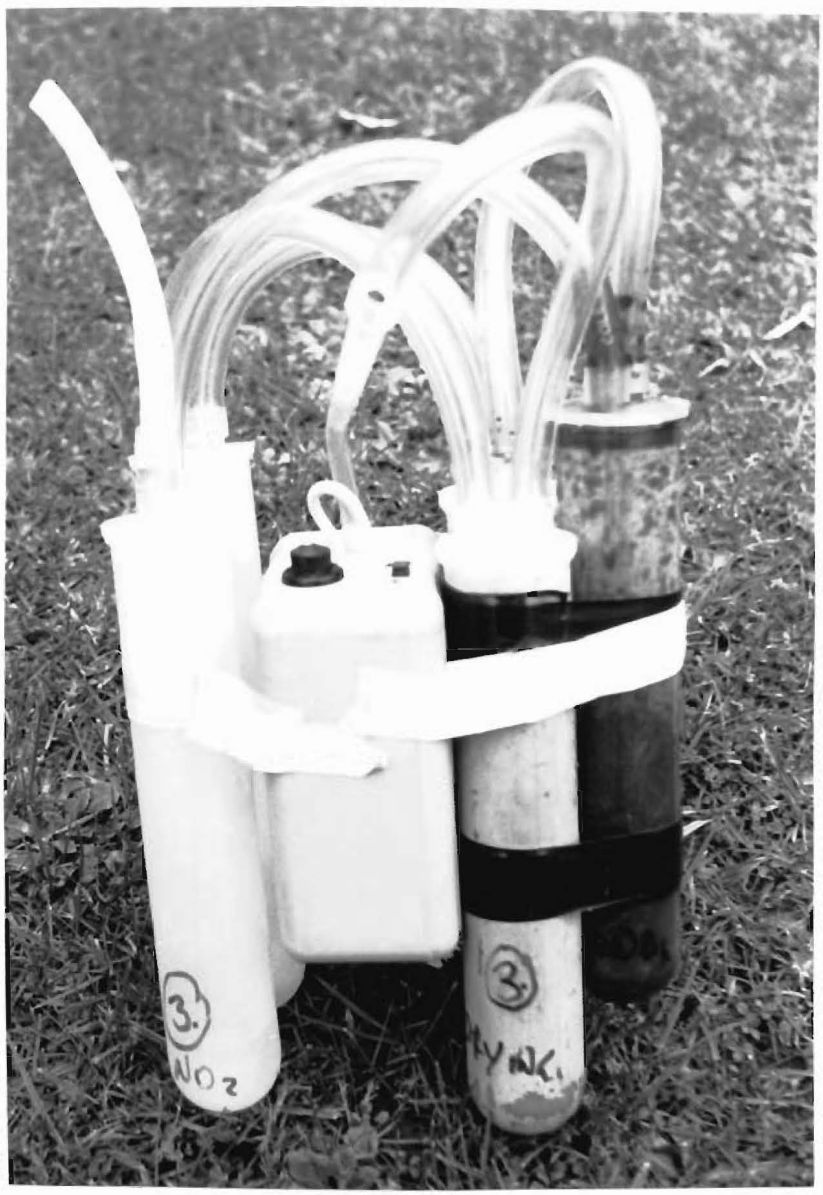

PLATE A.3 Kytoon Nitrogen Oxides Sampler Showing Portable Pump and Bubblers.

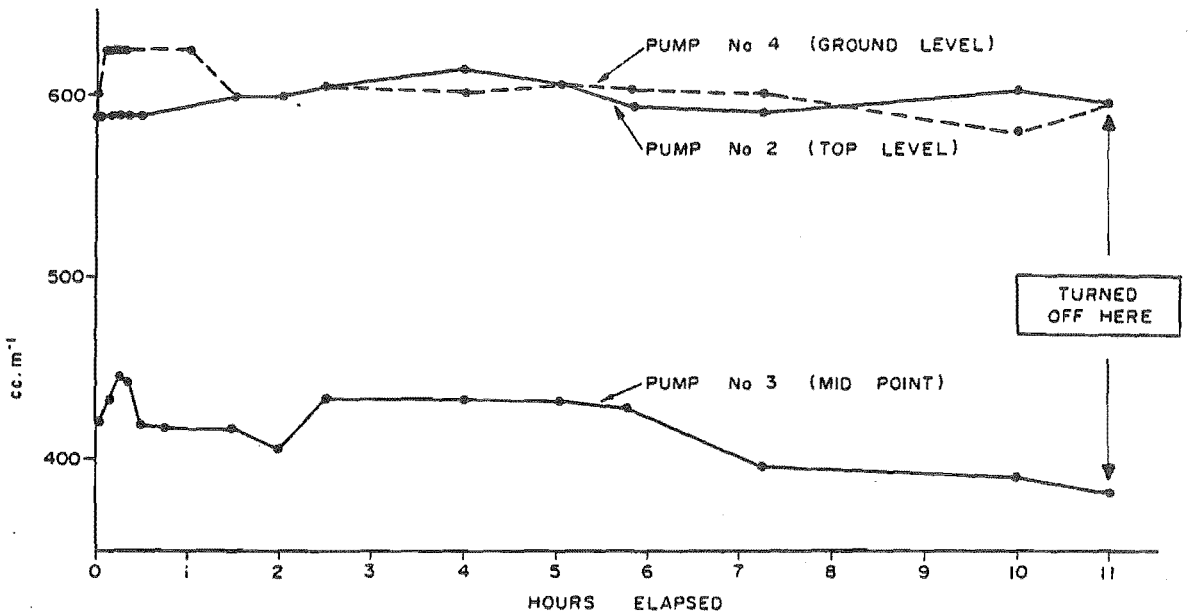

FIGURE A.6 Flow Rates for NOx Pumps on Kytoon-System (Under Load).

Monitor Laboratories Nitrogen Oxides Analyzer would suggest (Table A.4). Complete agreement is not expected because of the distance between the kytoon site and the caravan containing the surface based air pollution equipment (Figure 3.2).

Three complete sets of apparatus were used in the kytoon system; one at ground level, the second 75 m below the kytoon and the last immediately beneath the kytoon. Height placement of the upper sensor varied according to the prevailing windspeed, but generally ranged between 150 and 200 m above ground level.

TABLE A.4 Comparison of ground level total nitrogen oxides ($NO + NO_2$) measured with kytoon sampling apparatus and adjacent Monitor Laboratory Nitrogen Oxides Analyser.

SAMPLING TIME (HOURS)	KYTOON APPARATUS (NOX - $\mu g\ m^{-3}$)	M.L. ANALYSER (NOX - $\mu g\ m^{-3}$)	% DIFFERENCE (NOX - $\mu g\ m^{-3}$)
2.3	40	45	11
1.4	113	80	40
1.6	232	240	3
2.0	78	64	22
1.0	100	60	60
1.5	207	180	15
1.6	400	450	11
			$\bar{X}$ 24%

APPENDIX IV

STANDARDIZING OF PAIRED PROFILES

Profile correction procedures used in this study can be divided into two categories; one in which profiles were made after the time of maximum screen level temperature (evening flights) and the other where profiles were made after the time of minimum screen level temperature (morning flights). Most paired profiles are in the first category and the profiles of the second of the two paired flights (generally for the Lincoln Site) was adjusted to the time of the first flight in the manner described below.

Anfossi *et al.* (1976) developed a theoretical model to calculate the vertical distribution of air temperature in the lower atmosphere during clear, calm, night-time conditions (consistent with the present study). The model, using as input temperatures measured at screen level, is a modification of the classical Brunt model (Sutton, 1953) and differs from previous models in that an upper boundary variable in time and height is calculated above which temperature variations vanish. The starting time of the process is made to coincide with the time the diurnal thermal wave attains its maximum value, before decreasing. The temperature T (^{o}C) at a height (z) and time (t) after the maximum screen level temperature is given by:-

$$T(z,t) = T(0,0) - [T(0,0) - T(0,t)] \{\exp[-(z/z_i)^2] - z/z_i(\pi)^{\frac{1}{2}} \text{ erfc } \ldots$$

$$(z/z_i) + 0.278\ (z/z_i) \qquad \ldots\ldots \text{A.3}$$

with $z_i = 70(t)^{\frac{1}{2}}$ A.4

where, z_i is the depth of the layer influenced by surface radiation and erfc is an error function term. The constant used in the calculation of z_i is derived experimentally from measurements in the Po Valley by Anfossi *et al.* In the above formulation radiative heat exchange is assumed dominant and the thermal diffusion coefficient (included in the calculation of z_i) is kept constant with height and time. The method cannot account for water vapour condensation at ground level. Equations A.3 and A.4 have been integrated into the computer programme 'Tempro' which is included here. Anfossi *et al.* (1976) found good agreement between observed and predicted temperature profiles on the north Italian Plains, particularly when condensation did not occur at ground level. Despite its' inability to account for condensation (often observed during Christchurch flights), 'Tempro' appears to give reasonable predictions of temperature change aloft over Christchurch where consecutive measured profiles are available for comparison. Figure A.7 shows the measured and predicted temperature changes aloft for the evening of 7 July, 1979 at Lincoln. In this diagram the decrease of temperature at altitude with time predicted by the model has been applied to the measured profile using the 1530 h profile as a starting point. Since the predicted curve is defined by a parabolic cooling function it cannot replicate irregularities in the measured profile, nevertheless, there is reasonable agreement.

In the Christchurch application the method was applied retrospectively to allow correction of the second of the paired profiles to the time of the first. Since only short time differences were involved (approximately 1 hour) and profiles were evolving at a slower rate than indicated in Figure A.7 (most profiles were undertaken between

```
20 REM "TEMPPRO"  - VERTICAL TEMP PROFILES FROM MAX SCREEN
30 REM TEMP AND SUBSEQUENT SCREEN TEMP MEASUREMENTS
40 DIM T1(20),T2(20),T3(30)
50 REM DEFINE CONSTANTS:A1=.278393:A2=.230389:A3=.000972:A4=.078
100
60 REM ENTER LOCATION ETC:INPUT "ENTER LOCATION",L$:INPUT "ENTER
 DATE",D$
70 INPUT "ENTER MAX SCREEN TEMP(C)",T0:INPUT "ENTER TIME OF MAX
TEMP (HRS)",T4:N=1
80 INPUT "ENTER SUBSEQUENT TIMES(T1) AND SCREEN TEMPS(T2):T1=99T
O END",T1(N):IF T1(N)=99 THEN 100:INPUT T2(N)
90 N=N+1:GOTO 80
100 SELECT PRINT 215(80):PRINT HEX(0E),"TEMPERATURE PROFILES FOR
 ";L$:PRINT HEX(0E),"DATE ";D$:PRINT "MAX SCREEN TEMP=  ";T0;" C
 AT   ";T4;" HRS"
110 FOR I=1 TO N:PRINT HEX(0C),"TEMPERATURE PROFILE FOR ";T1(I);
" HRS":PRINT "SCREEN TEMPERATURE= ";T2(I);" C":PRINT "HEIGHT(M)
   TEMP(C)":FOR L=1 TO 20:PRINT "-";:NEXT L:PRINT
120 FOR J=1 TO 30:Z=J*10:Z1=70*(T1(I)-T4)^0.5:Z2=Z/Z1
125 E=1/(1+A1*Z2+A2*Z2^2+A3*Z2^3+A4*Z2^4)^4
130 T3(J)=T0-(T0-T2(I))*(EXP(-Z2^2)-(Z/Z1*SQR(#PI)*E)+.278*Z2)
140 PRINTUSING 150,Z,T3(J)
150 %  ###       +#####.##
160 NEXT J :FOR L=1 TO 20:PRINT "-";:NEXT L:PRINT :NEXT I
170 INPUT "MORE DATA(Y/N)",I$:IF I$="Y" THEN 60
180 END
```

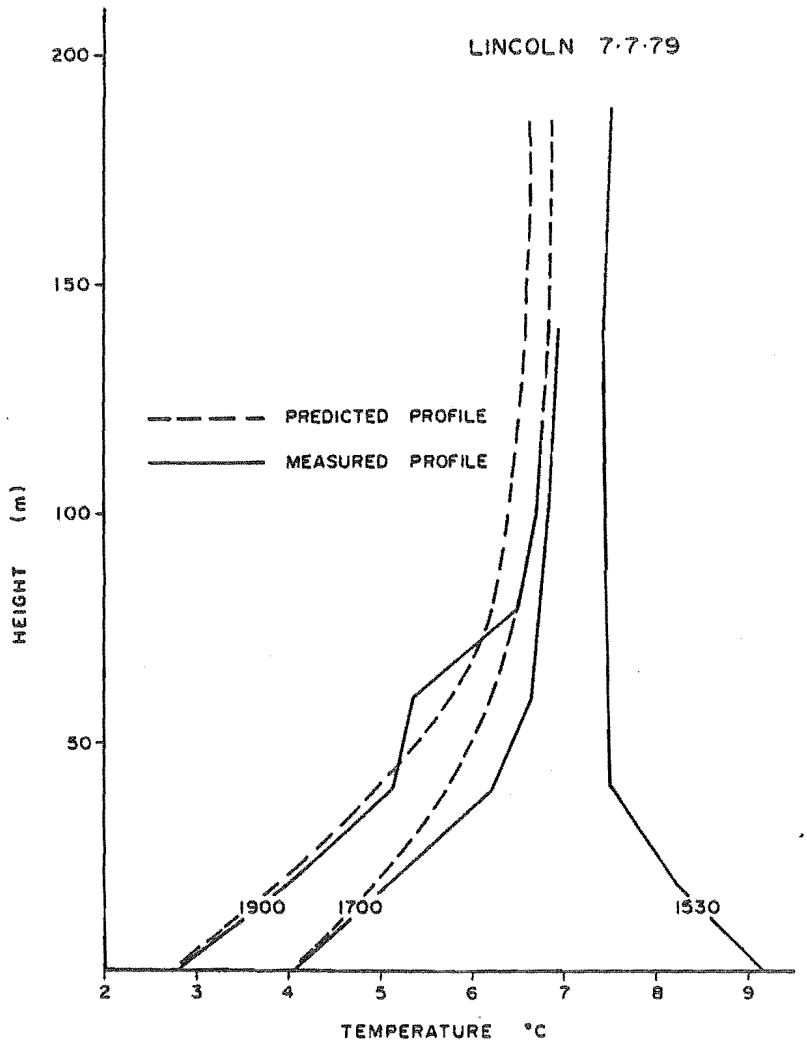

FIGURE A.7 Measured and Predicted (Anfossi *et al.* Equation) Temperature Profiles Aloft, 7 July, 1979.

2100 - 0000 h), adjustments involved were generally only small and any errors involved would be small also. Humidity profiles were adjusted according to the new temperature profile, assuming no change in atmospheric moisture.

The few, paired daytime profiles were standardized in the following arbitrary manner. Examination of measured profiles indicated that there was little temperature change above 200 m (this also substantiated by 'Tempro'), so a linear correction, reducing to zero adjustment at 200 m was applied according to the time progression of screen level temperature. Errors involved in such an approach are unknown but should not be significant as the variation in screen level temperature (hence the maximum correction) was generally quite small.

APPENDIX V

KYTOON PROFILES

All kytoon profiles used in this thesis have been microfilmed and are contained in an envelope inside the rear cover.

A key to the symbols used in the profiles appears below.

KEY:

*	INDICATES THAT THE LINCOLN FLIGHT IS PAIRED WITH A CENTRAL CITY FLIGHT.
	WIND 040° AT 7·5 $m.s^{-1}$ (= 5·0 $m.s^{-1}$, — = 1 $m.s^{-1}$)
	NO WIND SPEED RECORDED
60(26)	NOX, NO_2 BRACKETED ($\mu g.m^{-1}$)
N.P.R.	NO POLLUTION RECORDED
Z.M.S.	NO POLLUTION MEASURED

APPENDIX VI

PROGRAMME LISTING OF 'FINALE'

The programme 'Finale' calculates incoming infra-red radiation from vertical soundings of temperature and humidity in the atmosphere. 'Finale' was written in Basic language for use with the Geography Departments WANG 2200T minicomputer. Full documentation is given below and the listing follows on subsequent pages.

DOCUMENTATION OF 'FINALE'

LINES 40 - 110 — Reads from disk file emissivity tables according to Staley and Jurica (1970). Six tables involved; A - Flux emissivity table for H_2O; AA - Flux emissivity table for CO_2; BA, BB, BC, BD - Tables for H_2O - CO_2 overlap for $-70^{\circ}C$, $-40^{\circ}C$, $-10^{\circ}C$ and $+20^{\circ}C$ respectively.

LINES 150 - 170 — Calculates a pressure/height relationship for use with kytoon data (where only height is known). Pressures and heights obtained from nearest radiosonde flight.

LINES 200 - 250 — Allows input of profile data by height (kytoon) or pressure (radiosonde) and calculates mean pressure, temperature, and humidity characteristics of the

individual layer. Also scales pressure at the layer to standard atmospheric pressure.

LINES 260 - 420 — Calculates and prints out humidity characteristics necessary for the calculation of optical depth of water vapour for the layer. Uses the Groff-Gratch formulas for computation of saturation vapour pressures (Smithsonian Meteorological Tables, p. 350).

LINE 450 — Calculates optical water path with a square root pressure correction in the manner of Robinson (1947) and Kondratyev (1969). Cumulates layer water optical depth with that of previous layers and then calculates the logarithm of total optical path.

LINES 510 - 620 — Using two-dimensional linear interpolation the flux emissivity table for H_2O is entered with the mean layer temperature and log water optical path to give a cumulative all-layer emissivity.

LINES 630 - 660 — Actual layer H_2O emissivity and IR↓ due to water vapour is derived in the method of Robinson (1947, Table IV).

LINES 680 - 740 — In absence of measurements a mean mixing ratio of CO_2 of 5×10^{-4} gg^{-1} was assumed throughout the tropopause, this giving a depth of CO_2 of 0.033 cm in a 1 metre column of air at standard pressure. The value given is a mean observed CO_2 mixing ratio near the earth's surface (Staley and Jurica, 1972). The optical depth of CO_2 in the layer is calculated and pressure scaling performed according to Kondratyev (1969).

LINES 740 - 880 Calculates layer IR↓ emission due to CO_2 in a similar manner to that described in lines 510 - 660 for H_2O.

LINES 890 - 1040 Calculates a negative correction to account for overlap in the contribution of H_2O and CO_2. Overlap correction tables are entered in the same way as described for the H_2O and CO_2 emissivity tables.

LINE 1050 IR↓ emission for the individual layer due to H_2O and CO_2 is calculated.

LINES 1160 - 1200 IR↓ emission from all layers due to H_2O and CO_2 is summated and an addition made for IR↓ contributed by O_3. In the manner of Staley and Jurica (1972) O_3 atmospheric emissivity was assumed throughout to be 0.05 and screen level temperatures were used to calculate ozone IR↓. As the total contribution of O_3 is small, the errors involved in such assumptions are not crucial (Staley and Jurica, 1972).

```
10  REM PROGRAM "FINALE" TO CALCULATE INCOMING IR RADIATION FROM
 VERTICAL SOUNDINGS.
20 DIM A(30),D1(4,14),X1(40),D2(4,14),D3(14,8),D4(14,8),D5(14,8)
,D6(14,8)
30 SELECT PRINT 005
40 FOR I=1TO 6:PRINT "ENTER NAME OF EMISSIVITY TABLE (A,AA,BA,BB
,BC,BD)";I:INPUT B$:INPUT "NO OF COLS AND ROWS",M1,N1:MAT REDIM
X1(M1),D6(M1,N1)
50 DATA LOAD DC OPEN F B$:FOR J=1TO N1:DATA LOAD DC X1():FOR K=1
TO M1:D6(K,J)=X1(K):NEXT K:NEXT J
60 ON I GOTO 70,80,90,100,110,120
70 MAT REDIM D1(M1,N1):MAT D1=D6:GOTO 120
80 MAT REDIM D2(M1,N1):MAT D2=D6:GOTO 120
90 MAT REDIM D3(M1,N1):MAT D3=D6:GOTO 120
100 MAT REDIM D4(M1,N1):MAT D4=D6:GOTO 120
110 MAT REDIM D5(M1,N1):MAT D5=D6:GOTO 120
120 NEXT I
130 SELECT PRINT 005
140 Y2=0:G2=0:X1=0:X3=0
150 PRINT "PRESSURE AT SURFACE(P1), 1ST SIGNIFICANT LEVEL(P2) AN
D HEIGHT AT P2(Y)";:INPUT P1,P2,Y
160 REM Z IS PRESSURE HT RELATIONSHIP.
170 Z=(P1-P2)/Y
180 PRINT "NO OF LAYERS";:INPUT N
190 FOR I=1TO N:SELECT PRINT 005
200 PRINT "INPUT BY HEIGHT(1) OR PRESSURE(2)";:INPUT X
210 ON X GOTO 220,240
220 PRINT "TEMP, HUMID, HT AT THE TOP AND BOTTOM OF THE LAYER";:
INPUT T1,T2,H1,H2,Z1,Z2
230 Z3=((Z1*Z)*(-1))+P1:Z4=((Z2*Z)*(-1))+P1:GOTO 250
240 PRINT "TEMP, HUMID,PRESS AT TOP AND BOTTOM OF LAYER";:INPUT
T1,T2,H1,H2,Z3,Z4
250 T3=(T1+T2)/2:H3=(H1+H2)/2:Z5=(Z3+Z4)/2:Z6=Z4-Z3:Z7=Z5/1013.2
5
260 REM THE FOLLOWING CALCULATES HUMIDITY CHARACTERISTICS FOR TH
E LAYER
270 E1=2.3026:DEFFNW(T)=10^(-7.90298*((373.16/T)-1)+5.02808*LOG(
373.16/T)/E1-1.3816E-7*(10^(11.344*(1-T/373.16)))-1+8.132E-3*(10
^(-3.49149*((373.16/T)-1))-1)+LOG(1013.246)/E1)*10
280 DEFFNI(T)=10^(-9.09718*((273.16/T)-1)-3.56654*LOG(273.16/T)/
E1+.876793*(1-(T/273.16))+LOG(6.1071)/E1)
290 SELECT PRINT 215:PRINT "CALCULATIONS OF HUMIDITY AND RADIATI
ON  CHARACTERISTICS FOR LAYER";I
300 PRINT "TD   PRESSURE   VAP PRESSURE   SPECIFIC HUMIDITY"
310 PRINT "(C)      (MB)         (MB)                (G/KG)"
320 B2=T3+273.16:IF B2<273.16THEN 330:S1=FNW(B2):GOTO 340
330 S1=FNI(B2)
340 R1=H3:R=R1/100:S2=R*S1:W3=B2:W4=W3-40:W2=(W3+W4)/2
350 IF W2<273.16 THEN 360:S3=FNW(W2):GOTO 370
360 S3=FNI(W2)
370 IF ABS(S2-S3)>0.01THEN 400:IF S3<S2THEN 380:W3=W2:W2=(W2+W4)
/2:GOTO 350
380 W4=W2:W2=(W2+W3)/2:GOTO 350
390 W1=W2-273.16
400 E=R*S1*Z7:G=(.622*E/(Z5-(0.378*E)))*1000:SELECT PRINT 215
```

```
410 PRINTUSING 420,T3,25,E,Q
420%##.#   ####.#         ##.###          ##.###
430 SELECT PRINT 005
440 REM CALCULATES LOG H20 PATH LENGTH
450 Y1=10^(-3.0)*Q*((25/1013.25)^0.5)*26:Y2=Y1+Y2:L1=(LOG(Y2)/LO
G(10))
460 PRINT "H20 PATH LGTH,CUM PTH LGTH,LOG PTH LGTH,MEAN TEMP IS
";Y1,Y2,L1,T3
470 SELECT PRINT 215
480 PRINT "LOG H20 PATH LENGTH IS";L1
490 SELECT PRINT 005
500 REM CONVERTS TEMP(T3) AND LOG PATH LENGTH TO CORRESPONDING M
ATRIX CO-ORDINATES
510 T5=(T3+100)/30:L5=15+(L1-2)*2
520 REM  INTERPOLATE REQUIRED EMISSIVITY(F1)
530 M1=4:N1=14
540 K=1
550 IF T5<KTHEN 560:K=K+1:GOTO 550
560 IF T5>M1THEN 570:A9=T5-K+1:J=1:GOTO 580
570 PRINT "TABLE OVERFLOW MAX VALUE USED":A9=T5-M1+1:J=1:K=M1
580 IF L5<JTHEN 590:J=J+1:GOTO 580
590 IF L5>N1 THEN 600:B9=L5-J+1:GOTO 610
600 PRINT "TABLE OVERFLOW MAX VALUE USED":B9=L5-N1+1:J=N1
610 F1=(1-A9)*(1-B9)*D1(K-1,J-1)+B9*(1-A9)*D1(K-1,J)+A9*(1-B9)*D
1(K,J-1)+A9*B9*D1(K,J)
620 PRINT "CUMULATIVE ALL LAYER H20 EMISSIVITY(%) IS";F1
630 X2=F1-X1:X1=F1
640 PRINT "RESULTANT LAYER EMISS IS";X2
650 H8=((5.67*10^(-8.0))*B2^4)*(X2/100)
660 PRINT "LAYER H20 IR EMISSION (W/M-2) IS";H8
670 REM CALCULATES LOG CO2 PATH LENGTH
680 IF X=2THEN 710
690 Z9=Z1-Z2:G1=0.033*Z9*((25/1013.25)^0.8):GOTO 730
700 REM IF ORIGINAL INPUTS WERE BY PRESSURE, HERE USES INPUT HT
TO CALCULATE CO2 DEPTH WITH A PRESSURE CORRN.
710 PRINT "INPUT HT OF TOP, BOTTOM OF LAYER CONCERNED";:INPUT Z1
,Z2
720 Z9=Z1-Z2:G1=0.033*Z9*((25/1013.25)^0.8)
730 G2=G1+G2:L2=(LOG(G2)/LOG(10))
740 L6=13+(L2-2)*2
750 PRINT "LOG CO2 PATH LENGTH IS";L2
760 REM INTERPOLATES REQUIRED EMISSIVITY (F2)
770K=1
780 IF T5<KTHEN 790:K=K+1:GOTO 780
790 IF T5>M1THEN 800:A9=T5-K+1:J=1:GOTO 810
800 PRINT "TABLE OVERFLOW MAX VALUE USED":A9=T5-M1+1:J=1:K=M1
810 IF L6<JTHEN 820:J=J+1:GOTO 810
820 IF L6>N1 THEN 830:B9=L6-J+1:GOTO 840
830 PRINT "TABLE OVERFLOW MAX VALUE USED":B9=L6-N1+1:J=N1
840 F2=(1-A9)*(1-B9)*D2(K-1,J-1)+B9*(1-A9)*D2(K-1,J)+A9*(1-B9)*D
2(K,J-1)+A9*B9*D2(K,J)
850 PRINT "CUMULATIVE ALL LAYER CO2 EMISSIVITY IS";F2
860 X4=F2-X3:X3=F2
870 C1=((5.67*10^(-8.0))*B2^4)*(X4/1000)
880 PRINT "LAYER CO2 IR EMISSION (W/M-2) IS";C1
890 L7=L2+5:K=1:M1=14:N1=8
```

```
900 IF L5<K THEN 910:K=K+1:GOTO 900
910 IF L5>M1 THEN 920:A9=L5-K+1:J=1:GOTO 930
920 PRINT "TABLE OVERFLOW MAX VALUE USED":A9=L5-M1+1:J=1:K=M1
930 IF L7<J THEN 940:J=J+1:GOTO 930
940 IF L7>M1 THEN 950:B9=L7-J+1:GOTO 960
950 PRINT "TABLE OVERFLOW MAX VALUE USED":B9=L7-M1+1:J=M1
960 IF T3<-55 THEN 970:IF T3<=-25 THEN 980:IF T3<=5 THEN 990:GOT
O 1000
970 F3=(1-A9)*(1-B9)*D3(K-1,J-1)+B9*(1-A9)*D3(K-1,J)+A9*(1-B9)*D
3(K,J-1)+A9*B9*D3(K,J)
980 F3=(1-A9)*(1-B9)*D4(K-1,J-1)+B9*(1-A9)*D4(K-1,J)+A9*(1-B9)*D
4(K,J-1)+A9*B9*D4(K,J)
990 F3=(1-A9)*(1-B9)*D5(K-1,J-1)+B9*(1-A9)*D5(K-1,J)+A9*(1-B9)*D
5(K,J-1)+A9*B9*D5(K,J)
1000 F3=(1-A9)*(1-B9)*D6(K-1,J-1)+B9*(1-A9)*D6(K-1,J)+A9*(1-B9)*
D6(K,J-1)+A9*B9*D6(K,J)
1010 F4=F3*10^(-6)
1020 PRINT "LAYER H2O-CO2 OVERLAP CORRECTION IS";F4
1030 Z1=((5.67*10^(-8.0))*B2^4)*F4
1040 PRINT "H2O-CO2 OVERLAP CORRECTION (W/M-2) IS";Z1
1050 A(I)=H8+C1-Z1
1060 SELECT PRINT 215
1070 PRINT "H2O RESULTANT EMISS (%)";X2
1080 PRINT "H2O IR (W/M-2)";H8
1090 PRINT "CO2 RESULTANT EMISS (%)";X4
1100 PRINT "CO2 IR (W/M-2)";C1
1110 PRINT "EMISS CORR (%)";F4
1120 PRINT "IR CORR.(W/M-2)";Z1
1130 PRINT "LAYER IR (W/M-2) IS";A(I)
1140 NEXT I:IF I=N THEN 1150
1150 S=0
1160 FOR J=1 TO N:S=S+A(J):NEXT J
1170 REM CALCULATES THE CONTRIBUTION OF OZONE IN MANNER OF ROBIN
SON    (1947) AND STALEY AND JURICA (1972).
1180 PRINT "WHAT IS SCREEN LEVEL TEMPERATURE";:INPUT T9
1190 O3=((5.67*10^(-8.0))*(T9+273.16)^4)*0.05
1200 T=S+O3
1210 SELECT PRINT 005
1220 PRINT "OZONE IR RADIATION (W/M-2) IS";O3
1230 PRINT "TOTAL INCOMING IR RADIATION (W/M-2) IS";T
1240 SELECT PRINT 215
1250 PRINT "OZONE IR RADIATION (W/M-2) IS";O3
1260 PRINT "TOTAL INCOMING IR RADIATION (W/M-2) IS";T
1270 SELECT PRINT 005
1280 PRINT "ANOTHER DATA SET (YES=1,NO=2)";:INPUT Q
1290 ON Q GOTO 140,1300
1300 END
```